Struvite Crystallization from Nutrient Rich Wastewater

Thesis submitted by

Md. Imtiaj Ali *BSc* (Civil Engineering) Rajshahi University of Engineering and Technology (Bangladesh), *MSc* (Civil-Environment Engineering) University Technology Malaysia (Johor), *MIEAust*

July 2005

For the degree of Doctor of Philosophy

In the School of Engineering

James Cook University

ELECTRONIC COPY

I, the undersigned, the author of this work, declare that the electronic copy of this thesis provided to the James Cook University Library, is an accurate copy of the print thesis submitted, within the limits of the technology available.

_____ _____

Signature Date

STATEMENT OF ACCESS

I, the undersigned, the author of this work, understand that James Cook University will make this thesis available for use within the University Library and, via the Australian Digital Theses network, for use elsewhere.

I understand that, as an unpublished work, a thesis has significant protection under the copyright Act and;

In consulting this thesis I agree not to copy or closely paraphrase it in whole or in part without the written consent of the author, and to make proper public written acknowledgement for any assistance, which I may have obtained from it.

Beyond this, I do not wish to place any restriction on access to this thesis.

_____ _____

Signature Date

STATEMENT OF SOURCES

DECLARATION

I declare that this thesis is my own work and has not been submitted in any form for another degree or diploma at any university or other institute of tertiary education. Information derived from the published or unpublished work of others has been acknowledged in this text and a list of references is given.

_____ _____

Signature Date

ACKNOWLEDGEMENTS

I would like to thank a number of people for their help during the course of this research. I am particularly indebted to my supervisor Dr. Philip Andrew Schneider, for providing me with the opportunity to study with him, for his help and encouragement throughout all stages of this work.

I would also like to thank the AAC staff at JCU particularly Dr. Yee Hu and Dr. Kevin Blake. I am also indebted to Mr. David Kaupilla at JCU mechanical workshop for the technical support of the reactor set up. I also want to extend my thanks to Dr. Paul Britton for his help with the temperature controller set up.

Special thanks are due to Neale Hudson (Queensland DPI) for providing financial and technical support to conduct this research. I am grateful to JCU School of Engineering, JCU research office to provide my scholarship.

Finally I would like to thank my family and friends for their unconditional support, encouragement, willingness to help, and friendship.

DEDICATION

Dedicated to

My Mother

ABSTRACT

Discharge of untreated nutrient-rich wastewater is a problematic issue, which may cause root burning and eutrophication of receiving water. It is also a problematic issue due to the formation of crystalline deposits in waste water systems. The recovery of nutrients using a crystallization technique may provide a value added product. The recovered product is struvite, which is chemically known as magnesium ammonium phosphate hexahydrate. The key focus of this research is the modeling and simulation of struvite growth, which incorporates solution chemistry and thermodynamics, kinetics of growth and process description of the recovery system. This research also focuses on the strategy of struvite crystallization in a fed batch system, to avoid spontaneous precipitation. A fully integrated control strategy in pilot scale is developed in this research. This control strategy is based on feedback control, maintaining constant supersaturation throughout the crystallization. The development and commissioning of experiments includes investigation of suitable seeds, automatic temperature control, operating zone of crystallization and correct design of the pilot scale reactor. Experimental investigation showed a precise stability of the controlled supersaturation. Moreover, size independent growth is indicated in this investigation. An ensemble of experimental data is combined with a dynamic model to carry out parameter estimation of struvite growth kinetic parameters using gPROMS.

TABLE OF CONTENTS

LIST OF TABLES

LIST OF FIGURES

CHAPTER 1

INTRODUCTION

1.1 Problem Statement

Effluent discharge has become a major issue for pig farmers over the last three decades due to livestock intensification. The conventional approaches of nutrient management of livestock wastewater include the spreading of nutrient-rich water on cropland and the dumping of this into receiving waters. Increasing nutrient loads, mainly ammonium and phosphate, causes eutrophication in surface water-bodies and the burning of roots. Eutrophication causes aquatic diversity by producing toxic algae, which devastates fish and other aquatic life.

Occasionally, high mineral content causes encrustation of pipelines, pumps and wastewater related equipment, leading to difficulties in operating piggeries. Excess nutrient content also causes soil acidification, which causes the death of trees. Over the last few decades, Australian pig farms have become more densely populated for commercial reasons, leading to increased nutrient loads in smaller areas (AWA 2000). In Australia, 300,000 sows produce 75 million litres of liquid manure per day (Kruger *et al.* 1995).

One proposed solution to this problem is the recovery of nutrients using crystallization. The key feature of this recovery technique is the combined removal of ammonium, phosphate and magnesium from supersaturated solutions. The by-product of this technique is magnesium ammonium phosphate (MAP), which is commonly known as

struvite. Struvite may be utilized as a valuable source of slow release fertilizer due to its solubility characteristics (Nelson *et al.* 2003). Production of struvite incorporates a chemical reaction among magnesium, ammonium and phosphate ions (equation 1.1) and combines six molecules of water.

$$Mg^{2+} + NH_4^{+} + PO_4^{3-} + \mathbf{6}H_2O \rightarrow MgNH_4PO_4.\mathbf{6}H_2O \qquad \textbf{(1. 1)}$$

1.2 Objectives

The main goal of this research is to develop a clearer understanding of struvite (MAP) crystallization, relating to solution thermodynamics and crystallization kinetics. This research incorporates experimentation, coupled with model simulation. Specific goals of this research are as follows:

1. Design of an isothermal pilot scale struvite reactor based on a sensor-based feedback control system.
2. Demonstration of a strategy to maintain fed-batch (semi-continuous) controlled struvite crystallization using a pilot scale reactor.
3. Description of struvite solution chemistry relating to solution thermodynamic equilibria.
4. Derivation of a more rigorous struvite growth model in which growth kinetics incorporates solution thermodynamic equilibria rather than unconnected process parameters (concentration and pH value). This growth model is derived in fed-batch (semi-continuous) controlled supersaturation mode.
5. Determination of the suitable seed material.

1.3 Layout of the Thesis

This thesis describes the fundamentals of struvite crystallization relating to thermodynamics and kinetics. The design and commissioning of the fed-batch struvite crystallization is also described in this thesis. The chapter wise key summary of this thesis is given below.

1.3.1 Chapter 1 - Introduction

This chapter describes the problem statement relating to nutrient-rich wastewater and its recovery technique. The objectives of this research are also included in this chapter.

1.3.2 Chapter 2 - Literature Review

This chapter describes the background of the research, including the basic understanding of struvite crystallization. The background information included in this chapter is the identification of struvite and its crystallization technique relating to thermodynamics, nucleation and growth. A detailed description of the struvite reactor design and control strategy of struvite crystallization is also included in this chapter.

1.3.3 Chapter 3 - Derivation of the Mathematical Model

This chapter describes the mathematical description of struvite thermodynamics and solution chemistry. A detailed mathematical description of struvite growth kinetics and mathematical modeling of the process is also included in this chapter.

1.3.4 Chapter 4 - Experimental Setup

This chapter describes the experimental procedure, including the design and commissioning of controlled crystallization in fed-batch mode. The design and commissioning of controlled crystallization includes the identification of the operating zone of struvite crystallization, determination of the drying temperature of struvite, design of the struvite reactor, determination of suitable seeds, control of the experimental temperature and the technique of analyzing samples.

1.3.5 Chapter 5 - Results and Discussion from Experiments

This chapter describes the results of the fed-batch experimental control, the growth pattern of struvite, the operating zone of struvite crystallization and the drying temperature of struvite.

1.3.6 Chapter 6 - Results and Discussion from Simulation

An ensemble of experimental data of pilot scale controlled crystallization was included in gPROMS[♣] to estimate struvite growth parameters. The simulation response relating to struvite growth kinetics is described in this chapter. The kinetic response also includes the model validation based on the experimental data. The model based thermodynamic and solution chemistry of struvite is also included in this chapter.

[♣] Process System Enterprise Limited, Bridge Studios, 107a Hammersmith Bridge Road, London, W6 9DA, United Kingdom, email: info@presenterprise.com

1.3.7 Chapter 7 - Conclusion

This chapter describes the brief outcome of this research including the experiment and simulation results.

1.3.8 Chapter 8 – Recommendations for Future Research

This chapter describes the brief recommendation for the future directions of the present research.

CHAPTER 2

LITERATURE REVIEW

2.1 Research Perspective

Integration of process components by means of single controlling parameter (pH value) is an important control strategy for economical and technological reasons (Amjad *et al.* 1978; Toumi and Engell 2004). Amjad *et al.* (1978) investigated an approximate control strategy for hydroxyapatite crystallization in constant supersaturation with no representative data. Van der Houwen and Valsami-Jones (2001) implemented a constant supersaturation strategy for hydroxyapatite crystallization with some representative data of constant concentration as well as constant operating pH. Bouropoulos and Koutsoukos (2000) investigated experimental control of struvite crystallization. Control strategy of struvite crystallization in constant supersaturation was implemented in a small-scale 250 ml reactor. Moreover, robust control strategy is required to identify the reality and problem of the struvite process in large-scale controlled crystallization. Strategic development of controlled supersaturation is essential to maintain product quality and to acquire technically representative data.

Literature suggests that various types of materials are used as seeds in different types of crystallization system. Phosphate rock, bone charcoal, magnesia clinker, zirconium hydroxide, pumice stone, borosilicate glass, struvite, quartz sand, marble, calcium carbonate, activated carbon, bone char, mother crystal (struvite) are the possible candidates of seeds (Nancollas 1968; Joko 1984; Nelson 2000; Paraskeva *et al.* 2000; Munch and Barr 2001; Nelson *et al.* 2003). Theory suggests that chemical inactivity in

mother liquor, isomorphism with mother crystal and adequate surface area in suspension are the predominant properties of ideal seeds (McCabe *et al.* 1985; Mullin 1993; Myerson 1993), which, however, is not confirmed yet by experimental investigation. Thus, this research incorporated experimental investigation of seeds to clarify that mother crystal acts as an efficient source of surface area for crystal growth (Ali and Schneider 2005). Different types of materials such as struvite seeds, borosilicate glass seeds and quartz sand seeds were considered in this research.

Solubility product expresses the saturation of struvite in solution. The value of the struvite solubility product is well documented in the literature (Bube 1910; Taylor *et al.* 1963; Snoeyink and Jenkins 1980; Ohlinger *et al.* 2000). Solution supersaturation and pH value are the key parameters of struvite precipitation. Experimentally, the apparent pH for struvite crystallization has been documented 7.5 - 11.0 (Snoeyink and Jenkins 1980; Buchanan *et al.* 1994; Stumm and Morgan 1996; Ohlinger 1999), depending on the concentration of reactants (magnesium, ammonium and phosphate) and impurities.

Solution thermodynamics is another key factor that plays a predominant role in commencing crystallization. The basic understanding of struvite solution chemistry and the relevant supersolubility is available in the literature (Booram *et al.* 1975; Snoeyink and Jenkins 1980; Ohlinger *et al.* 1998; Ohlinger 1999; Ohlinger *et al.* 2000), however, the detailed results have not yet been published. The thermodynamic modeling of struvite crystallization explored a better understanding on struvite solution chemistry and respective precipitation. This approach was conducted by thermodynamic simulation using gPROMS.

The general form of crystal growth and nucleation kinetics is available in the literature (White 1971; Randloph and Larson 1991; Sohnel and Garside 1992; Mullin 1993; Myerson 1993). Heterogeneous nucleation kinetics and the simple growth kinetic of struvite were investigated by previous researchers (Harrison 1999; Ohlinger 1999; Bouropoulos and Koutsoukos 2000; Nelson 2000; Ohlinger *et al.* 2000; Nelson *et al.* 2003). The mechanism for preferential struvite accumulation using field effluent of nutrient-rich wastewater was also investigated (Ohlinger 1999). Ohlinger (1999) also described a steady state model of struvite incorporating mass deposition and the solubility product. The model described by Ohlinger (1999) offers little understanding of struvite growth, since it does not incorporate thermodynamic and growth kinetics.

Nelson 2000 investigated a nucleation model and carried out a simple kinetic study of struvite precipitation, using anaerobic swine effluent. This study was based on batch experiments, considering mass deposition and concentration decay governed by nucleation. The growth model derived by Harrison (1999) offers a better understanding than the others, since it incorporates the particle size of growing struvite, reactive solution concentration and operating pH. However, Harrison's (1999) growth model appears to be inaccurate, since the process pH value and the reactive solution concentration was considered separately, which is rather impractical. Moreover, the Harrison (1999) model was derived in small-scale, semi-batch (semi-continuous) experiments with controlled pH for a shorter duration of growth. Hence, more reproducible and representative data is required to derive a robust growth model of struvite. Therefore, this research incorporates the derivation of a struvite growth model, which included solution chemistry of struvite along with growing struvite size in controlled supersaturation. To acquire reproducible and representative data,

experimental observations should be conducted in a pilot-scale controlled fed-batch (semi-continuous) mode.

2.2 Livestock Intensification

Pig effluent contains water (90%), complex carbohydrates, pathogenic organisms, salts and nutrients (AWA 2000). Nutrients in pig manure include major nutrients (nitrogen, phosphorus, potassium), minor nutrients and trace elements. Salts in pig effluent mainly include Na^{+}, Ca^{2+}, Mg^{2+}, Cl^{-} and CO_3^{-}.

The growing demand for efficient pork production in Australia has led to a significant reduction in the number of pig farms with increased numbers of pigs in each farm. The number of pig farmers reduced from approximately 40,000 in 1969 to approximately 3000 in 1999. However the pig population has remained stable during that period (Meo and Cleary 2000). The average herd size increased from 8 to over 100. This structural change in pig farming has lead to the production of higher volumes of pig manure in smaller areas, which is very difficult to manage using traditional practices. It is worthwhile pointing out that besides pig manure, nutrient-rich wastewater comes from different sources, such as abattoirs, feedlots, poultry, prawn farming, anaerobic effluent from domestic wastewater treatment plants and fertilizer production plants (Harrison 1999).

2.3 Perspective of Fertilizer Value of Piggery Wastewater

Basic nutrition for plants include NH_4^{+} and NO_3^{-}, $H_2PO_4^{-}$, HPO_4^{2-}, K^{+}, Ca^{2+}, Mg^{2+}, Zn^{2+}, Fe^{2+}, Fe^{3+}, Mn^{2+}, MoO_4^{2} (Dhingra 1995). A survey of Queensland piggeries

(Hudson 2003), shown in Table 2.1, demonstrates the available chemicals in pig effluent; some of them are considered as the basic component for plant nutrition. The available nutrients in pig effluent can improve soil fertility when applied to fields within allowable concentration limits.

Plant roots absorb the nutrient contents from soil pores by mass flow action (Wild 1993). Excess nutrients wash out due to rainfall or flood, when conventional methods of disposal are applied. One of the major concerns of nutrient-rich wastewater is the nitrification of ammonium to nitrate within a few weeks of disposal. Nitrification of ammonium causes several health hazards, which include the restriction of oxygen into circulating blood, the occurrence of gastric cancer, methemoglobinemia (blue baby syndrome) and creating hazards for grazing animals, *etc* (Wild 1993).

Excess loading of nitrogen and phosphorus to receiving waters may cause an increase in phytoplankton production and decrease light penetration. When nutrient supplies are exhausted by either excessive phytoplankton growth or shortage of nutrient supply in dry weather, these unicellular plants die and sink to the bottom. Dissolved oxygen is consumed by deposited algae and results in killing of worms, and causes the removal of the cooler deep water causing damage in the habitat for fish and shellfish communities (Sharpley 2000). Light reduction through water causes turbidity, which prevents the submersed aquatic vegetation (SAV) from preparing food and it is the prime factor for very substantial SAV losses (Sharpley 2000). The resulting eutrophication restricts the use of surface water from aesthetic fisheries, recreation, industry, and drinking purposes.

The most popular chemical fertilizers used in agriculture are $(NH_4)_2SO_4$ (ammonium sulphate), NH_4NO_3 (ammonium nitrate), NH_4NO_3 plus $CaCO_3$ (calcium ammonium nitrate), $CO(NH_2)_2$, anhydrous NH_3, aqueous NH_3, $Ca(H_2PO_4)_2$ plus $CaSO_4.2H_2O$ (single superphosphate), $Ca(H_2PO_4)_2$ (triple superphosphate), $(NH_4)_2HPO_4$ (di-ammonium phosphate), $Ca_5(PO_4)_3F$ (rock phosphate), KCl (potassium chloride), K_2SO_4 (potassium sulphate) to provide supplements of K, N and P (Wild 1993). Recovery of P and N, using crystallization, may provide valuable fertilizer and can reduce the cost of effluent management. Literature suggests that hydroxyapatite and struvite are the most popular by-products, whereas no research has been reported for the crystallization of potassium ammonium phosphate (KMP) since Taylor *et al.* 1963.

2.4 Concepts of Struvite Crystallization

2.4.1 Background of Struvite

Magnesium ammonium phosphate hexa-hydrate ($MgNH_4PO_4.6H_2O$) is more commonly known as struvite. Struvite is a threat for nutrient-rich wastewater streams due to encrustation onto the exposed surface of wastewater distribution system. The morphology of struvite crystal is orthorhombic (Figure 2.1), however its shape may be spherical or dendrite, and cubic shapes of struvite crystal are also known. Struvite is slowly soluble in neutral water (Nelson *et al.* 2003).

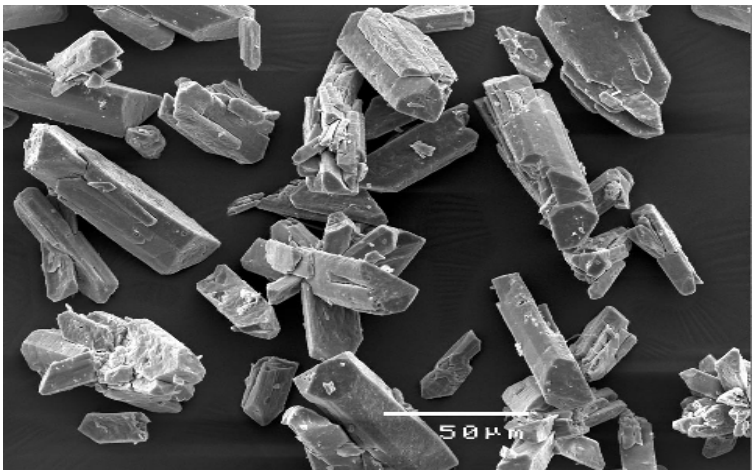

Figure 2. 1 Electron Micrograph of the typical struvite crystal observed in this research

Its genuine slow release property prevents the burning of plant roots, even when applied in excess quantities. Moreover, the insoluble nature of struvite in neutral water prevents eutrophication of surrounding waterways and restricts leaching into groundwater, providing efficient and economical use of fertilizer. Therefore, struvite has the potential to be used as a popular boutique fertilizer in horticulture, nurseries and golf courses (Schuling and Andrade 1999).

Table 2. 1 Characteristics of pig effluent of different Queensland's piggeries: concentrations are in mg/l (Hudson 2003)

THIS TABLE HAS BEEN REMOVED DUE TO COPYRIGHT RESTRICTIONS

Crystalline deposits of struvite characteristically form around specific sections of wastewater treatment infrastructures in the high turbulence zone (Schuling and Andrade 1999). The very sensitive zones for struvite formation are valves; bends in pipe-works, separating screens and pumps. The formation of crystalline deposits can be extensive, which leads to operational failure by clogging wastewater distribution lines (Snoeyink and Jenkins 1980). Figure 2.2 demonstrates one example of struvite formation in digester pipeline.

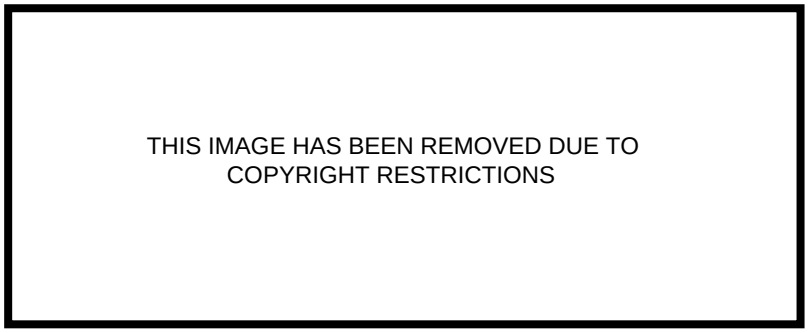

Figure 2. 2 Struvite deposition in digester pipeline (Snoeyink and Jenkins 1980)

2.4.2 Thermodynamics of Struvite

Thermodynamics is the study of energy transformation in chemical reaction and phase equilibria, which reveals the reaction or transition properties and the state of chemical equilibrium (Mullin 1993; Myerson 1993). Solubility is the key parameter in solution thermodynamics, which depends on Gibbs free energy transformation (equation 2.2). The Thermodynamic Solubility Product of struvite (K_{so}) depends on the free ion concentration (C_i), ionization fraction (α_i) and the activity coefficient (γ_i) of the struvite

constituents (Mg^{2+}, NH_4^+ and PO_4^{3-}). Ohlinger *et al.* (2000) documented the Conditional Solubility Product (P_s), as it relates to the Thermodynamic Solubility Product (K_{so}), total or analytic concentration ($C_{T,i}$), ionization fraction (α_i), and activity coefficient (γ_i) to illustrate the solubility status of field effluent (equations 2.1 and 2.3). Numerical comparison between the Conditional Solubility Product (P_s) and the Thermodynamic Solubility Product (K_{so}) identifies the solubility state of the solution.

$$K_{so} = \left(\alpha_{mg^{2+}} \gamma_{mg^{2+}} C_{T,mg^{2+}}\right)\left(\alpha_{NH_4^+} \gamma_{NH_4^+} C_{T,NH_4^+}\right)\left(\alpha_{PO_4^{3-}} \gamma_{PO_4^{3-}} C_{T,PO_4^{3-}}\right) \quad \textbf{(2. 1)}$$

$$K_{so} = \exp\left(-\frac{\Delta G_0}{RT}\right) \quad \textbf{(2. 2)}$$

$$P_S = C_{T,Mg} C_{T,NH_3} C_{T,PO_4} = \frac{K_{so}}{\alpha_{mg^+} \alpha_{NH_4^{+2}} \alpha_{PO_4^+} \gamma_{mg^+} \gamma_{PO_4^{3-}} \gamma_{NH_4^+}} \quad \textbf{(2. 3)}$$

Experimental investigations on the struvite solubility product are well established in the available literature (Bube 1910; Taylor *et al.* 1963; Snoeyink and Jenkins 1980; Ohlinger *et al.* 2000). Bübe (1910) first conducted a successful investigation on a struvite solubility product and documented a pK_{so} value of 12.60. Snoeyink and Jenkins (1980) used a pK_{so} value of 12.6, which was repeatedly cited by the other researchers (Webb and Ho 1992; Mamais *et al.* 1994; Lowenthal *et al.* 1995). More recent investigations in this perspective were conducted by Ohlinger (1999), who documented a pK_{so} product value of 13.26±0.04. Ohlinger (1999) determined the range of possible pK_{so} value by an iterative computational analysis, considering a theoretical concentration and pH, along with their complexes. The solubility product of struvite (K_{so}), proposed by Ohlinger (1999), is employed in this research for further theoretical and experimental investigation.

2.4.3 pH for Struvite Precipitation Potential

Undersaturated solution, consisting of struvite components (Mg^{2+}, NH_4^+, PO_4^{3-}), commences crystallization when supersaturation is attained. The increase of solution saturation can be carried out by either of the following two techniques.

1. Increasing the reactant concentration.
2. Increasing the solution pH.

Logically, increasing the reactant concentration to commence crystallization is not feasible or desirable. Hence, increasing the solution pH to commence crystallization is more appropriate. The apparent pH of minimum struvite solubility is documented in the range of 9.0 to 11.0 (Snoeyink and Jenkins 1980; Buchanan *et al.* 1994; Stumm and Morgan 1996; Ohlinger 1999). However, struvite precipitation can commence at lower pH values, i.e. 7.5 (Doyle *et al.* 2000; Doyle *et al.* 2001). Wrigley *et al.* (1992) investigated struvite precipitation at a pH value of 10, achieving a 75% recovery of nutrients. von Munch and Barr (2001) implemented struvite precipitation at pH 8.5, with more than 80% recovered phosphate. Buchanan *et al.* (2000) investigated struvite crystallization at pH of 7-11. Schuling and Andrade (1999) documented struvite crystallization at pH of 9, using animal wastewater. Doyle *et al.* (2000) employed a pH of 8.0 for struvite precipitation, providing evidence that it could also occur at pH value of 7.5.

Literature already cited indicates that pH is not the only parameter that effects struvite crystallization. More precisely, a wide range of pH values was implemented, since solution concentrations varied widely. Therefore, it can be concluded that struvite

crystallization depends on both pH as well as solution concentration, which can be more accurately described by solution thermodynamics.

2.4.4 Nucleation Thermodynamics

The classical theory of nucleation was derived for the condensation of vapor and the scope was extended to crystallization from melts and solution (Becker and Doring 1935; Volmer 1939; Gibbs 1948; Mullin 1993). Critical cluster formation is the first step of crystallization. Critical clusters do not posses any distinct shape, however, they are described as miniature particles that take part in surface diffusion (Hoare and McInnes 1982).

The first step of nucleation is the formation of clusters and thereafter formation of critical clusters by combining the newly born clusters (Mullin 1993). Clusters produced at very high supersaturation do not take part in crystal growth, leading to the production of fines (Randloph and Larson 1991; Myerson 1993). Besides, crystallization from a very low supersaturated solution induces miniature and unstable clusters, which redissolve very easily (Randloph and Larson 1991; Mullin 1993; Myerson 1993). Therefore, the optimum level of operating supersaturation is recommended for crystallization to arrest excessive nucleation and enforce crystal growth (Hirasawa 1996; Davey and Garside 2000).

2.4.5 Mode of Nucleation

Nucleation is characteristically divided into primary nucleation and secondary nucleation. Primary nucleation is further divided into homogeneous nucleation and

heterogeneous nucleation. Homogeneous nucleation occurs in the absence of any foreign particles, a condition that practically does not exist. Heterogeneous nucleation occurs by the influence of foreign particles. Heterogeneous nucleation occurs at reduced supersaturation. However, it is virtually impossible to achieve solution completely free from foreign bodies (Davey and Garside 2000), therefore homogeneous nucleation is unlikely to exist.

Secondary nucleation occurs in the presence of parent crystals, imposing local interactions of existing crystals with reactor's walls and impeller. Parent crystals have a catalyzing effect on nucleation, causing local fluctuations in supersaturation, thus nucleation occurs at unpredictably lower supersaturation. Secondary nucleation is a problematic issue in industrial crystallization where product quality is an important factor (Tavare 1995). The governing factors of secondary nucleation are: initial or dust breeding, needle breeding, collision breeding, impurity concentration gradient nucleation, and fluid shear (Myerson 1993).

2.5 Fundamentals of Crystal Growth

Growth is the second part of crystallization kinetics, which occurs when clusters aggregate themselves or diffuse onto the surface of diffusive bodies. Several mechanisms, including surface energy theory, adsorption layer theory and diffusion reaction theory, have been proposed to explain crystal growth. Among these theories, only diffusion reaction theory can, in fact, explain crystal growth effectively (Myerson 1993). However exceptions exists in which the growth phase is described by adsorption layer theory (Babic-Ivancic *et al.* 2002). According to the diffusion reaction theory,

crystal clusters and solute molecules are transported from the bulk fluid phase to the solid surface, followed by the integration of the solid molecules (Figure 2.3).

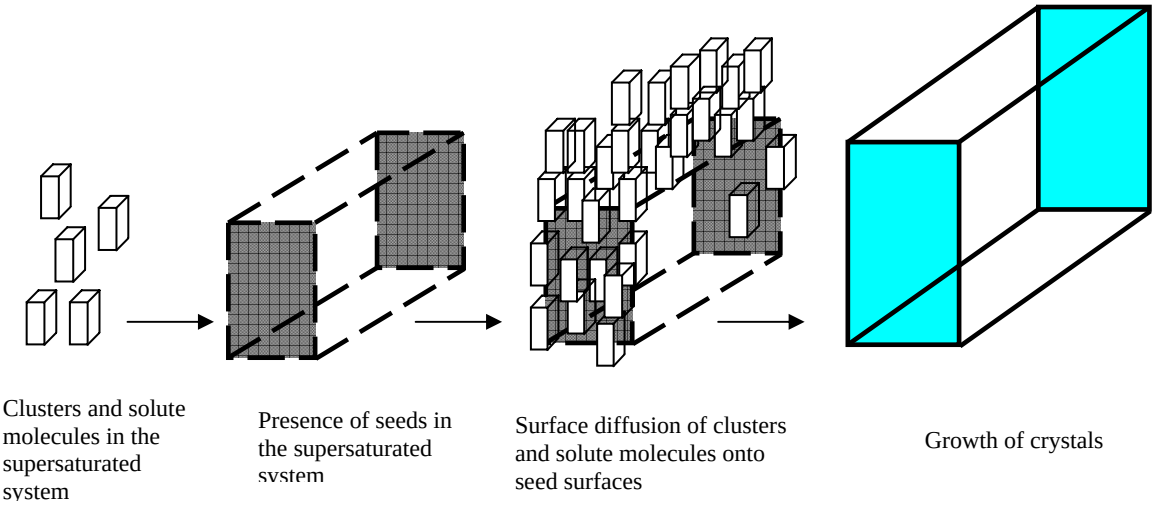

Figure 2. 3 Schematic of diffusion integration process

The rate of crystal growth can be expressed as the rate of linear displacement of crystal faces. For a specified crystal, such linear growth rate is different for different crystallographic faces (Sohnel and Garside 1992). For engineering purposes, the rate of crystallization is expressed by the specific rate of mass deposition (R), which incorporates growth order (y), growth constant (K), crystal surface area (A_T) and supersaturation (S) (Tavare 1995).

$$R = \frac{1}{A_T}\frac{dW}{dt} = KS^{y} \qquad \textbf{(2. 4)}$$

The overall growth rate constant (K_g) depends on temperature, crystal size, and the presence of impurities.

It is convenient to express the overall linear rate (dL/dt) for an ensemble with a constant population of crystal, relating to reaction temperature (T), seeds size (L), nucleation rate (N) and mixing intensity (I) (McCabe *et al.* 1985; Randloph and Larson 1991; Sohnel and Garside 1992; Mullin 1993; Myerson 1993; Tavare 1995; Davey and Garside 2000). In equation (2.5), $\boldsymbol{K_g}$ is the growth rate constant and $\boldsymbol{g}$ is the growth order.

$$G = \frac{dL}{dt} = K_g S^g \qquad \textbf{(2. 5)}$$

$$K_g = f(T, L, N, I, \cdots) \qquad \textbf{(2. 6)}$$

2.6 Struvite Crystallization in the Metastable Region

Thermodynamically, the metastable zone is defined as the critical zone of supersaturation of solution where crystallization is not governed by nucleation and thus avoids the rapid precipitation.

Figure 2.4 illustrates the saturation states of struvite crystallization relating to the negative log value of the conditional solubility product (pP_{so}) and the solution pH value. The chemical composition of struvite is $MgNH_4PO_46H_2O$. The relevant chemical complexes of struvite are Mg^{2+}, $MgOH^+$, $MgH_2PO_4^+$, $MgHPO_4$, $MgPO_4$, H_3PO_4, $H_2PO_4^-$, HPO_4^{2-}, PO_4^{3-}, $MgPO_4^-$ NH_3, NH_4^+ (Bouropoulos and Koutsoukos 2000; Ohlinger *et al.* 2000). As demonstrated in Figure 2.4, Ohlinger *et al.* (2000) documented several solubility limit curves (saturation curves) at different ionic strength *(μ)* and different negative log values of the solubility product (pP_{so}). The chemical complexes include in saturation curves 1-3 are Mg^{2+}, $MgOH^+$, $MgHPO_4$, H_3PO_4,

$H_2PO_4^-$, HPO_4^{2-}, PO_4^{3-}, $MgPO_4^-$, NH_3, NH_4^+, whereas saturation curve 4 (Figure 2.4) includes Mg^{2+}, $MgOH^+$, H_3PO_4, $H_2PO_4^-$, HPO_4^{2-}, PO_4^{3-}, $MgHPO_4$, $MgPO_4^-$, NH_3, NH_4^+, $MgHPO_4$, $MgH_2PO_4^+$ and $MgPO_4$. For further reference, this research includes saturation curve 4, since it includes all the chemical complexes of struvite solution chemistry and applicable for reasonably high ionic strength ($\mu = 0.1$).

Table 2. 2 Clarification of struvite solubility based on Figure 2.4

Demonstrated points/ Graphs	**State of Solubility**	**Remarks/ Notes**
XY	Saturation curve	Growth type crystallization may be possible between these two curves
X_1Y_1	Minimum solubility limit spontaneous precipitation	
A	Undersaturation	No crystallization occurs
B	Saturation	Unlikely to occurs
C	Metastable supersaturation zone	Heterogeneous crystallization
D	Minimum solubility limit of spontaneous precipitation	Maximum solubility limit of heterogeneous crystallization
E	Labile supersaturation	Homogeneous crystallization

The graphical presentation of XY (line 4 in Figure 2.4) represents the saturation curve in typical conditions as demonstrated by Ohlinger (1999). However, the state of saturation may vary to some extent depending on the solution ionic strength and/or equilibrium solubility product. Graphical presentation of X_1Y_1 demonstrates an arbitrary minimum limit for spontaneous precipitation. Literature suggests that the minimum solubility limit of spontaneous precipitation depends on solution properties (Hirasawa 1996). The solubility zone, between the saturation curve (XY) and the arbitrary minimum limit of spontaneous precipitation (X_1Y_1) is called the metastable zone. Crystallization in the metastable zone is heterogeneous. Homogeneous crystallization occurs when the saturation level of solution is above the minimum solubility limit of spontaneous precipitation. The full demonstration of solubility and saturation based on Figure 2.4 is given in Table 2.2.

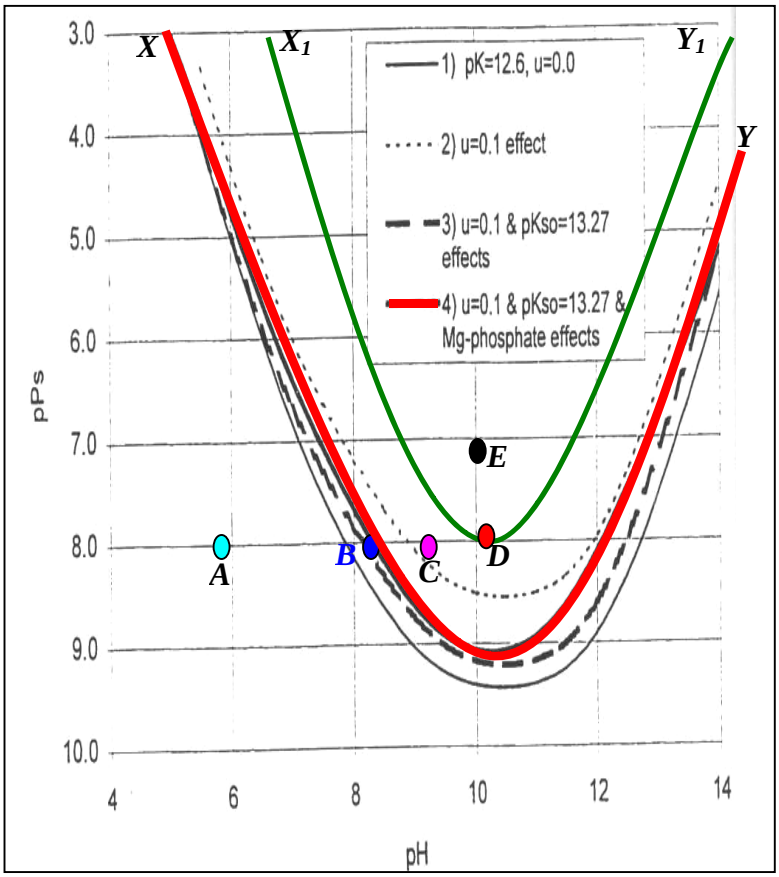

Figure 2. 4 Operating range of struvite crystallization (Ohlinger 1999)

The thermodynamic driving force in supersaturated solutions supplies energy for cluster formation. The time lag between the supersaturation of solution and the first appearance of concentration decay is called the induction time (Mullin 1993). A highly supersaturated solution has a shorter induction, whereas relatively lower supersaturation is characterized by a longer or even infinite induction time. One disadvantage of infinite induction time is the re-dissolving of induced crystals in solution due to high-energy consumption from a relatively lower driving force. In this circumstance, preliminary additions of seed materials induce surface diffusion of newly born clusters and govern crystal growth (Munch and Barr 2001). In industrial crystallization, metastable zone technique is widely practiced due to a smoother continuous operation at controlled supersaturation (Thaller *et al.* 1981; McPherson 1988; Srinivasakannan *et al.* 2002). Figure 2.5 demonstrates the schematic diagram of crystallization at uncontrolled and controlled supersaturation.

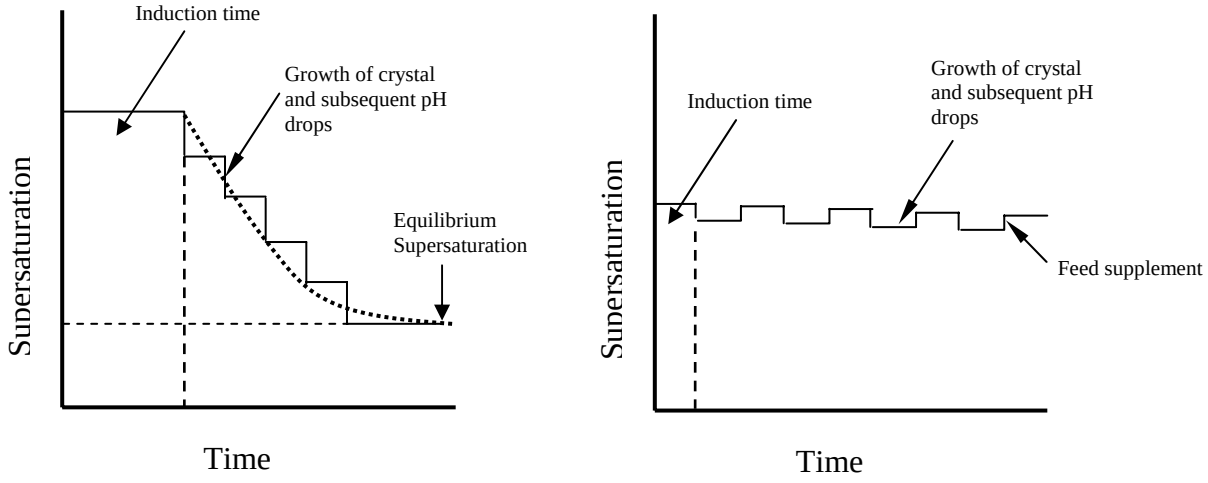

Figure 2. 5 Schematic presentation of crystallization at higher supersaturation and controlled (constant) supersaturation

The metastable zone width is a characteristic property of crystallization, which plays an important role in industrial crystallization to maintain product quality (Kim and

Mersmann 2001). Hirasawa (1996) documented an experimental approach to determine the metastable zone width for hydroxyapatite crystallization, relating to solution supersaturation, pH value, and the minimum solubility limit of crystallization. Crystallization at very close to saturation is ultimately a challenging issue (Penkova *et al.* 2003). However, seed crystals offer assistance for crystal growth (Mullin 1993). A longer or even an infinite induction time is required for crystallization at lower supersaturation. In this circumstance, the presence of seeds generally reduces the induction period; therefore, crystals grow even at lower supersaturation in the presence of seeds.

2.7 Selection of Seeds materials

Often research on struvite (MAP) recovery was conducted using unspecified seed size (Harrison 1999). The Kurita process (Joko 1984) used phosphate rock of 0.5-1.0 mm. Ohlinger *et al.* 2000 used struvite seeds of larger than 1 mm (1-1.36 mm) to perform batch and continuous struvite crystallization. Sydney Water conducted a struvite recovery experiment using 10 micron seeds (Angel 1999). Literature suggests that chemical inactivity of seeds in the mother liquor, isomorphism with mother crystal and adequate surface area in suspension are the predominant properties of ideal seeds (McCabe *et al.* 1985; Mullin 1993; Myerson 1993).

Various types of materials are being used as seed materials in crystallization. Among them phosphate rock, borosilicate glass, struvite, quartz sand, parent crystals (struvite) are the most popular candidate of seeds for struvite crystallization (Nancollas 1968; Joko 1984; Paraskeva *et al.* 2000; Munch and Barr 2001).

2.8 Control Strategy

The control strategy is a key feature for the continuous or semi-continuous (fed-batch) systems of struvite crystallization. The sensor-based control strategy is divided into automatic and feedback control (Green 1983; Trystram 1986; Trystram and Dumoulin 1990; Trystram and Courtois 1994). Automatic control includes the automatic stoppage of the machine at the time of a process upset and is followed by the activation of an alarm. Feedback control includes the electronic continuous control of a system by monitoring and manipulating the process input variables to influence the expected control. In struvite crystallization, the control system is sensor based feedback control by means of pH as the process controlling parameters (Joko 1984; Momberg and Oellermann 1992; Battistoni *et al.* 2000; Munch and Barr 2001; Piekema and Giesen 2001). Integration of process components by means of a single controlling parameter (solution pH) is an important control strategy for economical and technical aspects (Toumi and Engell 2004). An improved control system, incorporating a pH value as the controlling parameter, was applied in small scale for hydroxyapatite crystallization (van der Houwen and Valsami-Jones 2001). Integrated sensor based control of somewhat larger operational volume, i.e. 2.5 litres, was employed by Adnan *et al.* (2003, 2004) for struvite crystallization. Adnan *et al.* (2003, 2004) successfully controlled experimental pH in a continuous system by proving the mixing of solution through a recirculation pump. However, the experimental control of phosphate concentration (Adnan *et al.* 2003; Adnan *et al.* 2004) appeared to be in a steady state and no statement has been made regarding the sensitivity of the control unit.

Precise stability of the experimental control is highly desirable to accomplish a better understanding of struvite growth kinetics (Moscosa-Santilla *et al.* 2000). Application of

the sensor based feedback control in struvite crystallization is a problematic issue in large-scale crystallizations. The major source of faulty control occurs due to the insertion point of a pH probe in the dead zone of crystallizer, loss of sensitivity of the sensor and the other controlling equipment and excessive sensitivity of the dosing point due to local fluctuation of supersaturation (Mangin *et al.* 2004). Failure of the above mentioned control elements degrade the system's performance.

2.9 Growth Type Crystallization

The key concept of the growth type crystallization is to prevent spontaneous precipitation and to allow existing crystals to take part in growth. An efficient way to improve crystal morphology is to maintain optimum supersaturation (Ali and Schneider 2005). Controlled crystallization supports the integration of clusters efficiently (Mullin 1993); hence good product quality can be achieved. Crystallization at very high supersaturation produces elongated shaped crystals (Sohnel and Garside 1992). The key stress of high supersaturation is the imbalance energy transformation between crystal and solution in growth phase. Hence a significant amount of fines is produced in this circumstance. The detailed explanation of the energy transformation during crystal growth is described in the following paragraph.

As described in Section 2.5, crystallization is induced by the formation of clusters in the supersaturated system. Assuming the spherical shape of clusters, Gibbs free energy equation (equation 2.7) describes the required energy change to form a cluster of a given size (Myerson 1993).

$$\Delta G = 4\pi r^2\sigma - \left(\frac{4\pi r^3}{3v}\right)RT\ln(1+S) \qquad \textbf{(2. 7)}$$

Where

r = Radius of the cluster

σ = Solid-liquid interfacial tension

R = Gas constant

T = Temperature in Kelvin scale

S = Degree of supersaturation

V_m= Molecular volume

The first term of the equation 2.7 is the Gibbs free energy change for forming the surface *(ΔG_s)* and the second term is for the volume *(ΔG_v)*. It is worthwhile pointing out that the rate of nucleation is a function of supersaturation (equation 2.8), given that $\boldsymbol{k}$ is the Boltzman constant, $\boldsymbol{T}$ is the temperature, $\boldsymbol{S}$ is the supersaturation, $\boldsymbol{A}$ is the Arrhenius reaction constant, $\boldsymbol{\gamma}$is the interfacial tension and $\boldsymbol{V_m}$ is the molecular volume of the cluster. At very low supersaturation, the rate of nucleation is negligible. Therefore, the number of cluster formations is limited. For small numbers of clusters the total Gibbs free energy change is positive (Myerson 1993), since the second part of equation 2.7 is negligible at low supersaturation *(S)*. This means that clusters are unstable and will dissolve at very low supersaturation. In contrast, at very high supersaturation the critical size of clusters decreases (equation 2.9), leading to the occurrence of an unstable crystallization system (Myerson, 1993).

$$J = A\exp\left[-\frac{\boldsymbol{16}\pi\gamma^{\boldsymbol{3}}V_m{}^{\boldsymbol{2}}}{\boldsymbol{3}k^{\boldsymbol{3}}T^{\boldsymbol{3}}(\ln S)^{\boldsymbol{2}}}\right] \qquad \textbf{(2. 8)}$$

$$r_c = \frac{2V_m \sigma}{RT \ln(1 + S)} \qquad \textbf{(2. 9)}$$

Destruction of fines will have a positive impact on improving product quality (Davey and Garside 2000), which however needs substantial extra equipment. Provision of a elutriation leg is a competent way of improving product quality (Sohnel and Garside 1992; Tavare 1995; Davey and Garside 2000; Mersmann 2001). This has been implemented successfully in the industrial and field scale (Munch and Barr 2001).

2.10 Agitation and Mixing

Hydrodynamics and mixing plays an important role in preventing local supersaturation. Even small degrees of local supersaturation may cause spontaneous nucleation and produce smaller crystals with lower mean particle diameters and higher coefficients of variance of the crystal size distribution (CSD).

Mixing energy can be supplied by the recirculation of fluid streams, impeller operation and/or air purging. It is demonstrated that an increase in agitation and mixing does not always lead to an increase in nucleation (Mullin and Raven 1961, 1962). In other words, gentle agitation causes stable nucleation, whereas vigorous agitation considerably enhances nucleation, but the transition between the two conditions may not be continuous (Mullin 1993). The optimum mixing energy prevents the crystal from breaking and suspends it just as required.

2.11 Operating Mode Struvite Reactor

Numbers of different techniques are currently being used in struvite crystallization, and are based on fluidized bed, mixed suspension mixed product removal (MSMPR) and packed bed condition. Packed beds effectively reduce nutrient concentration, however periodic regeneration is required due to media cementation (Ohlinger *et al.* 2000). Fluidized bed, providing continuous flow of mother liquor, keeps crystals in suspension (McCabe *et al.* 1985). In the MSMPR type of crystallizer, solid particles remain in a continuously mixed state using an external source of mixing energy (forced circulation) such as an impeller operation. Particle size distribution cannot be effectively controlled in MSMPR. The schematic diagrams of different types of reactors are demonstrated in Figure 2.6.

The Draft Tube-baffled reactor is the other type of struvite crystallizer, in which a baffle controls the circulation of magma, and a downward-directed propeller agitator provides a controllable circulation within the crystallizer (McCabe *et al.* 1985). The flow of mother liquor is regulated by an additional circulation system driven by a circulating pump outside the crystallizer.

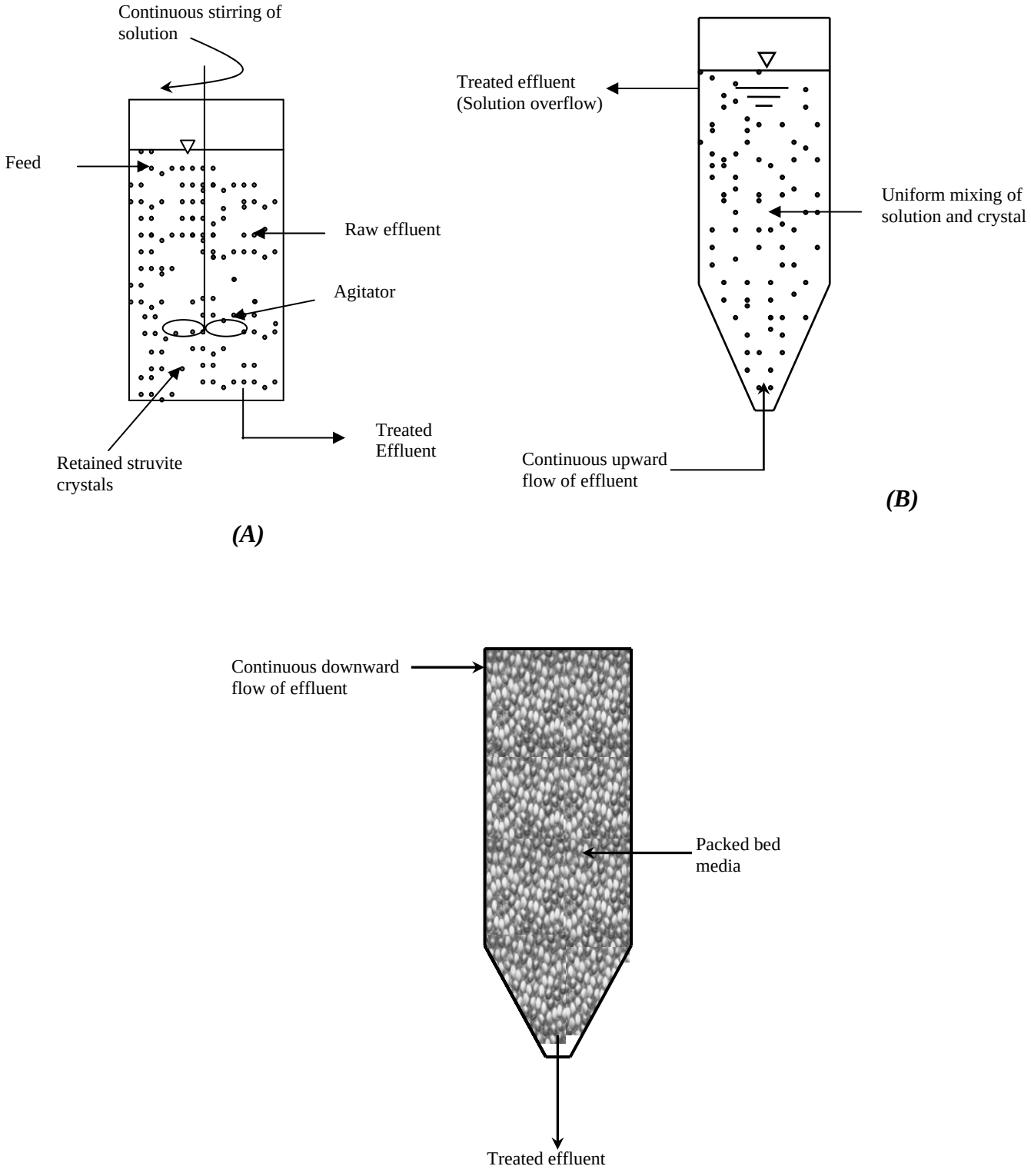

Figure 2. 6 Schematic of MSMPR (A), Fluidized bed reactor (B), and packed bed reactor (C)

2.12 Chapter Summary

This chapter describes the theoretical understanding of struvite crystallization, relating to solution thermodynamics and the kinetics of crystal growth. The background information of reactor design and operation in controlled supersaturation system shows that the fed-batch struvite crystallization in pilot scale (maintained at controlled supersaturation) is a critical issue. Design of controlled struvite crystallization requires several critical data sets, including the solubility product and the thermodynamics of struvite crystallization. Controlled struvite crystallization should also include some techniques to reduce spontaneous precipitation, along with the condition of proper mixing and the correct composition of feed solution. Background information also shows that struvite recovery from livestock wastewater has the potential to reduce environmental pollution. The recovered product has the potential to be used as a commercial fertilizer.

Based on the information cited in this chapter, this research incorporates the following studies.

- Design and Commissioning of a pilot scale struvite reactor to conduct a fed-batch experiment is controlled supersaturation (chapter 4 and 5).
- Derivation of a thermodynamic and kinetic model (chapter 3) and the simulation of this model using the gPROMS process simulation software (a programming language). The result of simulation is shown in the chapter 6.

CHAPTER 3

DERIVATION OF MATHEMATICAL MODEL

3.1 Introduction

Struvite contains magnesium, ammonium and phosphate. The crystallization of struvite is governed by supersaturation. The value of supersaturation can be computed by incorporating the detailed solution chemistry and thermodynamic equilibria of magnesium, ammonium and phosphate. The kinetics of struvite growth incorporates struvite thermodynamics and a mathematical description of the crystallization mechanism. The coding of a mathematical model in gPROMS (a process simulation software) leads to an estimation of the kinetic parameters and a preliminary design of the experiment.

3.2 Thermodynamic Modeling

Solution chemistry plays a key role in struvite crystal formation. In a supersaturated solution, struvite forms by the chemical reaction of the free Mg^{2+}, NH_4^+ and PO_4^{3-} ions (equation 3.1).

$$Mg^{2+} + NH_4^+ + PO_4^{3-} \rightleftarrows MgNH_4PO_4 \qquad \textbf{(3. 1)}$$

Additionally, the formation of struvite crystal normally incorporates six molecules of water, as water of hydration: therefore struvite is known as magnesium ammonium phosphate hexahydrate ($MgNH_4PO_4.6H_2O$).

Supersaturation of the solution is the key parameter leading to crystallization, which in turn depends on solution pH and reactive solution concentration. Solutions consisting of Mg, NH_4 and PO_4 form ions and complexes including Mg^{2+}, $MgOH^{+}$, $MgH_2PO_4^{+}$, $MgHPO_4$, $MgPO_4^{-}$, H_3PO_4, $H_2PO_4^{-}$, HPO_4^{2-}, PO_4^{3-}, NH_3 and NH_4^{+} (Bouropoulos and Koutsoukos 2000; Ohlinger *et al.* 2000). Thermodynamic equilibria for different complexes are presented in equations (3.2)-(3.9), provided that *{i}* represents the activity based concentration of each ion and complex described above, and K_i is the equilibrium constant of the specified ion complex.

$$K_{MgOH^+} = \frac{\{Mg^{2+}\}\{OH^-\}}{\{MgOH^+\}} \quad \textbf{(3. 2)}$$

$$K_{NH_4^+} = \frac{\{H^+\}\{NH_3\}}{\{NH_4^+\}} \quad \textbf{(3. 3)}$$

$$K_{HPO_4^{2-}} = \frac{\{H^+\}\{PO_4^{3-}\}}{\{HPO_4^{2-}\}} \quad \textbf{(3. 4)}$$

$$K_{H_2PO_4^-} = \frac{\{H^+\}\{HPO_4^{2-}\}}{\{H_2PO_4^-\}} \quad \textbf{(3. 5)}$$

$$K_{H_3PO_4} = \frac{\{H^+\}\{H_2PO_4^-\}}{\{H_3PO_4\}} \quad \textbf{(3. 6)}$$

$$K_{MgH_2PO_4^+} = \frac{\{Mg^{2+}\}\{H_2PO_4^-\}}{\{MgH_2PO_4^+\}} \quad \textbf{(3. 7)}$$

$$K_{MgHPO_4} = \frac{\{Mg^{2+}\}\{HPO_4^{2-}\}}{\{MgHPO_4\}} \quad \textbf{(3. 8)}$$

$$K_{MgPO_4^-} = \frac{\{Mg^{2+}\}\{PO_4^{3-}\}}{\{MgPO_4^-\}} \quad \textbf{(3. 9)}$$

The total constituent concentrations for Mg^{2+}, NH_4^+ and PO_4^{3-}, denoting C_{T_Mg}, C_{T_NH4}, C_{T_PO4}, are the sum of the ionic concentration of their complexes and free ions, which are illustrated in equations (3.10)-(3.12).

$$C_{T\_PO_4} = [H_3PO_4] + [H_2PO_4^-] + [HPO_4^{2-}] + [PO_4^{3-}] + [MgH_2PO_4^+] + [MgHPO_4] + [MgPO_4^-] \quad \textbf{(3. 10)}$$

$$C_{T\_Mg} = [Mg^{2+}] + [MgOH^+] + [MgH_2PO_4^+] + [MgHPO_4] + [MgPO_4^-] \quad \textbf{(3. 11)}$$

$$C_{T\_NH_4} = [NH_3] + [NH_4^+] \quad \textbf{(3. 12)}$$

The thermodynamic relations presented in equations (3.2)-(3.9) incorporate equilibrium constants of the different complexes. The values of the thermodynamic constant of the relevant complexes are given in Table 3.1. These thermodynamic equilibria further relate to solution pH through the concentration of H^+ and OH^- ions, provided that the ionization constant of water (K_w) is equal to 10^{-14} (equations 3.13 and 3.14).

$$[H^+] = \mathbf{10}^{-pH} \quad \textbf{(3. 13)}$$

$$K_w = [H^+][OH^-] \quad \textbf{(3. 14)}$$

Bulk fluid ionic strength *(I)* is employed to determine the activity coefficient *(γ_i)* of each component ion (Mg^{2+}, NH_4^+ and PO_4^{3-}). The solution ionic strength *(I)* can be calculated by the defined relations, based on each species of ionic concentration, C_i (Mg, NH_4 and PO_4) and its respective charge, Z_i (equation 3.16). The activity coefficient can be determined using a variety of empirical relations, including the DeBye-Hückel equation, DeBye-Hückel with Güntelberg approximation, Davies

equation and Bromley equation (Sohnel and Garside 1992; Mullin 1993). The mathematical form of the DeBye-Hückel equation is shown in equation (3.16), whereas the modified DeBye-Hückel equation and Davies equations are demonstrated in equations (3.17) and (3.18), respectively.

Table 3. 1 Values of equilibrium constants for complexes presented in equations 3.2 - 3.9 and 3.14

Equilibrium Constant	Values	References
K_{MgOH}	$10^{-2.56}$	(Childs 1970)
$K_{NH_4^+}$	$10^{-9.25}$	(Taylor *et al.* 1963)
$K_{HPO_4^{3-}}$	$10^{-12.35}$	(Morel and Hering 1993)
$K_{H_2PO_4^-}$	$10^{-7.20}$	(Morel and Hering 1993)
$K_{H_3PO_4}$	$10^{-2.15}$	(Martell and Smith 1989)
$K_{MgH_2PO_4^+}$	$10^{-0.45}$	(Martell and Smith 1989)
K_{MgHPO_4}	$10^{-2.91}$	(Martell and Smith 1989)
$K_{MgPO_4^-}$	$10^{-4.80}$	(Martell and Smith 1989)
K_w	10^{-14}	(Snoeyink and Jenkins 1980)

$$I = \frac{1}{2}\sum C_i Z_i^2 \qquad \textbf{(3. 15)}$$

$$-Log\gamma_i = AZ_i^2 I^{1/2} \qquad \textbf{(3. 16)}$$

$$-Log\gamma_i = AZ_i^2\left[\frac{I^{1/2}}{1+I^{1/2}}\right] \qquad \textbf{(3. 17)}$$

$$-Log\gamma_i = AZ_i^2\left[\frac{I^{1/2}}{1+I^{1/2}}\right] - 0.3I \qquad \textbf{(3. 18)}$$

Where

γ_i = Activity of solution

I = Ionic strength in molar

Z_i = Valency of the corresponding elements

A = DeBye-Hückel constant, has a value of 0.493, 0.499, 0.509 and 0.519 at 5, 15, 25 and 35°C, respectively (Mullin 1993).

For ionic strength as high as 6 molar, the solution activity coefficient can be determined using the Bromley equation (Sohnel and Garside 1992), as shown in equation (3.19). The constant B_1 in Bromley equation consists of the ionic contribution of the solution species, as shown in equation (3.20). For struvite solutions, the detailed ionic contribution is shown in Table 3.2.

$$\frac{1}{Z_i^{\,2}} Log\gamma_i = -0.511 \frac{\sqrt{I}}{1+\sqrt{I}} + \frac{(0.06 + 0.6 B_1) I}{\left(1 + 1.5 I / Z_i\right)^2} + \frac{B_1 I}{Z_i^{\,2}} \qquad \textbf{(3. 19)}$$

$$B_1 = B_+ + B_- + \delta_+ + \delta_- \qquad \textbf{(3. 20)}$$

Table 3. 2 Ionic contributions B_+, B_-, δ_+, δ_- for determination of constant B_1 according to equation (3.20) (Sohnel and Garside 1992)

The literature suggests that DeBye-Hückel equation is applicable for ionic strengths less than 5×10^{-3} molar (Snoeyink and Jenkins 1980; Mullin 1993). The modified form of the DeBye-Hückel equation with the Güntelberg approximation is applicable for sparingly soluble electrolytes, however no specific limit is documented (Mullin 1993). In general, this research incorporates the Davies equation to calculate the activity coefficient, since it is capable of performing activity calculations for higher ionic strengths, i.e. the maximum computable limit of *I* is 0.2 molar (Mullin 1993).

The ionization fractions of Mg^{2+}, NH_4^+ and PO_4^{3-} ($\alpha_{Mg^{2+}}, \alpha_{PO_4^{3-}}, \alpha_{NH_3}$) can be defined by the quotient of free ion concentration and the total concentration of each chemical component (equations 3.21- 3.23).

$$\alpha_{Mg^{2+}} = \frac{[Mg^{2+}]}{C_{T,Mg}} \quad \textbf{(3. 21)}$$

$$\alpha_{PO_4^{3-}} = \frac{[PO_4^{3-}]}{C_{T,PO_4}} \quad \textbf{(3. 22)}$$

$$\alpha_{NH_3} = \frac{[NH_4^+]}{C_{T,NH_3}} \quad \textbf{(3. 23)}$$

Two types of solubility products describe the solubility status, which include the Conditional Solubility Product (P_{cs}) and the Product of the Analytical Molar Concentration (P_{so}) (Snoeyink and Jenkins 1980). The conditional Solubility Product (P_{cs}) relates to the solution properties, including ionization fraction (α_i), activity coefficients (γ_i) and the minimum struvite solubility product (K_{so}) (Ohlinger 1999). The Product of the Analytical Molar Concentration relates to the total concentrations of

reactive constituents ($C_{T,i}$), where "i" represents the concentration of magnesium, ammonium, and phosphate, as required (Snoeyink and Jenkins 1980). The mathematical definition of the minimum solubility product of struvite is shown in equation (3.24).

$$K_{so} = C_{T,Mg^{2+}} \alpha_{Mg^{2+}} \gamma_{Mg^{2+}} . C_{T,PO_4^{3-}} \alpha_{PO_4^{3-}} \gamma_{PO_4^{3-}} . C_{T,NH_3} \alpha_{NH_4^{+}} \gamma_{NH_4^{+}} \quad \textbf{(3. 24)}$$

The mathematical formulation of the Conditional Solubility Product (P_{cs}) and the Product of the Analytical Molar Concentration (P_{so}) are demonstrated in equations (3.25) and (3.26), respectively. Solutions with a higher value of the Concentration Product than the Conditional Solubility Product ($P_{so} > P_{cs}$) refer to a supersaturated solution. Equal numerical values of P_{cs} and P_{so} characterize the saturated condition of solution, whereas $P_{so} < P_{cs}$ demonstrates the undersaturated condition of a solution (Snoeyink and Jenkins 1980). The negative logarithmic value of the minimum struvite solubility product value *(pK_{so})* applied in this thermodynamic modeling is 13.26 (Ohlinger 1999).

$$P_{cs} = \frac{K_{so}}{\alpha_{Mg^{2+}} \gamma_{Mg^{2+}} \alpha_{NH_4^{+}} \gamma_{NH_4^{+}} \alpha_{PO_4^{3-}} \gamma_{PO_4^{3-}}} \quad \textbf{(3. 25)}$$

$$P_{so} = C_{T,Mg} . C_{T,PO_4} . C_{T,NH_3} \quad \textbf{`(3. 26)}$$

The solution thermodynamic properties specify the state of saturation, free ion concentrations, molar concentration of ion complexes and the state of precipitation. The precipitation of struvite occurs in supersaturated solutions, which is particularly

influenced by the pH of the solution and the reactant concentration (Al-Khayat and Garside 1990; Mullin 1993).

The thermodynamic relations described above are appropriate for pure solutions containing only ammonium, magnesium and phosphate ions. This process is based on the magnesium ammonium phosphate precipitation using synthetic solution of magnesium chloride with ammonium dihydrogen phosphate at a sufficiently high pH value. The presence of base allows the solution to increase free ions of phosphate (equation 3.27), thereby increasing the solution supersaturation.

$$H_3PO_4 \Leftrightarrow H_2PO_4^- + H^+ \Leftrightarrow HPO_4^{2-} + 2H^+ \Leftrightarrow PO_4^{3-} + 3H^+ \qquad \textbf{(3. 27)}$$

For real effluent, the abovementioned thermodynamic equilibria should also include other chemical complexes, since real effluent contains various dissolved impurities (including the dissolved chemical species), which affect the fundamental solution chemistry of struvite and may retard or enhance the struvite crystallization rate. For example, the presence of Ca^{2+} ions prompts the formation of different complexes of Ca^{2+} such as $CaHPO_4$, $CaH_2PO_4^+$, $CaOH^+$, $CaPO_4^-$ (Parkhurst 1999), thus decreasing the free [PO_4^{3-}] ions and increasing the free [Mg^{2+}] ions.

3.3 Struvite Growth Kinetics

3.3.1 Definition of Supersaturation

The active mass of each reactant (free ion concentration) and the rate of chemical reaction for struvite precipitation are proportional to the degree of supersaturation

(Mullin 1993; Ohlinger 1999). The supersaturation of a crystallization system can be expressed in a number of ways. The simplest form of supersaturation is expressed in terms of the single component concentration of solution. In struvite systems, supersaturation is often calculated based on the phosphate concentration (Harrison 1999), as follows in equation (3.28). All the concentrations in equation (3.28) are expressed in mg/l. Given that, C_p is the total phosphate concentration and C^*_p is the equilibrium phosphate concentration.

$$S = C_p - C^*_p \qquad \textbf{(3. 28)}$$

Based on the single component concentration, supersaturation is often expressed in terms of the concentration driving force (ΔC), the supersaturation ratio (S') and the relative supersaturation (S_r) (Mullin 1993), as shown in equations (3.29) – (3.31). Given that, C is the total concentration of any solution species that takes part in crystal formation and C^* is the equilibrium concentration of that solution species.

$$\Delta C = C - C^* \qquad \textbf{(3. 29)}$$

$$S' = \frac{C}{C^*} \qquad \textbf{(3. 30)}$$

$$S_r = \frac{\Delta C}{C^*} = S' - \boldsymbol{1} \qquad \textbf{(3. 31)}$$

Of the above expressions for supersaturation (equations 3.29- 3.31), only equation (3.29) is dimensional, unless the solution concentration is expressed in molar or mg/l.

The expression of supersaturation in terms of the single component concentration (i.e., total PO_4) is suitable for the solution systems, which consists of a single reactant. For the multi-component system, single component supersaturation does not reflect the actual state of solubility, since the solubility status of solution depends on all the reactants. Hence, this research incorporated the actual solubility of solution relating to all the reactants present in the crystallization system as shown in the following paragraphs.

Often, the degree of supersaturation is expressed by the critical supersaturation ratio (S_c) relating to the Thermodynamic Conditional Solubility Product (P_{cs}) and the Concentration Product of the reactants (P_{so}), as shown in the equation (3.32) (Snoeyink and Jenkins 1980; Ohlinger 1999). Based on the chemical formation, the number of species in anhydrous struvite is $\nu = 3$.

$$S_c = \left(\frac{P_{so}}{P_{cs}} \right)^{1/\nu} \quad \textbf{(3. 32)}$$

$$S_c = \left(\frac{C_{T,Mg} C_{T,NH_3} C_{T,PO_4}}{\left(K_{so} / \gamma_{Mg^{2+}} \gamma_{NH_4^+} \gamma_{PO_4^{3-}} \alpha_{Mg^{2+}} \alpha_{NH_4^+} \alpha_{PO_4^{3-}} \right)} \right)^{1/3} \quad \textbf{(3. 33)}$$

$$S_c = \left(\frac{\left(\gamma_{Mg^{2+}} \alpha_{Mg^{2+}} C_{T,Mg} \right) \left(\gamma_{NH_4^+} \alpha_{NH_4^+} C_{T,NH_3} \right) \left(\gamma_{PO_4^{3-}} \alpha_{PO_4^{3-}} C_{TPO_4} \right)}{K_{so}} \right)^{1/3} \quad \textbf{(3. 34)}$$

$$S_c = \left(\frac{\left(\gamma_{Mg^{2+}} \left[Mg^{2+} \right] \right) \left(\gamma_{NH_4^+} \left[NH_4^+ \right] \right) \left(\gamma_{PO_4^{3-}} \left[PO_4^{3-} \right] \right)}{K_{so}} \right)^{1/3} \quad \textbf{(3. 35)}$$

$$S_c = \left(\frac{\{Mg^{2+}\}\{NH_4^{+}\}\{PO_4^{3-}\}}{K_{so}} \right)^{1/3} \quad \textbf{(3. 36)}$$

$$S_c = \left(\frac{IAP}{K_{so}} \right)^{1/3} \quad \textbf{(3. 37)}$$

Further simplification of equation (3.32) through equation (3.37) shows that the critical supersaturation ratio (S_c) can also be expressed in terms of the Ion Activity Product (IAP) and the minimum struvite Solubility Product (K_{so}), which is often used to calculate the solution supersaturation (Mullin 1993). However, for the kinetic investigation, this research employed oversaturation (S) to compute solution supersaturation (equation 3.38). It is worth while pointing out that the value of critical supersaturation (S_c) refers to equation (3.32) or equation (3.37), which give identical results. However, this research incorporated equation (3.32) to compute critical supersaturation ratio (S_c) and equation (3.38) to compute solution supersaturation (S) and to solve the kinetic model.

$$S = S_c - 1 \quad \textbf{(3. 38)}$$

Often supersaturation is expressed in terms of the Saturation Index (SI), as shown in equations 3.39 and 3.40 (Allison *et al.* 1991; Parkhurst 1999).

$$SI = Log(IAP) - LogK_{so} \quad \textbf{(3. 39)}$$

$$SI = Log\left(\frac{IAP}{K_{so}} \right) \quad \textbf{(3. 40)}$$

Where, IAP = Ion Activity Product of Magnesium, Ammonium and Phosphate

K_{so} = Minimum Solubility Product of struvite

However, equation (3.41) is identical to equation (3.39) in expressing the Saturation Index (SI), following the simplifying procedure of equation (3.32) through equation (3.37).

$$SI = Log(P_{so}) - Log(P_{cs}) \quad \textbf{(3. 41)}$$

$$SI = Log\left(\frac{P_{so}}{P_{cs}}\right) \quad \textbf{(3. 42)}$$

Where, P_{so} = Concentration Product of the total Magnesium, Ammonium and Phosphate

P_{cs} = Conditional Solubility Product of the solution

As described in the previous paragraph of this section, this research employed equation (3.32) and (3.38) to compute the solution supersaturation in the struvite kinetic modeling. This research also incorporates investigations of struvite kinetics based on the Saturation Index (SI) as shown in equation (3.41) to compare the kinetic trends based on SI and S. However, for the further investigation, this research will adhere to oversaturation (S) to compute solution supersaturation and the relevant struvite growth kinetics.

3.3.2 Growth Rate Expression

In general, the growth rate of crystal from aqueous solution depends on the supersaturation, temperature, fluid hydrodynamics (agitation and mixing), impurities concentration, size of crystal (for size dependant growth) and the past history of crystals including imperfections, cracks and size dispersions (White 1971). However,

supersaturation, temperature, fluid hydrodynamics have the most direct effect on the crystal growth (Sohnel and Garside 1992). It is also documented that the presence of seeds may have a direct effect on crystallization (Myerson 1993). Therefore, the linear growth rate of struvite is presented as a function of supersaturation (S), temperature (T), mixing intensity (N), and the mean size of crystals as seeds (L), as shown in equations (3.43) and (3.44). The constants *K* and *n* applied in the equation (3.43) are the struvite growth kinetic parameters, and depend on the experimental conditions as described in the equation 3.44.

A growth rate expression, incorporating supersaturation (S) and particles size (L), may also be considered (equation 3.45) in this research. The constant K_1 is the growth rate constant, *n* is the growth order due to supersaturation and n_1 is the growth order due to particle size (equation 3.45).

$$G = \frac{dL}{dt} = KS^{n} \qquad \textbf{(3. 43)}$$

$$n,\ K = f(T, L, N, \cdots) \qquad \textbf{(3. 44)}$$

$$G = \frac{dL}{dt} = K_1 S^{n} L^{n_1} \qquad \textbf{(3. 45)}$$

Ideally, crystal may grow in a well-mixed vessel in the presence of seeds of size L_0. The newly born clusters diffuse onto exposed seeds and increase the crystal size from L_0 to L. It is convenient to assume that both seeds and growing struvite crystals are spherical. Based on the preliminary assumption that crystals are spherical in shape, the volume and mass increase of a single particle is shown in equations (3.50) and (3.52), provided that the density of a struvite particle is ρ_c.

$$V = \frac{1}{6}\pi L^3 \quad \textbf{(3. 46)}$$

$$\therefore \frac{dV}{dt} = \frac{d}{dt}\left(\frac{1}{6}\pi L^3\right) \quad \textbf{(3. 47)}$$

$$\frac{dV}{dt} = \frac{dV}{dL} \cdot \frac{dL}{dt} \quad \textbf{(3. 48)}$$

$$\frac{dV}{dt} = \frac{1}{2}\pi L^2 \frac{dL}{dt} \quad \textbf{(3. 49)}$$

$$\frac{dV}{dt} = \frac{1}{2}\pi L^2 G \quad \textbf{(3. 50)}$$

$$\frac{dm}{dt} = \rho_c \frac{dV}{dt} = \rho_c \frac{\pi}{2} L^2 G \quad \textbf{(3. 51)}$$

$$\frac{dm}{dt} = \frac{1}{2}\pi \rho_c L^2 G \quad \textbf{(3. 52)}$$

Further substitution of the struvite growth rate expression (equation 3.45) in equation (3.52) offers a more practical expression of the single particle struvite mass deposition rate (equation 3.53).

$$\frac{dm}{dt} = \frac{1}{2} K\pi\rho_c L^2 S^n L^{n_1} \quad \textbf{(3. 53)}$$

The crystal population is characterized by assuming a point-sized distribution of crystal, considering a spherical shape. Hence, crystal number *(N)* is a function of the initial mass of seeds (m_0), density of struvite crystal (ρ_c) and initial size (volume equivalent diameter) of seeds, L_0 (equation 3.54).

$$N = \frac{m_0}{\frac{\pi}{6}\rho_c L_0^{\,3}} \qquad \textbf{(3. 54)}$$

Total mass deposition, dM/dt, can now be presented by equation (3.55), incorporating single particle mass deposition $\left(dm/dt\right)$ and the number of crystals in the crystal population. This research incorporates the volume equivalent analysis of mean particle size, since particle size analysis was conducted using the Malvern particle sizer, which measures a spherical equivalent diameter.

Therefore,

$$\frac{dM}{dt} = \frac{1}{2} KN\pi\rho_c L^2 S_c^{\,n} L^{n_1} \qquad \textbf{(3. 55)}$$

3.4 Process Modeling

The schematic of a continuous struvite crystallization process is shown in Figure 3.1. This system is a continuous flow system in terms of the liquid phase and discrete with respect to the solid phase, since it is assumed that all struvite crystals are retained within the reactor. The assumption of perfect mixing enables a simple set of ordinary differential equations to be used to model this system. A point-sized distribution is assumed for the crystal population, which, while incorrect, dramatically simplifies the modeling of the system. Furthermore, it is assumed that the number of crystals in the reactor is constant, after the system is seeded, since nucleation is assumed not to occur.

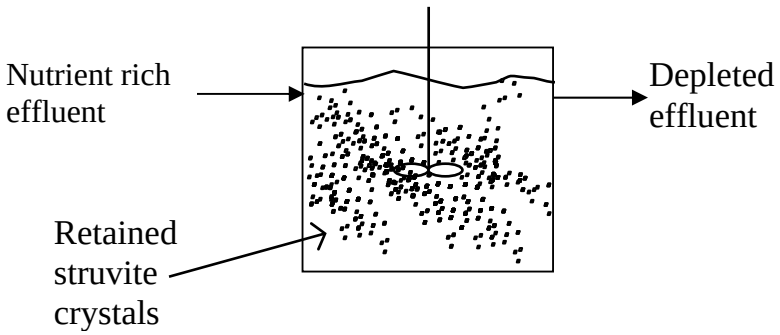

Figure 3. 1 Schematic of continuous-discrete struvite reaction system

Equation (3.56) describes the volume change of reactive solution in terms of inlet flow (F_{in}) of feed solution and outlet flow (F_{out}) of feed solution.

$$\frac{dV}{dt} = F_{in} - F_{out} \qquad \textbf{(3. 56)}$$

The solution mass balance of $Mg^{2+}/NH_4^{+}/PO_4^{3-}$ after reaction takes place $\left(\frac{dC_i'}{dt}\right)$ depends on the inlet and outlet flow rates (F_{in}, F_{out}), inlet and outlet concentrations ($C_{i,in}$, $C_{i,out}$), and crystallization rate of struvite $\left(dM/dt\right)$. Equation (3.57) describes the change of reactive solute mass in the continuous system.

$$\frac{dC_i'}{dt} = F_{in}C_{i,in} - F_{out}C_{i,out} - \frac{dM}{dt}\left(\frac{MW_{c_i}}{MW_s}\right) \qquad \textbf{(3. 57)}$$

Where

$\frac{dC_i'}{dt}$ = Total change of individual solution species in mg/h (Mg^{2+}, NH_4^{+} and PO_4^{3-})

F_{in}, F_{out} = Inlet and outlet flow rate (l/h)

$C_{i,in}$, $C_{i,out}$ = Inlet and outlet solution concentration of specific species (mg/l)

$\frac{dM}{dt}$ = Mass deposition of struvite crystal (mg/h)

MW_s = Molecular weight of struvite

MW_{c_i} = Molecular weight of individual solution species (Mg^{2+}, $NH_4^+$and PO_4^{3-})

In a fed-batch process of constant supersaturation, the rate of crystallization is equal to the rate of feed addition. The discrete nature of the fed-batch system retains solution in the reactor, since the outlet flow *(F_{out})* is set to zero.

$$\frac{dC_i'}{dt} = F_{in}C_{i,in_i} - \frac{dM}{dt}\left(\frac{MW_{c_i}}{MW_s}\right) \quad \textbf{(3. 58)}$$

$$-\frac{dC_i'}{dt} = \frac{dM}{dt}\left(\frac{MW_{c_i}}{MW_s}\right) \quad \textbf{(3. 59)}$$

$$\frac{dC}{dt} = \frac{dC'/dt}{V(t)} \quad \textbf{(3. 60)}$$

Therefore, the mass balance of reactive solution in a fed-batch (semi-continuous) system can be presented by equation (3.58). In a batch system (with no inlet or outlet stream, *i.e.* $F_{in} = 0$; $F_{out} = 0$) the mass balance can be described by equation (3.59). The deposited mass is simply equivalent to the concentration decay in the solution. The change of constituent's concentration $\left(\frac{dC}{dt}\right)$ can be calculated using equation (3.60).

This research incorporates a fed-batch process model (equations 3.58 and 3.60), operating at constant supersaturation. This process is based on feed solutions of $NH_4H_2PO_4$ and $MgCl_2$ as the source of NH_4^+, PO_4^{3-} and Mg^{2+}. For the selected reagents ($NH_4H_2PO_4$ and $MgCl_2$), each mole formation of struvite liberates 2 moles of H^+, leading to a drop in the solution pH due to the reaction (equation 3.61).

$$NH_4H_2PO_4 + Mg^{2+} \rightarrow MgNH_4PO_4 + 2H^+ \quad \textbf{(3. 61)}$$

The amount of liberated hydrogen ions (H^+) and the change of pH for an equivalent deposited struvite mass (M_{MAP}) can be predicted for a known volume of reactor (V) and the molecular weight of struvite crystal (MW_{MAP}). For a specified duration of fed-batch reactor operation, the required volume of NaOH (V_{NaOH}) of known concentration (C_{NaOH}) can be quantified by simple stoichiometric relations (equations 3.62-3.64). It is worthwhile noting that the H^+ and NaOH concentrations (equations 3.62-3.64) are measured in moles/L, mass of struvite (M_{MAP}) is measured in grams, molecular weight of struvite (MW_{MAP}) is measured in gram molecular weight and the volume of reactive solution (V) is measured in liter. In terms of the described units of process parameters in equation 3.62, the concentration of hydrogen ion (H^+) is measured in moles/L.

$$\frac{dH^+}{dt} = 2 \times \frac{d}{dt} \frac{(M_{MAP})}{MW_{MAP}.V} \quad \textbf{(3. 62)}$$

$$pH_1 = -Log_{10} H^+ \quad \textbf{(3. 63)}$$

$$V_{NaOH}.C_{NaOH} = V.H^+ \quad \textbf{(3. 64)}$$

Coding of this series of algebraic, differential equations describing the thermodynamic, kinetic and process models was carried out using gPROMS process simulation software.

3.5 Chapter Summary

This chapter presented the derivation of a struvite growth model, incorporating the thermodynamics of solution, kinetics of struvite growth and the modeling of the fed-batch process of controlled struvite crystallization. Detailed solution chemistry and possible thermodynamic complexes of struvite constituents are included in the thermodynamic modeling to describe the state of solution saturation.

A growth rate expression, incorporating the supersaturation and mean particle size along with the mass deposition of struvite is presented to describe struvite growth kinetics. A point size distribution is assumed for the crystal population. A mathematical description of the controlled fed-batch process of struvite crystallization is also included in this modeling to solve the struvite growth kinetics.

Coding of equations was conducted in gPROMS (process simulation software and equation solver). Detailed simulation response, including solution chemistry and kinetic, will be described in Chapter 6, “Results and Discussion from Simulation.”

CHAPTER 4

EXPERIMENTAL SETUP

4.1 Introduction

Experiments were conducted in pilot-scale and operated in a constant supersaturation mode. Scale-up of the reactor in pilot scale and development of fed-batch crystallization experiments led to some preliminary outcomes prior to the main set of experiments. The preliminary outcomes are given below.

(1) Development of a strategy to maintain correct stoichiometry of the feed solutions.

(2) Design of an automatic system to maintain constant experimental temperature.

(3) Identification of suitable seeds to maximize crystallization rates and to provide efficient media for diffusion during crystallization.

(4) Determination of a suitable drying process for struvite.

(5) Calibration of electronic equipment such as the dosing pumps and pH controller.

4.2 Determination of the Operating Zone of Struvite Crystallization

A series of batch experiments were conducted using synthetic solutions of 0.003, 0.004, 0.005 and 0.007-M (equimolar) of magnesium, ammonium and phosphate. Sigma Aldrich analytical grade $MgCl_2$ and $NH_4H_2PO_4$ were used to make up these solutions. A series of batch scale experiments were conducted using one liter volume of solutions

in the absence of seeds. A helium neon laser light, passing through the reactive solution, gave an indication of the onset of nucleation in the reactive solution. The reactive solution was agitated using a mechanical impeller of 2.5 inches diameter rotating at 35 rpm. In each batch, the solution pH was slowly adjusted using 0.25M of NaOH solution at the initial stage until the solution supersaturation approached close to saturation limit. The solution saturation limit was preliminary investigated by thermodynamic modeling. After initial adjustment of pH value, NaOH solution of 0.1M was used for further pH adjustment until the appearance of first nuclei. In every circumstance, 15 minutes intervals were given after each drop of NaOH addition. Every batch experiment was conducted in a dark room for clear visualization of nuclei in the laser light.

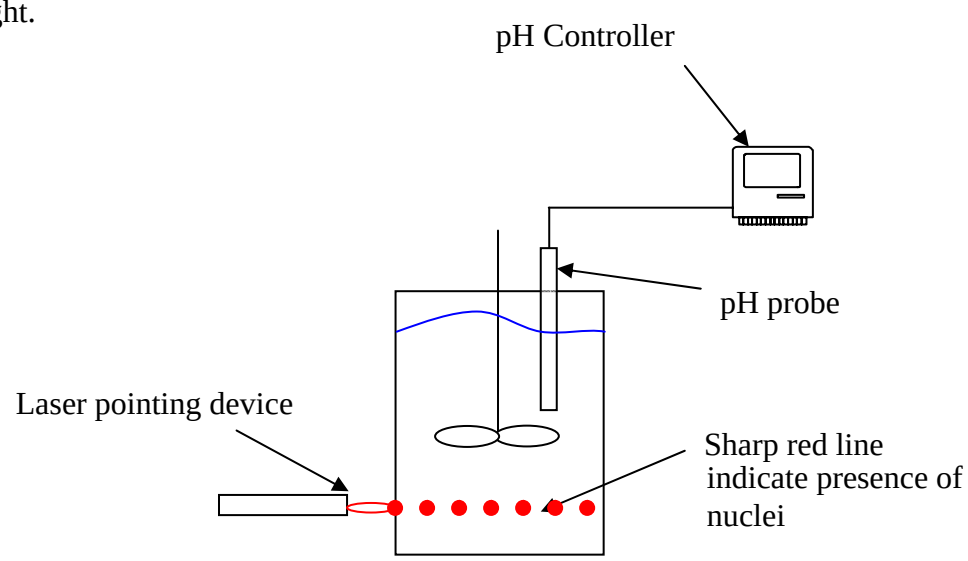

Figure 4. 1 Schematic of experimental set-up to determine operating zone of struvite crystallization

4.3 Selection of Seed Materials

Experiments were conducted using different seed materials, which included quartz sand, borosilicate glass grindings and struvite. Graded quartz sand was crushed and sieved using 45-63-µm ASTM standard sieves, followed by 24 hours of oven drying at

105°C. Broken laboratory glassware was used as the raw materials of borosilicate glass seeds. Treatment by acid washing, followed by normal washing and drying was employed for these raw materials and thereafter crushing and sieving was employed to make a final seed size of 45-63 μm. Previously generated struvite crystals of size 45-63 μm were used as struvite seeds.

Each solution was seeded with 1 g of the respective seed material. Each experiment was carried out at the uniform agitation of 35rpm impeller speed, along with slow addition of NaOH solution to make the solution supersaturated. NaOH of 0.25 M was used at the initial stage of experiment start-up, whereas NaOH of 0.1 M was used when solution pH approached to the expected point of supersaturation. All experiments were conducted within the determined metastable zone, just above solution saturation. A data logger recorded trends of pH change for the 24 hours duration of the experiment.

4.4 Moisture Analysis

The moisture analysis of struvite was conducted to identify the effect of drying temperature on the struvite morphology and the amount of crystalline water. This experiment was conducted using a moisture analyzer (Sartorius MA-45) with operating temperature of 40, 50, 60 and 100°C for 90 minutes duration. The tolerance limit of the moisture analysis using the Sartorius MA 45 is ±1mg. Each experiment was conducted using 8g of previously generated struvite of size 150-250 μm. Struvite crystal employed in this experiment was graded using wet sieving and followed by 12 hours of fan drying, 1 hour sun drying and 7 days air drying.

4.5 Design of the Fed-batch Pilot Scale Reactor

A schematic diagram of the struvite fed-batch system is shown in Figure 4.2. Unfortunately no standard design approach exists for struvite crystallization. However, some common techniques such as suspension bed, seedings, feed addition are widely used (Bouropoulos and Koutsoukos 2000; van der Houwen and Valsami-Jones 2001; Kofina and Koutsoukos 2003; Adnan *et al.* 2004; Kofina and Koutsoukos 2005).

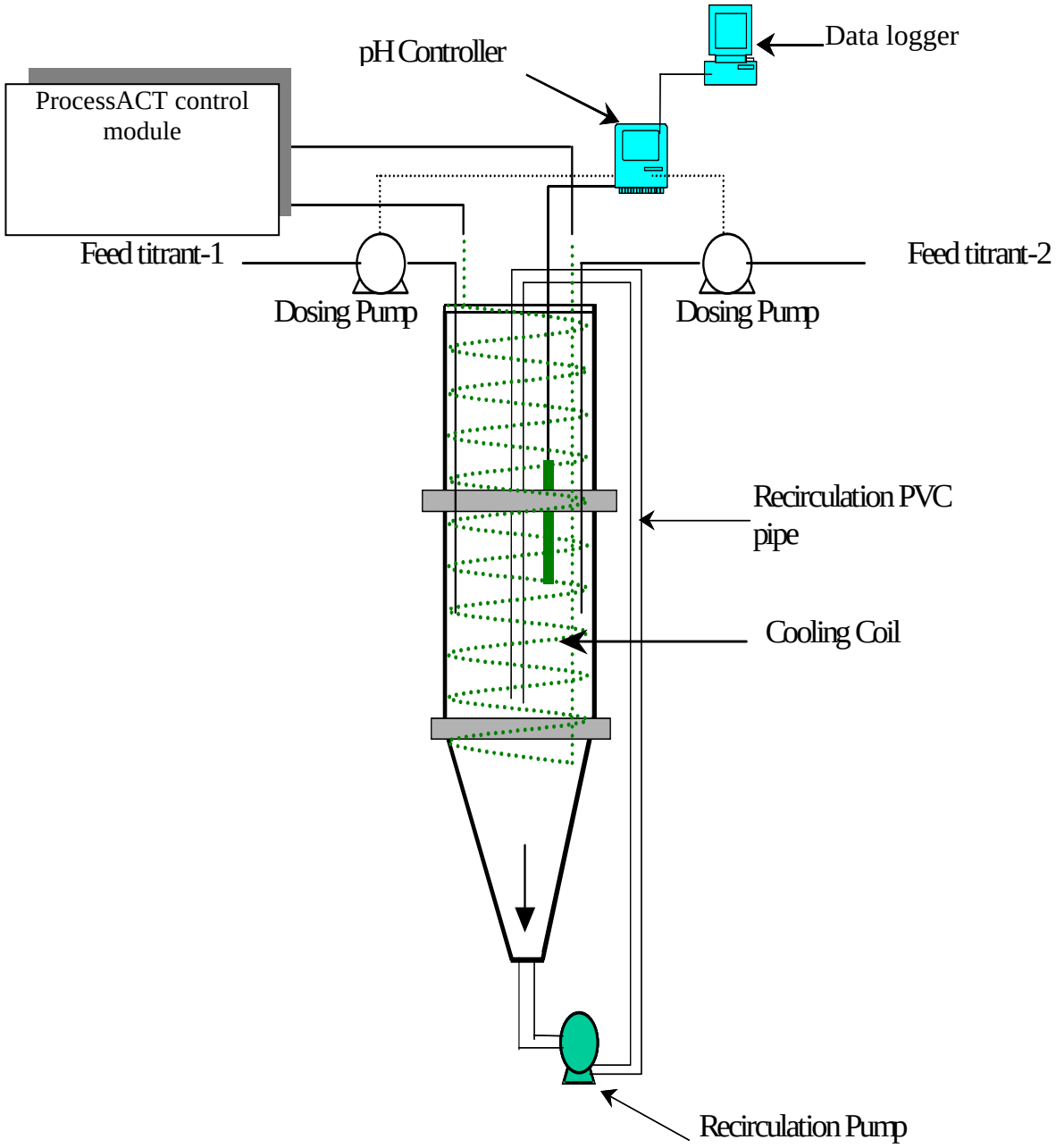

Figure 4. 2 Schematic of controlled struvite crystallization

A struvite reactor of 44-litre volume, made of clear perspex, was used in this study (Figure 4.3). The reactor was operated as a suspended bed, allowing seeds and crystals to keep in uniform and full suspension. A pH controller (αlpha 2000W) controlled the pH set point and triggered feed addition when solution pH dropped below the set point. Two dosing pumps (Grundfos DME-12) were operated for titrant (feed solution) additions based on the output signal sent from the pH controller. The pH controller was operated in pulse frequency control mode together with a proportional integral control strategy.

Mixing of the reactive solution was carried out by a centrifugal pump (Onga; model 413) together with a solution recirculation loop, composed of PVC pipe of 1-inch diameter. The capacity of the pump (model 400 series) against different pump heads is demonstrated in Figure A.2 (Appendix-A). A variable transformer (variac) controlled flow rate of the pump. The reactor was seeded with 30 g of previously generated struvite crystal of size range 63-125 μm. Samples of crystal suspension were collected at the pump outlet (Figure 4.4) and filtered using 0.45 μm filter paper. The top portion of the PVC pipe was connected with an adjustable and flexible recirculation system to avoid short-circuiting of recirculated streams (Figure 4.5).

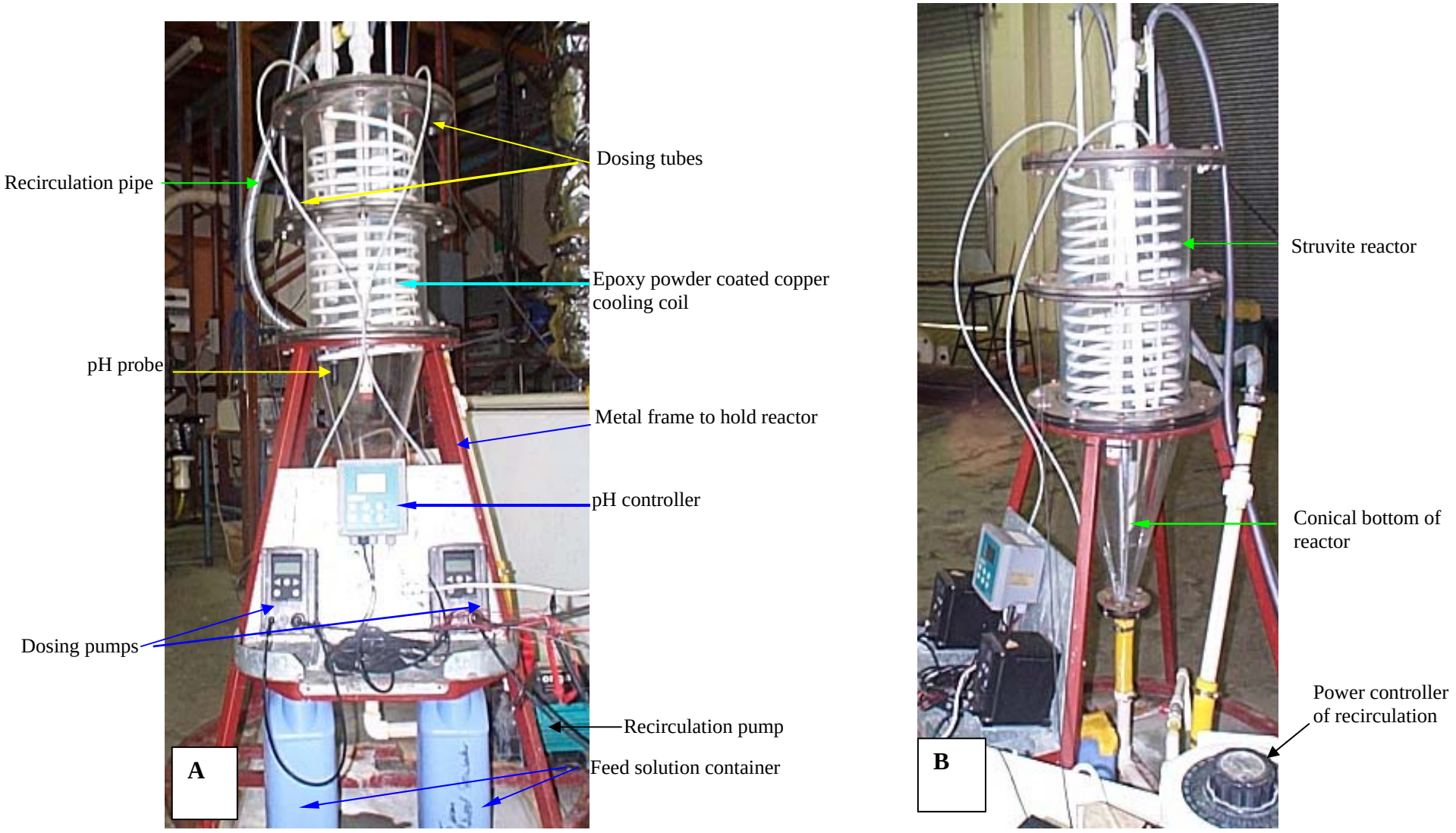

Figure 4. 3 (A) Front view of struvite reactor, (B) Side view of struvite reactor

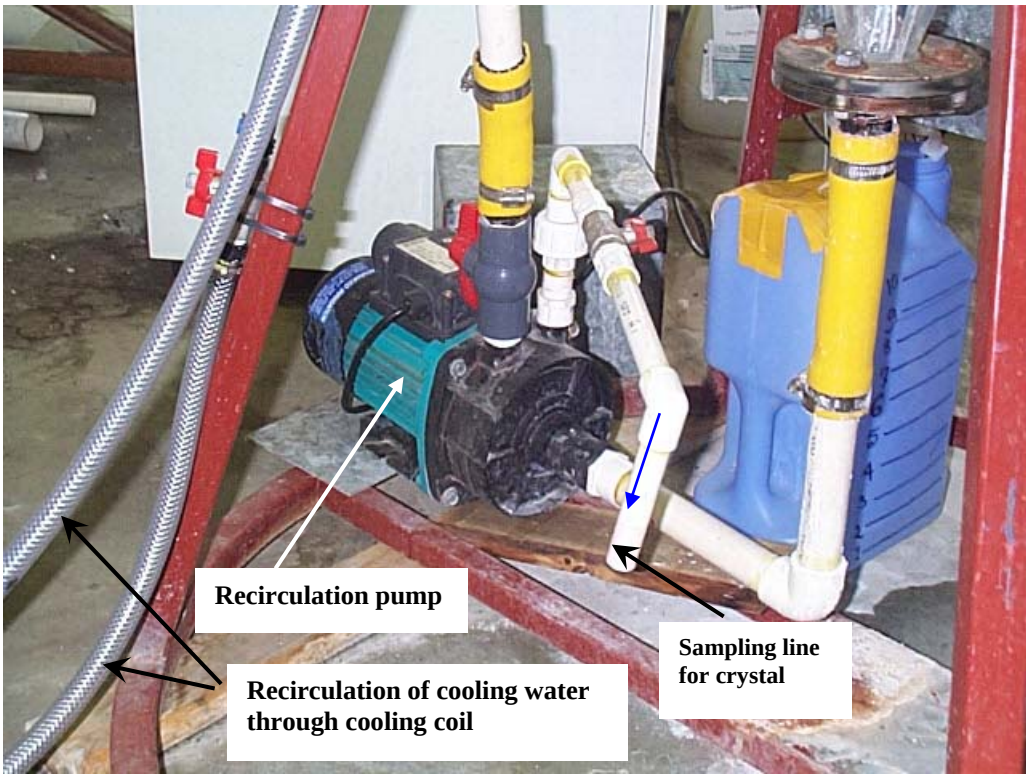

Figure 4. 4 Sampling of struvite crystal through recirculation pump

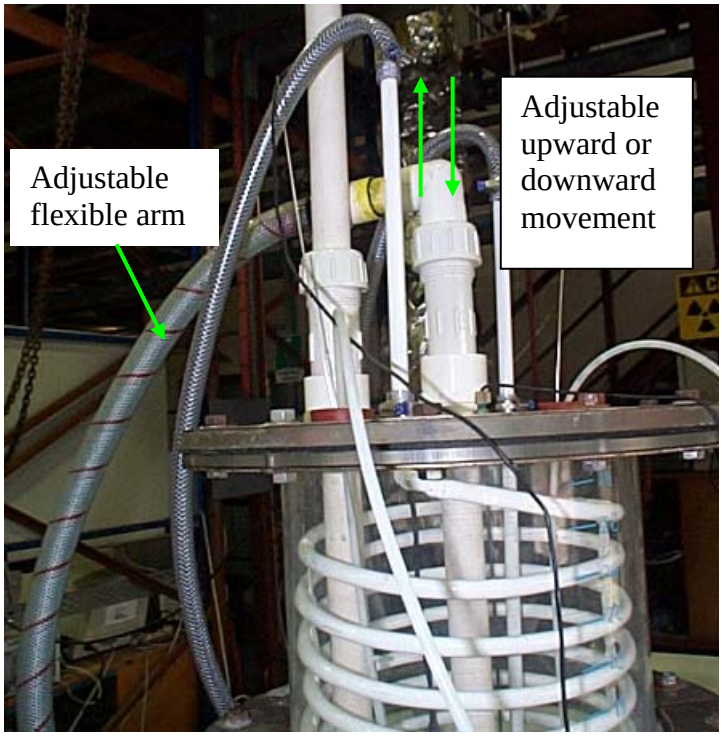

Figure 4. 5 Photographic presentation of adjustable recirculation arm of reactor

Continuous operation of the recirculation pump led to temperature rise in the reactor. Significant increases of solution temperature caused offset (drift) in the pH value. Therefore, it was necessary to maintain constant operating temperature, enabling effective supersaturation control. The automatic temperature control system is pictured in Figure 4.6. In Figure 4.6, *P* represents the recirculation pump, B_1 represents the normally open solenoid valve, B_2 represents the normally closed solenoid valve and *A* represents the control module. Constant operating temperature was maintained by an automatic temperature control system, encompassing a plastic-coated copper-cooling coil (C), resistive temperature device (RTD) and solenoid valve. Using a plastic coated cooling coil was required to avoid corrosion of exposed copper. A detailed description of automatic temperature controller is provided in Appendix-A.

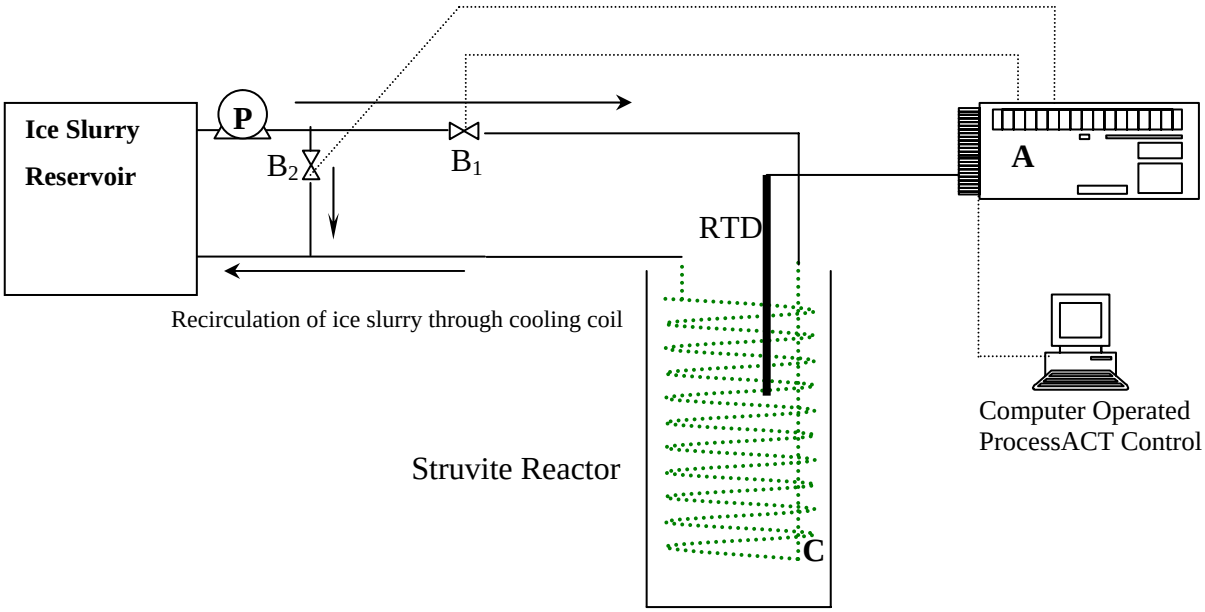

Figure 4. 6 Schematic of automatic temperature control system

It was observed in struvite crystallization that application of sensor based control was problematic due to the location of the insertion point of the pH probe, loss of sensitivity of the sensor, loss of sensitivity of the controlling unit including pH controller and

dosing pump and dosing point. Failure of the abovementioned control elements degrades systems performance.

4.6 Design of Experiment

The fed-batch system was maintained using two feed solutions, i.e., titrant-1 (NaCl+ $NH_4H_2PO_4$) and titrant-2 (NaOH + $MgCl_2$). The main purpose of NaCl addition in titrant-1 is to maintain a constant level and moderately high ionic strength. The pH value of titrant-1 was adjusted to 6.0; more precisely, the relative difference of pH between titrant-1 and reactive solution of 1.0- 1.25 unit provided better control. A set of fed-batch experiments was conducted in pilot scale control supersaturation mode. The key experimental data required for simulation are the mean particles size of growing struvite and seeds, reactant concentration and pH value, flow rate of feed solution, and concentration of feed solutions.

4.6.1 Chemical and Physical Analyses

High-resolution images of growing crystals were taken using a Scanning Electron Microscope (model JOEL JSM-5410LV), which had a magnifying range of 35 to 200,000. Analysis of crystal was also done by a powder X-ray diffraction technique, using Siemens D5000 front-loading X-ray Diffractometer. Phosphate and Magnesium were analyzed using Inductively Coupled Plasma Optical Emission Spectrophotometer (model Varian Type Liberty Series II).

4.6.2 Sample Preservation and Storage

For chemical analysis of magnesium, ammonium and phosphate, it is important to keep solutions frozen for long term preservation (Hurd and Spencer 1991; Horowitz *et al.* 1992; van Loon 2000). For the purpose of chemical analysis, double separation of crystal and solution was done using Millex-HA filters of 0.45 μm. Sampling of struvite crystal was done using 0.45 μm Whatman paper filters. Crystal sampling was conducted using 200 ml of well-mixed reactive solution, collected from the recirculation pump outlet. Samples for analytical measurement of phosphorus (phosphate) were preserved in a plastic bottle to prevent any interference of adsorbed phosphate into the glassware (Fresenius *et al.* 1987; van Loon 2000). Moreover, preserved solution pH was set to about 5.0 to prevent any unexpected crystal formation at the time of sample preservation. Rigorous cleaning of laboratory glassware was conducted using dilute HCl (10%) by soaking overnight and rinsing with distilled water (Hanrahan *et al.* 2003). Detergent use was avoided for the cleaning of experimental apparatus, since it may lead to unwanted addition of phosphate into the solution (Rand *et al.* 1975).

4.7 Chapter Summary

This chapter covers the detailed experimental plan including the design of pilot scale struvite reactor operated at constant supersaturation. The design of controlled crystallization scheme of struvite also includes some preliminary outcomes, such as determination of operating zone of struvite crystallization, suitable seeds, suitable drying temperature of struvite, design of temperature controller. The experimental

outcome of this research will be discussed in the chapter entitled “Results and Discussion from Experiments (Chapter 5)”.

CHAPTER 5

RESULTS AND DISCUSSION FROM EXPERIMENT

5.1 Introduction

This chapter presents the results of the design and commissioning of a controlled struvite crystallization system, which incorporates an investigation of the operating zone of struvite crystallization, determination of effective seed materials, drying technique of struvite, identification of feed composition and control of the experimental temperature. Based on the preliminary outcomes of Sections 5.2- 5.6, a set of fed-batch controlled experiments were conducted. The preliminary outcomes supported the development of controlled struvite crystallization. The experimental results of the fed-batch pilot scale struvite crystallization are presented in the Section 5.8.1 and 5.8.2. The summary of this chapter is presented in Section 5.11.

5.2 Identification of the Metastable Supersaturation Zone

This is a preliminary investigation to identify the optimal operating supersaturation to be maintained in fed-batch controlled crystallization experiments. Based on the experimental investigations described in Section 4.2 of Chapter 4, this section demonstrates a typical diagram of metastable zone for struvite crystallization. The metastable zone represents a potential zone of optimal supersaturation at which nucleation may have a limiting effect. In this circumstance, crystallization process may be encouraged to avoid spontaneous precipitation.

The experimental outcome of pH for spontaneous precipitation (identified by laser light scattering) was plotted along with the model predicted pH for minimum struvite solubility to identify the metastable zone of struvite crystallization. Thermodynamic equilibria of struvite chemistry were simulated and the simulated response was verified with thermodynamic modeling using the PHREEQC* solution thermodynamics-modeling package (Parkhurst 1999) and the derived data of the Ohlinger's (1999) solubility limit curve. The graphical presentation of the investigated pH for struvite precipitation is shown in Figure 5.1.

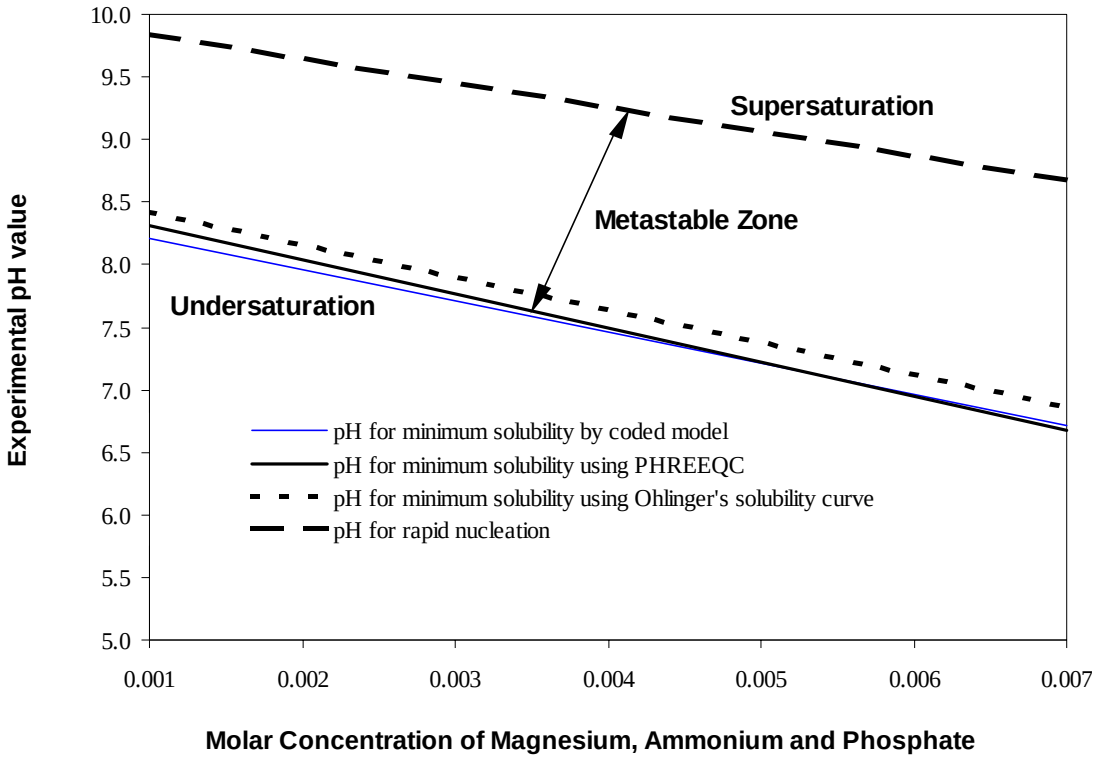

Figure 5. 1 Identification of the metastable zone for struvite crystallization

The range of maximum and minimum pH limit is known as the operating pH range of struvite crystallization. The operating zone of crystallization is known as the metastable zone of crystallization. Crystallization, operating close to saturation within the

* U.S. Geological Survey, Hydrologic Analysis Software Support Program, 437 National center, Reston VA 20192, email: h2osoft@usgs.gov

metastable zone, may encourage crystal growth by limiting nucleation (Pareena and Flood 2005). Crystal growth in this circumstance is governed by surface diffusion (layering) of clusters onto seed particles (Henning 1990; Kim and Mersmann 2001; Mersmann 2001).

5.3 Effect of Seed Type on Struvite Crystallization

This is a preliminary experimental outcome to identify the suitable type of seed to be used in controlled fed-batch (semi-continuous) experiments. Based on the experimental investigation in Section 4.3, this section shows the typical characteristics of struvite growth using different types of seeds. The kinetic investigation relates to the reaction rate of struvite crystallization, crystal size distribution of struvite, induction times, electron micrographs of growing struvite crystals. Based on the experimental outcome this section discusses the characteristics of struvite growth using quartz sand, borosilicate glass grinding and struvite as seed materials.

The trend of pH change during the preliminary stage of crystallization is shown in Figures 5.2-5.4. The release of H^+ in the supersaturated struvite system is an indirect expression of the chemical reaction rate. On the basis of equation (5.1), each mole of pH drop in the supersaturated struvite system represents the release of 2 moles of H^+ and the resulting formation of 1 mole of struvite (Bouropoulos and Koutsoukos 2000). Therefore, the rate of pH reduction is an alternative expression of struvite formation rate, as shown in Figures 5.2-5.4.

$$Mg^{2+} + NH_4H_2PO_4 + \mathbf{6}H_2O \Leftrightarrow MgNH_4PO_4.\mathbf{6}H_2O + \mathbf{2}H^+ \qquad \textbf{(5. 1)}$$

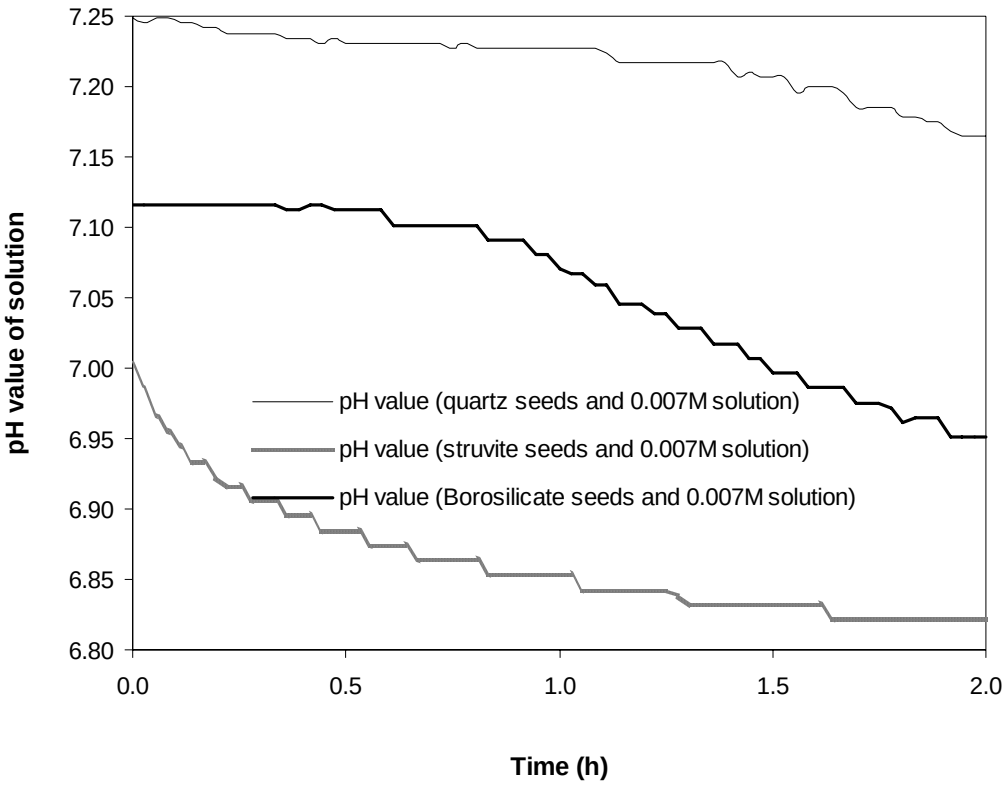

Figure 5. 2 Reaction kinetics during experiment using 0.007 M solution

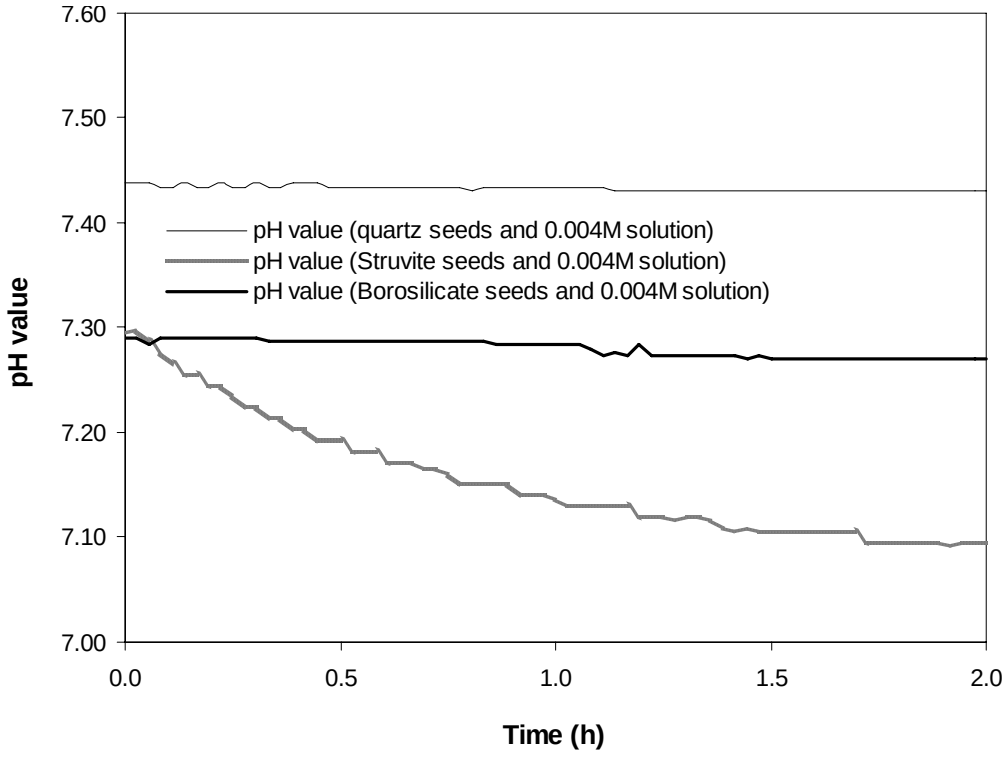

Figure 5. 3 Reaction kinetics during experiment using 0.004 M solution

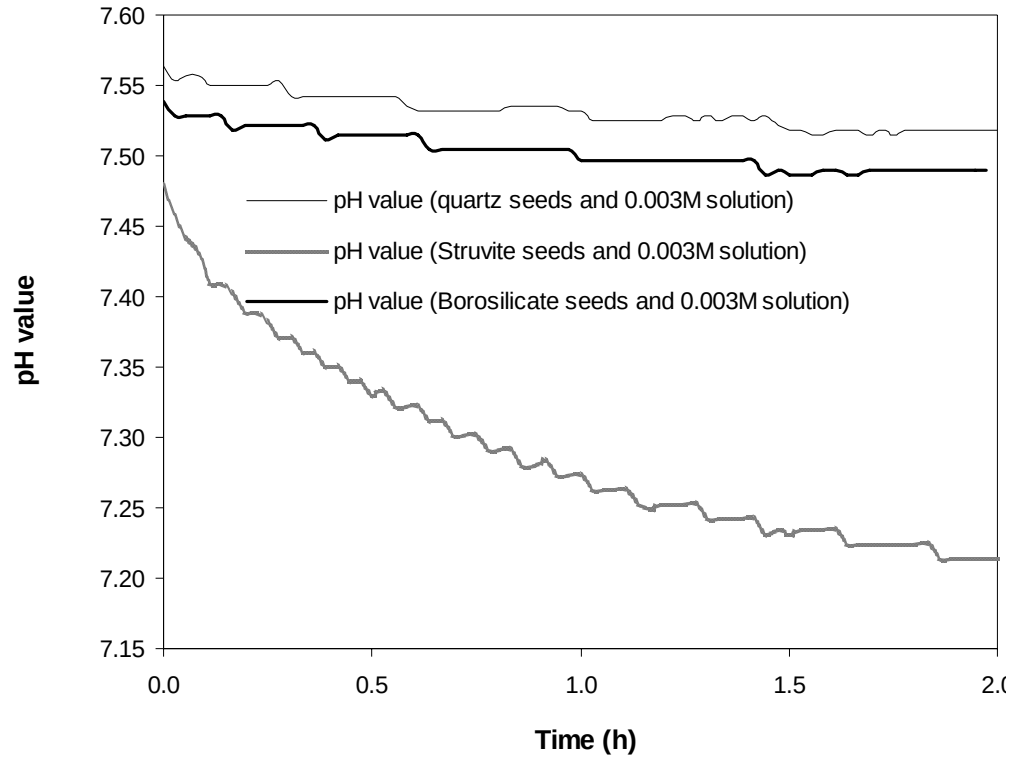

Figure 5. 4 Reaction kinetics during experiment using 0.003 M solution

During struvite crystallization, slower reaction rates were observed for quartz sand and borosilicate seeds, whereas higher reaction rates were observed for struvite seeds (Figure 5.2-5.4). Struvite seeds intensified the reaction rate of crystallization due to the similarity of the lattice structure of seeds and newly born clusters in the supersaturated system (Mullin 1993; Mersmann 2001). Crystallization in the stable-metastable region (close to saturation) induced thermodynamically unstable clusters due to very high-energy consumption from the solution of very low thermodynamic driving force. Proper seedings have the potential of lowering the activation energy for nucleation. Non-isomorphous seeds (borosilicate seeds and quartz sand seeds) change the type of nucleation required for crystal growth from homogeneous primary nucleation to heterogeneous primary nucleation. Heterogeneous nucleation lowers the activation energy required for nucleation, however, nucleation is still required if isomorphous seeds are not provided (Mullin 1993). Struvite seeds add surface area for integration of

molecules (magnesium, ammonium, phosphate and hydrates) and struvite clusters, and therefore, crystallization occurs without the need of nucleation (Mersmann 2001).

The de-supersaturation curves, represented in Figures 5.2-5.4, illustrate a simultaneous nucleation and growth of struvite. The horizontal portions of each curve (Figures 5.2-5.4) express a slow nucleation lag along with simultaneous diffusion of clusters, and afterwards a slow pulse of de-supersaturation. No nucleation lag time was observed for struvite seeds, since the available surface area for crystal growth is already provided. The other types of seeds (borosilicate and quartz sand) required nucleation, and hence there was a lag time during crystallization.

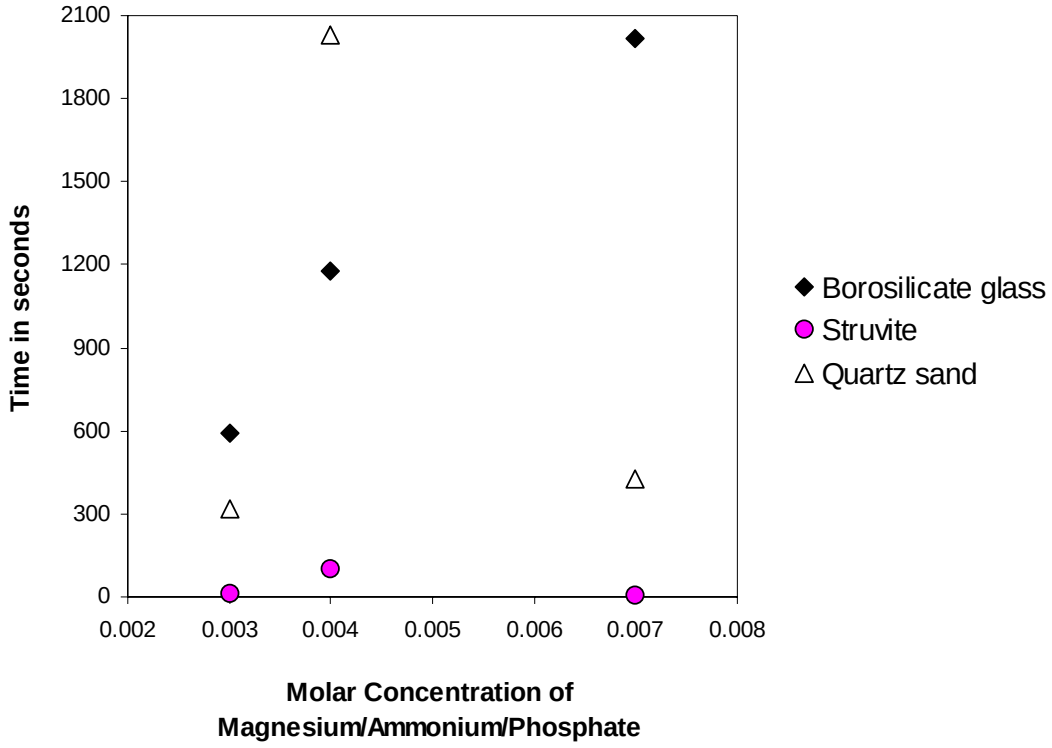

Figure 5. 5 Induction time in struvite system using different seed

Non-isomorphous seeds acted as a diffusive body but did not take part in the integration step and therefore unstable clusters re-dissolved (Mersmann 2001), leading

to longer or even infinite induction time (Figure 5.5). However, isomorphous seeds (struvite) provided the available surface area for clusters and solute molecules (magnesium, ammonium, phosphate and hydrate ions) diffusion. The diffused unit (clusters and solute molecules) were integrated into the boundary layer of seeds and solution. Therefore, the presence of available surface area for struvite growth (struvite seeds) intensified the rate of crystallization and reduced and/or eliminated the induction time.

Figures 5.6-5.9 describe the SEM (Scanning Electron Microscopic) view of struvite growth, using different types of seed. When quartz seeds and borosilicate glass seeds were used, there is no noticeable growth (Figures 5.6-5.8), however some struvite crystals formed, due to the nucleation and subsequent growth of stable nuclei. The SEM view in Figure 5.9 demonstrates the similarity of typical orthorhombic shape of struvite seeds and growing struvite crystals. Noticeable increase of size of struvite seeds was observed after crystallization.

The similarity of the lattice structure between struvite seeds and newly born struvite nuclei enhance the diffusion integration process (Eberl *et al.* 1998; Bergfors 2003). However, the diffusion integration process for other types of seeds is less likely due to redissolving of unstable nuclei as explained by the Gibbs Thompson effect of energy transformation during crystallization (Mullin 1993). It is worthwhile noting that the experiment was conducted very close to the saturation region as investigated previously by thermodynamic modeling.

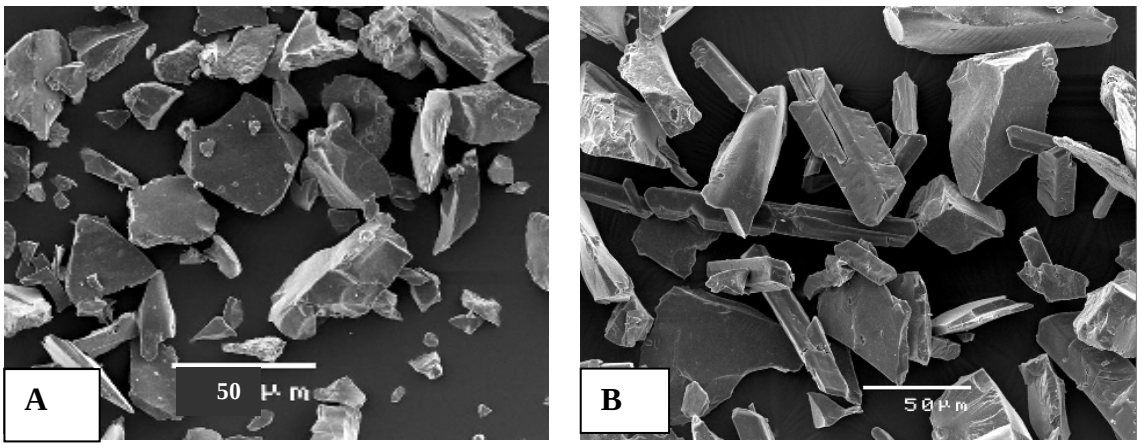

Figure 5. 6 Scanning electron microscopic view of quartz sand seeds (A), Growing struvite with quartz sand seeds (B)

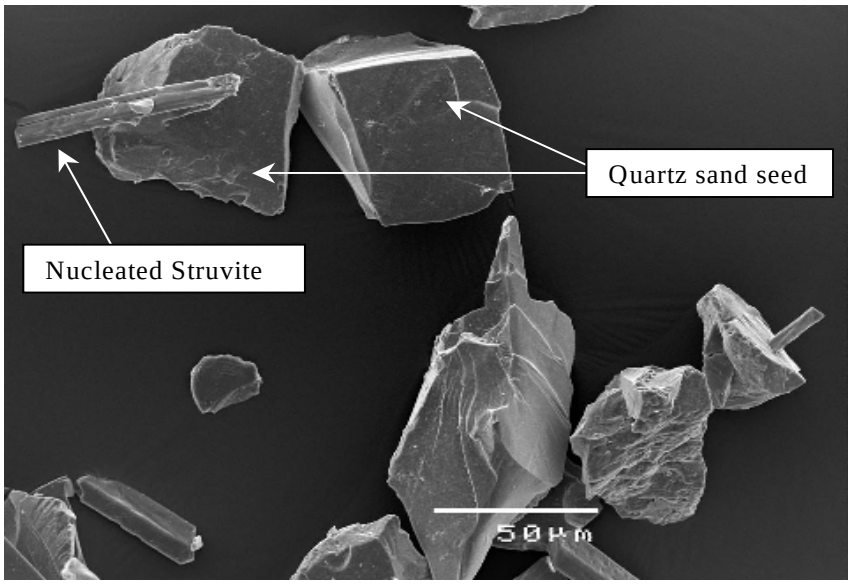

Figure 5. 7 Magnified scanning electronic microscopic view of growing struvite and quartz sand seeds

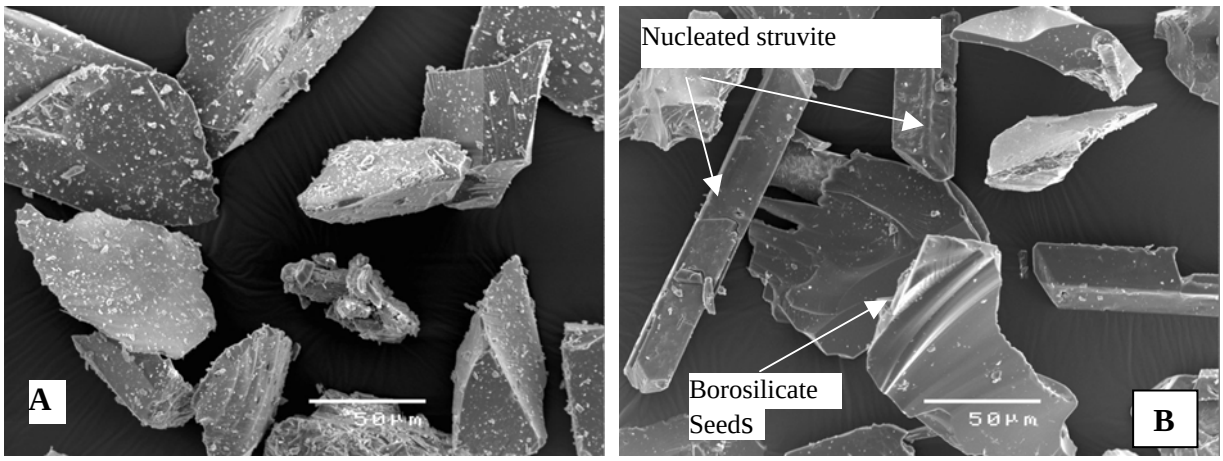

Figure 5. 8 Scanning Electron Microscopic view of borosilicate seeds (A), Growing struvite along with borosilicate seeds (B)

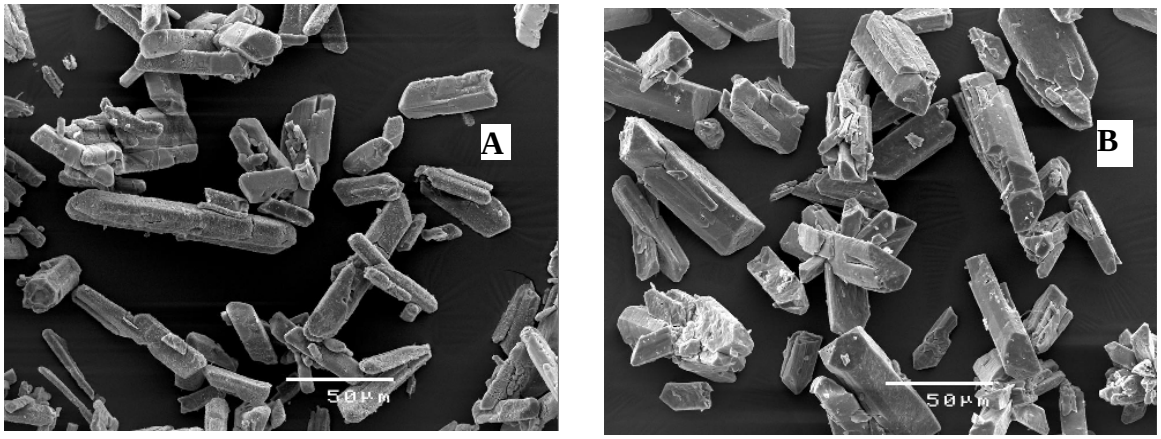

Figure 5. 9 Scanning Electronic Microscopic View of struvite seed (A), Growing struvite along with struvite seeds (B)

Analysis of the crystal CSD, using the Malvern particle-sizer, indicates a size-independent growth for struvite, since the CSD curve shifted almost identically to the right (Figure 5.10). Borosilicate glass seed and quartz sand seeds experienced less effective growth, since area under the CSD curve of seeds and growing struvite remained almost unchanged. The combined effect of nucleation and agglomeration of fines along with the breakage of seeds also influence the CSD curves of Figures 5.10.

Finally, the results of the batch crystallization using different types of seeds are summarized in Table 5.1. The results show higher growth of struvite when previously generated struvite crystals were used as seeds. Hence, this research incorporated struvite crystals as seed for further experimental development in fed-batch control.

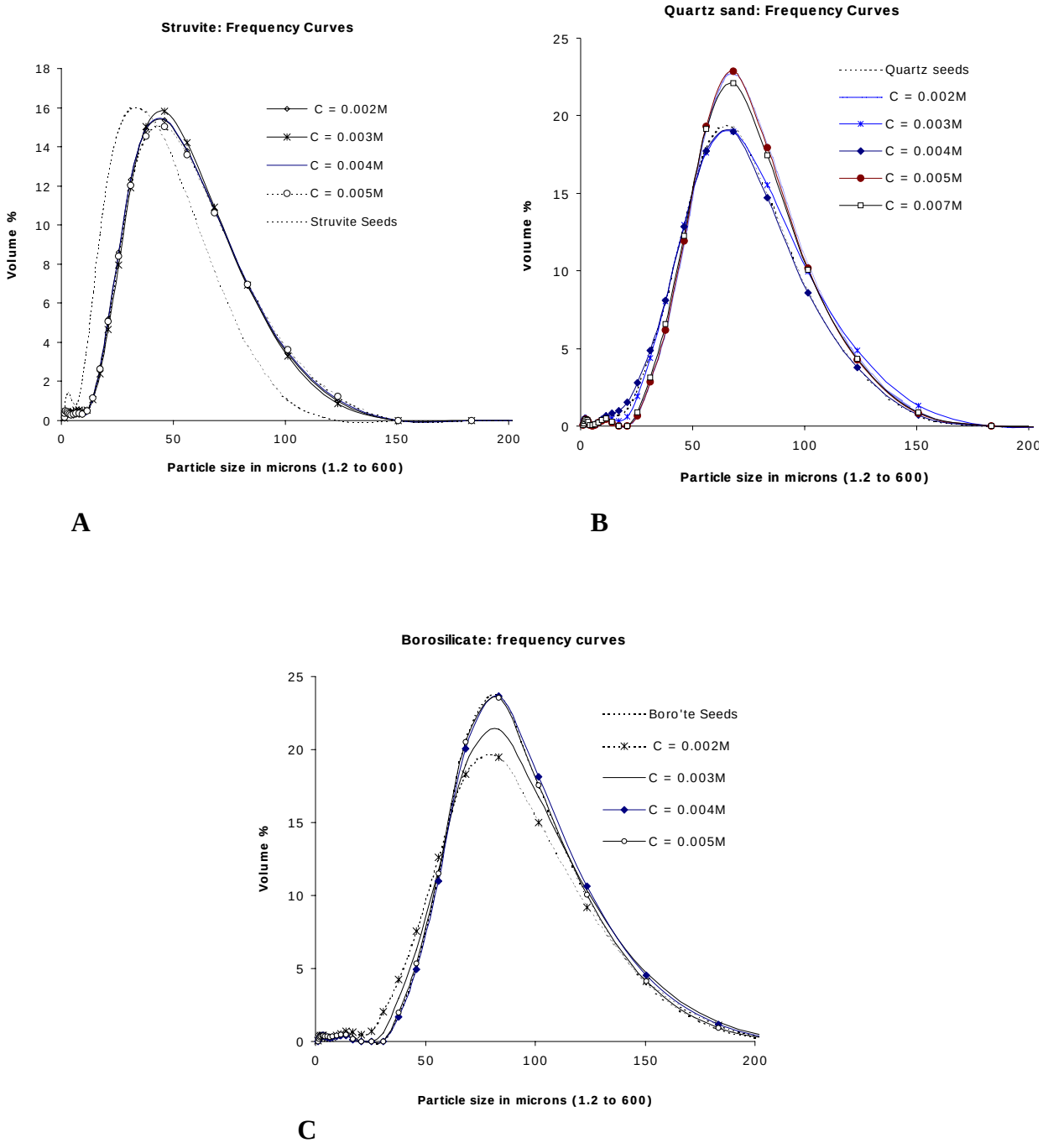

Figure 5. 10 Development of struvite crystals using different types of seed materials

Table 5. 1 Summary of experiment of struvite crystal growth using different seed particles

Conc. (M)	**pH (S)**	**pH (Q)**	**pH (B)**	**SI (S)**	**SI (Q)**	**SI (B)**	**ΔL (S)**	**OT (S)**	**ΔL (Q)**	**OT (Q)**	**ΔL (B)**	**OT (B)**	**Ionic Strength (S/B/Q)**
0.003	7.48	7.637	7.54	0.06	0.11	0.08	**13.44**	12.29	**4.96**	12.57	**0.53**	14.67	0.0085
0.004	7.294	7.564	7.29	0.02	0.32	0.02	**11.81**	12.14	**4.42**	14.67	**1.99**	18.51	0.01085
0.007	7.004	7.245	7.116	0.22	0.51	0.36	**11.44**	23.64	**-0.19**	22.17	**-3.73**	19.62	0.0176

Notes: S = Struvite seeds; Q = Quartz sand seeds; B = Borosilicate seeds; M = Molar Concentration; SI = Saturation Index; ΔL = Increase of crystal size in μm;

OT = Operation time in hour

5.4 Analysis of Moisture Content of Struvite

This section describes the preliminary experimental outcome to identify the optimal drying temperature for struvite. The identification of optimal drying temperature for struvite is important when previously generated dry struvite crystal is used as seeds. It is worthwhile noting that over-drying of struvite may transform the original crystal into delicate form due to the loss of crystalline water (Figure 5.11). Over-dried struvite seed may cause excessive breakage due to hydro-dynamics and mixing during the reactor operation, leading to the generation of faulty experimental data (Figure 5.12).

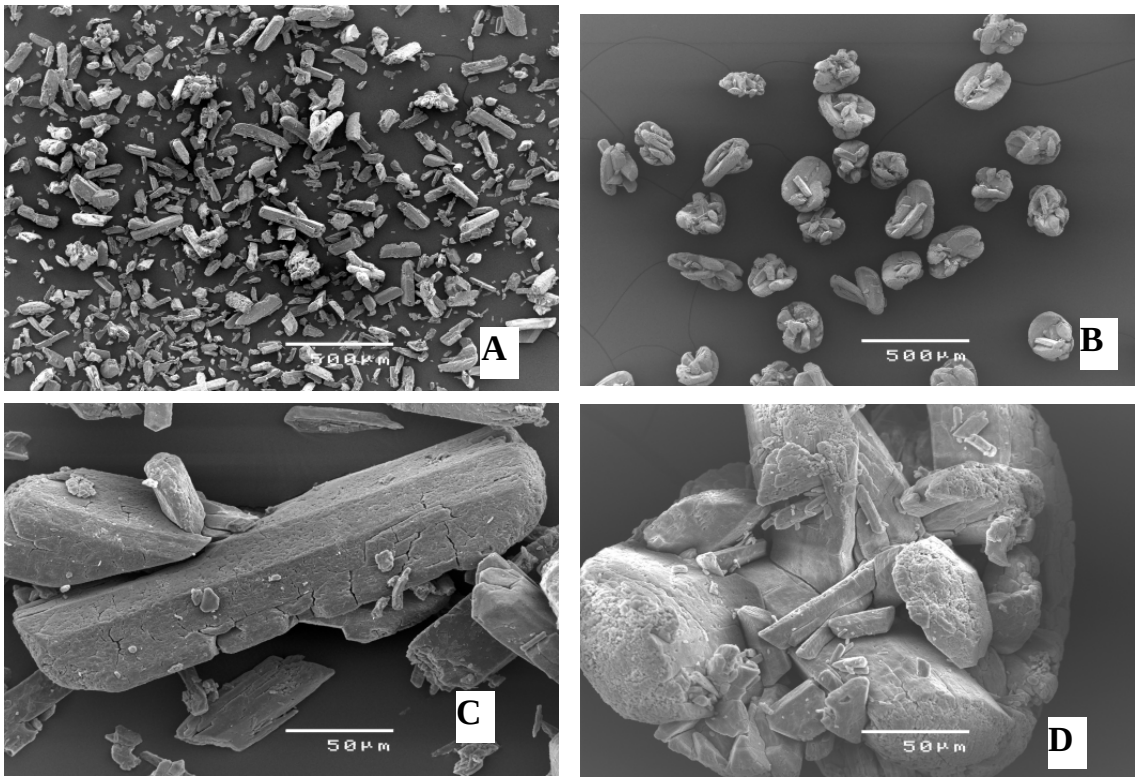

Figure 5. 11 SEM view of air-dried struvite (A); magnified view of air-dry struvite (C); temperature dry (100°C) struvite (B); magnified View of temperature dry struvite (D)

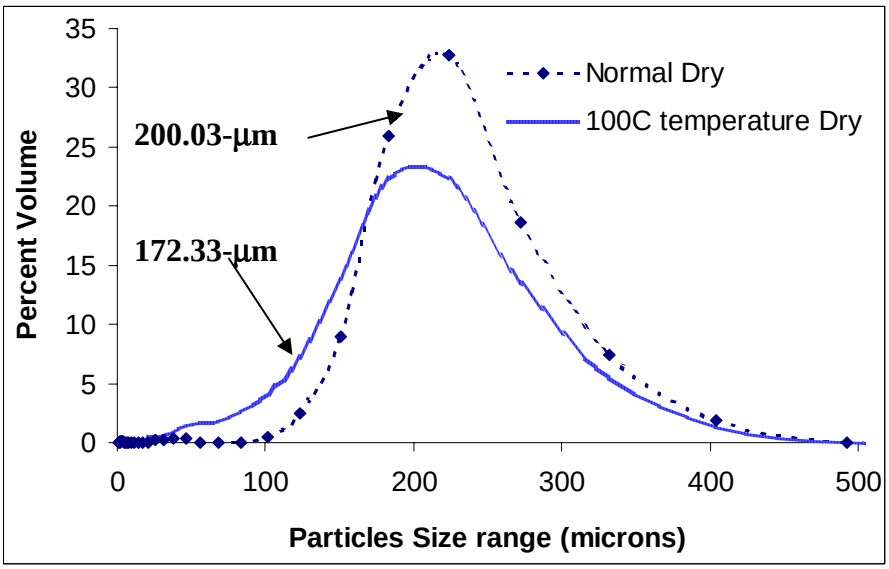

Figure 5. 12 Frequency curves of struvite at different drying conditions

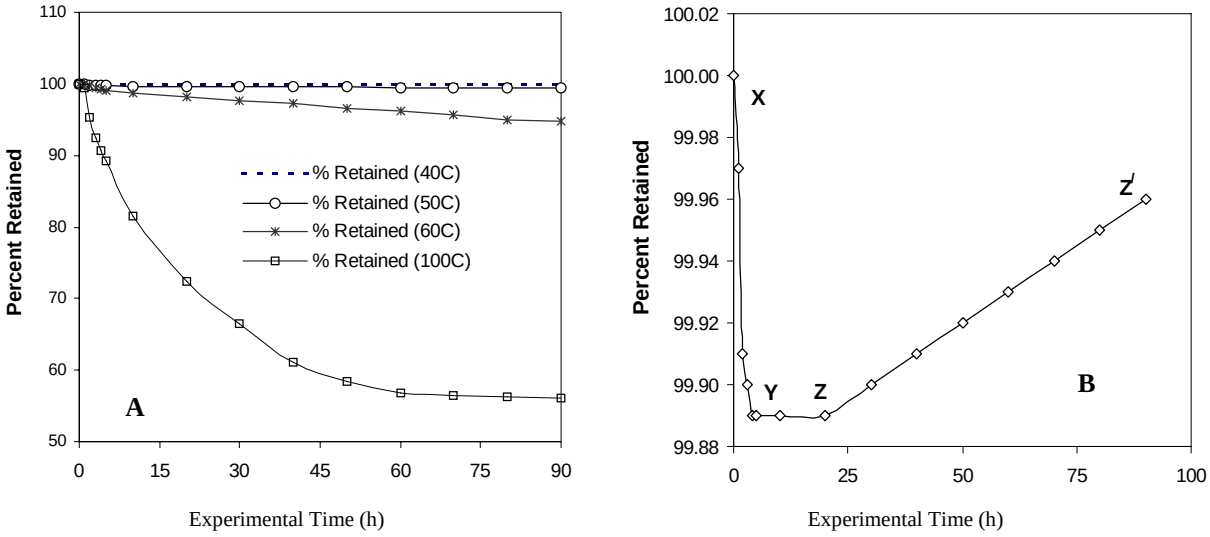

Figure 5. 13 Decline of struvite moisture content at different temperature (A), Retention of total mass in drying process at 40°C temperature (B)

Depletion of struvite moisture at different temperatures is demonstrated in Figure 5.13(A). Referring to equation 5.2 and 5.3, diminution of struvite moisture at high temperature occurred mainly due to the loss of crystalline water (Ramalingom *et al.* 2001).

$$MgNH_4PO_4.nH_2O \Rightarrow MgNH_4PO_4.(n-x)H_2O + xH_2O \quad \textbf{(5. 2)}$$

$$MgNH_4PO_4.(n-x)H_2O \Rightarrow MgNH_4PO_4 + (n-x)H_2O \quad \textbf{(5. 3)}$$

However, atmospheric moisture caused very negligible interference in the drying process, which can be illustrated at drying temperature of 40ºC (Figure 5.13B). Given full explanation of crystal drying at 40°C (Figure 5.13B), escape of available surface moisture from struvite surface occurs due to drying *(xy)*, followed by no gain of moisture *(yz)*. It is worthwhile pointing out that the escape of free surface moisture caused 0.13% reduction of the retained struvite mass. Dry struvite, free from any surface moisture, also caused some insignificant absorption of atmospheric moisture *(zz')*, leading to increase of total mass of about 0.11%. Therefore, it is concluded that perfectly dry struvite may cause very minor atmospheric moisture interference, leading to free moisture transport to and from struvite surface. Based on the results and discussion presented in this section, struvite crystal should be dried at 40-50°C temperature to prevent any moisture loss from the crystal molecule.

5.5 Control Strategy

A key focus of this research was the controlled struvite crystallization carried out in a pilot scale crystallizer (reactor). To develop a strategy in controlled struvite crystallization, the following concerns required attention.

- Correct combination of feed solution
- Correct stoichiometry of feed solution
- Poor control due to preliminary loss of reactive solution concentration
- Poor control due to acid base neutralization

Each of these setbacks imposed considerable influence on experimental design. The key concerns involved in effective process control of struvite crystallization are outlines below.

5.5.1 Composition of Feed Solution

As described in the Chapter 4 (section 4.5), this research aimed at struvite crystallization using fed-batch controlled supersaturation. Synthetic solutions of $MgCl_2$ and $NH_4H_2PO_4$ were used as the source of magnesium, ammonium and phosphate. The constant supersaturation was maintained using controlled dosing of magnesium, ammonium and phosphate feed. The automatic dosing of NaOH maintained the constant solution pH value. Possible combinations of feed solutions using $MgCl_2$, $NH_4H_2PO_4$ and NaOH are listed below in Table 5.2.

Table 5. 2 Possible combination of feed solution

Feed Type	Components-1 (Titrant-1)	pH	Components-2 (Titrant-2)	pH
M_1	$MgCl_2$ + NaOH	≈ 10-11	$NH_4H_2PO_4$	≈ 3.8
M_2	$NH_4H_2PO_4$ + NaOH	≈ 9.0	$MgCl_2$	≈ 7.0
M_3	$NH_4H_2PO_4$ + $MgCl_2$	≈ 5.3	NaOH	≈ 12.5

Significant amounts of $Mg(OH)_2$ precipitated (equation 5.4) when $MgCl_2$ and NaOH solutions were mixed to make up titrant-1 (Feed type M_1). Thermodynamic predictions in Figure 5.14, using the PHREEQC thermodynamic modeling package, demonstrate the trend of Mg^{2+} in titrant-1 when composition type M_1 and M_3 are maintained. Precipitation of $Mg(OH)_2$ formed in the alkaline feed solution did not take part in feed

addition, since it had settled to the bottom. This precipitate caused the loss of magnesium ion in the feed solution (Figure 5.14A), leading to unbalanced and undesired level of reactant concentration (magnesium, ammonium and phosphate) in the system. It is worthwhile pointing out that the loss of soluble magnesium (30%) was computed at the natural pH (pH ≈ 11) of titrant 1 (feed type M_1) using thermodynamic modeling.

$$\begin{aligned} &\mathbf{4}MgCl_2 + \mathbf{8}NaOH \Leftrightarrow OH^- + H^+ + H_2O + \mathbf{8}Cl^- + Mg^{2+} \\ &+ MgOH^+ + \mathbf{7}Na^+ + NaOH + O_2 + Mg(OH)_2 + MgO \end{aligned} \qquad \textbf{(5. 4)}$$

Conversely, mixing of $NH_4H_2PO_4$ and NaOH solution to make up titrant-1 (feed type M_2) led to an imbalanced control of the experiment due to the transformation of NH_4^+ to volatile NH_3. The transformation of NH_4^+ to NH_3 in the feed solution caused the significant loss of NH_4^+ (100% - 70% ≈ 30%) in the form of NH_3 (Figure 5.14B), leading to an alteration of the desired supersaturation in the reactive solution. The loss of soluble ammonium (≈ 30%) was computed at the default feed solution pH (pH ≈ 9) of titrant 1 (feed type M_2) using thermodynamic modeling.

Mixing $MgCl_2$ and $NH_4H_2PO_4$ to make up titrant-1 (feed type-M_3) also led to a poor control, due to crystal formation in the titrant (feed) solution. The unexpected formation of struvite crystal in the feed solution caused an alteration of original feed concentration and change in the experimental control.

As described previously in this section, it was therefore imperative to use feed solutions according to M_1 to minimize losses of Mg^{2+}, NH_4^+ and PO_4^{3-}. Continuous stirring of

titrant 1 set the feed solution in motion, thus avoided the settling of $Mg(OH)_2$ precipitate. This $Mg(OH)_2$ precipitate redissolve on entry to the reactor.

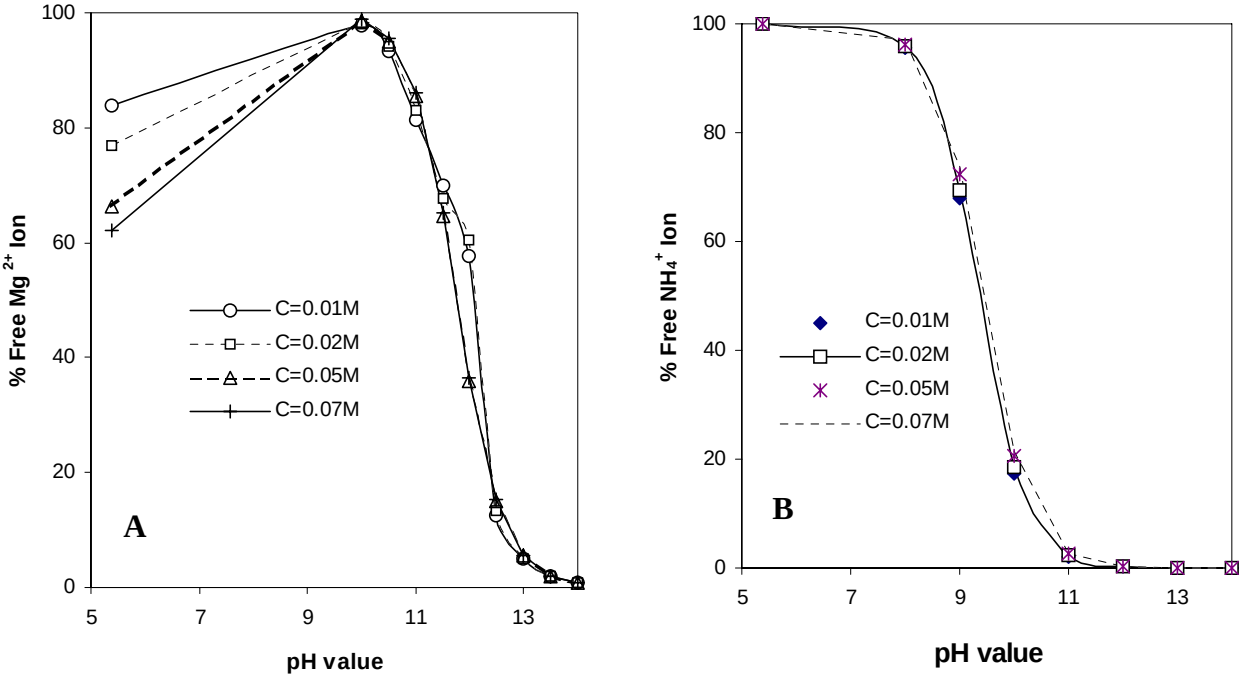

Figure 5. 14 (A) Free Mg^{2+} Concentration in Feed-type M_1 and M_3 of Titrant-1; (B) Free NH_4^+ and NH_3 Concentration in Feed-type M_2 and M_3 of Titrant-1 (computed using PHREEQC thermodynamic modeling package)

5.5.2 Stoichiometry of Feed Solution

Experimental control depends on the correct stoichiometry of feed solution, following the fundamental reaction of struvite crystallization (Bouropoulos and Koutsoukos 2000; Adnan *et al.* 2004; Ali and Schneider 2006), as described in equation 5.5.

$$Mg^{2+} + NH_4H_2PO_4 \Leftrightarrow MgNH_4PO_4 + 2H^+ \qquad \textbf{(5. 5)}$$

A struvite reactor, operating at constant pH and constant reactant concentration of magnesium, ammonium and phosphate, was required for the experiment. The reactor consisted of an initial volume (v liter) of reactive solution of x_1 equimolar concentration of magnesium, ammonium and phosphate. The schematic diagram of the feed addition system is shown in Figure 5.15. The feed solutions must be split into two streams, since the presence of magnesium, ammonium and phosphate in the same stream may cause the formation of struvite crystal in the feed solution. Based on the previous discussion (Section 5.5.1), combination of feed solution must be maintained as followed by equations (5.6) and (5.7).

$$\text{Titrant - 1}: NaOH + MgCl_2 \qquad \textbf{(5. 6)}$$

$$\text{Titrant - 2}: NH_4H_2PO_4 \qquad \textbf{(5. 7)}$$

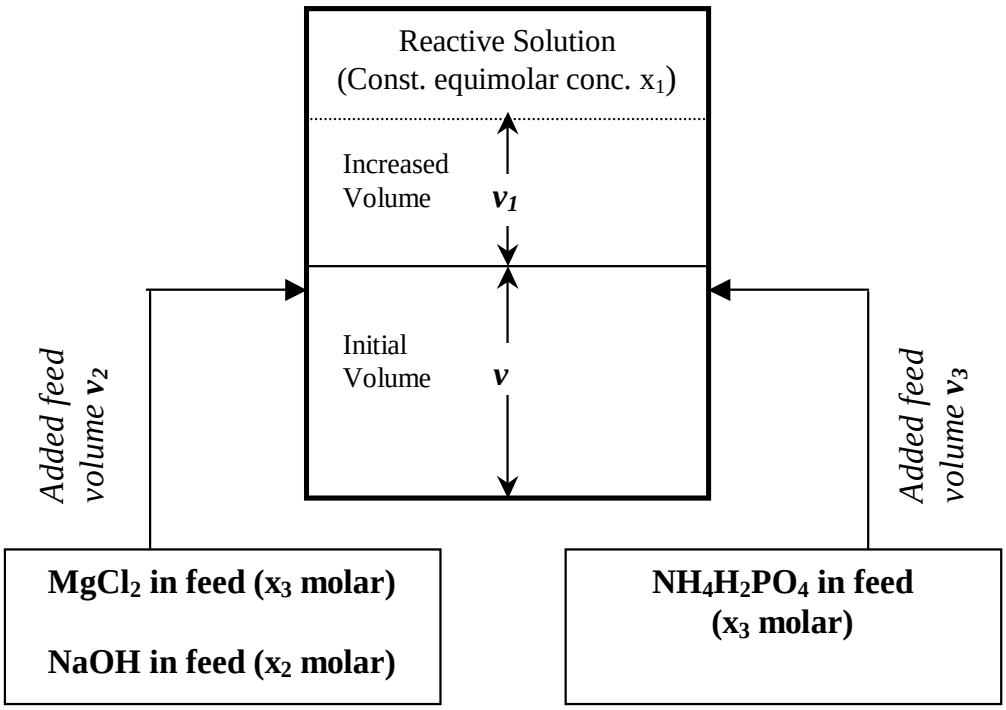

Figure 5. 15 Schematic of feed solution addition (following feed type M_1)

Assume that, the concentration of Mg^{2+}, NH_4^+ and PO_4^{3-} in the feed solution is x_3 molar, and NaOH concentration in the feed solution is x_2 molar. Due to the fed-batch action, v_2 liter of titrant-1 and v_3 liter of titrant-2 are added into the reactor. Based on the struvite stoichiometry (equation 5.5), equal volumes of feed solutions (equation 5.8) are required to maintain constant equimolar concentration of Mg^{2+}, NH_4^+ and PO_4^{3-} in the reactive solution.

$$v_2 = v_3 \quad \textbf{(5. 8)}$$

After the unit operation time, v_1 liter of reactive solution is increased in the crystallizer due to the fed-batch action, leading to an added volume of titrant-1 and titrant-2 (v_2 and v_3). Equation (5.9) represents the mole balance of the reactants (magnesium, ammonium and phosphate) due to the fed-batch action of the crystallizer.

$$vx_1 + v_1 x_1 = v_3 x_3 \quad \textbf{(5. 9)}$$

$$(v + v_2 + v_3)x_1 = v_3 x_3 \quad \textbf{(5. 10)}$$

$$(v + \boldsymbol{2}v_3)x_1 = v_3 x_3 \quad \textbf{(5. 11)}$$

$$x_3 = \frac{v}{v_3} x_1 + \boldsymbol{2}x_1 \quad \textbf{(5. 12)}$$

$$x_3 = Ax_1 + \boldsymbol{2}x_1 \quad \textbf{(5. 13)}$$

Equation (5.12) presents the standard equation to present the molar concentration of Mg^{2+}, NH_4^+ and PO_4^{3-} in fed solution, which is obtained by simplifying equation (5.9). Considering $A = v/v_3$ in equation (5.12), the standard equation to present molar

concentration of Mg^{2+}, NH_4^+ and PO_4^{3-} in the feed solution can be presented by equation (5.13). Please note that ***A*** is a chosen constant to maintain feed solution concentration sufficiently strong. This research considered **A** is equal to**10** to establish the longer duration of fed-batch (semi-continuous) operation. It would be worthwhile noting that the value of **A** depends on the crystallization rate and the expected duration fed-batch operation. Therefore, for higher rate of crystallization (higher supersaturation) stronger feed concentration should be maintained. In this context, larger value of the constant **"A"** would lead to good experimental control.

The release of H^+ in supersaturated struvite system is an indirect approach of monitoring the chemical reaction rate. On the basis of equation (5.14), pH drop in the supersaturated struvite system indicates the occurrence of reaction. During the reaction, 2 moles of H^+ are released for every one mole of struvite formed (Bouropoulos and Koutsoukos 2000). Therefore, 2 moles of NaOH (source of OH^- ion) are required to neutralize the acidic effect of H^+ ion. Equation (5.15) presents the mole balance of NaOH. Equation (5.16) is the simplified form of equation (5.15). By substituting $A = v/v_3$, equation (5.17) shows the theoretical molar concentration of NaOH feed solution. As described before, ***A*** is a chosen constant. This research considered **A** is equal to **10** to compute the feed concentrations.

$$2 v_3 x_3 = v_2 x_2 \qquad \textbf{(5. 14)}$$

$$2 v_2 \left(vx_1 / v_3 + 2 x_1 \right) = v_2 x_2 \qquad \textbf{(5. 15)}$$

$$2 \frac{v}{v_3} x_1 + 4 x_1 = x_2 \qquad \textbf{(5. 16)}$$

$$x_3 = 2Ax_1 + 4x_1 \quad \textbf{(5. 17)}$$

It is worthwhile pointing out that equation (5.17) is the theoretical formula of NaOH feed concentration (M). However, experimental outcome in the fed-batch system showed that the NaOH feed as followed by equation (5.18) provided good control. The selection of arbitrary value ***A*** is supported by the existing literature (Bouropoulos and Koutsoukos 2000).

$$x_3 = 2Ax_1 - 2x_1 \quad \textbf{(5. 18)}$$

The dissimilarity of theoretical and practical observations of NaOH feed concentration (equations 5.15 and 5.18) is most likely due to (i) the difference in pH between the titrant-2 and reactive solution and (ii) the complex chemical nature of reactive solution. The first reason most probably relevant to the natural pH of feed solutions itself due to the complex feed mixture. The second reason relevant to this context is described in the next paragraph.

In the supersaturated system of magnesium, ammonium and phosphate the most likely solid phases include Newberyite [$MgHPO_4.3H_2O$], Bobieryite [$Mg_3(PO4)_2.8H_2O$], Farringtonite [$Mg_3(PO_4)_2$], alongside struvite [$MgNH_4PO_4.6H_2O$]. However, this research incorporated a series of XRD analysis for newberyite, bobieryite and farringtonite, and found the existence of bobieryite alongside struvite. Please note that produced struvite using equimolar concentration of 0.0045M along with operating pH of 7.35 was used in XRD analysis. In addition to bobieryite, XRD analysis also showed the presence of dittmarite ($MgNH_4PO_4.H_2O$) alongside struvite. It is worthwhile noting

that dittmarite does not appear in the PHRREQC database, although it appears in the machine's database of diffractometer (powder X-ray Diffractometer: model Siemens D5000) used in this research.

5.5.3 Preliminary Reduction of Supersaturation of Reactive Concentration

A fed-batch experiment, conducted using 0.002M of reactant concentration (operating pH 8.5) along with the stated formulation of feed solutions, indicated an initial reduction of reactant concentration during the start-up phase of the experiment (Figure 5.16A). Significant reductions of about 25% and 40% were observed for Mg^{2+} and PO_4^{3-}, respectively. The preliminary reduction of reactant concentration occurred due to uncontrolled and undesirable nucleation during the start-up phase of the experiment. After 28 hours of operation, loss of about 65% and 71% was encountered for Mg^{2+} and PO_4^{3-}, respectively (equations 5.19 and 5.20). It is worthwhile pointing out that the measured initial concentrations for Mg^{2+} and PO_4^{3-} were 60 mg/l and 237 mg/l, respectively.

$$\text{Reduction of } Mg^{2+} \text{ after 28 hours of operation} = \frac{(60 - 21.1)}{60} \times 100 = 65\% \qquad \textbf{(5. 19)}$$

$$\text{Reduction of } PO_4^{3-} \text{ after 28 hours of operation} = \frac{(237 - 68.64)}{237} \times 100 = 71\% \qquad \textbf{(5. 20)}$$

At this stage, the reactive solution had reached an equilibrium state. Continual depletion of reactive concentration was observed even though the process maintained controlled pH during this phase of the operation. Figure 5.16B demonstrates the trend of P/Mg control, which expresses the loss of effective control in the reactor. Note that the

measured concentrations of phosphorous (P) and magnesium (Mg) in the Figure 5.16 is in mg/l.

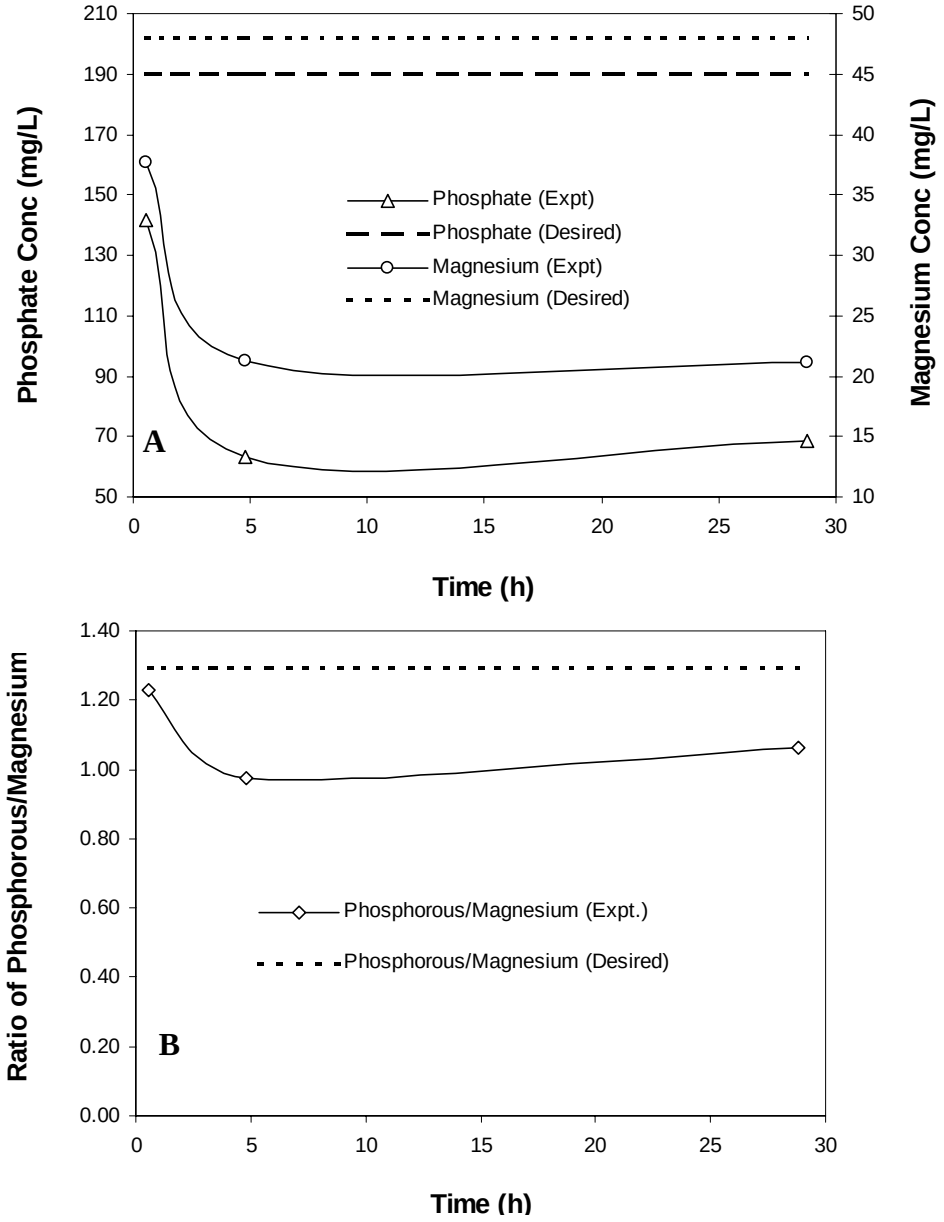

Figure 5. 16 (A) Faulty control due to preliminary reduction of reactant concentration; (B) trend of control expressing P/Mg value of the system

Due to reduction of reactant concentration during the start-up of the process, the reactive solution never attains the desired process conditions. Virtually no

crystallization resulted, since the reactive solution was essentially undersaturated. Simple thermodynamic modeling, using PHREEQC, confirmed the undersaturation of solution with a resulting value of the Saturation Index (SI) of 0.37. Detailed explanation of the Saturation Index (SI) is shown in chapter 3.

5.5.4 Poor Control (Extreme Supersaturation) due to Acid-base Neutralization

Another experiment was conducted with 0.002M of reactive solution along with a preliminary set point of pH 8.75. The composition of titrant was according to M_3 (Table 5.2 in Section 5.4.1). An excessive feed rate was observed during the experiment (Figure 5.17A). A new pH set point of 8.25 was employed 10 minutes after the experiment set up to reduce supersaturation.

During this period, reactant concentration increased and the pH never achieved its targeted set point. At the end of the experiment pH of the reactive solution was 6.88, which was far below the set point and surprisingly 8L of each feed solution was added in about 0.7 hours. Instead of maintaining the control Mg^{2+} and PO_4^{3-} at 48 and 190 mg/l, the reactive solution concentration increased to 120 and 750 mg/l for Mg^{2+} and PO_4^{3-}, respectively.

Figure 5.17B shows the P/Mg ratio during the process, given that the concentrations of phosphorous (P) and magnesium (Mg) is presented in mg/l. As described in Figure 5.17A and 5.17B, decline of control occurred due to the acid base neutralization as described previously, where the acidic feed solution (titrant-2) of pH 3.8 neutralized a fraction of OH^- ions. This acid-base neutralization affect caused the addition of extra

feed and increased the generation of fines. In this circumstance, the solution turned into milky-white and crystallization was controlled by spontaneous precipitation. Due to the excessive feed addition, pH and constituent concentrations never achieved the targeted set point. Hence, a continuous increase in concentration of the reactive solution occurred, along with simultaneous depletion of pH.

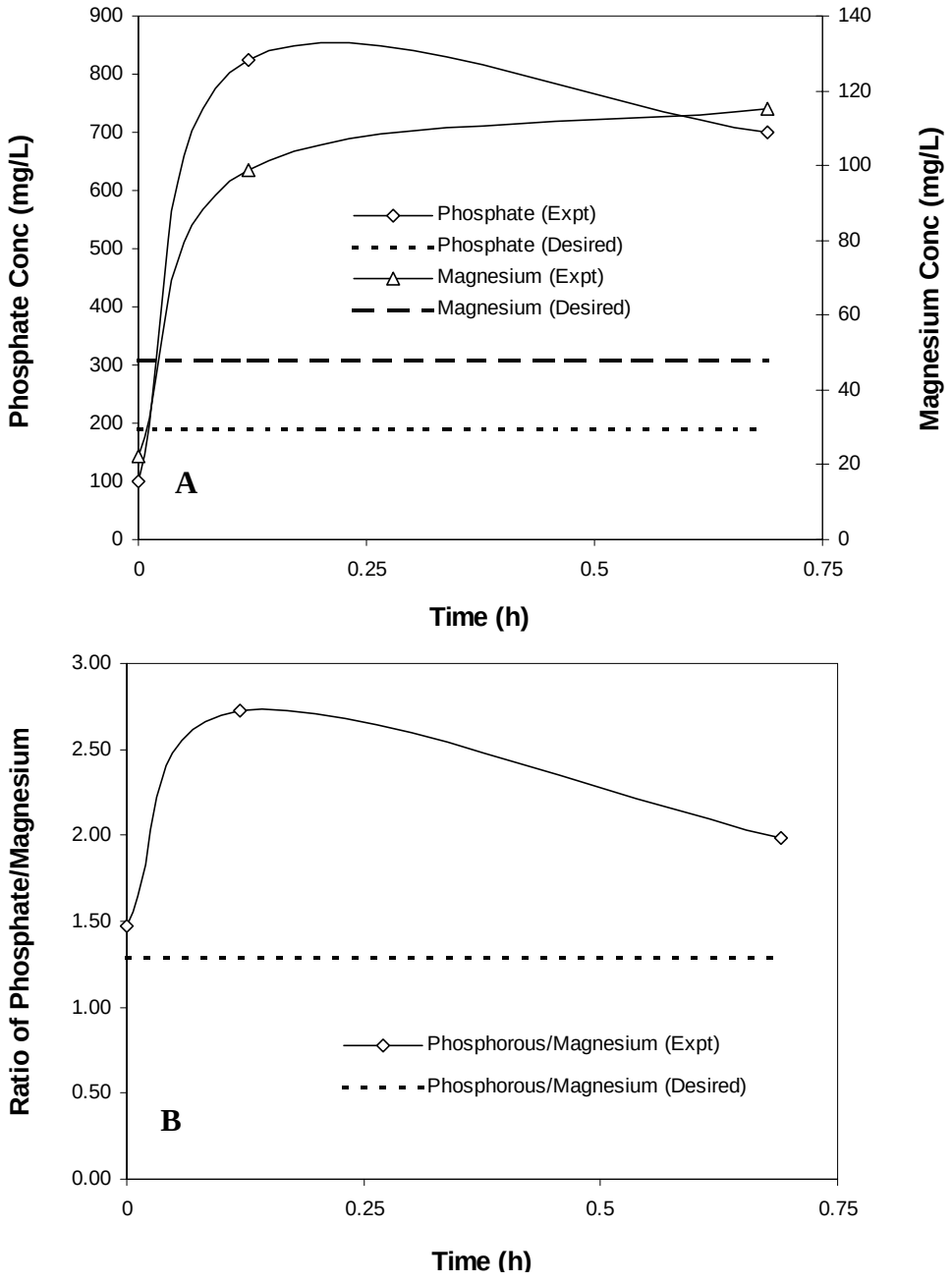

Figure 5. 17. (A) Poor control due to acid-base neutralization; (B) trend of control expressing P/Mg value of the system

Thermodynamic modeling using PHREEQC showed the increase of supersaturation during the experiment. The initial value of Supersaturation Index (SI) was computed as 0.67, whereas it increased to 1.55 at the end of the fed-batch experiment. As described in the previous paragraph, the starting experimental concentration of Mg^{2+} and PO_4^{3-} was 48 and 190 mg/l, which increased to 120 and 750 mg/l, respectively, at the end of the experiment.

5.5.5 Summary of the Control Strategy

The previous discussion in this section (section 5.5.1) on feed composition described how the fed-batch system should be maintained using two feed solutions. The first titrant is composed of NaOH (for pH maintenance) and $MgCl_2$ (the magnesium source). The second is a solution of $NH_4H_2PO_4$ (the ammonia and phosphate source) and NaCl (to maintain ionic strength), pH-adjusted to 6.0. Composition factors for the feed solutions are $12x_1$ (Mg^{2+}, NH_4^+ and PO_4^{3-}) and $18x_1$ (NaOH), where x_1 is the equimolar reactive solution concentration (Section 5.5.2).

To avoid the unexpected undersaturation of the reactive solution during the startup of the experiment, it is required to increase solution pH stepwise allowing sufficient time for proper mixing. van der Houwen and Valsami-Jones (2001) implemented the stepwise increase of solution pH at the start-up of experimental control for hydroxyapatite crystallization. As for example, Figure 5.18 shows the detailed of the experimental startup for experiment-2. This method of experimental initialization was universally applied throughout all fed-batch controlled crystallization experiments.

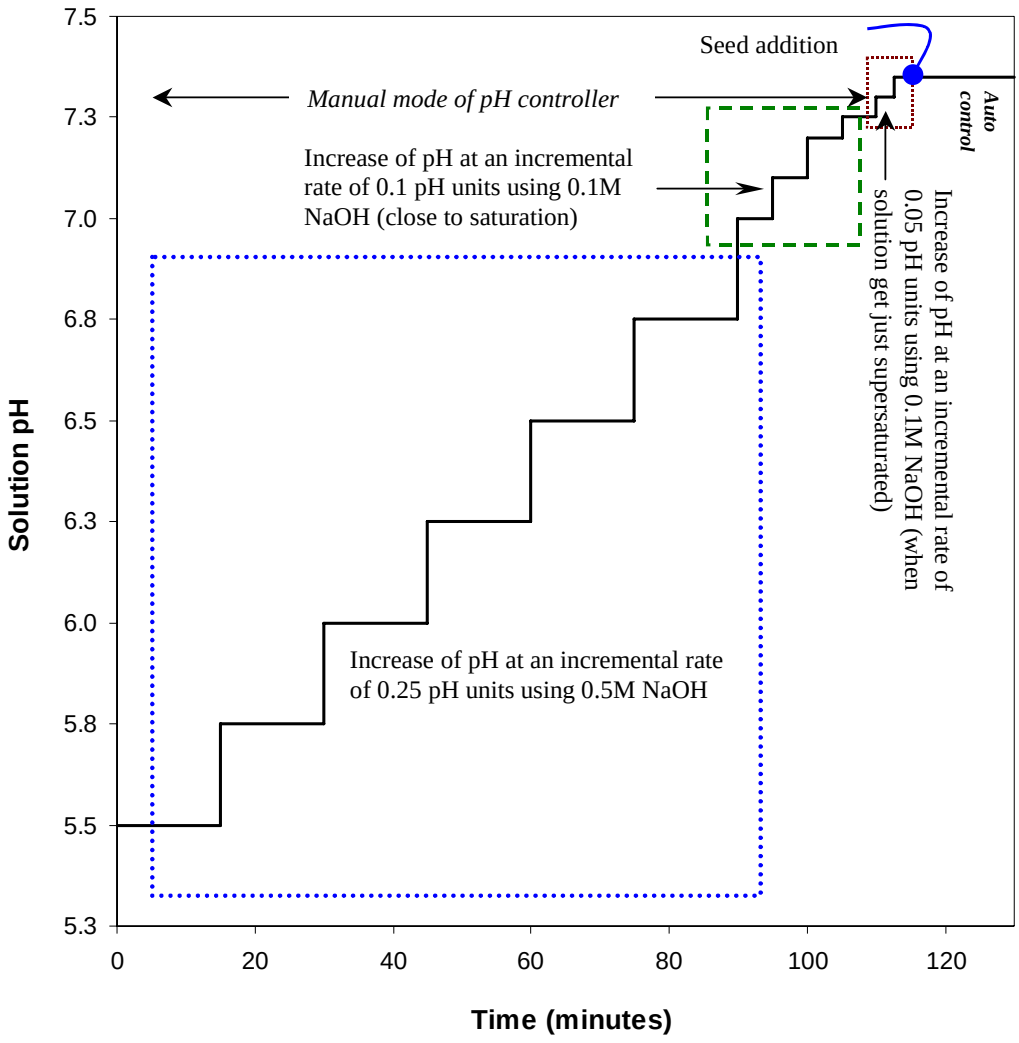

Figure 5. 18 Initialization of fed-batch controlled crystallization system

Maintaining 0.1M of NaCl in the reactive solution altered the ionic strength of the reactive solution. Considering the dilution effect of the combined feed addition, 0.2-M of NaCl was required in the feed solution (titrant-2 of feed type M_1) to maintain 0.1-M concentration of NaCl in the reactive solution. Addition of 0.2-M of NaCl reduced pH value of titrant-1 to 3.70. In this circumstance "acid base neutralization" occurred in the reactive solution when both titrants were added at the same flow rate to maintain constant stoichiometry (Section 5.5.4). Adjustment of the pH was thus required to minimize the acid base neutralization effect. Experimental investigation showed that the

pH difference between titrant-2 and reactive solution of 1.00-1.25 maintained reasonably consistent control of the process.

5.6 Other Operational Issues

The successful operation of struvite reactor is also associated with the temperature control, minimal breakage of particles and dosing point selections. The detailed outcomes of these operational issues are described in the sections 5.6.1-5.6.3.

5.6.1 Temperature Control during Crystallization

This section describes the response of the temperature controller, which was developed and used to maintain constant experimental temperature. The detailed setup and design of the temperature controller is described in Section 4.5 of chapter 4.

There was an increase of the solution temperature of 40°C when the reactor was operated continuously for 48-hours. Uncontrolled process temperature affected the pH sensor and impacted on the process stoichiometry by causing inaccurate solution pH due to the drift in the electrode response.

The second impact is the drift in the pH of the solution. The combined effect of these two events caused faulty control, since the solution supersaturation was under predicted or over predicted. The faulty response of the pH sensor caused the discontinuity and/or stopping of the process at various stages. Therefore, it is imperative to maintain a constant operating temperature of reactive solution. The trend of temperature rise (TT_1)

during the reactor operation is illustrated in Figure 5.19. This temperature control system maintained smoother control of temperature (Figure 5.20).

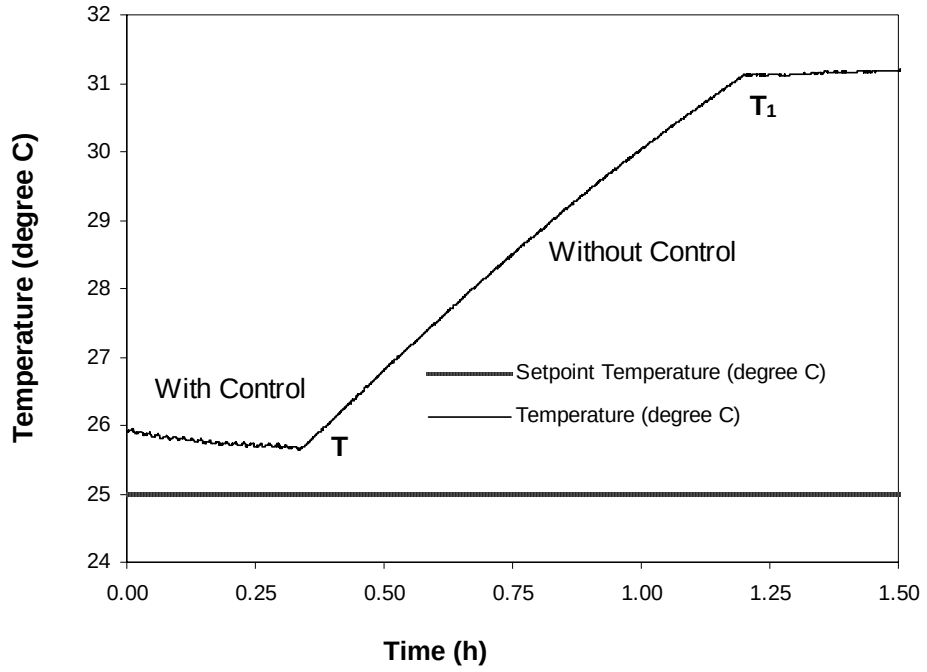

Figure 5.19 Rise of temperature of reactive solution due to recirculation pump operation

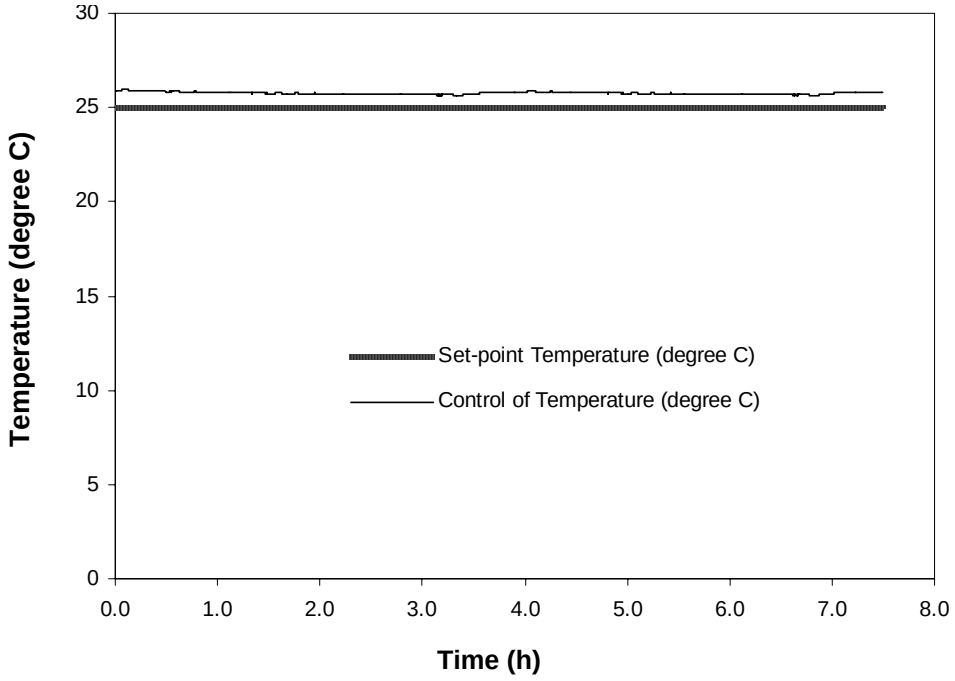

Figure 5. 20 Control of temperature by automatic temperature control system

5.6.2 Particle Breakage Investigations

This section describes the experimental outcome to identify the potential of particles breakage due to the solution hydrodynamic and mixing during reactor operations. To conduct this investigation, quartz sand was used as the surrogate particles of struvite, since struvite in normal water may cause unexpected dissolution.

This experiment was conducted at 25°C using 40L of tap water (roughly free of any reactive components) together with added size-graded quartz sand of 250-450 μm, in order to quantify breakage effects due to the recirculation pump. This experiment included quartz sand as the surrogate particles of struvite. Struvite crystals in normal water led to undesired dissolution, therefore, data of struvite breakage was not representative. Several limitations are involved in this experiment, which are described as follows.

a) Breakage of struvite may be different to that of quartz sand due to different particle hardness and morphology as well as size.
b) The results may be comparable if struvite is harder than quartz sand, but otherwise the elongated shape of struvite may make it more susceptible to breakage.

Micro-hardness test of the quartz sand and struvite could overcome these difficulties (Mersmann 2001), however, these micro-hardness tests were unable to be conducted. Hence, this research incorporated a viable alternative approach, which included the condition of maximum breakage of particles. The condition of the maximum breakage for the surrogate particles was provided during the experiment by carrying out vigorous

mixing of the solution. This was done using the recirculation pump, operating at 80% of the full system's capacity.

Figure 5.21 demonstrates the particle size distribution at different times under this operating condition. Experimental outcome (Figure 5.21) shows that hydrodynamic and mixing causes minimal breakage of quartz sand particles.

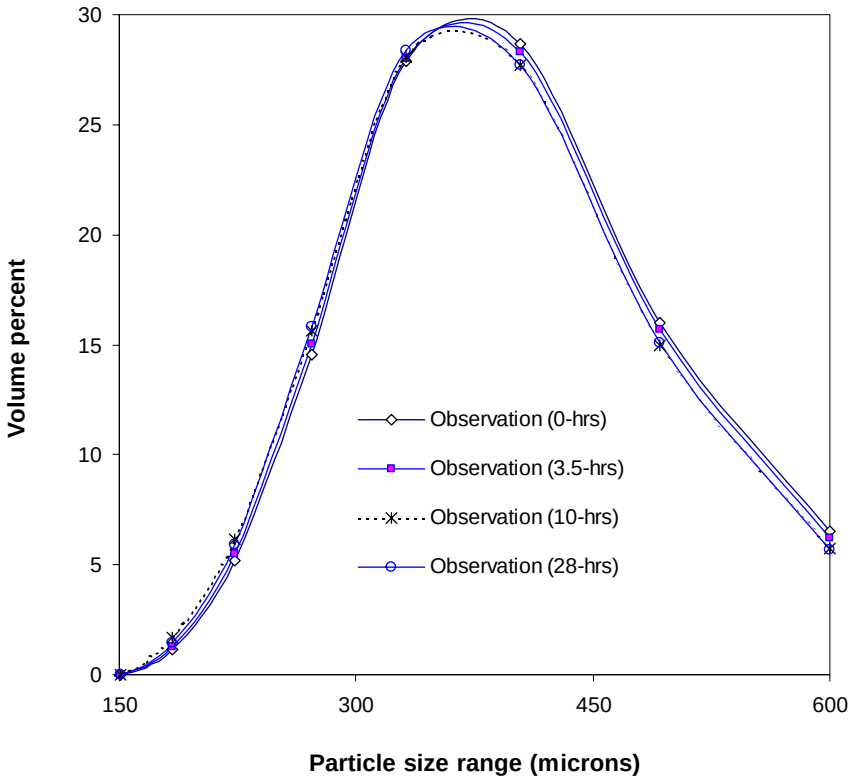

Figure 5. 21 CSD of quartz sand particles during experiment

5.6.3 Dosing Point Selection

This section describes the outcome of a preliminary observation to identify the sensitivity of dosing points and the potential of fines production due to faulty dosing.

Fed-batch controlled crystallization, conducted using solution concentration of 0.005-M along with operating pH of 7.35, imparted significant production of fines due to the

close proximity of the two dosing points (Figure 5.22). The likelihood of fines formation was due to spatial variations in supersaturation of the solution, which resulted in the occurrence of fines (Sohnel and Garside 1992; Tavare 1995; Bouropoulos and Koutsoukos 2000; Mersmann 2001). Therefore, it is necessary to keep the dosing points apart to prevent local supersaturation fluctuation (Mangin *et al.* 2004).

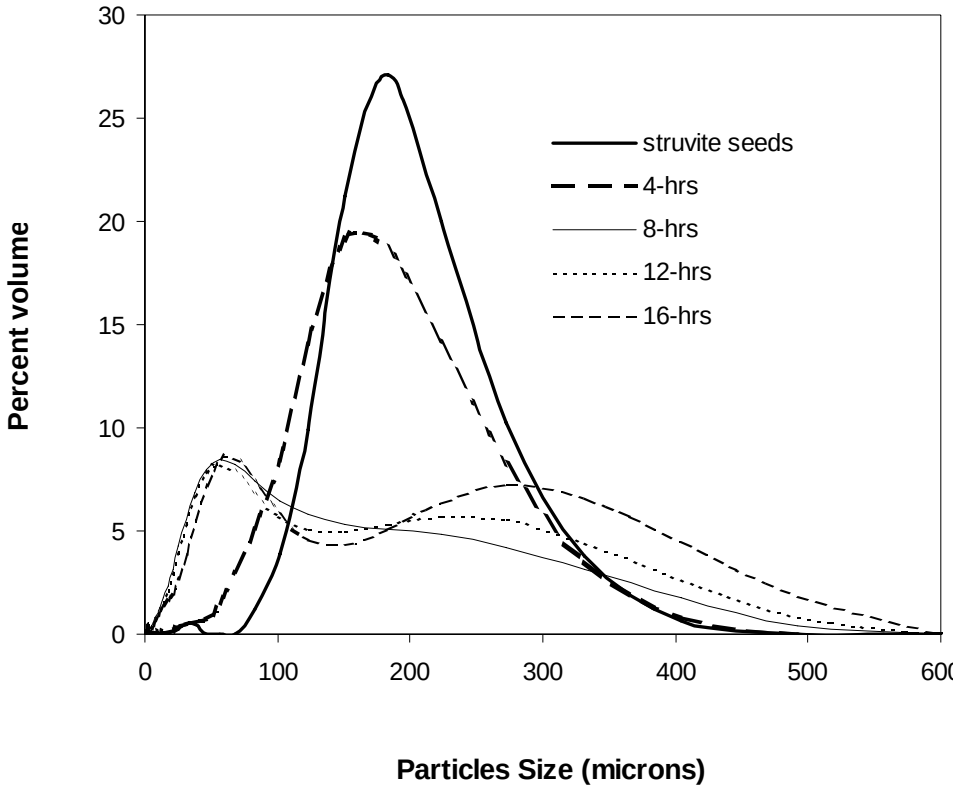

Figure 5. 22 Characteristics of struvite CSD in faulty dosing of titrants

5.7 Conditions for the Controlled Fed-batch Experiments

Detailed outcome of the Design and Commissioning of Experiment, described in Sections 5.2- 5.6, concludes the following requirements for reasonable control of supersaturation in fed-batch crystallization.

- Metastable operating zone of supersaturation should be maintained to avoid spontaneous precipitation (Section 5.2).
- Parent crystal provides effective surface area for newly born clusters, leading to intensified growth of struvite crystals (Section 5.3).
- Over-dried struvite crystals should be avoided as seed due to its susceptibility to breakage. Over-drying of struvite crystals above 40°C may cause the transformation of compact crystal to delicate form due to the loss of crystal forming water molecule. The delicate over-dried crystals may cause breakage due to recirculation and mixing of parent solution during the fed-batch experiment (Section 5.4).
- Proper stoichiometry of feed solutions (Table 5.2) must be maintained for accurate experimental control of supersaturation (Section 5.5.1). Moreover, alterations of pH of titrant-2 close to reactive parent solution (1-1.25 unit pH difference) along with slow increase of solution supersaturation during start-up of the experimental control are mandatory for reasonably accurate supersaturation control in fed-batch struvite crystallization (Section 5.5.2 and 5.5.4).
- Reactive solution temperature must be maintained constant during the fed-batch controlled experiment, since temperature change can cause alteration of original solution thermodynamics (Section 5.6.1). Moreover, two dosing points should be positioned away from one another to avoid spatial variations in supersaturation of the solution (Section 5.6.3).

Based on the abovementioned schemes, a set of fed-batch experiments was conducted using 30-g of previously generated (size classified) struvite seeds. ASTM standard sieve

of 63-125 μm were used to prepare size-classified seeds using a wet sieving technique, followed by air-drying. Each of the experiments was conducted using 15L initial volume of reactive solution. Table 5.3 illustrates the key parameters of these fed-batch experiments. Detailed experimental results will be discussed in Section 5.8.

Table 5. 3 Different conditions of experiments

Experiment	Desired Equimolar Concentration of Reactive Solution	Desired pH of Reactive Solution
1	0.0055M	7.51
2	0.0045M	7.35
3	0.0060M	7.22

5.8 Results of Controlled Fed-batch Experiments

Extensive experimental outcomes in fed-batch show that a reasonable accuracy of experimental control is achievable, if the investigated preliminary parameters (Section 5.7) are properly established.

5.8.1 Characterization of Experimental Control

Figures 5.23(A)-5.25(A) illustrate the control of struvite system at different process conditions. Good experimental control of supersaturation was achieved, since the reactant concentrations and pH remained reasonably constant throughout the experiments (Figures 5.23A, 5.24A and 5.25A). Figures 5.23B-5.25B shows the increase of reactant volume due to the fed-batch action during crystallization.

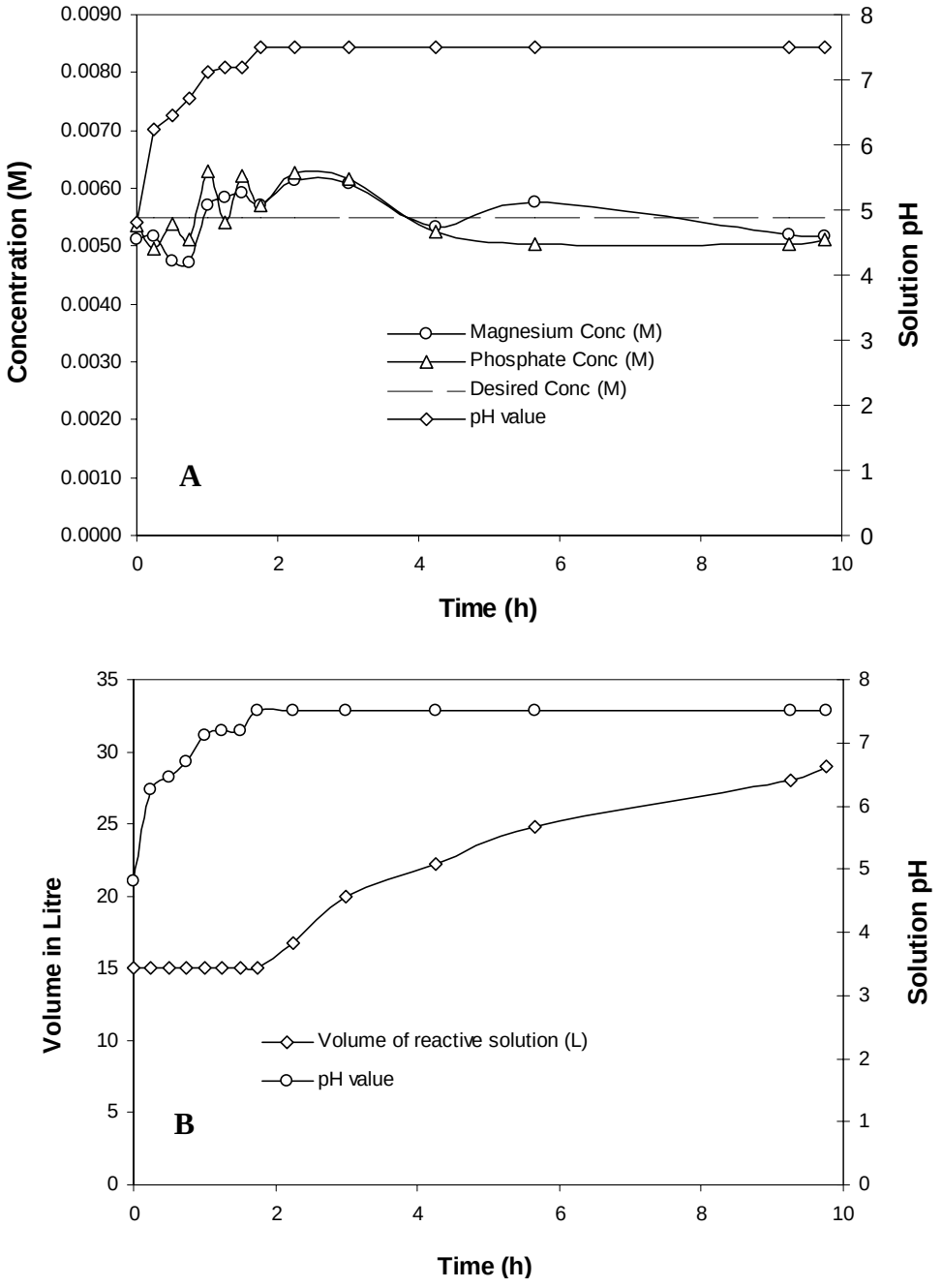

Figure 5. 23 (A) Experimental control; (B) Operating volume in fed-batch action (Expt-1)

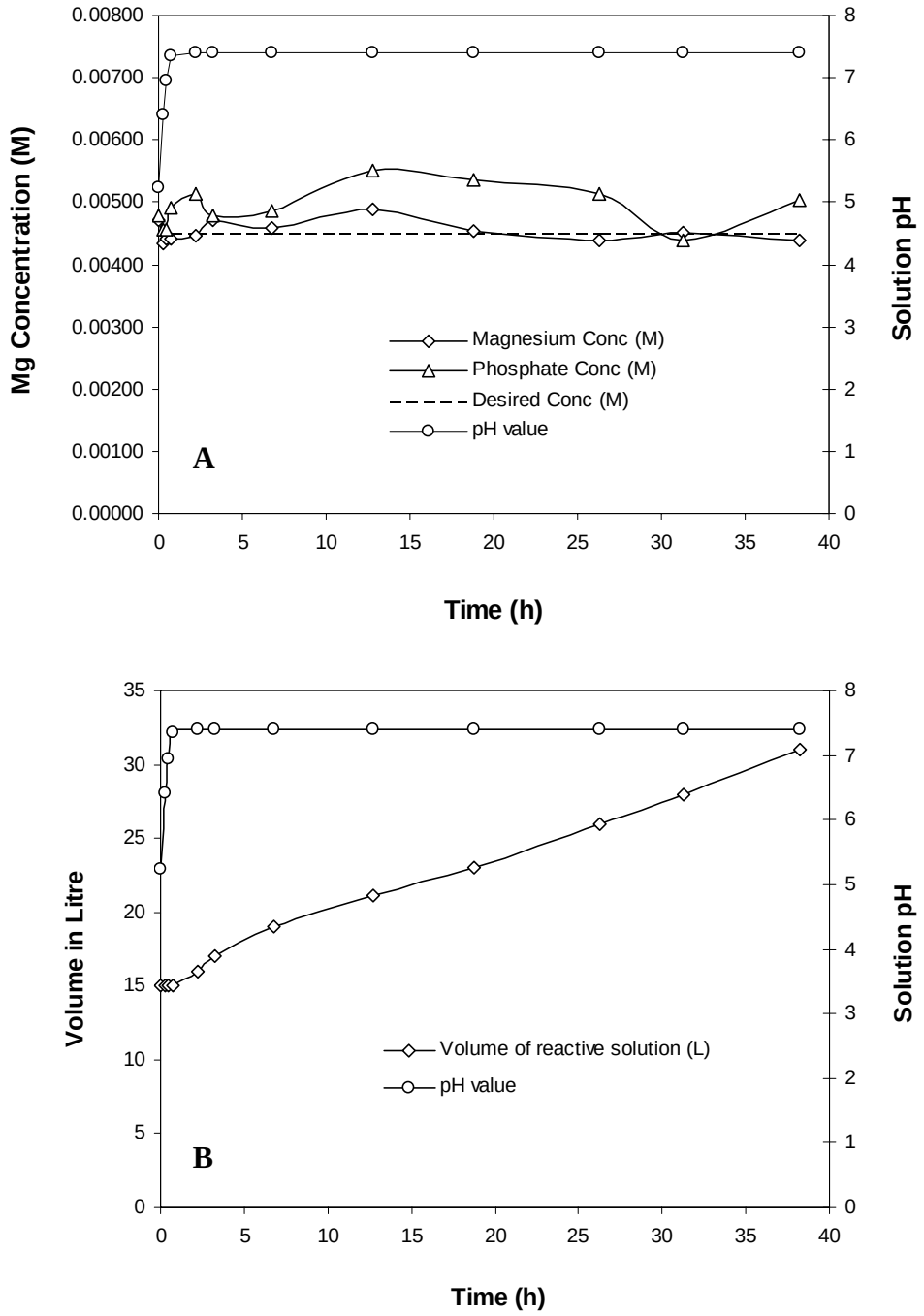

Figure 5. 24 (A) Experimental control; (B) Operating volume in fed-batch action (Expt-2)

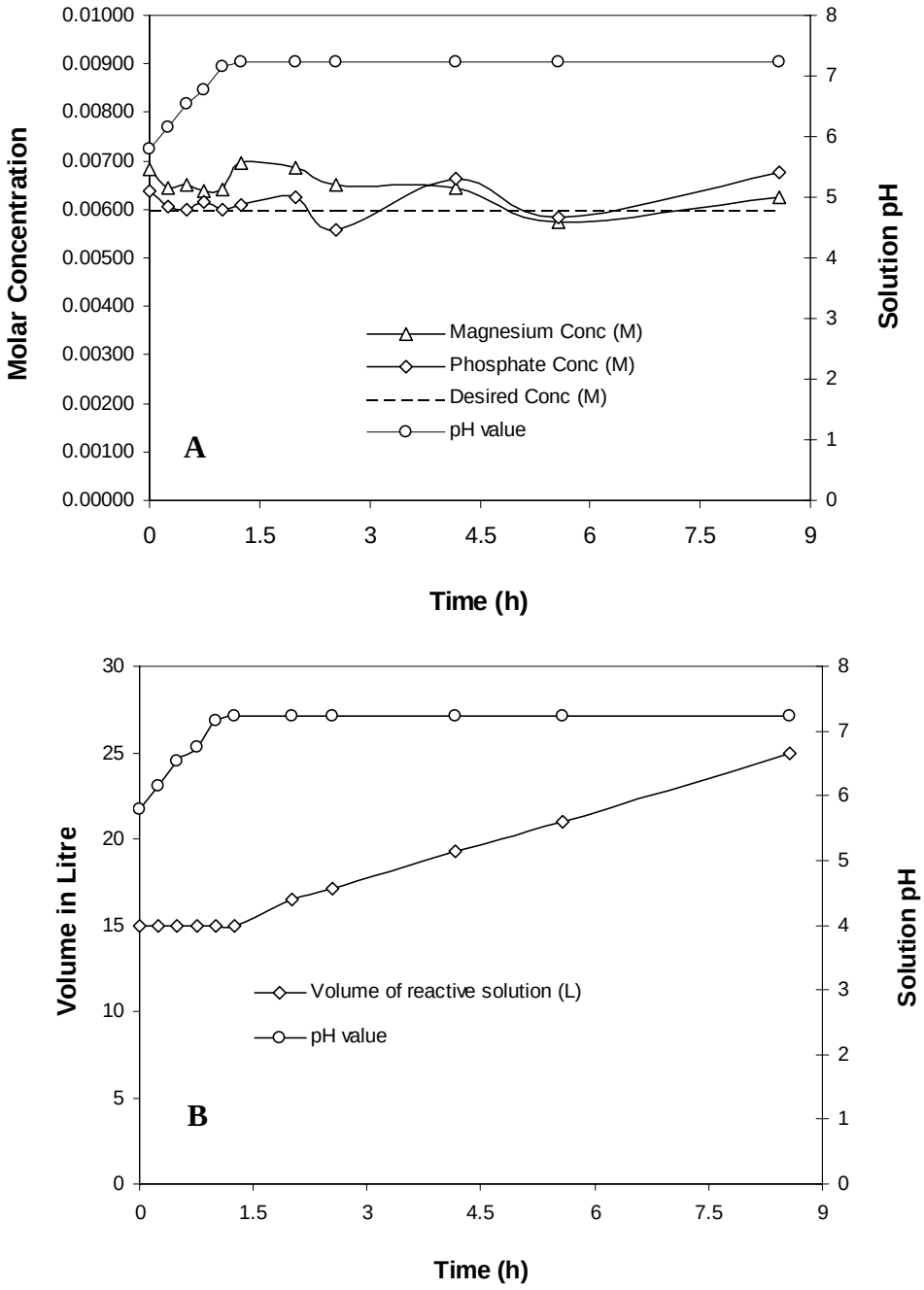

Figure 5. 25 (A) Experimental control; (B) Operating volume in fed-batch action (Expt-3)

Following each experiment, product struvite crystal was separated from mother liquor using an ASTM standard sieve of aperture 63 μm. Collected struvite was air dried and then dry sieved to separate further fines, smaller than 63 μm. A mass recovery of 65-

70% of expected total struvite mass was found in each experiment. The generation of smaller struvite crystals was due to reduction of fines as a consequence of lack of sufficient seeds, very minor breaking effects of growing crystals/seeds due to impeller action of the recirculation system (pumps, pipe *etc*). The crystal produced was identified as struvite by XRD analysis (Figure 5.26).

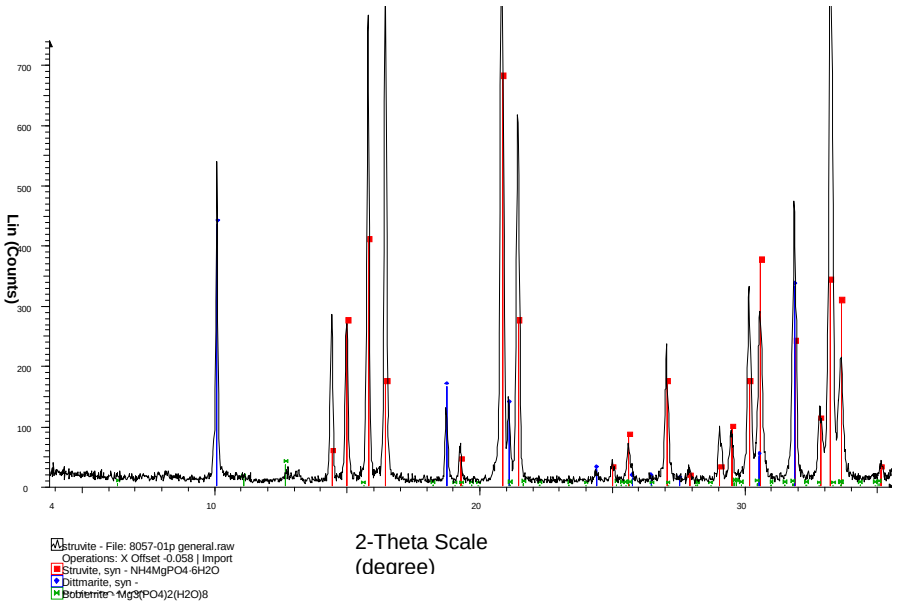

Figure 5. 26 Analysis of struvite by powder XRD analysis

Table 5.4 describes the flow-rate of reactant addition. Based on struvite stoichiometry, any quantifiable drop of pH triggered the addition of both feed titrants; hence the rate of feed addition was an indirect measure of the crystallization rate. Table 5.4 indicates that the rate of crystallization depends on solution supersaturation (Saturation Index). Detail definition of the Saturation Index is shown in Chapter 3.

Table 5. 4 Flow-rate of reactant feed at different Saturation Index

SI	Duration of reactor operation (h)	Preliminary start-up time (h)	Duration of control (h)	Total added feed (L)	Reactant volume added (L)	Flow-rate of reactant feed (L/h)
0.57	9.75	1.75	8	14	7	0.875
0.38	8.57	1.25	7.32	10	5	0.683
0.32	38.25	2.25	36	16	8	0.222

5.8.2 Characterization of Struvite Crystal

In each specified experiment (Table 5.3), the frequency curves of the harvested crystal size distribution indicates a reasonable size independent growth without size dispersion (White 1971), since the frequency curves shifts to the right almost identically to each other (Figure 5.27- 5.29). It is worthwhile noting that a longer tail along the larger particle size range reflects the higher growth for larger particles. A very minor agglomeration among the fine particles is also observed, which causes the increase of elevation of the frequency curves (White 1971).

The magnified view of a frequency curve, in the size range of fine crystals, is demonstrated in Figure 5.30. Produced fines took part in growth and agglomeration, which shifts the developing of frequency curve along Y-axis as well as X-axis.

A plot of mean particle size against operating volume is shown in Figure 5.31. Depletion of mean particle size of growing struvite was observed when the operating solution exceeds 25 litres. In these circumstances a significant amount of fines was produced, which reduced the mean particle size. The cause of fines production was the

insufficient mixing caused by remoteness of inlet and outlet of recirculation stream into the reactor, which made the reactive solution stagnant and local supersaturation fluctuation caused the generation of fines for that period of operation. Increased recirculation pump speeds was employed together with an upward adjustment of the recirculation outlet (Figure 5.31), however, this problem remained. Therefore, it is recommended to use both impeller mixing and conventional mixing to avoid this difficulty.

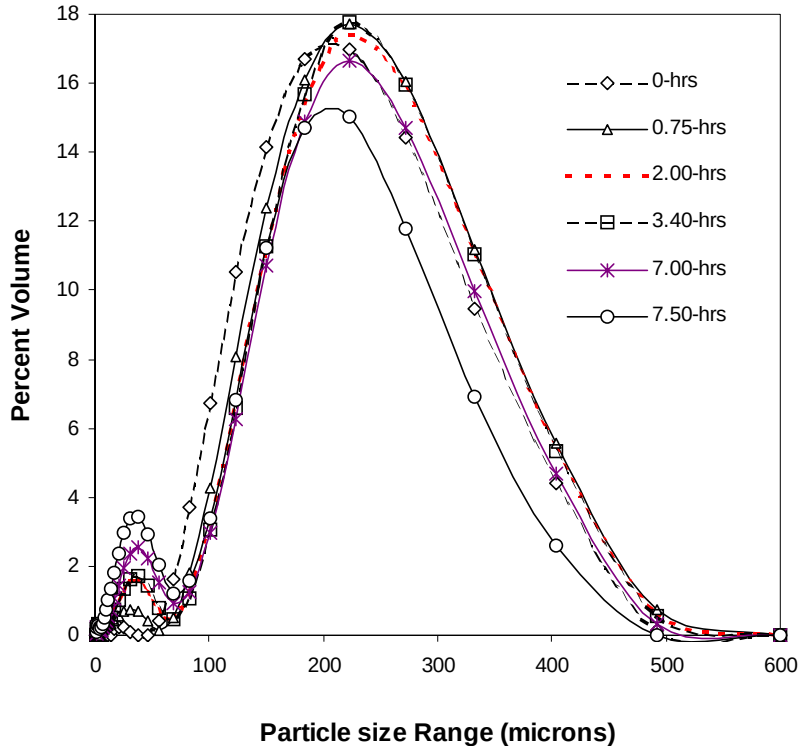

Figure 5. 27 Characterization of mean particle size of struvite (Expt-1)

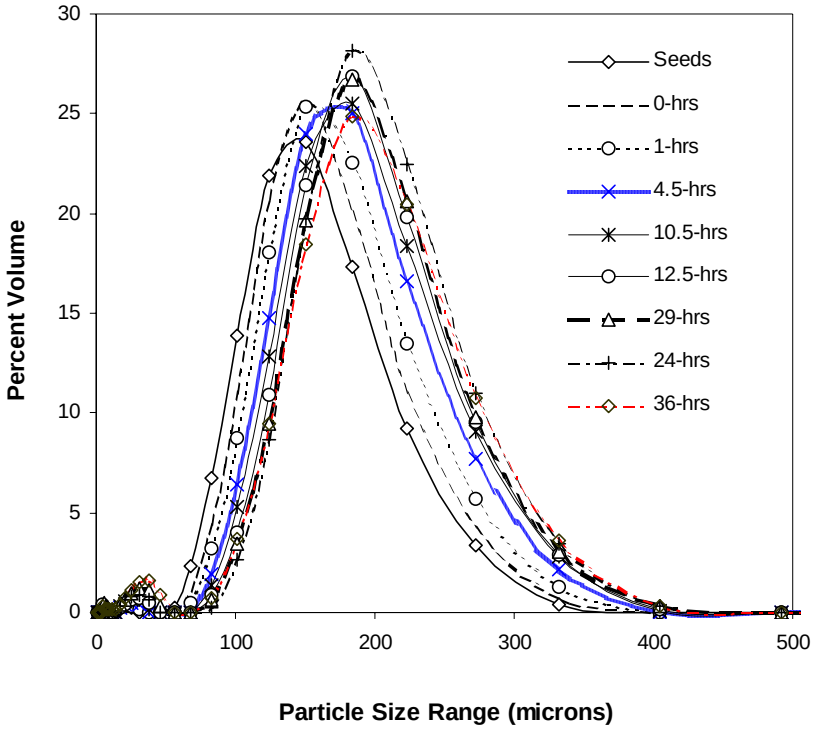

Figure 5. 28 Characterization of mean particle size of struvite (Expt-2)

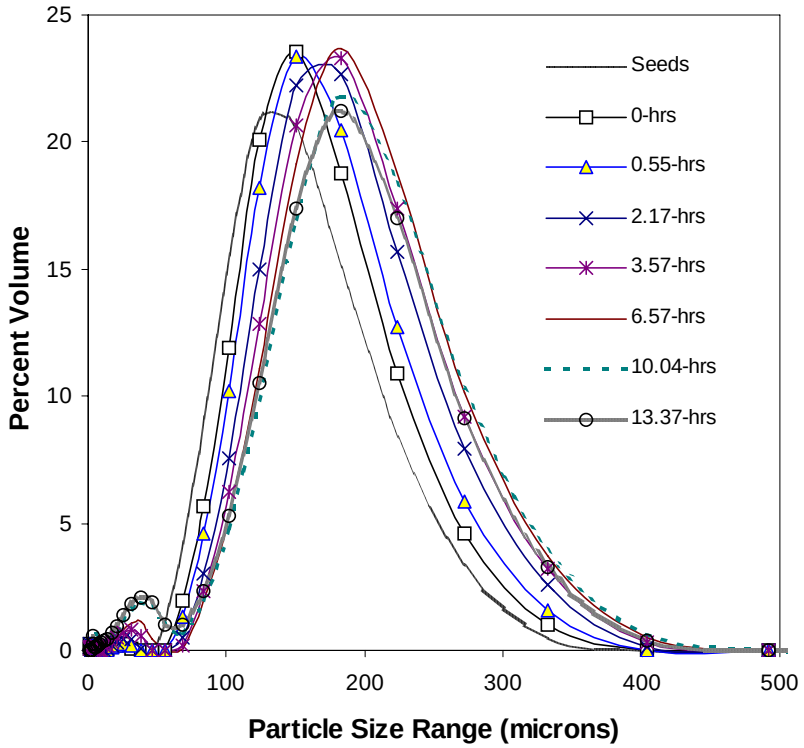

Figure 5. 29 Characterization of mean particle size of struvite (Expt-3)

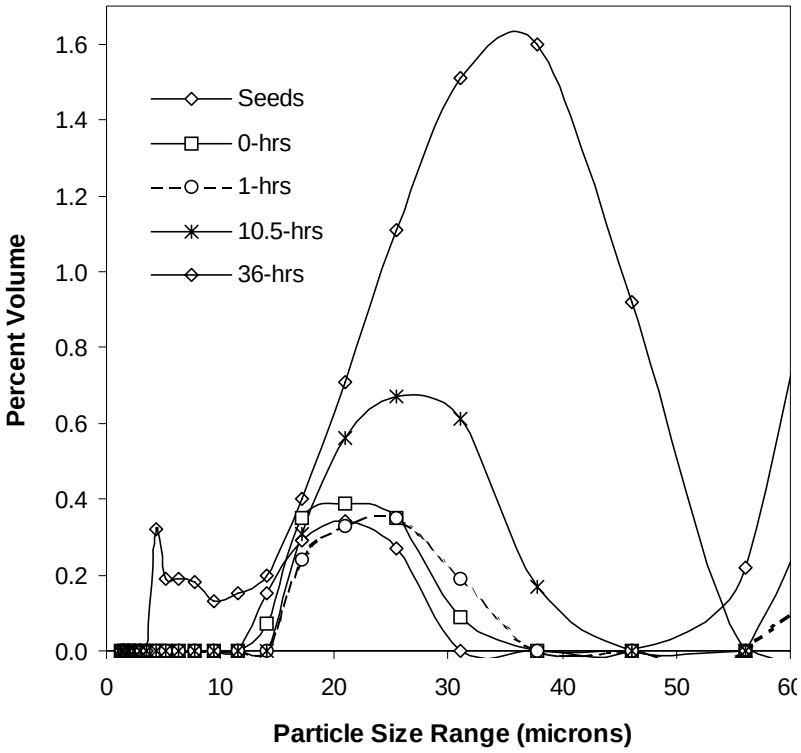

Figure 5. 30 Characterization of fines during crystallization (Expt- 2)

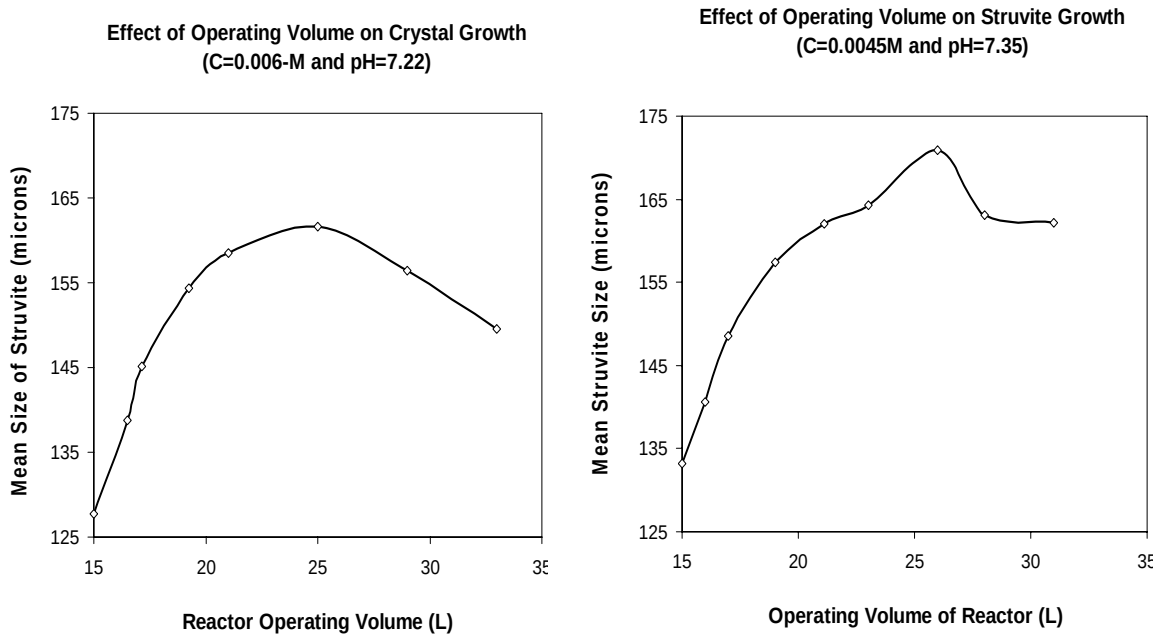

Figure 5. 31 Effect of reactive solution volume on the mean particle size of struvite

5.9 Yield Analysis

The yield analysis of produced struvite mass in fed-batch controlled (constant) supersaturation system involved some difficulties, as described below.

- Difficulties in handling large volumes of reactive solution during the separation of crystal from solution.
- Due to the controlled fed-batch crystallization, reactive solution concentration remained constant. Therefore, a yield analysis using desupersaturation data is not applicable.

At the first step of yield analysis, the reactive solution was filtered using ASTM standard sieve of 105 μm after each fed-batch experiment. Wet sieving was employed to separate crystals (>105 μm) from solution. Subsequent to the separation of crystals from crystal slurry, further separation of fines was required using mild alkaline water (pH = 8.5) to avoid any dissolution of crystal (struvite) during wet sieving. Air-drying was employed for 7 days to remove surface moisture from crystal surface. Dry struvite was weighed using an electronic balance. The recovered dry weight of crystals (>105 μm) were 98, 70.32 and 110 g for experiment 1, experiment 2 and experiment 3, respectively (Table 5.5). In each experiment, the fraction of total struvite mass retained on 105μm sieve was generated by the growth of seeds, whereas the fraction of total struvite mass that passed through the sieve of 105 μm was likely to be generated by nucleation and/or breakage. It is worthwhile noting out that ASTM standard sieve of 105-150 μm were used to separate size-classified seed, which was used in the pilot scale experiments.

The filtered solution was kept in a large container for 24 hours to let the fines settle at the bottom. Fine crystals, setteled at the bottom, were filtered using 0.45 μm Whatmann

filter papar. Subsequent to filtration, fine crystals were air-dried for 7 days and weighed using electronic balance. The measured mass of fines were 42.1, 25.13 and 57.28 g for experiments 1, 2 and 3, respectively. Therefore, the total mass of the recovered struvite (fines + growing struvite) were 140.1, 95.45, 167.28 g for experiments 1, 2 and 3, respectively.

Assume that the equimolar concentration of the reactive magnesium, ammonium and phosphate is x_1 and the volume of solution after experiment is v_1. Referring to the Section 5.5.2, deposited mass of struvite due to feed addition (M) can be calculated by the equation (5.21), provided that W_s is the gram molecular weight of struvite and M_s is the mass of seed employed in each experiment.

$$M = x_1 v_1 W_s + M_s \quad \textbf{(5. 21)}$$

The theoretical total mass of struvite deposition is equal to the accumulated mass of seeds and newly added struvite due to crystallization, which are calculated (equation 5.26) as 143, 96.15 and 171.12 g for experiment-1, 2 and 3, respectively, given the mass of seeds (M_s) is 30 g. Recovered mass of struvite (>105 μm) is 68.5%, 73.15% and 64.28%, for experiment 1, 2 and 3, respectively. Approximately 31.5%, 26.85% and 35.72% losses of produced struvite mass are occurred for experiments 1, 2 and 3, respectively. The losses of recovered mass are due to the presence of struvite particles smaller than 105 μm, which were occurred due to the production of fines by nucleation and/or breakage incident during crystallization. Please note that ASTM standard sieve of 105 μm was used to separate crystals from solution.

The yield analysis concludes that controlled supersaturation favors the growth of struvite by reducing nucleation, since 70% of the recovered product possesses good quality in terms of size. In commercial application, the controlled supersaturation technique can play an important role where the size of struvite crystal is an important criterion for commercial value.

Table 5. 5 Yield analysis of the fed-batch controlled experiment (expt 1, 2 and 3 as mentioned in the previous sections)

Expt. Number	Reactive solution concentration (M)	Concentration of $Mg/NH_4/PO_4$ in feed (M)	Total added volume of feed (L)	Volume of titrant-1/titrant-2 (g)	Mass of seeds used (g)	Total mass of seeds (Larger than mean size of seed) after expt. (g)	Total mass to be recovered for perfect growth (g)	Percentage recovered (Larger than mean size of seed)
1	0.0055	0.066	14	7	30	98.00	143.0	68.5
2	0.0045	0.054	10	5	30	70.32	96.15	73.15
3	0.0060	0,072	16	8	30	110.0	171.12	64.28

5.10 Discussion

This chapter discussed the controlled struvite crystallization in pilot scale to identify struvite growth kinetics. The strategy of controlled struvite crystallization was demonstrated previously in small scale of 250 ml (Bouropoulos and Koutsoukos 2000). This research incorporated the scale up of controlled struvite crystallization system in pilot scale of 44-litres, maintaining constant experimental concentration (magnesium, ammonium and phosphate) and constant operating pH. The design scheme included the identification of suitable seed, determination of optimum crystallization limit using metastable zone technique and the establishment of control strategy. A set of fed-batch controlled experiments was conducted to identify struvite growth.

Experiments conducted with different types of seed material shows that parent seed (struvite) have a catalyzing effect on struvite growth due to the efficient diffusion-integration of crystal clusters and solute molecules (magnesium, ammonium and phosphate ions). Efficient seeding is already a well-established areas (Mersmann 2001), however, no such observation relating to struvite is available in the literature.

Based on the thermodynamic modeling and experimental observation, this research incorporated the estimation of the metastable zone for struvite crystallization. Identification of the metastable supersaturation zone provided a better understanding of the required optimum supersaturation to maintain efficient crystal growth. This technique is well documented in the literature (Mullin 1993; Hirasawa 1996; Mersmann 2001) for the other types of crystallization. This research adopted the general phenomena of metastable supersaturation and applied this for struvite crystallization. To conduct this observation, this research incorporated thermodynamic modeling using

PHREEQC, gPRMOS coding and the existing solubility limit results (Ohlinger 1999) to identify the saturation limit. Laser scattering, using a set of batch experiments, identified the minimum limit of spontaneous nucleation. The area between the saturation limit and minimum limit of spontaneous precipitation is the metastable zone. For further experimental observations in the pilot scale, the crystallizer was operated in the metastable zone providing safe distance from the labile supersaturation.

This research adopted the concept of Bouropoulos and Koutsoukos (2000) to establish the control strategy of constant supersaturation. However, the main flaw of the existing concept by Bouropoulos and Koutsoukos (2000) is the incorrect presentation of the feed stoichiometry, as shown in equations (5.22) and (5.23).

$$x_2 = 10 + 2x_1 \quad \textbf{(5. 22)}$$

$$x_3 = 20 - 2x_1 \quad \textbf{(5. 23)}$$

Where

x_1 is the molar concentration of reactive solution (magnesium, ammonium and phosphate)

x_2 is the feed concentration of magnesium, ammonium and phosphate (M)

x_3 is the NaOH concentration in feed solution (M)

The abovementioned control strategy is not physically and/or stoichiometrically reliable, although, Bouropoulos and Koutsoukos (2000) implemented the correct approach in their experimental design. These textual errors, appeared in Bouropoulos and Koutsoukos (2000) research article, was confirmed by private communication

(Koutsoukos 2004). The present research established the correct strategy of the controlled struvite crystallization, and implemented it successfully in the pilot scale struvite crystallization. This research also showed substantial evidence of reliable experimental operation at pilot scale not previously reported in the literature.

The demonstrated strategy of the controlled supersaturation (in this research) also investigated the combination and mixing of the feed chemicals. This research showed that the feed solution must be split into two portions to avoid any undesired difficulties relating to experimental control. This is a significant contribution to the struvite research, leading to proper crystallizer design. This research also confirmed some other established guidelines, such as, the two dosing points should be positioned away from one another to avoid rapid local fluctuation of supersaturation (Mangin *et al.* 2004).

Rapid precipitation causes the production of fine and reduces crystal growth (Mullin 1993; Mersmann 2001). Therefore, controlled struvite crystallization is a significant contribution to struvite research, which may lead to proper experimental/ industrial design to avoid the production of fines during crystallization.

However, for field effluent this control strategy should be slightly different based on the effluent (different chemical species) and impurities concentration. Observation of the various effluent data shows the reasonably strong concentration of ammonium and the limiting concentration of magnesium and/or phosphate. In the circumstance of limiting magnesium/phosphate concentration, it is probably difficult to recover struvite due to very low supersaturation. Therefore, extra dosing of magnesium and/or phosphate could lead to the increase of supersaturation; therefore, struvite recovery would be

straightforward. However, a crystallizer cascade (Mersmann 2001) should be used in this circumstance, with the first crystallizer operated at controlled supersaturation and second crystallizer operated at uncontrolled supersaturation. In this way, first crystallizer can produce good quality struvite and the second crystallizer can treat effluent, making it safe for charge.

5.11 Chapter Summary

This chapter described the design of the pilot scale struvite crystallization system maintained at controlled supersaturation. The design strategy, described in this chapter, summaries the following key concerns.

- Struvite crystallization, operating at metastable supersaturation, supports heterogeneous nucleation and enhances crystal growth, leading to minimum spontaneous precipitation.
- Proper stoichiometry of feed solution maintains reasonably accurate experimental control of supersaturation.
- Use of air-dried parent crystal (struvite) as seed enhances struvite growth.
- Control of reactive solution temperature is an essential issue for controlled struvite crystallization.

Extensive experimental investigations show that reasonably accurate experimental control can be achieved when the experiment is designed properly as mentioned in the previous paragraph. Good control of supersaturation in struvite crystallization has a potential to enhance struvite growth by minimizing spontaneous precipitation.

The ensemble set of experimental data will be included to estimate kinetic parameters of struvite growth. Detailed simulation results will be discussed in Chapter 6.

CHAPTER 6

RESULTS AND DISCUSSION FROM SIMULATION

6.1 Introduction

Chemical reaction among free ions of magnesium, ammonium and phosphate causes the formation of struvite. Based on the modeling and simulation (Chapter 3) of struvite thermodynamic, kinetic and process, this chapter covers the following two components of struvite crystallization.

- Results of the thermodynamic simulation
- Results of the estimation of struvite growth parameters

Coding and simulation of the struvite thermodynamic equilibria using gPROMS provides a detailed insight of struvite solution chemistry. For the simulation of thermodynamic modeling, piggery effluent pond data is used as the model input. Based on the simulation response, detailed results of thermodynamic simulation will be discussed in Sections 6.2 and 6.3. With the given effluent concentrations (Table 6.1), the validation of solution speciation results (using gPROMS coding and simulation) was conducted by vMinteq (visual Minteq)[♣] (a specialized thermodynamic modeling package) to identify the acceptability of the developed thermodynamic model.

[♣] A Geochemical Assessment Model for Environmental System, U.S EPA National Exposure Research Laboratory, HydroGeoLogic Inc, Herndon, Virginia

The coding and simulation of struvite thermodynamic equilibria and the kinetics of struvite growth, along with the process modeling of struvite crystallization, allow the estimation of struvite growth parameters. A set of experimental data, conducted in a fed-batch, supersaturation controlled system, is included to solve the kinetic model using gPROMS process software. The detailed results of parameter estimation are presented in Sections 6.5 to 6.8.

6.2 Solution Chemistry of Struvite

Thermodynamic model predictions were made for the Cabarlah Park primary pond data, investigated by Queensland DPI. The concentration of magnesium, ammonium and phosphate of the Cabarlah Park primary pond effluent is shown in Table 6.1.

Table 6. 1 Pond data of magnesium, ammonium and phosphate (Hudson 2003)

THIS TABLE HAS BEEN REMOVED DUE TO COPYRIGHT RESTRICTIONS

Based on the simulation results using gPROMS, Figure 6.1 describes the ionization fraction at the given concentrations of nutrients. The computed value of the ionization fraction is a relative expression of the specified free ion concentration with respect to total concentration (Ohlinger 1999). An ionization fraction equal to one indicates the fully ionized form of the chemical species without forming any complexes (Snoeyink and Jenkins 1980). The thermodynamic simulation (using gPROMS) response of ionization fraction shows the stability of free Mg^{2+} ion concentration over the pH range

5 to10 (Figure 6.1). The ionization fraction of free PO_4^{3-} ion is very low over the specified range of pH 5 - 10, and increases with the increase of solution pH (Figure 6.1). Figure 6.1 also shows that free NH_4^+ ions are readily available $\left(\alpha_{NH_4^+} \approx 1\right)$ over the lower range of pH (pH<8), which, however decreases rapidly with the increase of pH value above 9.0. The model response of free Mg^{2+}, NH_4^+ and PO_4^{3-} ion concentrations over the pH range 5- 14 are shown in Appendix J (Table J.1).

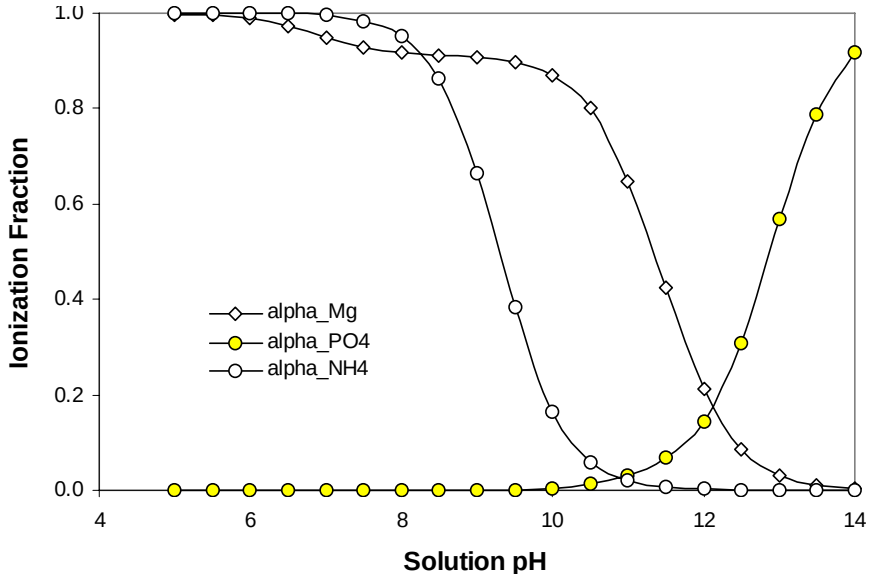

Figure 6. 1 Ionization fraction of fundamental struvite components (Mg^{2+}, NH_4^+, PO_4^{3-})

The ionic interactions between Mg^{2+} and the different PO_4^{3-} complexes (PO_4^{3-}, HPO_4^{2-} and $H_2PO_4^-$) cause the formation of magnesium phosphate ion ($MgPO_4^-$), aqueous magnesium mono-hydrogen phosphate ($MgHPO_4$) and magnesium di-hydrogen phosphate ($MgH_2PO_4^+$). The rest of the total magnesium remains as free Mg^{2+}. Figure 6.2 shows the log concentration of different magnesium and magnesium-phosphate complexes over the pH range 5 to 14. The ionization fraction of magnesium in Figure 6.1 also confirms this tendency shown in Figure 6.2. Therefore, in comparison to free

Mg^{2+} ions, small amounts of magnesium remain as magnesium-phosphate complexes. At higher pH (above 10.5) most of the total magnesium forms $MgOH^{+}$ complex. A validation of the model response for magnesium/ magnesium-phosphate complexes is made using vMinteq (a specialized thermodynamic modeling package). Very close similarities have been observed of the thermodynamic responses between gPROMS output and vMinteq output, which shows the acceptability of the thermodynamic modeling using gPROMS process simulation software. A small dissimilarity of $MgH_2PO_4^{+}$ responses between vMinteq and the developed thermodynamic model output occurred most likely due to the small differences of equilibrium constants and the relevant formation and/or dissolution equations along with the corresponding formation/dissolution ions (Childs 1970, Taylor *et al.* 1963, Morel and Hering 1993, Martell and Smith 1989, Allison *et al.* 1991). The Minteq database MINTEQA2 (V 4.0) was used to make this comparison (Allison *et al.* 1991).

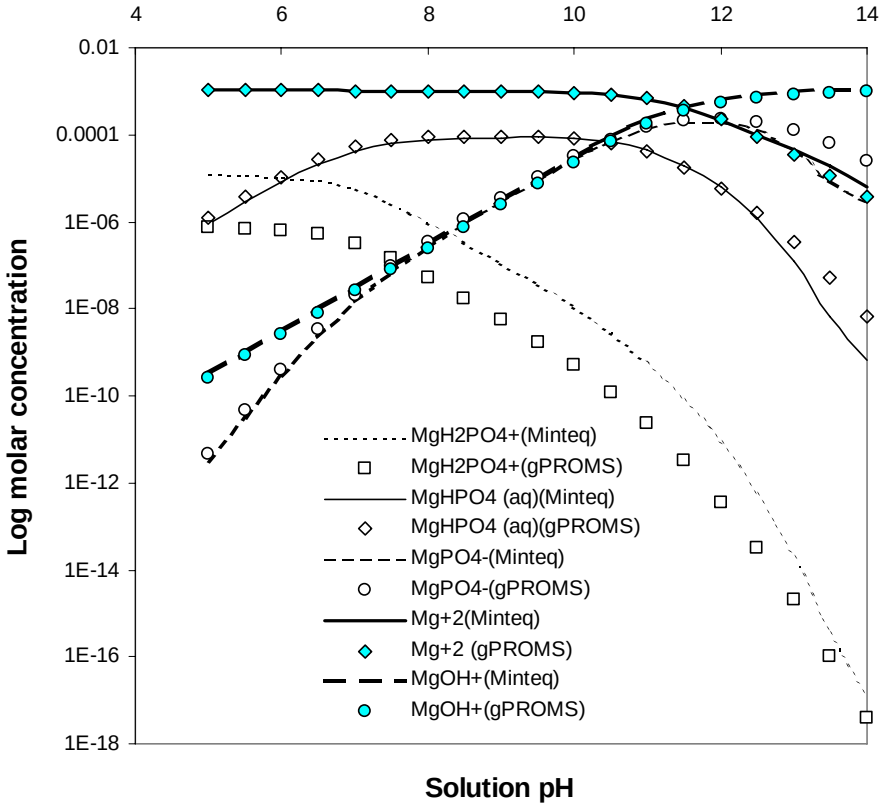

Figure 6. 2 Presence of different magnesium complexes in struvite system

Over the range of pH<10, the free PO_4^{3-} ion concentration is reasonably small when compared to Mg^{2+} ion (Figure 6.1 and Appendix J; Table J.2), since the major portion of phosphate remains as $MgPO_4^-$, $MgHPO_4$ (aq), $MgH_2PO_4^+$, $H_2PO_4^-$, H_3PO_4 and HPO_4^{2-} (Figures 6.2 and 6.3). However, above pH 10.5, the concentration of free PO_4^{3-} increases considerably due to the de-protonation of HPO_4^{2-}, $H_2PO_4^-$ and H_3PO_4 as described in the equation 3.27 in Chapter 3 (Seckler and Bruinsma 1996).

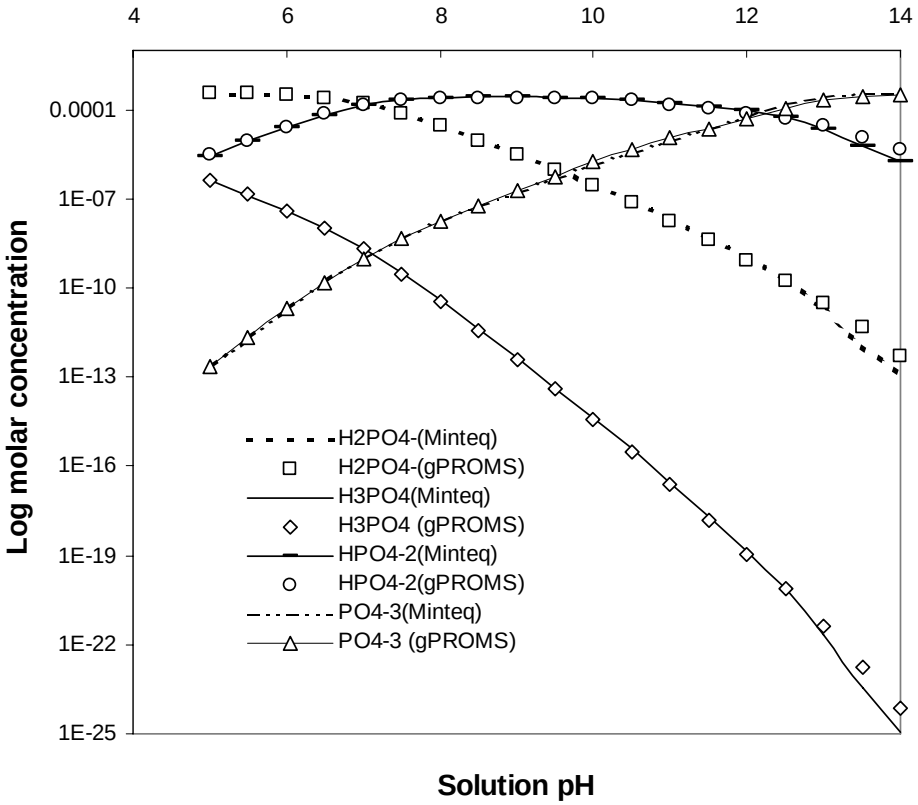

Figure 6. 3 Presence of different phosphate complexes in struvite system

With the given concentration (Table 6.1), the thermodynamic simulation results show that the major portion of total ammonium remains as free NH_4^+ ions below pH 8.5 (Figure 6.4), and decreases rapidly due to the transformation of NH_4^+ to NH_3 in the alkaline phase.

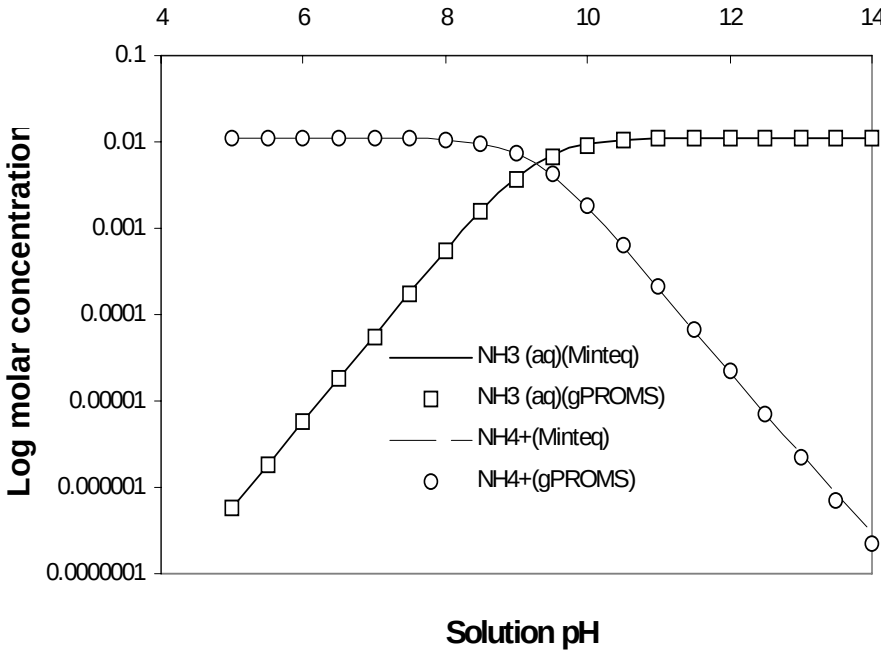

Figure 6. 4 Presence of different ammonium states in struvite system

The minimum solubility (saturated condition) of struvite occurs when the product of the ionization fractions are maximized (Snoeyink and Jenkins 1980). As shown in Figure 6.1, the ionization fractions of magnesium $\left(\alpha_{Mg^{2+}}\right)$, ammonium $\left(\alpha_{NH_4^+}\right)$ and phosphate $\left(\alpha_{PO_4^{3-}}\right)$ are a function of solution pH. The ionization fractions of magnesium and ammonium decrease with the increase of solution pH, and the ionization fraction of phosphate increases with the increase of solution pH. At a certain point of pH, the product of ionization fractions of magnesium ammonium and phosphate $\left(\alpha_{Mg^{2+}}\alpha_{NH_4^+}\alpha_{PO_4^{3-}}\right)$ approaches a maximum value, leading to the occurrence of the minimum conditional solubility product. With the concentrations given in Table 6.1, the minimum conditional solubility occurs at pH of about 10 (Figure 6.5). The computed concentration product of magnesium, ammonium and phosphate (P_{so}) exceeds the conditional solubility product (P_{cs}) at pH of about 8.1 and remains higher until the pH is about 12.1. Therefore, with the given solution concentration

indicated in Table 6.1, struvite precipitation is likely over the pH range 8.1 to 12.1, since the solution remains in supersaturated condition (Figure 6.6).

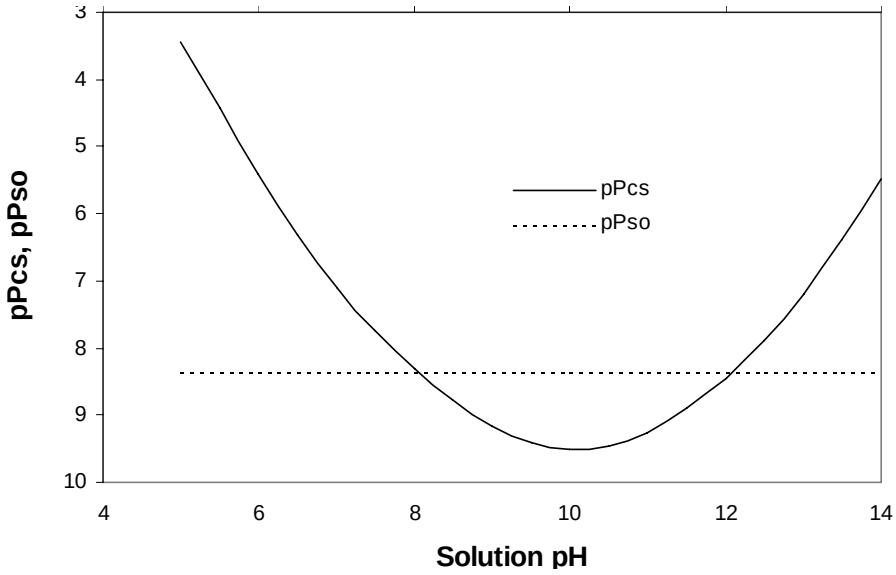

Figure 6. 5 Comparison of solubility products at different pH value

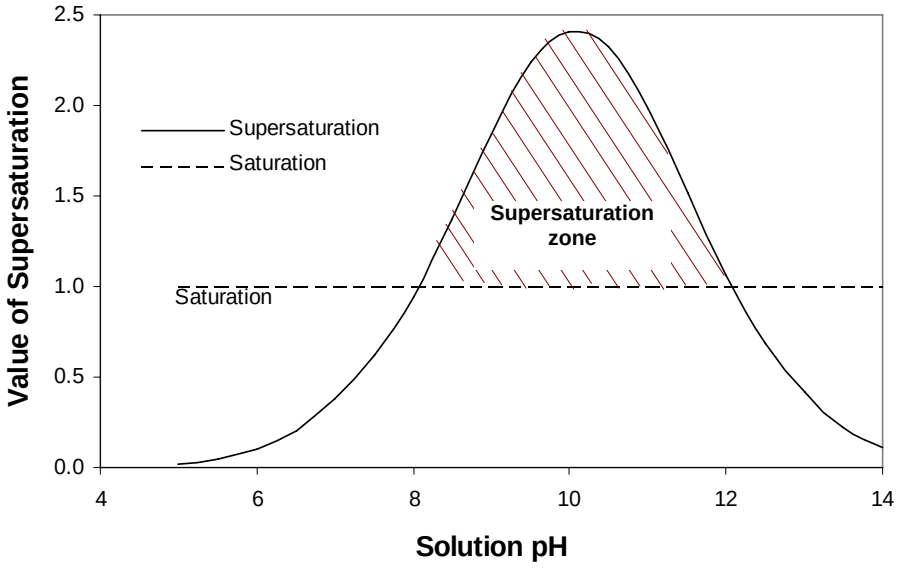

Figure 6. 6 Solution saturation at different pH value (based on the critical supersaturation ratio, S_c)

For the additional chemical species of the pond data (Chapter 2: Table 2.1), an extension to the gPROMS coding and simulation must be made. For example, addition of calcium in the gPROMS coding and simulation must incorporate the relevant thermodynamic equilibria between Ca^{2+} and PO_4^{3-} along with existing thermodynamic model.

6.3 Sensitivity of Supersaturation due to Solution Concentration

The previous section shows that solution supersaturation depends on reactant concentrations and pH. This section presents the sensitivity of the solution supersaturation (based on the critical supersaturation ratio, S_c), using different magnesium, ammonium and phosphate concentrations.

Table 6. 2 Input concentration for the sensitivity study

Cases	Total NH_4^+ (mg/l)	Total Mg^{2+} (mg/l)	Total PO_4^{3-} (mg/l)
1	199.7	26	34.1
2	199.7	***52***	34.1
3	199.7	26	***68.2***
4	***399.4***	26	34.1

Case 1 is the base case, with a concentration (Table 6.1) of magnesium, ammonium and phosphate, Case 2 uses double the magnesium concentration, Case 3 uses double the phosphate concentration and Case 4 uses double the ammonium concentration. Table 6.2 shows the concentration of magnesium, ammonium and phosphate used in this sensitivity study.

Figure 6.7 show that supersaturation increases when the concentrations of magnesium, ammonium and phosphate increase. The sensitivity of supersaturation due to each solution species shows that supersaturation of solution and the relevant reaction depends on each relevant solution species. The continuous surge and/or decline of effluent concentrations (magnesium, ammonium and phosphate) in any nutrient rich effluent stream/nutrient rich wastewater treatment plant, is a practical example of this, where the change in concentration often results in a change in the solution saturation levels.

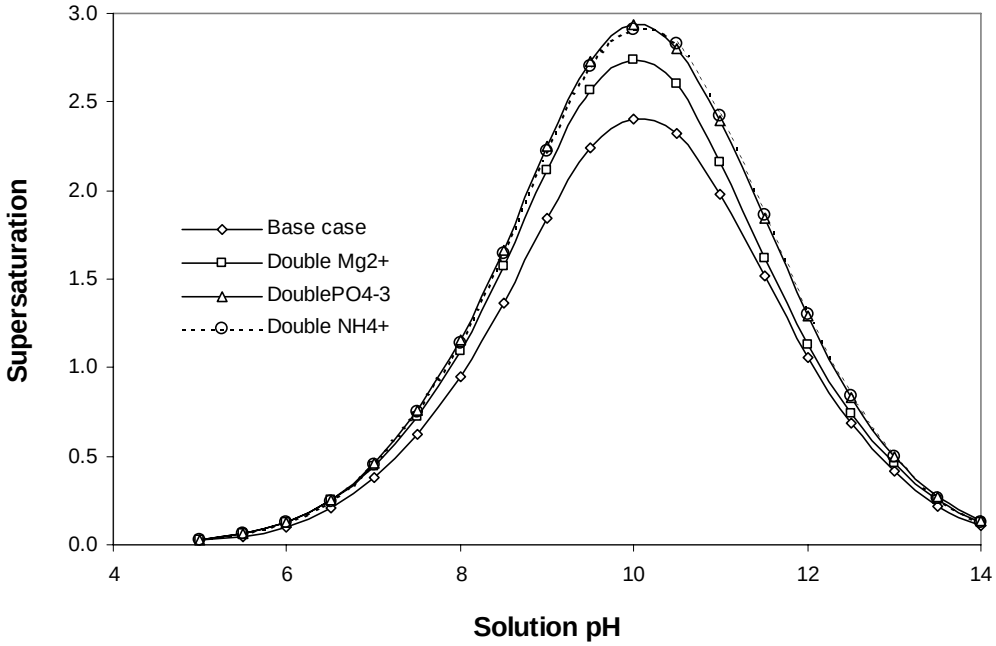

Figure 6. 7 Sensitivity of the critical supersaturation ratio to Mg^{2+}, NH_4^+ and PO_4^{3-} concentration

6.4 Parameter Estimation Modeling

The kinetic equation of struvite growth incorporates a mathematical relation between the increase of mean struvite crystal size and the solution supersaturation. The detailed description of the struvite growth model, incorporating the solution thermodynamic, kinetic of struvite growth and the mathematical description of struvite process model, was presented in Chapter 3. As shown in Chapter 3, supersaturation of solution is

computed in terms of oversaturation (relative supersaturation, S); however, Saturation Index (SI) is also included in the growth model.

The growth model of struvite is estimated (Est.) in six different modes, including **Est.type 1**, **Est.type 2**, **Est.type 3**, **Est.type 4**, **Est.type 5** and **Est.type 6**. The **Est.type 1** to **Est.type 3** employed relative supersaturation (oversaturation, S) to compute solution supersaturation. The simulation **Est.type 4** to **Est.type 6** employed Saturation Index (SI) to enumerate the solution supersaturation.

Est.type 1 was simulated to investigate the struvite growth kinetics incorporating oversaturation as the supersaturation model. The fundamental kinetic equation (Chapter 3, equation 3.43) in this case is described by equation (6.1).

$$\frac{dL}{dt} = KS^{n} \qquad \textbf{(6. 1)}$$

Est.type 2 incorporated an additional variable, i.e. crystal size (L), in the fundamental kinetic equation (Chapter 3, equation 3.45) to identify the effect of crystal size on struvite growth kinetic. In this case, the kinetic equation can be described by equation (6.2).

$$\frac{dL}{dt} = KS^{n} L^{n_1} \qquad \textbf{(6. 2)}$$

Est.type 3 incorporated the initial seed size (L_0) as an additional parameter to be estimated along with the fundamental growth parameters (K and n). The fundamental

growth equation is equivalent to equation (6.1). This approach is particularly important, since the size of seed is unknown at the beginning of experiment.

Est.type 4 incorporated Saturation Index (SI) into the struvite growth kinetic model. In this case, the fundamental growth model can be described by equation (6.3). Saturation Indices (SI) in equations (6.3) and (6.4) and the relevant estimations in **Est.types 4** to **6** are represented as S_i.

$$\frac{dL}{dt} = KS_i^{\,n} \qquad \textbf{(6. 3)}$$

Est.type 5 incorporated an additional variable, i.e. crystal size (L), in the kinetic equation (6.3) to identify the effect of crystal size on struvite growth kinetics. In this case, the struvite growth kinetic can be described by equation (6.4).

$$\frac{dL}{dt} = KS_i^{\,n} L^{n_1} \qquad \textbf{(6. 4)}$$

Est.type 6 included an additional variable (crystal size, L) to be estimated. This approach is similar to **Est.type 3**, however, supersaturation was computed in terms of Saturation Index (SI).

Based on the above discussions, the summary of parameter estimation approach is presented in Table 6.3.

Table 6. 3 Summary of parameter estimation approach

Parameter Set	Supersaturation Model			
	Oversaturation (S)		Saturation Index (S_i)	
K, n	Est.type 1	$\frac{dL}{dt} = KS^n$	Est.type 4	$\frac{dL}{dt} = KS_i^n$
K, n, n_1	Est.type 2	$\frac{dL}{dt} = KS^n L^{n_1}$	Est.type 5	$\frac{dL}{dt} = KS_i^n L^{n_1}$
K, n, L_0	Est.type 3	$\frac{dL}{dt} = KS^n$	Est.type 6	$\frac{dL}{dt} = KS_i^n$

Notes: K = Growth rate constant (µm/h), n = Growth order due to supersaturation, n_1 = Growth order due to particle size, Est.type = Identification of parameter estimation models

6.5 Est.type 1

Parameter estimation of a process is conducted by the real time parameter estimation and the offline parameter estimation method (Mendel 1973). The following sections describe the offline parameter estimation for struvite growth kinetics to provide the best fit of the measured and predicted data using the maximum likelihood method. Objective function is associated with this estimation problem. In general, struvite growth kinetics (Chapter 3) relating to the parameter estimation modeling can be described by equation (6.5).

$$f\left(x(t), \dot{x}(t), y(t), u(t), \theta\right) = \boldsymbol{0} \qquad \textbf{(6. 5)}$$

Where

$x(t)$ Differential variables, *i.e.* Crystal size (L) in µm, Mass of crystals (M) in grams, Reactive solution concentration (C_i) in mg/l, and Operational volume of the reactor (V) in liter

$y(t)$ Algebraic variables, *i.e.* pH, Feed concentration ($C_{i,\,in}$, C_{NaOH}) in mg/l,

Supersaturation (S)

$\dot{x}(t)$ Time derivative of the differential variables, *i.e.* dL/dt, dMg/dt, dPO_4/dt, dNH_4/dt, dM/dt and dV/dt

$u(t)$ Time varying control variables, *i.e.* NaOH feed rate in l/h (F_{NaOH}) and the Reactant feed rate in l/h (F_i)

θ Estimated parameters, *i.e.* $\boldsymbol{K}$ (µm/h) and $\boldsymbol{n}$

For the purposes of parameter estimation, the initial conditions of the equation (6.5) are defined in terms of the initial values of the differential variables, *i.e.* L(0), M(0), V(0) and $C_i(0)$, as shown in the equation (6.6).

$$Subset\{L(\boldsymbol{0}), M(\boldsymbol{0}), V(\boldsymbol{0}), C_i(\boldsymbol{0})\} = q \quad \textbf{(6. 6)}$$

Where, the value of component L(0) in the subset *q* is the initial crystal size, *i.e.* 140.06, 138.83 and 133.25 µm for experiments 1, 2 and 3, respectively. The initial mass of struvite, M(0), in the Subset *q* is equal to 30 g. The measured initial volume V(0) and the initial reactant concentrations, $C_i(0)$, are given in the Table 6.4.

The control variables are the flow-rate (l/h) of the reactant feed (F_i) and the NaOH feed (F_{NaOH}). Experimental data employed in the parameter estimation are the total concentration of Mg^{2+}, NH_4^+ and PO_4^{3-} along with the mean crystal size (L). The general mathematical form of the experimental data in this modeling is as follows.

$$\left(t_{ijk}, \tilde{z}_{ijk}\right) \quad \textbf{(6. 7)}$$

Where, $\tilde{z}_{ijk}$ is the k[th] value measured for variable z_j (Mg, NH_4 and PO_4 and L) during experiment i (i = 3), t_{ijk} is the time at which the measurement is taken. Detailed descriptions of the experimental data formation in the simulation are available in Appendices B and C.

Table 6. 4 Initial conditions of the solution concentration and reactor volume

Expt. No	C_{Mg} (mg/l)	C_{PO4} (mg/l)	C_{NH4} (mg/l)	V (liter)
1	108	487.25	92.32	16.0
2	165	594.52	112.64	16.5
3	147	594.52	112.64	16.8

The maximum likelihood method was used for the parameter estimation modeling. The maximum likelihood objective function associated with the parameter estimation can be described by equation (6.8) (gPROMS 2002a). Maximum likelihood method of parameter estimation is applied in this research due to its unbiased estimation properties and efficiency in handling both large and small data (Draper and Smith 1966).

$$\Phi = \frac{N}{2}\ln(2\pi) + \frac{1}{2}\min_{\theta}\left\{\sum_{i=1}^{NE}\sum_{j=1}^{NV_i}\sum_{k=1}^{NM_{ij}}\left[\ln\left(\sigma^2_{ijk} + \frac{\left(\tilde{z}_{ijk} - z_{ijk}\right)^2}{\sigma^2_{ijk}}\right)\right]\right\} \qquad \textbf{(6. 8)}$$

Where,

N = Total number of measurements taken during all experiments

θ = A set of model parameters to be estimated (***K*** and ***n***). The acceptable values may be subject to given lower and upper bounds, i.e. $\theta_L \le \theta \le \theta_U$

NE = Number of experiments performed

NV_i = Number of variables measured in the $\boldsymbol{i}^{th}$ experiment. The measured experimental variables are the total concentration of Mg^{2+}, NH_4^+, PO_4^{3-} and the mean size of the growing crystals *(L)*

NM_{ij} = Number of measurements of the $\boldsymbol{j}^{th}$ variables in the $\boldsymbol{i}^{\text{th}}$ experiment.

σ^2_{ijk} = Variance of the $\boldsymbol{k}^{th}$ measurement of variable *j* in the experiment i, i.e. variance of the Mg^{2+}, NH_4^+, PO_4^{3-} concentrations and mean crystal size (*L)* in each specified experiments.

$\tilde{z}_{ijk}$ = $\boldsymbol{k}^{th}$ measured value of variable *j* (Mg^{2+}, NH_4^+, PO_4^{3-}) in the experiment *i* *(i = 3)*

z_{ijk} = $\boldsymbol{k}^{th}$ model-predicted value of variable *j* in the experiment *i*.

The parameter estimation method employed includes different types of estimation procedure including the Constant Variance Model, Heteroscedastic Predicted/Measured Value Model, and the Least Square Model (gPROMS 2002a). This research incorporates the Heteroscedastic Predicted Value variance model to estimate the struvite growth kinetics. Based on the Heteroscedastic Predicted Value variance model, the measurement error is proportional to $z^{x/2}$ and the variance model description is as follows (equation 6.9).

$$\sigma^2 = \omega^2 \left(z^2 + \varepsilon\right)^x \qquad \textbf{(6. 9)}$$

Where,

σ^2 = Variance, which depends on the measured and predicted value of C_i, *L*, *K* and *n*.

ω = Standard deviation

x = A parameter employed to optimize the function (maximum value = 1)

ε = Absolute tolerance, which depends on the equation solver

z = Predicted value of the experimental variable

The process model described in the Chapter 3 and in general in equation (6.5) is developed in sequence, which includes the following steps:

1. Derivation of process dynamics (Chapter 3), which include material and population balances of struvite incorporating the solution thermodynamics and process kinetics.
2. Coding of the struvite process model, using gPROMS process simulation software.
3. Pre-designing of the experiment, which ascertains the solution's supersolubility. Pre-determination of the solution's supersolubility assists in conducting experiments across the wide range of solution concentration and pH.
4. Based on the experimental design (Chapter 4), fed-batch experiments were conducted in controlled supersaturation mode. These experiments provide the required data for the model input, which incorporates the CSD of growing struvite *(L)*, dynamic feed rate *(F_i, F_{NaOH})*, dynamic reactant concentration *(C_{Mg}, C_{NH4}, C_{PO4})* and experimental pH value.
5. Simulation of the parameter estimation model and investigation of its reliability based on statistical analysis.

The simulation of the model incorporates experimental and theoretical data. Assigned parameters, representing the fixed values of the model input are stated as SET value in the process entity. The defined parameters are the electron charge of struvite

components *(Z_i)*, density of struvite (g/cm^3), gram molecular weight of struvite, pH value of experiments, mass of seeds (g), NaOH feed (l/h) and pH values of reactant feeds.

The degrees of freedom in the simulation must be zero for successful model execution. To provide this necessary condition, underspecified variables are stated as ASSIGNED variables. The assigned variables act as model inputs, which include reactant concentrations of the feed solutions in mg/l, preliminary settings of feed rate in l/h and the assumed values of the estimated parameters (***K*** and ***n***). Specifying these variables provides the square system of the coding and permits the solution of equations (gPROMS 2002a).

The parameter estimation model automatically omits scheduling of the process and hence it is not necessary to include this section. *Scheduling* of a system in gPROMS coding is subject to the externally imposed manipulation, such as control action, disturbances and discontinuities and the duration of the process operation. In the parameter estimation modeling, the duration of the process is already stated in the experimental sections; therefore process simulation automatically omits the scheduling section (gPROMS 2002).

6.5.1 Results of Parameter Estimation Model (Est.type 1)

The parameter estimation model was simulated under the given experimental conditions, using the collected experimental data of solution concentrations *(C_{Mg}, C_{NH4}, C_{PO4})*, growing struvite crystal size *(L)* and controlled feed rate *(F_i and F_{NaOH})* to estimate the growth parameters ***K*** and ***n***.

The kinetic response of struvite growth model shows a value of growth order *(n)* equal to 1.48±0.162 and growth rate constant *(K)* equal to 46.64±8.06 (μm/h). Based on the estimated values of kinetic parameters (*K* and *n*), the struvite growth model can be described by equation (6.10), given that ***S*** is the relative supersaturation (oversaturation).

$$\frac{dL}{dt} = (\boldsymbol{46.64 \pm 8.026})S^{\boldsymbol{1.48\pm0.162}} \qquad \textbf{(6. 10)}$$

The overlay charts of experiments 1, 2 and 3 are presented in Figures 6.8 – 6.10. The overlay charts of the struvite growth (Figures 6.8- 6.10) show good agreement between the model-predicted and experimental values. The model-predicted and measured values of struvite growth agree within ±10% deviation (Table 6.5). The overlay charts of total phosphate concentration (Figures 6.8- 6.10) and total magnesium concentration (Figures 6.8- 6.10) also show an acceptable agreement in maintaining the controlled reactive concentration throughout the experimental period.

The model-predicted and measured values of the total reactive phosphate concentration agree within ±20% deviation and most of the predicted total magnesium concentrations agree with the measured total magnesium concentration within ±20% deviation. The percentage deviations of the experimental/predicted variables are calculated using the equation (6.11).

$$\%\ Deviation = \frac{(Experimental\ Measurements - Model\ Predictions)\times 100}{Experimental\ Measurements} \qquad (\textbf{6. 11})$$

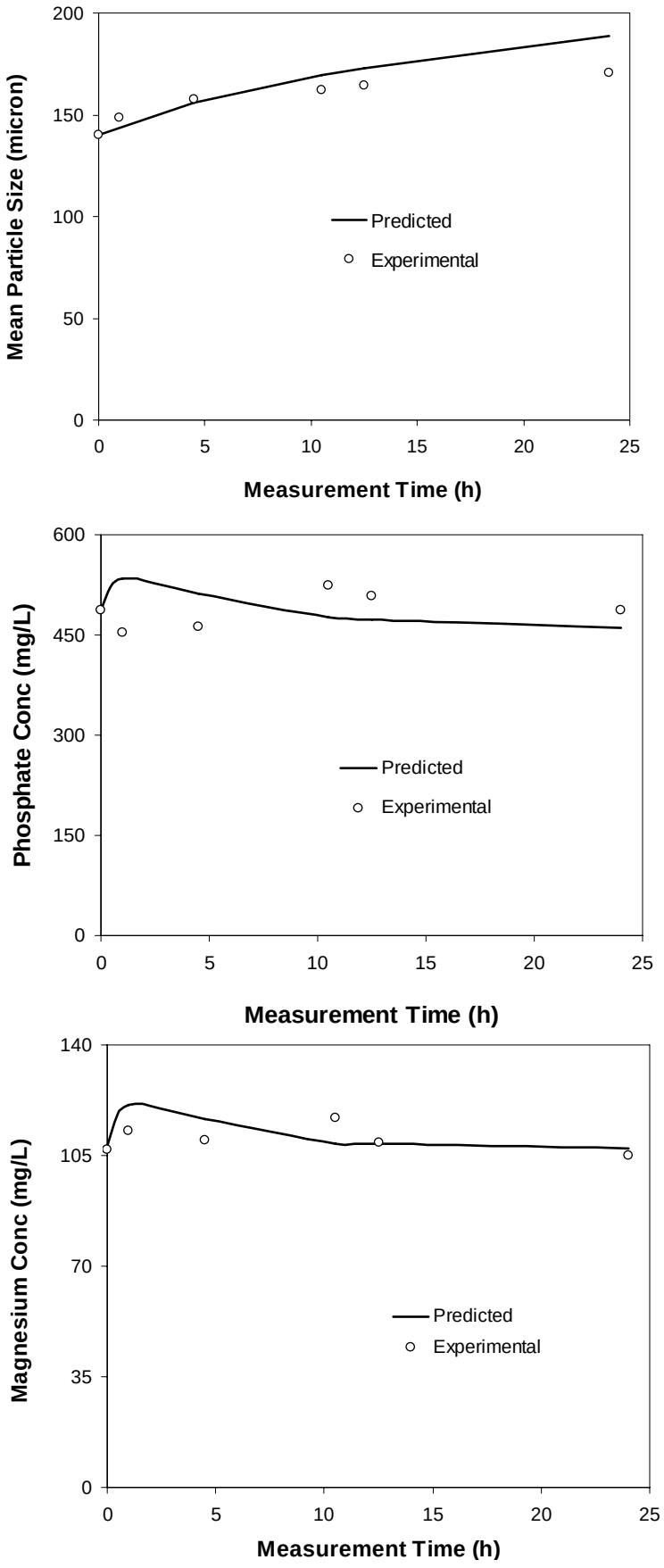

Figure 6. 8 Overlay charts of experiment 1 (Est.type 1)

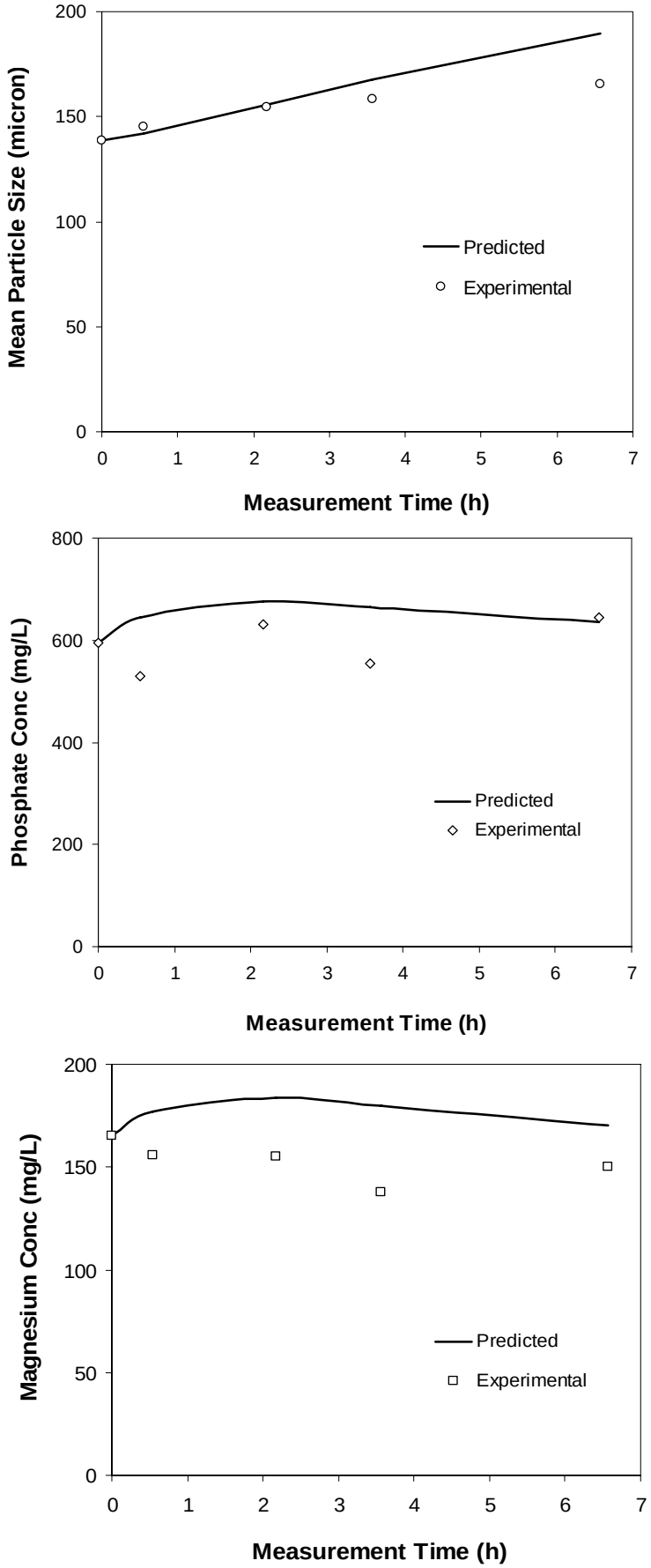

Figure 6. 9 Overlay charts of experiment 2 (Est.type 1)

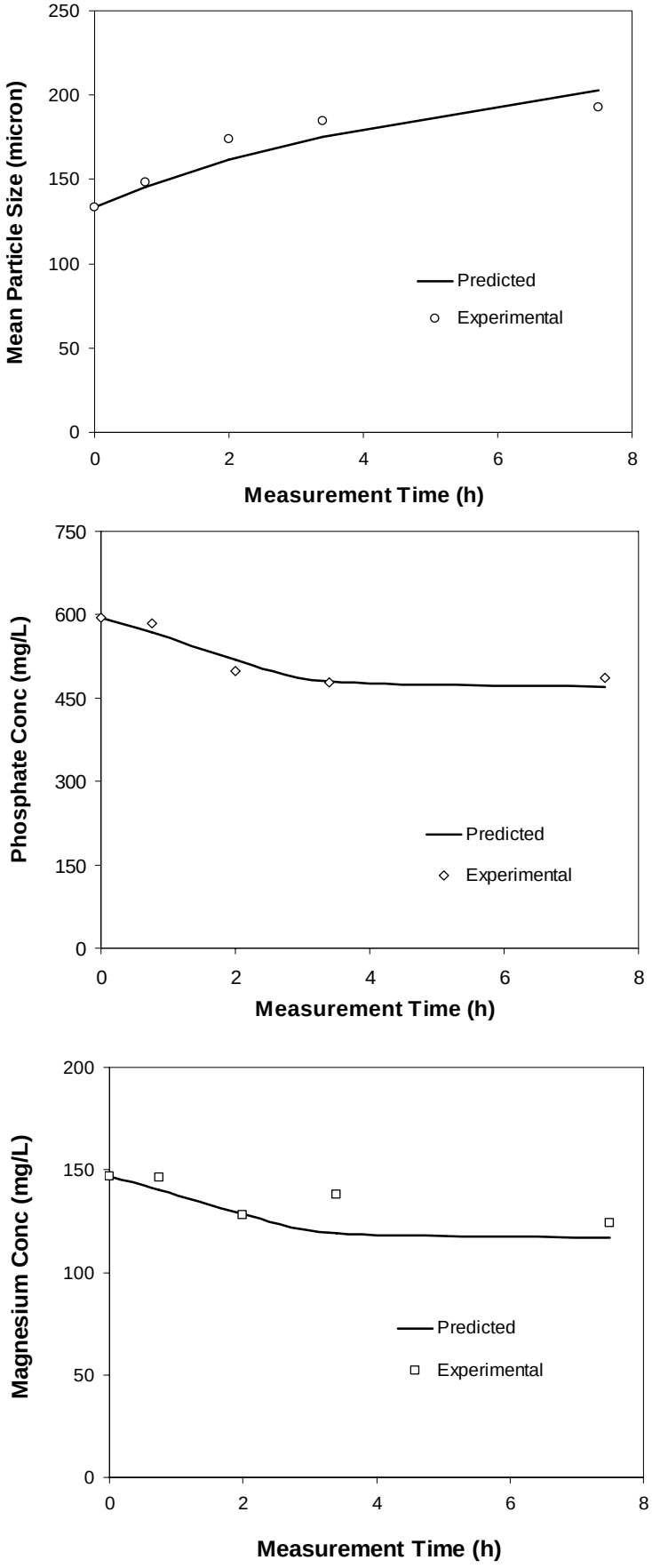

Figure 6. 10 Overlay charts of experiment 3 (Est.type 1)

6.5.2 Error Analysis (Est.type 1)

As described in the previous section, the model predictions for reactive solution concentration and the mean crystal size cover most of the measured data within the specified deviation limit. The individual consistency of the estimated parameters *K* and *n* is evaluated by making a comparison between the associated *t-value* of the estimated parameters and the reference 95% *t-value*. The model response associated the larger 95% *t-values* for estimated parameters *K* and *n* rather than the reference 95% *reference t-value* (Table 6.5), which presents an accurate estimation of the parameters (gPROMS 2002a). Moreover, the standard deviations of *K* and *n* are smaller than the relevant estimated values, which indicates that the estimated values of *K* and *n* are individually consistent (Draper and Smith 1966; Mandel 1984).

Table 6. 5 Major statistical information of the estimated response (Est.type 1)

Parameter	Optimal Estimate	90% CI[♣]	95% CI	99% CI	95% t-value	Standard Deviation
K	46.64	13.64	16.41	22.12	2.84	8.026
n	1.48	0.28	0.33	0.45	4.47	0.162
Reference t-value (95%): 1.70						

The joint statistical significance of the optimized parameters, including growth rate constant (K), growth order (n), standard deviation (ω) and optimization power (γ), are examined using *F-value* test within 95% confidence region. The null hypothesis (H_0) considered in this context is shown in equation (6.12). The notations of variables (6.12) is already presented in equations (3.43), (6.7) and (6.8) and the relevant texts.

[♣] CI refers to Confidence Interval

$$H_0 : K = n = \gamma_{ij} = \omega_{ij} = 0 \qquad \textbf{(6. 12)}$$

Based on the simulation responses, the detailed Fischer information matrix and the computed *F-value* for **Est.type 1** are presented in Appendix K; table K.1. The F-value within 95% confidence region is 1.96. The *critical F-value (F_{crit})* is identified using the function *F(α%, N, N-N_P)* (gPROMS 2002a), given that, N (N=48) is the total number of measurements taken, N_P (N_P=19) is the number of optimized parameters involved in the parameter estimation (Appendix K; Table K.1). The *critical F-value* for F(95%, 48, 29) is approximately 1.73 (Draper and Smith 1966). A smaller *F_{crit}-value* (F_{crit} = 1.73) rather than *F-value* (F-value = 1.96) indicates the rejection of null hypothesis (equation 6.12), therefore, validates the joint statistical significance of the optimized parameters. The detailed description of the parameters involved in the *F-test* is shown Appendix K; table K.1

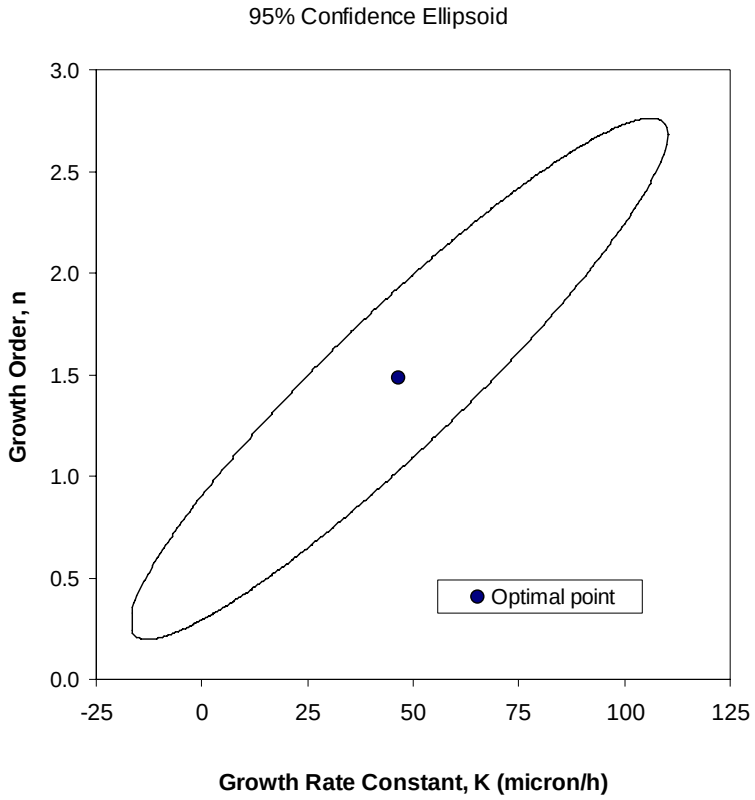

Figure 6. 11 Confidence ellipsoid of the estimated growth parameters

Based on the simulation response, the joint 95% confidence region (Figure 6.11) of the true parameter (*K* and *n*) shows a long thin ellipsoid and their optimized values. Strong positive correlation occurs between the estimated parameters, which means the increase of *K* and *n* values for higher struvite growth rate or *vise versa*.

The deviations between predicted and experimental results occurred (Table 6.6) due to experimental errors. The potential sources of errors are encountered due to the erroneous measurements of solution concentration and mean crystals size as well as faulty sampling and the sluggish responses of pH sensors.

As described previously in this Section, objective function describes the potential error involved in each specified experiment and the relevant experimental variables. Table 6.7 illustrates the objective function contributions to each experimental variable associated in the kinetic parameter estimation. The total objective function contributed at the optimal point is 198.609. The computed objective functions in Table 6.7 show that the experimental data of total phosphate and magnesium concentrations potentially cause larger inaccuracy than the mean crystal size, since the concentration encounters relatively higher objective function at the optimal point of the simulation. The numerical values of objective functions also show that the mean crystal size data causes some errors to this kinetic simulation (Table 6.7).

Table 6. 6 Percentage deviations of the measured and predicted values (Est.type 1)

Measurement Time (h)	Percentage Deviation for L	Percentage Deviation for total PO_4^{3-}	Percentage Deviation for total Mg^{2+}
Experiment-1			
0.00	0.00	0.00	-0.93
1.00	3.48	-17.90	-6.98
4.50	0.78	-10.45	-5.83
10.50	-4.70	9.24	6.99
12.50	-5.29	7.01	0.42
24.00	-10.43	5.40	-1.98
Experiment-2			
0.00	0.00	0.00	0.00
0.55	2.05	-21.51	-13.40
2.17	-0.93	-7.21	-18.46
3.57	-5.88	-19.95	-30.19
6.57	-14.53	1.14	-13.69
Experiment-3			
0.00	0.00	0.00	0.00
0.75	1.91	3.10	3.86
2.00	6.93	-4.10	-0.59
3.40	5.03	-0.63	13.64
7.50	-5.29	3.66	5.83

Table 6. 7 Objective function contributed for parameter estimation (Est.type 1)

Expt.	Variables	Variance Model	Objective Function Contribution
1	L	Heteroscedasticity Predicted Value	15.761
	Total PO_4^{3-}	Heteroscedasticity Predicted Value	25.964
	Total Mg^{2+}	Heteroscedasticity Predicted Value	13.091
2	L	Heteroscedasticity Predicted Value	14.292
	Total PO_4^{3-}	Heteroscedasticity Predicted Value	23.966
	Total Mg^{2+}	Heteroscedasticity Predicted Value	18.748
3	L	Heteroscedasticity Predicted Value	12.872
	Total PO_4^{3-}	Heteroscedasticity Predicted Value	15.972
	Total Mg^{2+}	Heteroscedasticity Predicted Value	13.832
Total Objective Function			*198.609*

6.6 Est.type-2

This section presents the kinetic parameter estimation of struvite growth, incorporating the crystal size effect of the kinetic model. As described in the previous section (section 6.5) this kinetic parameter estimation was conducted by the maximum likelihood method based on the general form of the system (equation 6.5). However, θ is a function of the estimated parameters $\boldsymbol{K}$ $\left(\mu m/hr\right)$, $\boldsymbol{n}$ and $\boldsymbol{n_1}$. Here, $\boldsymbol{K}$ is the struvite growth constant, $\boldsymbol{n}$ is the growth order due to solution supersaturation **(S)** and $\boldsymbol{n_1}$ is the growth order due to the effect of crystal size (L). The objective function associated with the parameter estimation is demonstrated in the equation (6.8) (section 6.5). However, the value of θ is related to the estimated parameters $\boldsymbol{K}$, $\boldsymbol{n}$ and $\boldsymbol{n_1}$. The heteroscedastic

predicted value variance model is employed for this estimation modeling as described in the equation (6.9) and the relevant text.

6.6.1 Results of Parameter Estimation Modeling (Est.type 2)

To identify the effect of mean particle size, the fundamental growth model (chapter 3, equation 3.43) transformed to a new equation (chapter 3, equation 3.45) incorporating the mean particle size *(L)*, and the order of equation due to the mean particle size (n_1). The fundamental growth model is demonstrated in the equation (6.13), and the growth model incorporating the effect of particle size *(L)* along with the relevant growth order (n_1) is demonstrated in equation (6.14).

$$\frac{dL}{dt} = KS^{n} \qquad \textbf{(6. 13)}$$

$$\frac{dL}{dt} = KS^{n} L^{n_1} \qquad \textbf{(6. 14)}$$

The estimation of kinetic parameters of equation (6.14) produced the following values.

$$K = \boldsymbol{27.72 \pm 108.18} \qquad n_1 = \boldsymbol{0.109 \pm 0.89} \qquad n = \boldsymbol{1.52 \pm 0.23}$$

Based on the numerical value of the estimated parameters, the struvite growth model, incorporating the effect of mean particle size, is described in equation (6.15). The order of the equation due to particle size effect (n_1) imparts a smaller value, which confirms the experimental observations that struvite growth is a size independent process within the specified range of crystal size (Chapter 5). However, it is recommended for future

research to test this model over the wider size range of struvite seeds, since the literature suggests a size dependent type of crystal growth for smaller particles (Mullin 1993). Please note that the explanation of the high standard deviations associated with the estimated parameters (K and n_1) is demonstrated in Section 6.6.2.

$$\frac{dL}{dt} = (\boldsymbol{27.83 \pm 108.18}) S^{\boldsymbol{1.52 \pm 0.23}} L^{\boldsymbol{0.109 \pm 0.89}} \qquad \textbf{(6. 15)}$$

The overlay charts of the struvite growth in Figures 6.12 – 6.14 show a reasonable agreement between the model-predicted values and the experimental values within ±10% deviation. The overlay charts of total magnesium and phosphate concentration in Figures 6.12-6.14 also show an acceptable agreement between model predicted and experimental results within ±20% deviation.

The deviations of measured and simulated results are encountered due to experimental and instrumental errors. The experimental errors occurred from the measured data of growing crystal size *(L)*, total magnesium concentrations $\left(C_{Mg^{2+}}\right)$ and total phosphate concentration $\left(C_{PO_4^{3-}}\right)$. The experimental controlled variables, *i.e.* flow-rate of reactant feed (F_i) and NaOH feed (F_{NaOH}), may also contains some error. Table 6.8 shows the values of contributed objective functions in each experimental variable associated with the kinetic estimation.

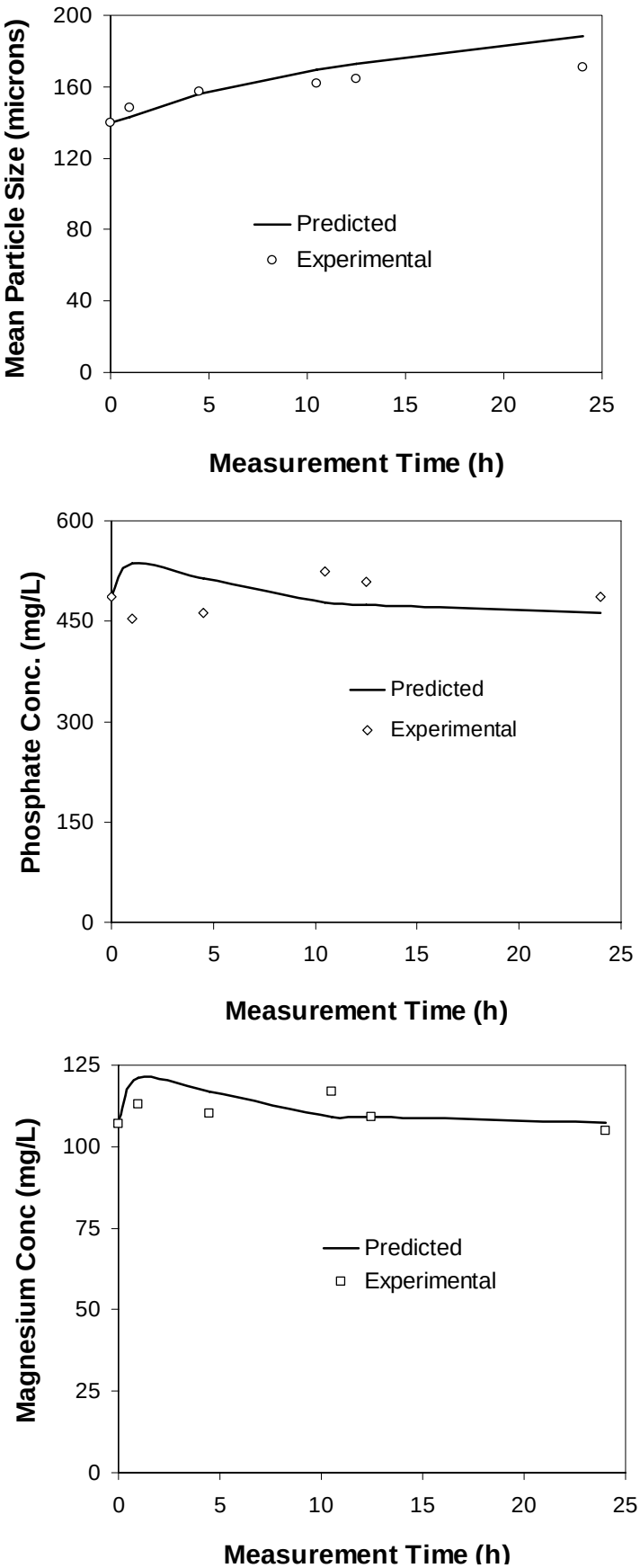

Figure 6. 12 Overlay charts of experiment 1 (Est.type 2)

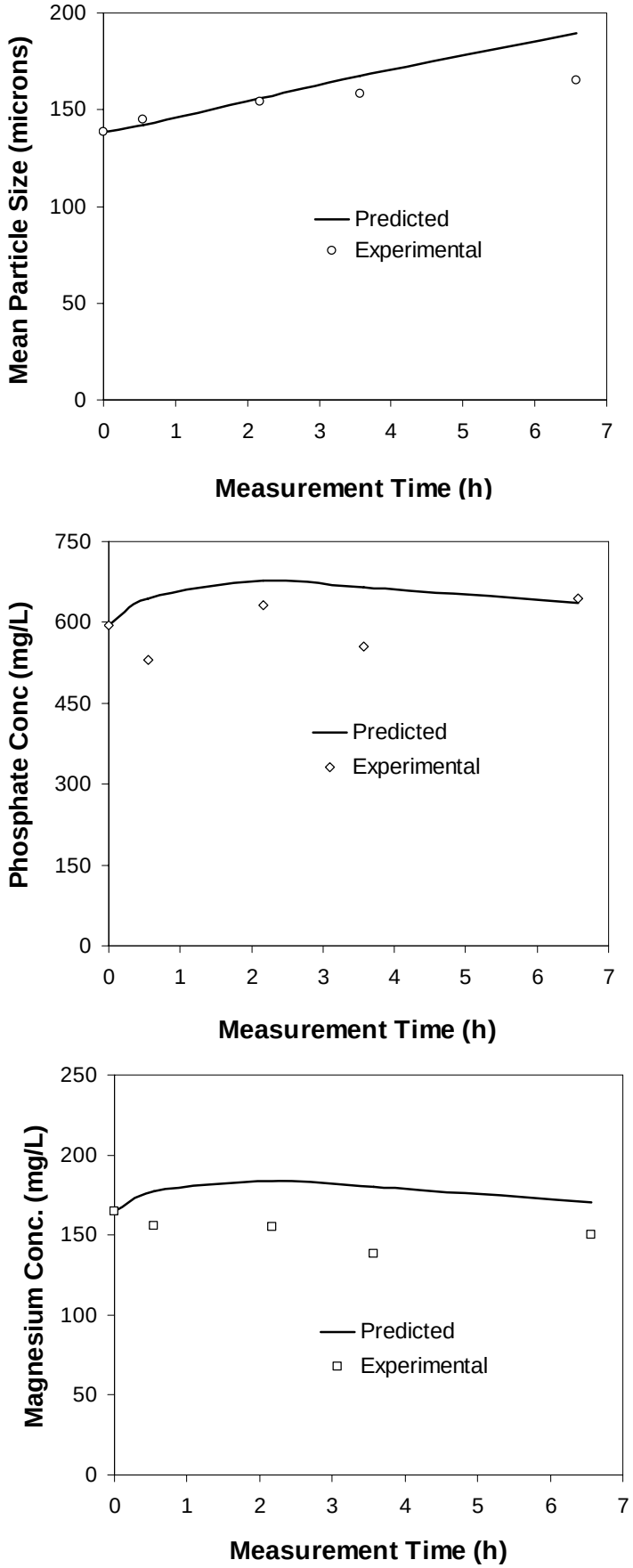

Figure 6. 13 Overlay charts of experiment 2 (Est.type 2)

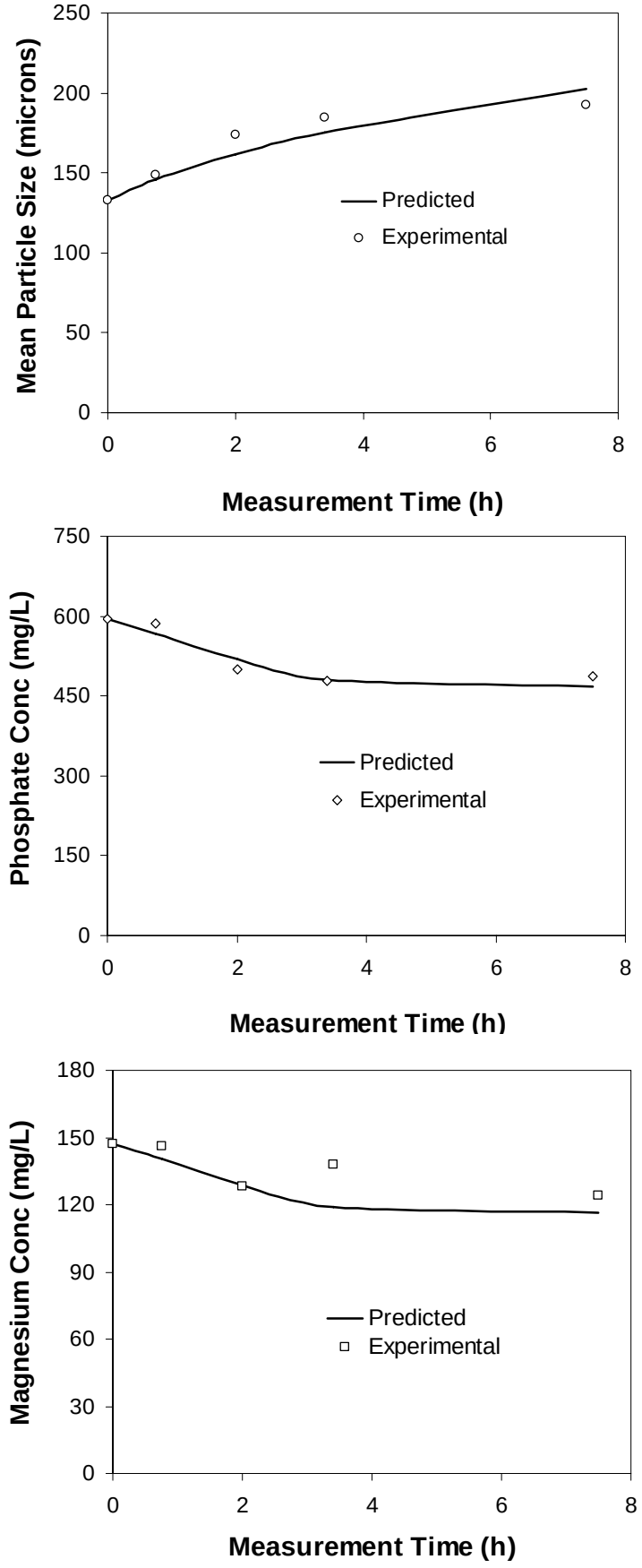

Figure 6. 14 Overlay charts of experiment 3 (Est.type 2)

Table 6. 8 Objective function contributed for parameter estimation (Est.type 2)

Experiments	Variables	Variance Model	Objective Function Contribution
1	L	Heteroscedasticity Predicted Value	15.785
	Total PO_4^{3-}	Heteroscedasticity Predicted Value	25.978
	Total Mg^{2+}	Heteroscedasticity Predicted Value	13.186
2	L	Heteroscedasticity Predicted Value	14.336
	Total PO_4^{3-}	Heteroscedasticity Predicted Value	24.004
	Total Mg^{2+}	Heteroscedasticity Predicted Value	18.782
3	L	Heteroscedasticity Predicted Value	12.887
	Total PO_4^{3-}	Heteroscedasticity Predicted Value	16.002
	Total Mg^{2+}	Heteroscedasticity Predicted Value	13.905
Total Objective Function			*198.993*

The numerical value of objective function represents the potential source of error associated with the experimental data and the relevant simulated outputs (gPROMS 2002a) at the optimal point of simulation. The numerical values of the objective function contribution show that the potential errors are encountered from the experimental data of growing crystal size and solution concentration. However, error encountered due to total phosphate concentration $\left(C_{PO_4^{3-}}\right)$ is higher than the error involved with the total magnesium concentration $\left(C_{Mg^{2+}}\right)$ and crystal size *(L)* data.

6.6.2 Error Analysis (Est.type 2)

The individual consistency of the estimated parameters *K*, *n* and n_1 are evaluated by *t-value* test. As shown in Table 6.9, the model response associated the smaller 95% *t-values* for the estimated parameters *K* and n_1 than the *reference 95% t-value*, which presents an inaccurate estimation of *K* and n_1 values. However, the parameter *n* is accurately estimated, since the *95% t-value* is larger than the *reference 95% t-value*. In addition, the higher standard deviations than the estimated values present the inaccurate estimation for *K* and n_1 (gPROMS 2002a).

Table 6. 9 Major statistical information of the estimated response (Est.type 2)

Parameter	Optimal Estimate	90% CI	95% CI	99% CI	95% t-value	Standard Deviation
K	27.83	184.30	221.94	299.75	0.13	108.18
n	1.52	0.40	0.48	0.65	3.17	0.23
n_1	0.11	1.36	1.63	2.21	0.07	0.80
Reference t-value (95%): 1.70						

The inaccurate estimations of struvite growth constant *(K)* and the growth order due to crystal size *(n_1)* are most likely due to the insufficient variations of the mean seed size, and consequently the insufficient variations of growing mean struvite crystal size. It is worthwhile noting that the mean crystal size of 140.06, 138.83 and 133.25 μm were employed for experiments 1, 2 and 3, respectively. Therefore, it is recommended to use wide variations of mean seed size to accurately estimate the effect of crystal size on struvite growth.

6.7 Est.type 3

This section presents the kinetic parameter estimation of struvite growth incorporating the flexible initial size of crystals as seeds. Referring to the background of parameter estimation in section 6.5.1, θ is related to the estimated parameters ***K***, ***n*** and $\boldsymbol{L_0}$. Here, ***K*** is the struvite growth rate constant, ***n*** is the growth order due to supersaturation and $\boldsymbol{L_0}$ is the estimated initial size of crystals as seeds.

6.7.1 Results of Parameter Estimation Modeling (Est.type 3)

The kinetic response of struvite shows an estimated value of growth order *(n)* equal to 1.45±0.16 and the growth rate constant *(K)* equal to 45.21± 7.89 μm/h. The estimated mean size of seeds (L_0) is equal to 134.96±1.82 μm. The estimated values of kinetic parameters, i.e. *K* and *n*, present the following kinetic model of struvite growth (Equation 6.16).

$$\frac{dL}{dt} = (\boldsymbol{45.21 \pm 7.89})S^{\boldsymbol{1.45 \pm 0.159}} \qquad \textbf{(6. 16)}$$

The overlay charts of struvite growth (Figures 6.15-6.17) show a reasonable agreement between the predicted and the experimental data within ±10% deviation (Table 6.10). The model predictions of total phosphate concentration validate most of the experimental data of total phosphate concentration (Figures 6.15-6.17) within ±20% deviation (Table 6.10). The predicted total magnesium concentrations also agree with the experimental data (Figures 6.15-6.17) within ±20% deviation (Table 6.10).

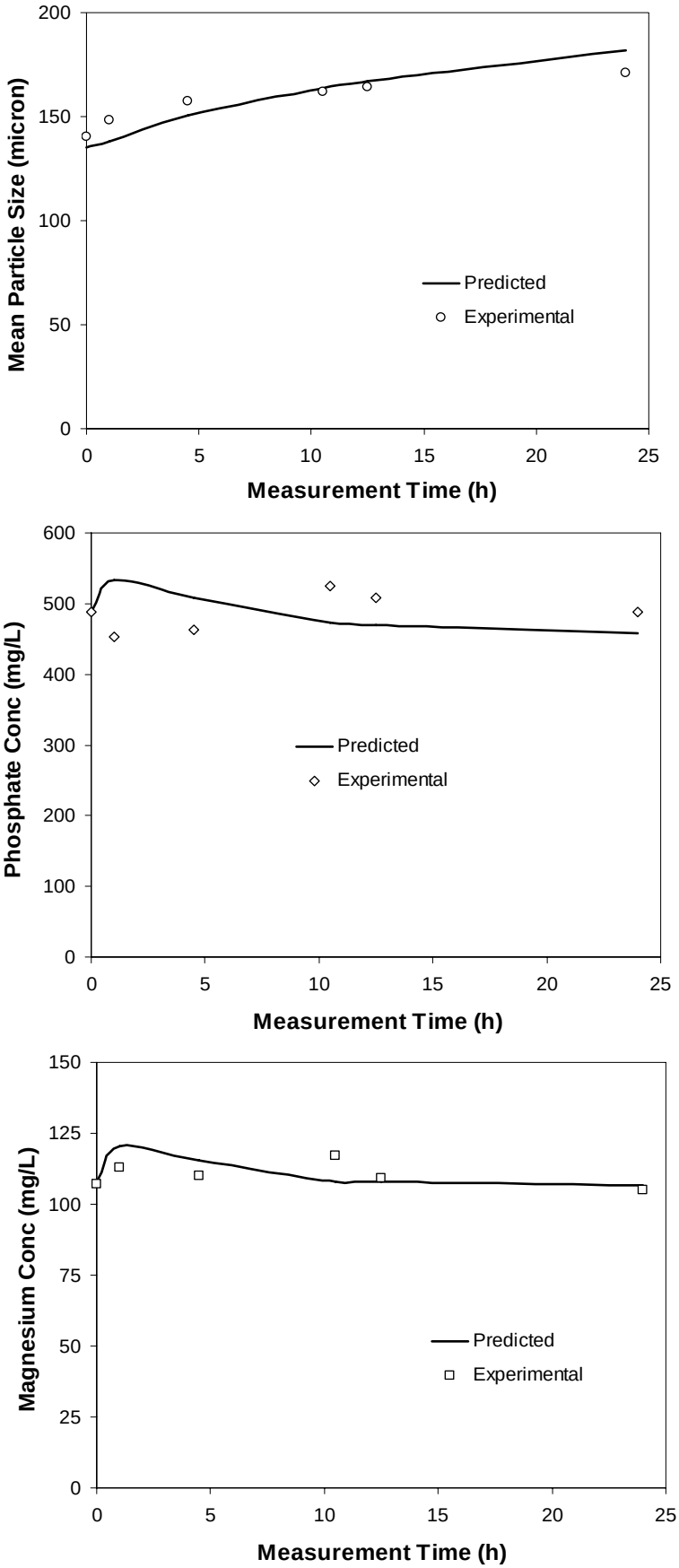

Figure 6. 15 Overlay charts of experiment 1 (Est.type 3)

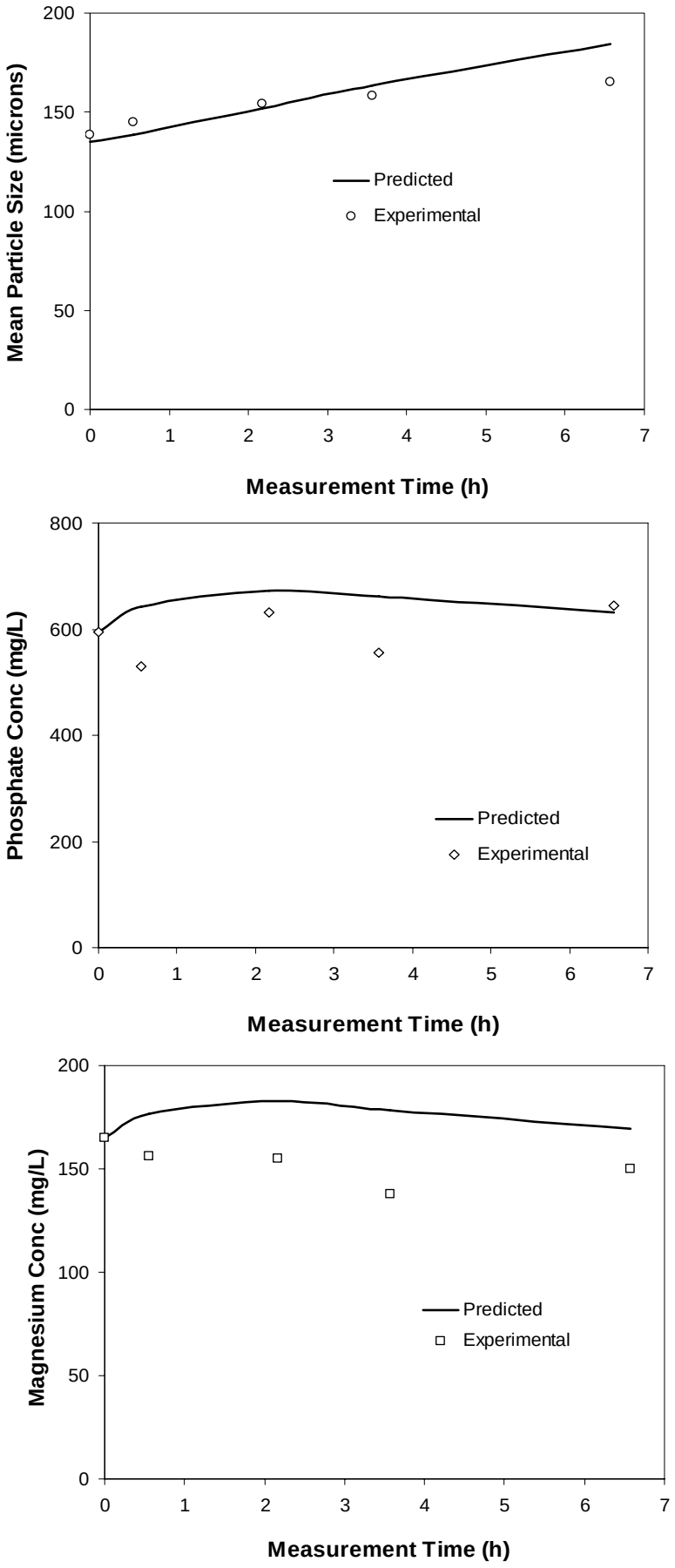

Figure 6. 16 Overlay charts of experiment 2 (Est.type 3)

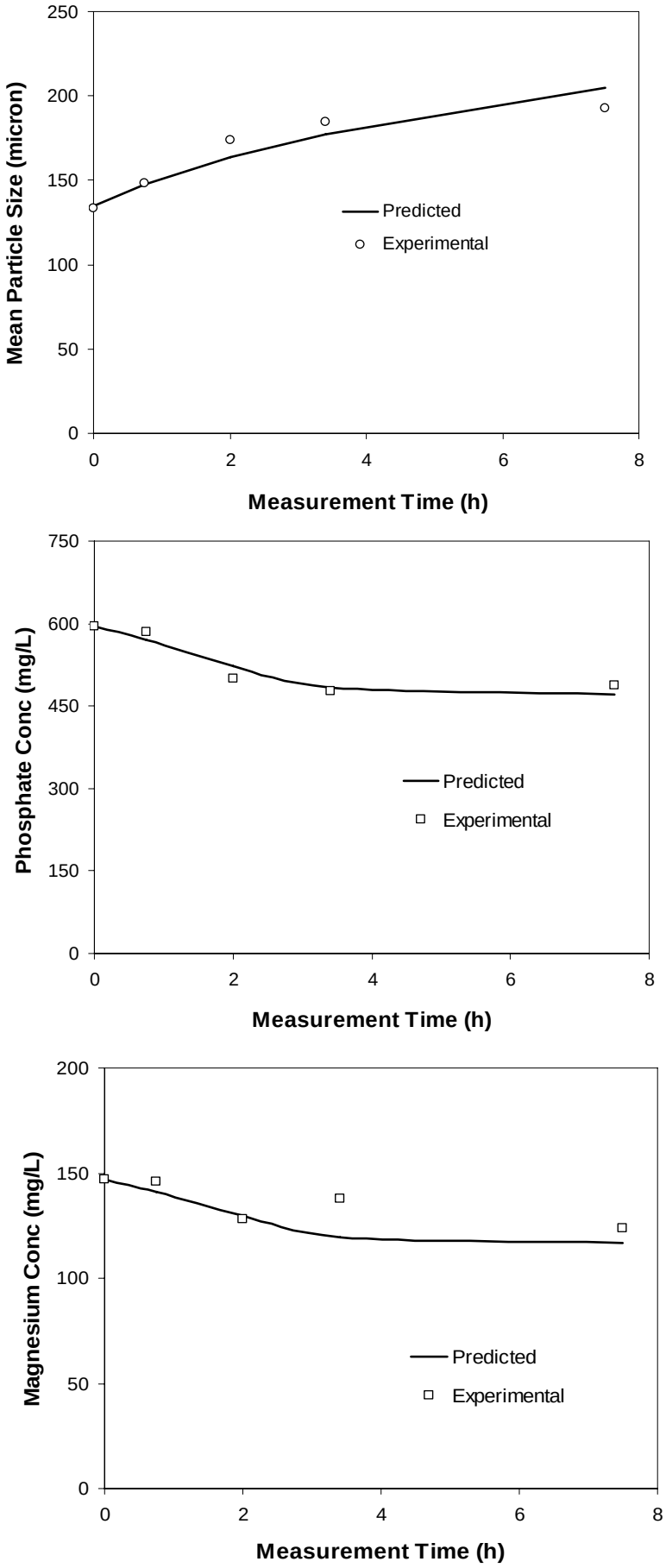

Figure 6. 17 Overlay charts of experiment 3 (Est.type 3)

Table 6. 10 Percentage deviations of the measured and predicted variables (Est.type 3)

Measurement Time (h)	Percentage Deviation for L	Percentage Deviation for total PO_4^{3-}	Percentage Deviation for total Mg^{2+}
Experiment-1			
0.00	3.64	0.00	-0.93
1.00	6.91	-17.90	-6.54
4.50	4.25	-9.69	-5.01
10.50	-0.98	9.77	7.58
12.50	-1.60	7.53	1.04
24.00	-6.48	5.87	-1.43
Experiment-2			
0.00	2.79	0.00	0.00
0.55	4.71	-21.24	-13.17
2.17	1.74	-6.61	-17.85
3.57	-3.08	-19.18	-29.40
6.57	-11.48	1.81	-12.96
Experiment-3			
0.00	-1.28	0.00	0.00
0.75	0.76	2.57	3.30
2.00	5.83	-4.70	-1.19
3.40	3.87	-1.03	13.29
7.50	-6.61	3.47	5.65

6.7.2 Error Analysis (Est.type 3)

The individual consistency of the estimated parameters (*K*, *n* and L_0) is evaluated by making a comparison between the associated *t-value* of the estimated parameters and the *reference* 95% *t-value*. The model response associated the larger 95% *t-values* for estimated parameters *K*, *n* and L_0 rather than the reference 95% *reference t-value* (Table 6.11), which presents an accurate estimation of the parameters (gPROMS 2002a).

Moreover, the standard deviations of *K*, *n* and L_0 are smaller than the relevant estimated values, which indicates that the estimated values of *K*, *n* and L_0 are individually consistent (Draper and Smith 1966; Mandel 1984).

Table 6. 11 Major statistical information of the estimated response (Est.type 3)

Parameter	Optimal Estimate	90% CI	95% CI	99% CI	95% t-value	Standard Deviation
K	45.21	13.44	16.19	21.86	2.79	7.89
n	1.45	0.27	0.33	0.44	4.42	0.159
L_0	134.96	3.10	3.73	5.04	36.16	1.82
Reference t-value (95%): 1.70						

The joint statistical significance of the optimized parameters, including growth rate constant (K), growth order (n), standard deviation (ω), optimization power (x) and the estimated size of seeds (L_0) are evaluated using *F-value* test within 95% confidence region. The null hypothesis (H_0) considered in this context is shown in equation (6.17). The notations of variables of equation (6.17) is already presented in equations (3.43), (6.7) and (6.8) and the relevant texts. Please note that, i is the number of conducted experiments (i =3) and j is the number of experimental variables in each parameter.

$$H_0 : K = n = \gamma_{ij} = \omega_{ij} = L_{0i} = \mathbf{0} \qquad \textbf{(6. 17)}$$

Based on the simulation responses, the detailed *Fischer information matrix* and the computed *F-value* are presented in Appendix K; Table K.3. The *F-value* within 95% confidence region is 1.962. The critical *F-value* (F_{crit}) was identified using the function

F(α%, N, N-N_P) (gPROMS 2002a), given that, N (N=48) is the total number of measurements taken, N_P (N_P=21) is the number of optimized parameters involved in the parameter estimation (Appendix K; Table K.3). Therefore, the *critical F-value* for F(95%, 48, 27) is approximately 1.71 (Draper and Smith 1966). A smaller F_{crit}*-value* (F_{crit} = 1.71) rather than *F-value* (F-value = 1.962) indicates the rejection of null hypothesis (equation 6.17), therefore, indicates the joint statistical significance of the optimized parameters. The detailed description of the parameters involved in the *F-test* is shown Appendix K; table K.3.

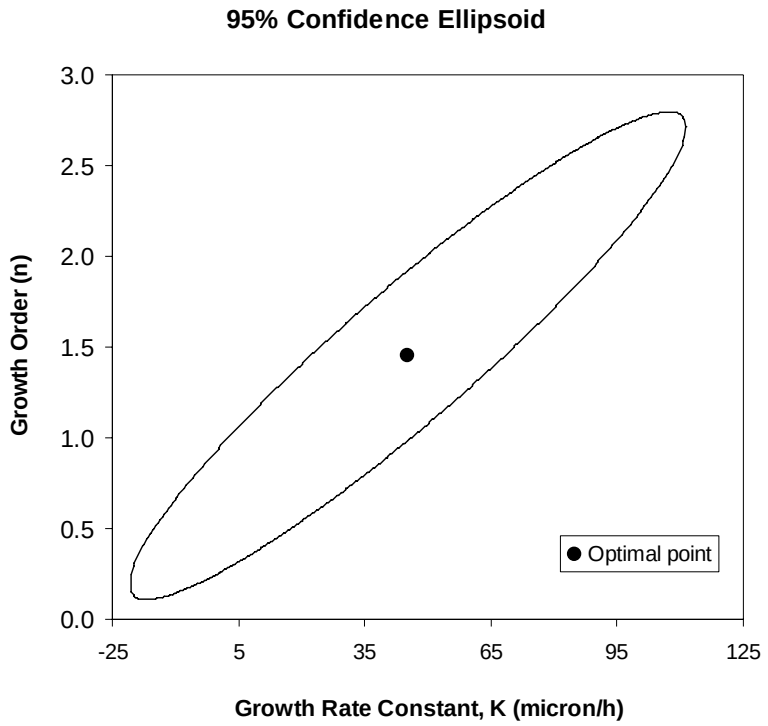

Figure 6. 18 Confidence ellipsoid of the estimated growth parameters

Based on the simulation response, the joint 95% confidence region (Figure 6.18) of the true parameters (*K* and *n*) shows long thin ellipsoid and the optimized values of *K* and *n*. Strong positive correlation occurs between the estimated parameters, which means the increase of *K* and *n* values for higher struvite growth rate or *vise versa*.

Table 6. 12 Objective function contributed for parameter estimation (Est.type 3)

Experiment	Variables	Variance Model	Objective Function Contribution
1	L	Heteroscedasticity Predicted Value	14.811
	Total PO_4^{3-}	Heteroscedasticity Predicted Value	25.973
	Total Mg^{2+}	Heteroscedasticity Predicted Value	12.961
2	L	Heteroscedasticity Predicted Value	13.497
	Total PO_4^{3-}	Heteroscedasticity Predicted Value	23.845
	Total Mg^{2+}	Heteroscedasticity Predicted Value	18.603
3	L	Heteroscedasticity Predicted Value	12.663
	Total PO_4^{3-}	Heteroscedasticity Predicted Value	16.002
	Total Mg^{2+}	Heteroscedasticity Predicted Value	13.691
Total Objective Function			*196.129*

The overlay charts (Figures 6.15- 6.17) confirmed that the model predictions of crystal growth and the total concentration of magnesium and phosphate validate the experimental observation within the specified tolerance limits. Different types of error cause deviation between the predicted and experimental results. The main sources of errors are the erroneous experimental data of crystals size and concentrations, together with the instrumental errors and the errors due to experimental controlled variables (F_i and F_{NaOH}).

Table 6.12 illustrates the objective function contributions to each experimental variable associated with the kinetic parameter estimation. The total objective function contributed at the optimal point of kinetic estimation is 196.129. The computed

objective functions in Table 6.12 show that the experimental data of phosphate and magnesium potentially causes more inaccuracy than the experimental data of crystal size, due to relatively higher value of objective function contribution at the optimal point of estimation. The numerical value of objective function contribution in each case of crystal growth also shows that crystal size data causes some errors to this kinetic simulation (Table 6.12).

6.8 Est.type 4, Est.type 5 and Est.type 6

Struvite growth kinetics were evaluated in terms of Saturation Index (SI). This section describes the struvite growth kinetics (Chapter 3, equation 3.43) incorporating Saturation Index (SI) as the mathematical expression of supersaturation (Chapter 3, equation 3.41). In this context, this research includes three types of kinetic study. The first type of estimation (identified as **Est.type 4**) was conducted using fundamental growth model as described in Chapter 3 (equation 4.43). **Est.type 5** incorporated particle size in the fundamental growth model of struvite. The other type of estimation (identified as **Est.type 6**) was conducted employing an extra estimated parameter (initial size of crystals as seeds, L_0), along with the fundamental kinetic.

The fundamental of kinetic estimation is already described in the previous sections (Sections 6.5- 6.7). Based on the simulated responses, the kinetic equation for struvite growth of **Est.type 4**, **Est.type 5** and **Est.type 6** are presented in equations (6.18) to (6.20). Kinetic equation (6.18) is equivalent to equation (6.10) (Est.type 1; for fundamental struvite growth model), and equation (6.20) is equivalent to equation (6.16) (Est.type 3; for estimated size of seeds). The major dis-similarity of the kinetic response between equations 6.10 and 6.18, equations 6.15 and 6.19 as well as equations

6.16 and 6.20 is the mathematical expression of supersaturation. Equations 6.10, 6.15 and 6.16 incorporate oversaturation (S) to compute supersaturation. Equations 6.18, 6.19 and 6.20 incorporate Saturation Index (SI) to compute supersaturation.

$$\frac{dL}{dt} = (\boldsymbol{47.06 \pm 8.521}) S_i^{\boldsymbol{1.64 \pm 0.193}} \qquad \textbf{(6. 18)}$$

$$\frac{dL}{dt} = (\boldsymbol{28.23 \pm 127.49}) S_i^{\boldsymbol{1.66 \pm 0.26}} L^{\boldsymbol{0.105 \pm 0.92}} \qquad \textbf{(6. 19)}$$

$$\frac{dL}{dt} = (\boldsymbol{49.16 \pm 8.562}) S_i^{\boldsymbol{1.68 \pm 0.183}} \qquad \textbf{(6. 20)}$$

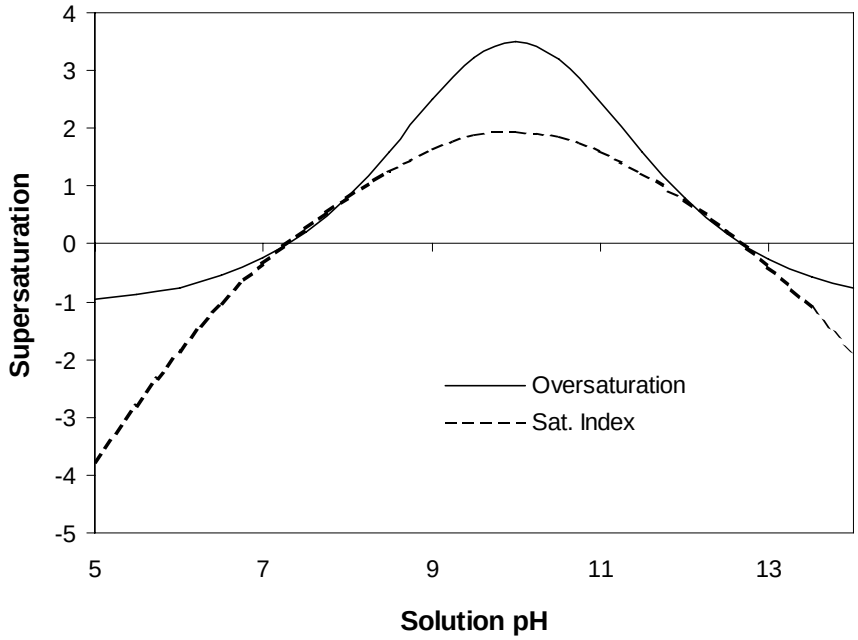

Figure 6. 19 Comparison of supersaturation expressed by oversaturation (S) and Saturation Index (SI) using the solution concentration of Expt 1

Based on thermodynamic simulation results, a close similarity was observed between the two types of kinetic equations. Small deviations of the estimated parameters were observed due to the difference of supersaturation values (Figure 6.19) at the specified range pH of given solution concentrations. As for example, solution concentration of 0.0045M equimolar of magnesium, ammonium and phosphate (roughly identical to

Expt-1) was employed to assess the similarity of the Saturation Index (SI) and Oversaturation. Based on the thermodynamic response of supersaturation (Figure 6.19), similar trends were observed for ***SI*** and ***S*** with slightly different numerical values.

6.8.1 Error Analyses

The individual consistencies of the estimated parameters are evaluated using *t-value* test (gPROMS 2002a). As described in Table 6.13, the model response associated the larger *95% t-values* for the estimated parameters *K* and *n* rather than *reference 95% t-value*, which indicates an accurate estimation of *K* and *n* values. In addition, the smaller standard deviations of the above parameters (*K* and *n*) than the relevant estimated values also indicate the individual consistency of the estimated parameters (*K* and *n*) for **Est.type 4**.

The major statistical information of the estimated response for **Est.type 6** (Table 6.15) also indicates an accurate estimation of the struvite growth rate constant (K), growth order (n) and the variable seed size (L_0). The individual statistical consistencies of K, n and L_0 is evaluated based on *95% t-values*, *reference 95% t-values* and the relevant *standard deviations* of the estimated parameters, as described in the previous paragraph. The more detailed statistical responses are presented in Appendices *K* to *N*.

Based on the simulation responses, the detailed *Fisher information matrices* along with *F-values* are presented in Tables K.4 and K.6 (Appendix K). The computed *F-value* within 95% confidence region is 1.9581 in both cases. The *critical F-values* (F_{crit}) in these contexts are approximately 1.73 and 1.71 (Draper and Smith 1966). The larger *F-values* rather than F_{crit}-values indicate the joint statistical significance of the estimated

parameters for **Est.type 4** and **Est.type 6** simulation. The detailed description of F-test is already presented in section 6.5.2 and 6.7.2.

Table 6. 13 Key statistical information of the estimated response (Est.type 4)

Parameter	Optimal Estimate	90% CI	95% CI	99% CI	95% t-value	Standard Deviation
K	47.06	14.48	17.43	23.49	2.70	8.521
n	1.64	0.33	0.39	0.53	4.16	0.193
Reference t-value (95%): 1.70						

Table 6. 14 Key statistical information of the estimated response (Est.type 5)

Parameter	Optimal Estimate	90% CI	95% CI	99% CI	95% t-value	Standard Deviation
K	28.23	217.20	261.56	353.25	0.11	127.49
n	1.66	0.44	0.53	0.72	3.12	0.26
n_1	0.105	1.57	1.89	2.56	0.06	0.92
Reference t-value (95%): 1.70361						

Table 6. 15 Major statistical information of the estimated response (Est.type 6)

Parameter	Optimal Estimate	90% CI	95% CI	99% CI	95% t-value	Standard Deviation
K	49.16	14.54	17.51	23.60	2.81	8.562
n	1.68	0.32	0.38	0.51	4.42	0.183
L_0	135.02	3.11	3.75	5.05	36.01	1.833
Reference t-value (95%): 1.70						

The model responses of **Est.type 5** (Table 6.14) associated the smaller 95% *t-values* for the estimated parameters K and n_1 than the *reference 95% t-value*, which presents an inaccurate estimation of K and n_1 values. However, the parameter n is accurately estimated, since the model **Est.type 5** encounters the larger *95% t-value* than the *reference 95% t-value*. In addition, the higher standard deviations than the relevant estimated values present an inconsistent estimation for K and n_1 (gPROMS 2002a). As described Section 6.6.2, the inaccurate estimations of K and n_1 are most likely due to the insufficient variations of mean seed size, and consequently the insufficient variations of growing mean struvite crystal size. Please note that the mean seed size of 140.06, 138.83 and 133.25 μm were employed for experiments 1, 2 and 3, respectively.

6.9 Selection of the Finest Model

Based on simulations, the summary of results is given in Table 6.16. On the basis of *t-value* test and the standard deviations of relevant parameters, **Est.type 2** and **Est.type 5** provide inconsistent estimation (Tables 6.9, 6.14 and 6.16) due to insufficient variations of mean seed sizes. Therefore, **Est.type 2** and **Est.type 5** are ignored in the discussion of model selection. Estimation types (**Est.type**) **1**, **3**, **4** and **6** shows statistically consistent results based on the *t-value* test, relevant *standard deviations* of the estimated parameters and the *F-value* test. Therefore, the selection of the finest model will be based on **Est.types 1**, **3**, **4** and **6**.

This section describes the selection of model based on total objective function contributions of each type of estimation (**Est.types 1**, **3**, **4** and **6**). As described in previous sections, **Est.types 1** and **4** is the fundamental struvite growth model incorporating different expression of supersaturation (Table 6.16). An extra flexibility

of the fundamental growth model is also considered by incorporating the variable size of seed (**Est.types 3** and **6**), since the mean size of seed at the beginning of experiment is unknown.

The total objective function contribution associated with the fundamental growth model (**Est.types 1** and **4**) provides slightly larger values than that of flexible growth model (**Est.types 3** and **6**). Therefore, it is concluded that unknown size of seed crystal may have some effect on the relevant parameter estimation (Table 6.17). This influence can be significant when seed size is largely unknown and/or altered due to initialization of experiment. However, the present investigation did not observe any significant differences between the fundamental (**Est.types 1** and **4**) and flexible growth model of struvite (**Est.types 3** and **6**). Thus, this research recommends the flexible type of estimation (**Est.types 3** and **6**) when there is large uncertainty of seed size at the beginning of experiments. However, for certain experimental data, fundamental type of growth model (**Est.type 1** and **4**) is suitable.

Table 6. 16 Responses of parameter estimation models

Supersaturation Model: Relative supersaturation (S)				Supersaturation Model: Saturation Index (S_i)			
Est.type	**Estimated values**	**Struvite growth equations**	**Total objective function**	**Est.type**	**Estimated values**	**Struvite growth equations**	**Total objective function**
1	K = 46.64±8.026 n= 1.48±0.162	$\frac{dL}{dt} = (46.64 \pm 8.026) S^{1.48 \pm 0.162}$	198.609	4	K = 47.06±8.521 n = 1.64±0.193	$\frac{dL}{dt} = (47.06 \pm 8.521) S_I^{1.64 \pm 0.193}$	198.431
2	K=27.72±108.18 n= 1.52±0.23 n_1= 0.109±0.079	$\frac{dL}{dt} = (27.72 \pm 108.18) S^{1.52 \pm 0.23} L^{0.109 \pm 0.89}$	198.993	5	K = 28.23±1127.49 n= 1.52±0.23 n_1= 0.109±0.079	$\frac{dL}{dt} = (28.23 \pm 127.49) S^{1.66 \pm 0.26} L^{0.105 \pm 0.92}$	198.863
3	K = 45.21±7.89 n= 1.45±0.159 L_0= 134.96±1.82	$\frac{dL}{dt} = (45.21 \pm 7.89) S^{1.45 \pm 0.159}$	196.129	6	K = 49.16±8.562 n = 1.68±0.183 L_0 = 135.02±1.833	$\frac{dL}{dt} = (49.16 \pm 8.562) S_I^{1.68 \pm 0.183}$	195.706

Selection of thermodynamic model between oversaturation *(S)* and saturation index *(SI)* may play some role in successful model execution. As described in Figure 6.19, both oversaturation *(S)* and saturation index *(SI)* show almost identical responses with slightly different values of supersaturation. The total objective functions contribution also shows the identical responses of parameter estimation. However, due to simplicity of mathematical expression, future investigation of this research should adhere to oversaturation *(S)* for the struvite growth model execution.

Table 6. 17 Estimated results of the seed size

Experiment	Supersaturation Model (S)		Supersaturation Model (SI)	
	Approximate seed size (μm)	***Estimated seed size (μm)***	***Approximate seed size (μm)***	***Estimated seed size (μm)***
1	140.06	134.96	140.06	135.02
2	138.83		138.83	
3	133.25		133.25	

6.10 Discussion

This chapter covers the simulation result of struvite thermodynamic and the estimation of struvite growth kinetic parameter. The thermodynamic simulation using the nutrient rich effluent pond data shows that the formations of complexes (among Mg^{2+}, NH_4^+ and PO_4^{3-}) depend on total concentration of magnesium, ammonium and phosphate as well as solution pH value. The major complexes and free ions present in struvite systems are $MgOH^+$, $MgH_2PO_4^+$, $MgHPO_4$, $MgPO_4^-$, H_3PO_4, $H_2PO_4^-$, HPO_4^{2-}, NH_3, NH_4^+, Mg^{2+} and PO_4^{3-}. The speciation of struvite solution (using gPROMS coding and simulation) is

validated by the solution speciation modeling using vMinteq (a specialized thermodynamic modeling package). The thermodynamic modeling response confirms the existing fact of struvite supersaturation (Taylor *et al.* 1963; Ohlinger 1999; Bouropoulos and Koutsoukos 2000; Kofina and Koutsoukos 2005); that struvite precipitation commences in a supersaturated solution and supersaturation is a function of solution concentration (magnesium, ammonium and phosphate) and pH.

As described in sections 6.5-6.8, this research incorporated the kinetic investigation of struvite growth by six different methods. Referring to Table 6.18, **Est.types 1-3** incorporate oversaturation *(S)* and **Est.types 4-6** incorporate Saturation Index *(SI)* to compute supersaturation. **Est.type 1** corresponds to the fundamental kinetic estimation of struvite growth, **Est.types 2** and **5** corresponds to the kinetic estimation of struvite growth incorporating the effect of particle size and **Est.type 3** corresponds to the kinetic estimation of struvite growth incorporating a variable mean size of seeds (L_0). **Est.type 4** corresponds to fundamental kinetic estimation of struvite growth using saturation index as the supersaturation model. **Est.type 6** corresponds to kinetic estimation using supersaturation index as supersaturation model and incorporating the estimated mean size of seeds (L_0) to provide a tolerance of seed size in the process. Based on the simulation response (using gPROMS coding and simulation), the values of estimated parameters and the other relevant information are shown in Table 6.18.

Other researchers have conducted kinetic investigation of struvite relating to concentration decay and concentration related desupersaturation. Nelson (2003) studied struvite kinetics relating to reduction of experimental phosphate concentration

$\left(C_{PO_4^{3-}} - C^*_{PO_4^{3-}}\right)$ and the rate of phosphate de-supersaturation $\left(dC_{PO_4^{3-}}/dt\right)$. A first order modified kinetic model (log form) in batch scale was documented in Nelson's (2003) study.

Table 6. 18 Key responses of the parameter estimation modeling

Estimated variables	Est.type	Estimated values	Est.type	Estimated values
		MS*[♣] = *S		***MS* = S_i**
• Growth rate constant *(K)* • Growth order *(n)* due to supersaturation	1	K = 46.64±8.026 *n* = 1.48±0.162	4	K = 47.06±8.521 *n* = 1.64±0.193
• Growth rate constant *(K)* • Growth order *(n)* due to Supersaturation • Growth order *(n_1)* due to L	2	K= 27.72±108.18 *n* = 1.52±0.23 n_1 =0.109±0.89	5	K = 28.23±127.49 *n* = 1.66±0.26 n_1 = 0.105±0.92
• Growth rate constant *(K)* • Growth order *(n)* due to Supersaturation • Initial mean crystal size *(L_0)*	3	K = 45.21±7.89 *n* = 1.45±0.159 L_0= 134.96±1.82	6	K = 49.16±8.562 *n* = 1.68±0.183 L_0= 135.02±1.833

A similar model to Nelson *et al.* (2003) kinetic study was also conducted very recently (Quintana *et al.* 2005). The abovementioned kinetic studies (Nelson *et al.* 2003; Quintana *et al.* 2005) showed very simple concentration-related struvite kinetics and actual struvite thermodynamic was largely ignored. Moreover, particle size distribution

♣ MS represents the Model of Supersaturation

of struvite crystal was not considered in the abovementioned investigations, causing no significant contribution to express struvite growth and the relevant solution supersaturation. Harrison's (1999) study is more practical in expressing the struvite growth kinetics, since it incorporates the mean particle size and the relevant growth of struvite crystal as a function of solution supersaturation. However, Harrison's (1999) study suffers a significant setback, since supersaturation is expressed in terms of total phosphate concentration decay instead of actual supersaturation. The mathematical presentation of supersaturation as a function of single component concentration $\left(C_{Mg^{2+}} / C_{PO_4^{3-}} / C_{NH_4^+}\right)$ is rather limited, since solution supersaturation depends on all the reactive concentration (magnesium, ammonium and phosphate) and the relevant solution pH, as described in the thermodynamic discussions of this thesis.

This research investigated a more rigorous growth kinetics model of struvite relating to the growth of mean crystal size as a function of thermodynamic related solution supersaturation.

6.11 Chapter Summary

This chapter shows the simulation results of struvite thermodynamics and growth kinetics. The thermodynamic simulation shows the complex solution chemistry of struvite. Based on the thermodynamic simulation results, the complexes and ions present in struvite solution system are $MgOH^+$, $MgH_2PO_4^+$, $MgHPO_4$, $MgPO_4^-$, H_3PO_4, $H_2PO_4^-$, HPO_4^{2-}, NH_3, NH_4^+, Mg^{2+} and PO_4^{3-}. The thermodynamic simulation results also show that the supersaturation of struvite system is a function of reactant

concentration (concentration of total magnesium, ammonium and phosphate) and solution pH.

The second part of this chapter shows the estimation of struvite growth kinetics using six different approaches. Different expressions of supersaturation were employed for the kinetic estimation to verify the responses of the kinetic model. The combined thermodynamic, kinetic and process modeling was collectively incorporated to identify the struvite growth kinetics. The estimation of growth kinetic incorporated statistical analysis, including *t-value test*, *F-value* test, relevant *standard deviations*, *percentage deviations*, *overlay charts* and *objective functions*, to identify the accuracy of the developed model.

CHAPTER 7

CONCLUSIONS

This research focused on the pilot scale controlled struvite crystallization and the investigation of struvite growth kinetics. The ***experimental*** part of this research included the design and commissioning of a pilot scale, controlled struvite crystallization system. The ***computational*** part of this thesis included the modeling and simulation of struvite growth kinetics by a parameter estimation technique, incorporating the rigorous modeling and simulation of struvite thermodynamics.

The development of the pilot scale struvite crystallization system included the design of the 44 litres struvite reactor by incorporating the preliminary experimental scheme using batch/fed-batch experiments and the thermodynamic simulation, together with the theoretical formulation of experimental control. Based on the preliminary experimental/ mathematical observations the following conclusions can be drawn.

- The series of batch experiments using different types of seed materials confirmed that parent crystal should be used as seed. The presence of parent crystal as seed provides a catalyzing effect on struvite growth, due to efficient diffusion integration of crystal clusters and solute molecules.
- Moisture analysis of struvite proved that air dried struvite crystal should be used as seeds. The loss of hydration water (due to over-drying) from the struvite lattice causes the formation of very fragile crystals. Air-dried struvite is compact and hard, and displays a typical orthorhombic shape. Oven-dried struvite remains as a lump with significant attachment of fines. The use of oven dry struvite seeds leads to inaccurate experimental data of particle size distribution.

- Struvite crystallization in the metastable zone has the potential to minimize spontaneous precipitation. Two steps of observation can identify the range of the metastable zone. The saturation limit of the metastable zone can be identified either by thermodynamic modeling or using an existing struvite solubility limit curve (Ohlinger 1999). The upper limit of the metastable zone is the minimum limit of spontaneous precipitation, which can be identified by a series of batch experiments incorporating the sensible visual identification of spontaneous precipitation using laser light scattering.
- This research scaled-up the existing concept of feed preparation (Bouropoulos and Koutsoukos 2000) to maintain controlled supersaturation. The existing control strategy was modified in this research (detail in chapter 5) based on the derivation of mathematical relations between the feed solution concentration and the reactive solution concentration together with the reaction mechanism and the relevant thermodynamic equilibria. The mathematical formulation of feed concentration relating to reactive solution concentration is as follows:

$$x_2 = 12\, x_1 \qquad \textbf{(7. 1)}$$

$$x_3 = 18\, x_1 \qquad \textbf{(7. 2)}$$

  Where, x_1 is the equimolar reactive solution concentration, x_2 is the equimolar feed concentration and x_3 is the NaOH molar feed concentration.
- In addition to the above control strategies, constant experimental temperature, efficient mixing of solution and effective dosing of feed solutions has significant effects on crystallization and the relevant crystal size distribution. Sufficient mixing intensity of the reactive solution must be employed to provide efficient surface diffusion of newly born struvite clusters. Care should be taken in the

design of struvite reactor to keep the feeding points apart from each other to avoid local fluctuations in supersaturation.

- Based on the preliminary experiments, a set of fed-batch, controlled struvite crystallization experiments was performed in pilot scale. The experimental results showed an acceptable control over a range of solution pH and reactive solution concentration (magnesium ammonium and phosphate). The strategy described in this thesis has a potential to cope with struvite crystallization at controlled supersaturation, since solution pH and reactant concentration can be maintained reasonably constant.

As part of the modeling and simulation, this research incorporated the coding and simulation of solution thermodynamics to describe the solution speciation of struvite. A combined thermodynamic, kinetic and process model was collectively incorporated in this research to identify the growth kinetic of struvite in different fashions. Brief results of the thermodynamic and kinetic responses are described below.

- The thermodynamic simulation shows that the formations of complexes (among magnesium, ammonium and phosphate ions) depend on the total concentration of magnesium, ammonium and phosphate, as well as solution pH. The major complexes and free ions present in struvite system are $MgOH^{+}$, $MgH_2PO_4^{+}$, $MgHPO_4$, $MgPO_4^{-}$, H_3PO_4, $H_2PO_4^{-}$, HPO_4^{2-}, NH_3, NH_4^{+}, Mg^{2+} and PO_4^{3-}. The speciation of struvite solution (using gPROMS coding and simulation) is validated by solution speciation modeling using vMinteq (a specialized thermodynamic modeling package). The thermodynamic modeling response confirms that struvite precipitation commences in a supersaturated solution and

supersaturation is a function of solution concentration (total magnesium, ammonium and phosphate) and pH.

- This research incorporated the estimation of struvite growth kinetics using six different approaches. The kinetic equation of struvite growth incorporates a mathematical relation of the increase of mean particle size and the solution supersaturation. Supersaturation is computed in terms of oversaturation (relative supersaturation, S) in **Est.type 1** to **Est.type 3**. **Est.type 4** to **Est.type 6** incorporated Saturation Index (SI) to compute supersaturation. Different expressions of supersaturation were employed for the kinetic estimation to verify the responses of the model. Moreover, due to the comparable response of the numerical value (saturation at zero) of oversaturation (S) and the Saturation Index (SI) this research employed these mathematical expressions of supersaturation to test the kinetic responses. The summary of the kinetic responses in different modes is demonstrated in Table 7.1.
- The *t-value* test and *F-value* test of the estimated process indicates acceptable estimations of the kinetic parameters for **Est.type 1**, **Est.type 3**, **Est.type 4** and **Est.type 6**. The overlay charts of the struvite growth show the acceptable match between the model predictions and the experimental results within 10% deviation limits. The predicted magnesium and phosphate concentrations agree with their respective experimental results within 20% deviation limits. The deviations of predicted and experimental results may have originated from (i) time varying control variables, *i.e.* feed rate of reactant (F_i) and feed rate of NaOH solution (F_{NaOH}) (ii) experimental data of crystal size (L), total concentration of magnesium and phosphate.

- The sensitivity of electronic equipment, *i.e.* pH sensor, pH monitor, dosing pumps, may also encounter some error leading to the deviations of predicted and experimental results.

Table 7. 1 Summary of the parameter estimation results

Supersaturation Model *(Relative supersaturation, S)*			**Supersaturation Model** *(Saturation Index, S_i)*		
Est.type	**Estimated values**	**Total objective function**	**Est.type**	**Estimated values**	**Total objective function**
1	K = 46.64±8.026 n= 1.48±0.162	198.609	4	K = 47.06±8.521 n = 1.64±0.193	198.431
2	K= 27.72±108.18 n = 1.52±0.23 n_1 =0.109±0.89	198.993	5	K = 28.23±127.49 n = 1.66±0.26 n_1 = 0.105±0.92	198.863
3	K = 45.21±7.89 n= 1.45±0.159 L_0= 134.96±1.82	196.129	6	K = 49.16±8.562 n = 1.68±0.183 L_0 = 135.02±1.833	195.706

- The objective function contribution of the simulation response shows that the experimental data of the reactive total phosphate and total magnesium concentration generated higher variability than the experimental data of crystal size. As for example, the simulation **Est.type 1 (Expt1)** contributed objective functions 15.76, 25.964 and 13.091 for crystal size (L), concentration of total phosphate $\left(C_{PO_4^{3-}}\right)$ and total magnesium $\left(C_{Mg^{2+}}\right)$, respectively. The simulation **Est.type 6 (Expt.-1)** contributed objective functions 14.48, 23.75 and 18.47 for

mean crystal size, and the concentration of total phosphates and total magnesium, respectively.

- The simulated response of n_1 in **Est.type 2** and **Est.type 5** (growth order due to crystal size effect) indicates roughly the size independent growth of struvite, since it encounters smaller value (n_1 = 0.109 and 0.105). Within the specified size range as described in the fed-batch experiments, the size independent growth of struvite was also indicated in the experimental investigation of this research. However, further simulation of **Est.type 2** and **Est.type 5** are required with sufficient variations of mean seed size to estimate the parameters accurately.
- The tendency of struvite growth kinetic relating to oversaturation *(S)* and the Saturation Index *(SI)* are almost identical in terms of the kinetic response of the estimated parameters and their relevant sensitivity, matching of experimental and predicted data and statistical significance. Therefore, both Saturation Index *(SI)* as well as oversaturation *(S)* can be used in the struvite growth kinetic equation. However, in future this research will adopt oversaturation *(S)* as the mathematical expression of supersaturation, due to the simplicity of mathematical expression.

CHAPTER 8

RECOMMENDATIONS

The predominant goals of this research were to identify the methods for controlled struvite crystallization and the development of a struvite kinetics model. The following recommendations are made for the future direction of this research.

- This research incorporated the design of an isothermal pilot scale struvite reactor using a feedback control system. The design of the pilot scale struvite reactor was based around a controlled supersaturation mode of operation. The control strategy, described in this thesis, may be implemented for the other types of reactive crystallization, such as for hydroxyapatite crystallization. Moreover, future investigations should include struvite and/or hydroxyapatite crystallization from different types of wastewater, including piggery wastewater, brine wastewater, industrial and municipal wastewater, poultry wastewater and mining wastewater. The use of a reactor in continuous system, by modifying the existing crystal retention strategy, is recommended.
- This research included the description of the struvite solution chemistry relating to thermodynamic equilibria of magnesium, ammonium and phosphate by simulating the thermodynamics using gPROMS. Future research may be directed to investigate the solution chemistry of real wastewater by incorporating additional thermodynamic equilibria with the present thermodynamic model.
- The present research incorporated the derivation of a more rigorous struvite growth model incorporating the solution thermodynamics and kinetics of struvite growth as well as the mathematical description of the struvite process.

Future research may include the extension of this model in more dynamic circumstances.

- Further research on struvite process modeling may include the coding and simulation of the complete process model of struvite crystallization in continuous, fed-batch and batch system. A complete model will assist in the preliminary design of large-scale systems for nutrient recovery.

REFERENCES

Adnan, A., M. Dastur, S. D. Mavinic and F. A. Koch (2004). "Preliminary Investigation into Factors Affecting Controlled Struvite Crystallization at the Bench Scale." Journal of Environmental Engineering Science **3**: 195-202.

Adnan, A., F. A. Koch and S. Mavinic (2003). "Pilot-Scale Study of Phosphorus Recovery through Struvite Crystallization- II : Applying in-reactor Supersaturation ratio as a Processes Control Parameters." Journal of Environmental Engineering Science **2**: 473-483.

Ali, M. I. and P. A. Schneider (2006). "A Fed-Batch Design Approach of Struvite System in Controlled Supersaturation." Chemical Engineering Science **61** (12): 3951-3961.

Ali, M. I., P. A. Schneider and N. Hudson (2005a). "Thermodynamics and Solution Chemistry of Struvite." Journal of Indian Institute of Sciences **85**(May-June): 141-149.

Ali, M. I., P. A. Schneider and N. Hudson (2004). Process Modelling of Struvite Crystallization. IWA Nutrient Recovery Conference, Asian Institute of Technology, Thailand. 143-147

Ali, M.I. and P. A. Schneider (2005). "Crystallization of Struvite from Metastable Region with Different Types of Seed Crystal." Journal of Non-equilibrium Thermodynamics **30**(2): 95-111.

Al-Khayat, A. and J. Garside (1990). Calcium Carbonate Precipitation: The Role and Importance of Solution Chemistry. 11th Symposium of Industrial Crystallization, Garmisch-Partenkirchen. 18-20

Allison, J. D., D. S. Brown and K. J. Novo-Gradac (1991). MINTEQA2/PRODEFA2: A Geochemical Assessment Model for Environmental Systems (Version 3.0 User Guide). Athens: Georgia, U.S Environmental Protection Agency (EPA).

Amjad, Z., P. G. Koutsoukos, M. B. Tomson and G. H. Nancollas (1978). "The Growth of Hydroxyapatite from Solution: A New Constant Composition Method." Journal of Dental Research **57**(9-10): 909.

Angel, R. (1999). "Removal of Phosphate from Sewage as Amorphous Calcium Phosphate." Environment Technology **20**(7): 709-720.

AWA (2000). Methane Generation and Use from Wastewater Treatment in Australia. Internal Report of FSA Australia, Environmental Protection Agency, South Australia.

Babic-Ivancic, V., J. Kontrec, D. Kralj and L. Brecevic (2002). "Precipitation Diagram of Struvite and Dissolution Kinetics of Different Struvite Morphologies." Croatia Chemeca ACTA **75**(1): 89-106.

Battistoni, P., G. Boccadoro, P. Pavan and F. Cecchi (2000). "Struvite Crystallization in Sludge Dewatering Supernatant Using Air Stripping: The New Full Scale Plant at Trevisco (Italy) Sewage Works." Water Resources **34**(11): 3033-3041.

Becker, R. and W. Doring (1935). "Kinetissche Behandlung der Keimbildung in Ubersattigen Dampfen." Annalen der Physik **24**: 719-752.

Bergfors, T. (2003). "Seeds to Crystals." Journal of Structural Biology **142**: 66-76.

Booram, C. V., R. J. Smith and T. E. Hazen (1975). "Crystalline Phosphate Precipitation from Anaerobic Animal Waste Treatment Lagoon Liquors." Transaction of the American Society of Agricultural Engineers **18**: 340-343.

Bouropoulos, C. Ch and P. G. Koutsoukos (2000). "Spontaneous Precipitation of Struvite from Aqueous Solutions." Journal of Crystal Growth **213**: 381-388.

Bube, K. (1910). "Uber Magnesiumammoniumphosphate." Z. Anal. Chem. **49**: 525-596.

Buchanan, J. R., C. R. Mote and R. B. Robinson (1994). "Struvite Control by Chemical Treatment." American Society of Agricultural Engineer **37**(4): 1301-1308.

Childs, C.W. (1970). "A Potentiometric Study of Equilibria in Aqueous Divalent Metal Orthophosphate Solutions." Journal of Inorganic Chemistry **9**(11): 2465-2469.

Davey, R. and J. Garside (2000). From Molecules to Crystallizers: An Introduction to Crystallization. Oxford Science Publication: Oxford University Press.

Dhingra, O. D. (1995). Basic Plant Pathology Methods. 2nd, Boca Raton, Lewis Publishers.

Doyle, J. D., K. Oldring, J. Churchley and S. A. Parsons (2001). Fundamental Chemistry and Control of Struvite Precipitation. Second International Conference on the Recovery of Phosphorus from Sewage and Animal Wastes, Noordwijkerhout, The Netherlands.

Doyle, J. D., R. Philip, J. Churchley and S. A. Parsons (2000). "Analysis of Struvite Precipitation in Real and Synthetic Liquors." Trans. IchemE. **Part B**: 480-488.

Draper, N.R. and H. Smith (1966). Applied Regression Analysis. New York, John Wiley and Sons, Inc.

Eberl, D.D., V.A. Drits and J. Srodon (1998). "Deducing Growth Mechanisms for Minerals from the Shapes of Crystal Size Distributions." American Journal of Science **298**: 499-533.

Fresenius, W., K. E. Quentin, Schneider. W. and H. H. Rump (1987). Water Analysis. New York, Springer-Verlag.

Gibbs, J. W. (1948). Collected Works: Thermodynamics. Yale University, New Haven. USA. **1**.

gPROMS (2002). gPROMS System Programming Guide. London, Process System Enterprise Ltd.

gPROMS (2002a). gPROMS Advanced User Guide. London, Process Systems Enterprise Ltd.

Green, D. A. (1983). The Use of Microprocessor for Control and Instrumentation in Food Industry. Engineering and Food. B. Backenna. London, Elsevier Science**:** 757-771.

Hanrahan, G., P. C. F. C. Gardolinski, M. Gledhill and P. J. Worsfold (2003). Environmental Monitoring of Nutrients. New York, USA, McGraw-Hill.

Harrison, M. (1999). Source Reduction of Nutrients from Abattoir Wastewater by Struvite Crystallization, PhD Thesis, Chemical Engineering, University of Queensland.

Henning, G. (1990). Industrial Crystallization. Garmisch, FRG.

Hirasawa, I. (1996). "Study on the Recovery of Ions in Wastewater by Crystallization." Memoirs of the School of Science and Engineering, **60**: 97-119.

Hoare, M. R. and J. McInnes (1982). "Protein Precipitation and Ageing." Transactions of the Institute of Chemical Engineers **60**: 79-87.

Horowitz, A. J., K. A. Elrick and M. R. Colberg (1992). "The Effect of Membrane Filtration Artifacts on Dissolved Trace Element Concentrations." Water Research **26**(6): 753-763.

Hudson, N. (2003). Pond Survey Data: Queensland Piggeries. Toowoomba, Queensland, Queensland DPI.

Hurd, D. C. and D. W. Spencer (1991). Marine Particles: Analysis and Characterization, American Geophysical Union, Geophysical Monograph 63.

Joko, I. (1984). "Phosphorus Removal from Wastewater by the Crystallization Method." Water Science and Technology. **17**: 121-132.

Kim, K. J. and A. Mersmann (2001). "Estimation of Metastable Zone Width in Different Nucleation Process." Chemical Engineering Science **56**: 47.

Kofina, A. N. and P. G. Koutsoukos (2003). Nucleation and Crystal Growth of Struvite in Aqueous Media: New Prospective in Phosphorus Recovery. WASIC, Istanbul, Turkey.

Kofina, A. N. and P. G. Koutsoukos (2005). "Spontaneous Precipitation of Struvite from Synthetic Wastewater Solutions." Crystal Growth and Design **5**(2): 489-496.

Koutsoukos, P. G. (2004). Email Communication: Control Strategy of Struvite Crystallization. P. A. Schneider and M. I. Ali.

Kruger, I., G. Taylor and M. Ferrier (1995). Effluent at Work. Australian Pig Housing Series, NSW Agriculture, Tamworth.

Lowenthal, R. E., U. R. C. Kornmuller and E. P. van Heerden (1995). "Modelling Struvite Precipitation in Anaerobic Treatment Systems." Water Science and Technology **30**(12): 107-116.

Mamais, D., P. A. Pitt, Y. W. Cheng, J. Loiacono and D. Jenkins (1994). "Determination of Ferric Chloride Dose to Control Struvite Precipitation in Anaerobic Sludge Digesters." Water Environmental Resources **66**(7): 912-918.

Mandel, J. (1984). The Statistical Analysis of Experimental Data. New York, Dover Publications Inc.

Mangin, D., S. Regy, J. P. Klein and C. Thronton (2004). Struvite Crystallization Reaction in a Semi-Continuous Reactor. International Conference on Struvite: Its Role in Phosphorus Recovery and Reuse, Cranfield University, UK.

Martell, A.E. and J. C. Smith (1989). Critical Stability Constants.

McCabe, W. L., J. C. Smith and P. Harriot (1985). Unit Operation of Chemical Engineering. 4th edition, McGraw Hill Book Company, USA.

McPherson, A. (1988). "The Use of Heterogeneous and Epitaxial Nucleation to Promote the Growth of Protein Crystals." Journal of Crystal Growth **90**(1-3): 47-50.

Mendel, J. M. (1973). Discrete Techniques of Parameter Estimation: The Equation Error Formulation. New York, Marcel Dekker Inc.

Meo, H. and G. Cleary (2000). Australian Pig Industry Handbook: Pig Stats99. APC & PRDC.

Mersmann, A. (2001). Crystallization Technology Handbook. 2nd edition, New York, USA, Marcel Dekker Inc.

Momberg, G. A. and R. A. Oellermann (1992). "The Removal of Phosphate by Hydroxyapatite and Struvite Crystallization in South Africa." Water Science and Technology **26**(5-6): 987-996.

Morel, F.M.M. and J.G. Hering (1993). Principles and Applications of Aquatic Chemistry. New York, John Wiley & Sons Inc.

Moscosa-Santilla, M., O. Bals, H. Fauduet, C. Porte and A. Delacroix (2000). "Study of batch crystallization and determination of an alternative temperature-time profile by on-line turbidity analysis application to glycine crystallization." Chemical Engineering Science **55**: 3759-3770.

Mullin, J. W. (1993). Crystallization. 3rd, Butterworth-Heinemann Publications, Ipswich, UK.

Mullin, J. W. and K. D. Raven (1961). "Nucleation in Agitated Solutions." Nature **190**: 251.

Mullin, J. W. and K. D. Raven (1962). "Influence of Mechanical Agitation on the Nucleation of Aqueous Salt Solutions." Nature **195**: 35-38.

Munch, E. V. and K. Barr (2001). "Controlled Struvite Crystallization for Removing Phosphorus from Anaerobic Digester Side streams." Water Resources. **35**(1): 151-159.

Myerson, A. S. (1993). Handbook of Crystallization. 1st, Boston USA, Butterworth-Heinmann Series in Chemical Engineering.

Nancollas, G. H. (1968). "Kinetics of Crystal Growth from Solution." Journal of Crystal Growth **3,4**: 335-339.

Nelson, N. O. (2000). Struvite Formation to Remove Phosphorus from Anaerobic Swine Lagoon Effluent as Struvite and its Use as Slow Release Fertilizer, Master Thesis, School of Science, North Carolina State University.

Nelson, N. O., R. Mikkelsen and D. Hesterberg (2003). "Struvite Precipitation in Anaerobic Swine Liquid: Effect of pH and Mg:P Ratio and Determination of rate Constant." Biosource Technology **89**: 229-236.

Ohlinger, K. N. (1999). Kinetics Effects on Preferential Struvite Accumulation in Wastewater, PhD Thesis, School of Science and Engineering, California State University.

Ohlinger, K. N., T. M. Young and E. D. Schroeder (1998). "Predicting Struvite Formation in Digestion." Water Research **32**: 3607-3614.

Ohlinger, K. N., T. M. Young and E. D. Schroeder (2000). "Postdigestion Struvite Precipitation Using a Fluidized Bed Reactor." Journal of Environmental Engineering **126**(4): 361-368.

Onga (2004). Onga Pumps: Water Systems Product Guide, www.Onga.com.au.

Paraskeva, C. A., P. G. Charalambous, L. E. Stokka, P. G. Klepetsanis, P. G. Koutsoukos, P. Read, T. Ostvold and A. C Payatakes (2000). "Sandbed Consolidation with Mineral Precipitation." Journal of Colloid Interface Science **232**: 326-339.

Pareena, P. and A. E. Flood (2005). "Effect of Growth Rate History on Current Crystal Growth: A Second Look at Surface Effects on Crystal Growth Rates." Crystal Growth & Design **5**(1): 365-371.

Parkhurst, L. D., Appelo, C. A. J. (1999). User's Guide to PHREEQC (2) - A Computer Program for Speciation, Batch- Reaction, One-Dimensional Transport, and Inverse Geochemical Calculations. Denver, Colorado, U.S. Department of the Interior & U.S. Geological Survey.

Penkova, A., I. Dimitrov and Chr. N. Nanev (2003). Nucleation of Insulin Crystals in a Wide Continuous Supersaturation Gradient. Micro gravity Transport Processes in Fluid, Thermal, Biological and Materials Sciences III, Davos, Switzerland.

Piekema, P. and A. Giesen (2001). Phosphate Recovery by the Crystallization Process: Experience and Developments. Second International Conference on the Recovery of Phosphorus from Sewage and Animal Wastes, Noordwijkerhout, The Netherlands.

Quintana, M., E. Sanchez, M. F. Colmenarejo, J. Barrera, J. Garcia and R. Borja (2005). "Kinetics of Phosphorus Removal and Struvite Formation by the Utilizationof by-product of Magnesium Oxide Production." Chemical Engineering Journal **11**: 45-52.

Ramalingom, S., J. Poddar and N. S. Kalkura (2001). "Crystallization and Characterization of Orthorhombic beta-$MgSO_4.7H_2O$." Crystal Research Technology **36**(12): 1357-1364.

Rand, M. C., A. E. Greenberg and M. J. Taras (1975). Standard Methods: For the Examination of Water and Wastewater. 14th edition, 1015 Eighteenth Street NW, Washington DC 20036, American Public Health Association.

Randloph, A. D. and M. A. Larson (1991). Theory of Particulate Process: Analysis and Techniques of Continuous Crystallization. Academic Press: Harcourt Brace Jovanovich Publishers.

Schuling, R. D. and A. Andrade (1999). "Recovery of Struvite from Calf Manure." Environmental Technology **20**: 765-768.

Seckler, M. M. and O. S. L. Bruinsma (1996). "Calcium Phosphate Precipitation in a Fluidised Bed in Relation of Process Condition: A Black Box Approach." Water Research **30**(7): 1577-1585.

Sharpley, A. N (2000). Agriculture and Phosphorus Management - The Chesapeake Bay. Blvd, Florida, Lewis Publisher, CRC Press LLC.

Snoeyink, V. L. and D. Jenkins (1980). Water Chemistry. John Wiley and Sons, USA.

Sohnel, O. and J. Garside (1992). Precipitation: Basic Principles and Industrial Applications. Butterworth-Heineman.

Srinivasakannan, C., R. Vasanthakumar, K. Iyappan and P. G. Rao (2002). "A Study on Crystallization of Oxalic Acid in Batch Cooling Crystallizer." Chemical and Biochemical Engineering Quarterly **16**(3): 125-129.

Stumm, W. and J. J. Morgan (1996). Aquatic Chemistry. New York, John Wiley and Sons, USA.

Tavare, S. N. (1995). Industrial Crystallization: Process Simulation Analysis and Design. New York and London, Plenum Press.

Taylor, A. W., A. W. Frazier and E. L. Gurney (1963). "Solubility Product of Magnesium Ammonium." Transaction Faraday Society **59**: 1580-1589.

Thaller, C., L. Weaver, G. Eichele, E. Wilson, R. Karlsson and J. Jansonius (1981). "Repeated Seeding Technique for Growing Large Single Crystal Structures of Proteins." Journal of Molecular Biology **147**: 465-469.

Toumi, A. and S. Engell (2004). "Optimization based Control of a Reactive Simulated Moving Bed Process for Glucose Isomerization." Chemical Engineering Science **59**: 3777-3792.

Trystram, G. (1986). State of Art of Computer Control of Food Processes. Engineering and Food. M. L. Manguer and P. Jelen. London, Elsevier Science. **2:** 459-474.

Trystram, G. and F. Courtois (1994). "Food Processing Control - Reality and Problems." Food Research International **27**: 173-185.

Trystram, G. and E. Dumoulin (1990). Process Control in the Food Industry. Engineering and Schubert. W. Spiess and H. Schubert. London, Elsevier Science. **1:** 705-718.

van der Houwen, J.A.M. and E. Valsami-Jones (2001). "The Application of Calcium Phosphate Precipitation Chemistry to Phosphorus Recovery: The Influence of Organic Ligands." Environmental Technology **22**: 1325-1335.

van Loon, G. W. (2000). Environmental Chemistry- A Global Perspective. London, Oxford University Press, UK.

Volmer, M. (1939). Kinetic der Phasenbildung. Steinkopff, Leipzig.

Webb, T. L. and G. E. Ho (1992). "Struvite Solubility and its Application to a Piggery Effluent Problem." Water Science and Technology **26**(9-11): 2229-2232.

White, E. T. (1971). Industrial Crystallization: A Short Course. University of Queensland.

Wild, A (1993). Soil and the Environment- An Introduction. Cambridge University Press, Great Britain.

NOMENCLATURE

Literature Review

A_T	Crystal surface area
α_i	Ionization fraction
ΔC	Concentration gradient
C_i	Free ion concentration
$C_{T,i}$	Total analytical concentration
dL/dt	Overall linear growth rate
I'	Mixing intensity
K_{so}	Thermodynamic Solubility Product of Struvite
K	Growth constant of crystal
K_g	Overall growth rate constant
g	Overall crystal growth order
L	Crystal size
N	Nucleation rate
T	Temperature
P_s	Conditional solubility product
pK_{so}	Negative logarithmic value of minimum solubility product of struvite
R	Specific rate of mass deposition
y	Crystal growth order
r	Radius of the clusters
σ	Solid-liquid interfacial tension
R	Gas constant
T	Temperature in Kelvin degree
Vm	Molecular volume
A	Arrhenius constant
ΔGs	Gibbs free energy change for forming the crystal surface
ΔGv	Gibbs free energy change for forming the crystal volume

Derivation of Thermodynamic Modeling

A	DeBye-Hückel constant (temperature dependent)
C_{T_Mg}	Total concentration of magnesium (molar)
C_{T_NH4}	Total concentration of ammonium (molar)
C_{T_PO4}	Total concentration of phosphate (molar)
$C_{i,in}$, $C_{i,out}$	Inlet and outlet solution concentration of specific species (mg/l)
C_{NaOH}	Concentration of NaOH in feed solution (molar)
dm/dt	Mass deposition of single crystals (g)
dM/dt	Total mass deposition of struvite (g)
$\frac{dC'_i}{dt}$	Change of solution concentration in the reactor (mg/l)

$\frac{dC_i}{dt}$	Total change of individual solution species in mg (Mg^{2+}, NH_4^+ and PO_4^{3-})
$\frac{dM}{dt}$	Mass deposition of struvite crystal
F_{in}	Inlet flow rate of effluent (l/h)
F_{out}	Outlet flow rate of treated effluent (l/h)
I	Ionic strength
I'	Mixing intensity
$[i]$	Ionic concentration (molar)
$\{i\}$	Activity concentration (molar)
K_w	Ionization constant of water
K	Growth rate constant of struvite kinetics (μm/h)
K_{so}	Minimum struvite solubility product (μm/h)
K_i	Equilibrium constant of the specified ion complexes
L_0	Mean diameter of seeds (μm)
L	Mean diameter of growing struvite (μm)
MW_{MAP}	Molecular weight of struvite
MW_{c_i}	Molecular weight (g) of individual solution species (Mg^{2+}, $NH_4^+$and PO_4^{3-})
M	Mass of struvite (g)
MW_s	Molecular weight of struvite (g)
$\{Mg^{2+}\}$	Activity concentration of magnesium ion (molar)
$\{NH_4^+\}$	Activity concentration of ammonium ion (molar)
n	Order of equation due to supersaturation
n_1	Order of equation due to crystal size
P_{cs}	Conditional Solubility Product
P_{so}	Molar concentration product of reactants
$\{PO_4^{3-}\}$	Activity concentration of phosphate ion
ρ_c	Density of struvite crystal (g/cm^3 or kg/L)
S_c	Critical supersaturation of solution
S	Relative supersaturation (oversaturation)
T	Temperature
V	Volume of the reactor
V_{NaOH}	Required volume of NaOH feed solution
Z	Chemical charge

Result and Discussion from Experiment

x_1	Reactive concentration of magnesium ammonium and phosphate (molar)
x_2	Concentration of feed solution (molar)
x_3	Concentration of NaOH in feed (molar)
ΔL	Increase of crystal size in μm

Result and Discussion from Simulation

$\alpha_{Mg^{2+}}$	Ionization fraction of magnesium

$\alpha_{PO_4^{3-}}$	Ionization fraction of phosphate
$\alpha_{NH_4^+}$	Ionization fraction of ammonium
$\gamma_{Mg^{2+}}$	Activity of magnesium
$\gamma_{PO_4^{3-}}$	Activity of phosphate
$\gamma_{NH_4^+}$	Activity of ammonium
K	struvite growth constant (μm/h)
n	struvite growth order due to supersaturation
n_1	struvite growth order due to crystal size
dL/dt	Growth of struvite
f	Functions of the specified variables
x(t)	Differential variables applied for parameter estimation modeling
$\dot{x}(t)$	Time derivatives of x(t) applied for parameter estimation modeling
y(t)	Algebraic variables applied for parameter estimation modeling
u(t)	Time varying control variables
θ	Parameters t be estimated
K	Struvite growth constant (μm/h)
n	Struvite growth order due to supersaturation
n_1	Struvite growth order due to particle size
L(0)	Initial mean crystal size (μm)
M(0)	Initial mass of seeds (g)
V(0)	Initial mean particle size (μm)
$C_i(0)$	Initial reactant concentration (mg/l)
i	Number of experiments performed
j	Number of variables in ith expt. and kth variables
k	Number of value in each expt. of any variable
z	Predicted variables
$\tilde{z}$	Measured variables
N	Total number of measurement taken during all experiments
θ	A set of model parameters to be estimated (***K*** and ***n***
NE	Number of experiments performed
NV_j	Number of variables measured in the ***i****th* experiments
NM_{ij}	Number of measurements of the ***j****th* variables
σ^2_{ijk}	Variance of the *kth* measurement of variable *j* in the experiment *i*

APPENDIX A

A.1 Automatic Temperature Control System

The automatic temperature control system was operated by computer operated ProcessACT operating system. Plastic coated copper cooling coil encompassed with cooling water circulation stream maintained cooling of reactor. The recirculation system was comprised of normally open solenoid valve (B_1), normally closed solenoid valve (B_2), recirculation pump (P) and ice slurry reservoir. A resistive temperature device (RTD), dipped into reactive solution and united with control module, sent signal to the solenoid valves to open or close accordingly based on process temperature. When reactor temperature drops below set point, control module send signal to close solenoid valve (B_1) and open the solenoid valve (B_2), so that coolant flows through smaller loop system (PB_2). On the other hand, when reactor temperature increases above the set point, control module close the solenoid valve (B_2) and open the solenoid valve (B_1) so that coolant flows through cooling coil and maintain the set-point temperature. Controlling of temperature reduces offset in pH reading. Offset in pH reading may have very adverse affect on process control.

A.2 Flow Diagram of Recirculation Pump (model: Onga 400 series)

Recirculation pump (Onga; model 413) was used for recirculation and mixing of reactive solution. The capacity of pump (model 400 series) against different pump head is demonstrated in Figure (A.1).

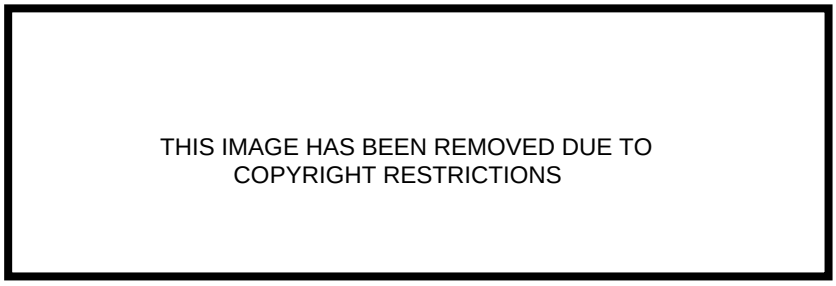

Figure A. 1 Description of recirculation pump capacity (Onga 2004)

APPENDIX B

B.1 Coding of Parameter Estimation Modeling in gPROMS (Est.type 1 and Est.type 4)

```
#  ***************************************************************************************************
#                    PARAMETER ESTIMATION
#  PARAMETER ESTIMATION MODEL CONSIDERING ALL THE IONIC COMPLEXES AND OHLINGER
#  (1999) SOLBILITY LIMIT DATA
#  INPUT DATA: PILOT SCALE EXPERIMENTAL DATA IN CONTROLLED SUPERSATURATION
#  MODEL LINK: Struvite_Modelling>Struvite_4_Control_PE>Est_bd>EST_BD>LC1,LC2,LC3
#  ***************************************************************************************************

PARAMETER
   K_w         AS REAL                  # Solubility Product of water
   A           AS REAL                  # DeBye-Huckel Constant
   Z_2         AS REAL                  # Valency of Mg
   Z_1         AS REAL                  # Valency of NH4
   Z_3         AS REAL                  # Valency of PO4
   MW_Mg       AS REAL                  # Molecular Weight of Mg (g)
   MW_NH4      AS REAL                  # Molecular Weight of NH4 (g)
   MW_PO4      AS REAL                  # Molecular Weight of PO4 (g)
   Density     AS REAL                  # Density of struvite in g/cm3 (Kg/L)
   MW_MAP      AS REAL                  # Molecular weight of struvite (g)
   pi          AS REAL                  # A constant : unitless
   NoComp      AS INTEGER               # Number of conducted experiments

   pH          AS ARRAY(NoComp) OF REAL        # Experimental pH value
   C_NaOH      AS ARRAY(NoComp) OF REAL        # Molar concentration of NaOH feed
```

```
  pH_Fi       AS ARRAY(NoComp) OF REAL      # pH value of the inlet solution
  V0          AS ARRAY(NoComp) OF REAL      # Initial volume of solution in the reactor (L)


VARIABLE
  C_T_PO4     AS ARRAY(NoComp) OF NoType    # Total Input Concentration of PO4(M)
  C_T_Mg      AS ARRAY(NoComp) OF NoType    # Total Input Concentration of Mg(M)
  C_T_NH4     AS ARRAY(NoComp) OF NoType    # Total Input concentration of NH4(M)

  Mg_Fi       AS ARRAY(NoComp) OF NoType    # Concentration of Mg in mg/l
  PO4_Fi      AS ARRAY(NoComp) OF NoType    # Concentration of PO4 in mg/l
  NH4_Fi      AS ARRAY(NoComp) OF NoType    # Concentration of NH4 in mg/l

  K_so        AS NoType                     # Solubility product of struvite
  L           AS ARRAY(NoComp) OF NoType    # Size of struvite crystal (microns)

  H3PO4       AS ARRAY(NoComp) OF NoType    # Activity concentration of H3PO4 (molar)
  H2PO4       AS ARRAY(NoComp) OF NoType    # Activity concentration of H2PO4 ion (molar)
  HPO4        AS ARRAY(NoComp) OF NoType    # Activity concentration of HPO4 ion (molar)
  PO4_i       AS ARRAY(NoComp) OF NoType    # Activity concentration of PO4 ion (molar)
  Mg_i        AS ARRAY(NoComp) OF NoType    # Activity concentration of Mg ion (molar)
  MgOH        AS ARRAY(NoComp) OF NoType    # Activity concentration of MgOH ion (molar)
  NH3         AS ARRAY(NoComp) OF NoType    # Activity concentration of NH3 ion (molar)
  NH4_i       AS ARRAY(NoComp) OF NoType    # Activity concentration of NH4 ion (molar)
  MgPO4       AS ARRAY(NoComp) OF NoType    # Activity Concentration of MgPO4 ion (molar)
  MgHPO4      AS ARRAY(NoComp) OF NoType    # Activity Concentration of MgHPO4 (molar)
  MgH2PO4     AS ARRAY(NoComp) OF NoType    # Activity Concentration of MgPO4 ion (molar)

  CMg_i       AS ARRAY(NoComp) OF NoType    # Ionic concentration of Mg ion (molar)
  CPO4_i      AS ARRAY(NoComp) OF NoType    # Ionic concentration of PO4 ion (molar)
  CNH4_i      AS ARRAY(NoComp) OF NoType    # Ionic concentration of NH4 ion (molar)
  CH2PO4      AS ARRAY(NoComp) OF NoType    # Ionic concentration of H2PO4 ion (molar)
```

```
CHPO4       AS ARRAY(NoComp) OF NoType    # Ionic concentration of HPO4 ion (molar)
CMgOH       AS ARRAY(NoComp) OF NoType    # Ionic concentration of MgOH ion (molar)
CH3PO4      AS ARRAY(NoComp) OF NoType    # Ionic concentration of H3PO4 (molar)
CNH3        AS ARRAY(NoComp) OF NoType    # Ionic Concentration of NH3 (molar)
CMgPO4      AS ARRAY(NoComp) OF NoType    # Ionic Concentration of MgPO4 ion (molar)
CMgHPO4     AS ARRAY(NoComp) OF NoType    # Ionic Concentration of MgPO4 ion (molar)
CMgH2PO4    AS ARRAY(NoComp) OF NoType    # Ionic Concentration of MgPO4 ion (molar)

alpha_Mg    AS ARRAY(NoComp) OF NoType    # Ionization Fraction of Mg
alpha_PO4   AS ARRAY(NoComp) OF NoType    # Ionization frationof PO4
alpha_NH4   AS ARRAY(NoComp) OF NoType    # Ionization frationof NH4

I           AS ARRAY(NoComp) OF NoType    # Ionic strength (molar)

Gamma_1     AS ARRAY(NoComp) OF NoType    # Activity coefficient of 1 charge ion
Gamma_2     AS ARRAY(NoComp) OF NoType    # Activity coefficient of 2 charge ion
Gamma_3     AS ARRAY(NoComp) OF NoType    # Activity coefficient of 3 charge ion
Gamma_0     AS ARRAY(NoComp) OF NoType    # Activity coefficient of 0 charge ion

H           AS ARRAY(NoComp) OF NoType    # Concentration of H ion
OH          AS ARRAY(NoComp) OF NoType    # Concentration of OH ion

NH4_Feed    AS ARRAY(NoComp) OF NoType    # Input concentration of NH4 feed (mg/l)
PO4_Feed    AS ARRAY(NoComp) OF NoType    # Input concentration of PO4 feed (mg/l)
Mg_Feed     AS ARRAY(NoComp) OF NoType    # Input concentration of Mg feed (mg/l)

V           AS ARRAY(NoComp) OF NoType    # Constant operative volume of reactor(Liter)
N_MAP       AS ARRAY(NoComp) OF NoType    # Number of struvite seeds
M_MAP       AS ARRAY(NoComp) OF NoType    # Mass of struvite into the reactor (g)
F_NaOH      AS ARRAY(NoComp) OF NoType    # Feed flowrate of NaOH in l/h

NH4         AS ARRAY(NoComp) OF NoType    # Mass of ammonium into the reactor (mg)
```

```
PO4             AS ARRAY(NoComp) OF NoType      # Mass of phosphate into the reactor (mg)
Mg              AS ARRAY(NoComp) OF NoType      # Mass of magnesium into the reactor (mg)

P_cs            AS ARRAY(NoComp) OF NoType      # Condition solubility product of struvite
P_so            AS ARRAY(NoComp) OF NoType      # Concentration product of struvite
S               AS ARRAY(NoComp) OF NoType      # Supersaturation of solution (Saturation Index)
SSR             AS ARRAY(NoComp) OF NoType      # Supersaturation Ratio of solution

Fi              AS ARRAY(NoComp) OF NoType      # Feed flowrate of solution (l/h)
H_Fi            AS ARRAY(NoComp) OF NoType      # H+ concentration of inlet solution (molar)
OH_Fi           AS ARRAY(NoComp) OF NoType      # OH+ concentration of inlet solution (molar)

Lchange         AS ARRAY(NoComp) OF NoType      # Change of mean particle size (microns)
L0              AS ARRAY(NoComp) OF NoType      # Initial mean particles size as seeds (microns)
M_MAP_0         AS ARRAY(NoComp) OF NoType      # Initial mass of struvite (Kg)
Mchange         AS ARRAY(NoComp) OF NoType      # Change of mean struvite mass (g)

K_kin           AS NoType_2         # Growth rate constant (microns/h)
n               AS NoType_1         # Order of the growth rate equation
```

EQUATION

```
Mg_Fi = C_T_Mg*MW_Mg*1000;
NH4_Fi = C_T_NH4*MW_NH4*1000;
PO4_Fi = C_T_PO4*MW_PO4*1000;

MgOH = 10^2.56 *Mg_i*OH ;
NH4_i = 10^9.252 *H*NH3 ;
HPO4 = 10^12.35 *H*PO4_i ;
H2PO4 = 10^7.20 *H*HPO4 ;
H3PO4 = 10^2.15 *H*H2PO4 ;
MgPO4 = 10^(4.8)*Mg_i*PO4_i;
```

```
MgHPO4 = 10^(2.91)*Mg_i*HPO4 ;
MgH2PO4 = 10^(0.45)*Mg_i*H2PO4;

K_so = 10^(-13.26);

CMg_i = Mg_i/Gamma_2;
CPO4_i = PO4_i/Gamma_3;
CNH4_i = NH4_i/Gamma_1;
CH3PO4 = H3PO4/Gamma_0;
CH2PO4 = H2PO4/Gamma_1;
CHPO4 = HPO4/Gamma_2;
CMgOH = MgOH/Gamma_1;
CNH3 = NH3/Gamma_0;
CMgPO4 = MgPO4/Gamma_1;
CMgHPO4 = MgHPO4/Gamma_0;
CMgH2PO4 = MgH2PO4/Gamma_1;

C_T_PO4 = CH3PO4 + CH2PO4 + CHPO4 + CPO4_i + CMgPO4 + CMgHPO4 + CMgH2PO4 ;
C_T_Mg = CMg_i + CMgOH + CMgPO4 + CMgHPO4 + CMgH2PO4;
C_T_NH4 = CNH3 + CNH4_i ;

H = 10^(-pH) ;
OH = K_w/H ;

alpha_Mg = CMg_i/C_T_Mg ;
alpha_PO4 = CPO4_i/C_T_PO4 ;
alpha_NH4 = CNH4_i/C_T_NH4 ;

I = 0.5*(C_T_Mg*Z_2*Z_2 +  C_T_NH4*Z_2*Z_2 + C_T_PO4*Z_3*Z_3);

Gamma_2= 10^(-(A*Z_2^2) * ((I^0.5/(1 + I^0.5))-0.3*I)) ;
Gamma_3=  10^(-(A*Z_3^2) * ((I^0.5/(1 + I^0.5))-0.3*I)) ;
```

```
Gamma_1= 10^(-(A*Z_1^2) * ((I^0.5/(1 + I^0.5))-0.3*I)) ;
Gamma_0 = 10^(-0.1*I);


 # Conditional solubility product (Pcs) and Concentration product (Pso)
 P_so = C_T_mg*C_T_NH4*C_T_PO4 ;
 P_cs = K_so/(alpha_Mg*Gamma_2*alpha_NH4*Gamma_1*alpha_PO4*Gamma_3);

 # Supersaturation of solution
  SSR = (P_so/P_cs)^0.33333 ;                          # Supersaturation ratio
  S = LOG10(P_so) - LOG10(P_cs);                       # Supersaturation Index

 # Growth rate of crystals (microns/h)
   $L = K_kin *((SSR-1)^n);                            # Based on Oversaturation (Oversaturation=SSR-1)
  # $L = K_kin *(S^n);                                 # Based on Saturation Index

 # Volume of solution in the reactor
    $V = Fi + F_NaOH ;

 # Ammonium mass balance in milligrams
    $NH4 = Fi*NH4_Feed - ($M_MAP*1000/MW_MAP)*MW_NH4 ;

 # Ammonia mass balance in milligrams
    $Mg = Fi*Mg_Feed - ($M_MAP*1000/MW_MAP)*MW_Mg ;

# Phosphate mass balance in milligrams
    $PO4 = Fi*PO4_Feed - ($M_MAP*1000/MW_MAP)*MW_PO4 ;
                          # Unit conversion:  1kg =1e6 mg

 # Transformation of total mass to concentrations (ppm)
    PO4_Fi = PO4/V;
    Mg_Fi = Mg/V;
```

```
    NH4_Fi = NH4/V;

  # struvite mass balance in grams
    $M_MAP = (10^(-12))*N_MAP*0.5*pi*Density*(L^2)*($L);


  # Determination of Number of struvite Crystals
     M_MAP_0 = (10^(-12)) *N_MAP*(pi/6)*Density *(L0^3);

  # Thermodynamic relation of H+ and OH- ions
     H_Fi = 10^(-pH_Fi);        # For feed solution
     OH_Fi = 10^(-14)/H_Fi;     # For feed solution

  # Minimization of error of mean particle size (microns)
     Lchange = L - L0;

 # Minimization of error of mean particle size (grams)
     Mchange = M_MAP - M_MAP_0;



UNIT
  E101 AS struvite_4_Control_PE

SET
WITHIN E101 DO
   K_w       :=10^(-14);       # Ionization Product of water
   A         := 0.5 ;          # DeBye-Huckel Constant
   Z_2       := 2.0;           # Valency of 2 chagre ions
   Z_1       := 1.0;           # Valency of 1 charge ions
   Z_3       := 3.0;           # Valency of 3 charge ions
```

```
   MW_Mg       := 24;                  # Molecular weight of Mg (g)
   MW_NH4      := 18;                  # Molecular weight of NH4 (g)
   MW_PO4      := 95;                  # Molecular weight of PO4 (g)

   Density     := 1.72;                # unit: Kg/L (g/cm3)
   pi          := 3.1416;              # unitless
   MW_MAP      := 245.10;              # Gram molecular weight of struvite-hexahydrate

   V0          := [16, 16.5, 16.8];                          # Unit: Liter
   C_NaOH      := [0.0045*18, 0.0060*18, 0.0055*18];         # Unit: molar
   pH_Fi       := [5.8, 5.75, 5.6];                          # Feed solution pH
   NoComp      := 3;                                         # Number of experiments
   pH          := [7.35, 7.22, 7.51];                        # Controlled pH of the reactive solution
END
```

ASSIGN

```
   WITHIN E101 DO
    NH4_Feed   := [0.0045*10*18000, 0.0060*10*18000, 0.0055*10*18000];     # unit: mg/l
    PO4_feed   := [0.0045*10*95000, 0.0060*10*95000, 0.0055*10*95000];     # unit: mg/l
    Mg_Feed    := [0.0045*10*24000, 0.0060*10*24000, 0.0055*10*24000];     # unit: mg/l

    L0         :=  [140.06, 138.83, 133.25];          # unit: micrometer

    Fi(1)      := 0.5;                                # unit: l/h
    Fi(2)      :=0.690909091;                         # unit: l/h
    Fi(3)      := 1;                                  # unit: l/h

    F_NaOH(1)  := 0.5;                                # unit: l/h
    F_NaOH(2)  :=0.690909091;                         # unit: l/h
    F_NaOH(3)  := 1;                                  # unit: l/h
```

```
    K_kin      := 25;                    # unit: microns/h
    n          :=1.5;                    # unitless

    M_MAP_0    := [30, 30, 30];          # unit: grams
END


INITIAL
   WITHIN E101 DO
      NH4_Fi(1)   = 92.32;               # unit: mg
      NH4_Fi(2)   = 112.64;              # unit: mg
      NH4_Fi(3)   = 112.64;              # unit: mg

      PO4_Fi(1)   = 487.25;              # unit: mg
      PO4_Fi(2)   = 594.52;              # unit: mg
      PO4_Fi(3)   = 594.52;              # unit: mg

      Mg_Fi(1)    = 108;                 # unit: mg
      Mg_Fi(2)    = 165;                 # unit: mg
      Mg_Fi(3)    = 147;                 # unit: mg

      V           = V0;                  # unit: Liter
      Lchange     = 0;                   # unit: microns
      Mchange     = 0;                   # unit: microns
END


SOLUTIONPARAMETERS
   gExcelOutput := "struvite_PE"

SCHEDULE
   CONTINUE for 30
```

ESTIMATE
E101.K_kin
25 20 80

ESTIMATE
E101.n
1.5 0.75 2

MEASURE
E101.L(1)
HETEROSCEDASTIC PREDICTED_VALUES (1 : 0.5 : 20; 0.5: 0.1: 1)

MEASURE
E101.PO4_Fi(1)
HETEROSCEDASTIC PREDICTED_VALUES (1 : 1E-20 : 20; 0.5: 0.1: 1)

MEASURE
E101.Mg_Fi(1)
HETEROSCEDASTIC PREDICTED_VALUES (1 : 0.5 : 20; 0.5: 0.1: 1)

MEASURE
E101.L(2)
HETEROSCEDASTIC PREDICTED_VALUES (1 : 0.5 : 10; 0.5: 0.1: 1)

MEASURE
E101.PO4_Fi(2)
HETEROSCEDASTIC PREDICTED_VALUES (1 : 0.5 : 20; 0.5: 0.1: 1)

MEASURE
E101.Mg_Fi(2)
HETEROSCEDASTIC PREDICTED_VALUES (1 : 0.5 : 20; 0.5: 0.1: 1)

MEASURE
E101.L(3)
HETEROSCEDASTIC PREDICTED_VALUES (1 : 0.5 : 20; 0.5: 0.1: 1)
MEASURE
E101.PO4_Fi(3)
HETEROSCEDASTIC PREDICTED_VALUES (1 : 0.5 : 20; 0.5: 0.1: 1)
MEASURE
E101.Mg_Fi(3)
HETEROSCEDASTIC PREDICTED_VALUES (1 : 0.5 : 20; 0.5: 0.1: 1)

RUNS
LC1
LC2
LC3

MEASURE
E101.L(1)
0.0 140.06
1.0 148.54
4.5 157.41
10.5 162.02
12.5 164.22
24.0 170.9

MEASURE
E101.PO4_Fi(1)

0.0 487.25
1.0 453.54
4.5 462.74
10.5 524.03
12.5 508.71
24.0 487.25

MEASURE
E101.Mg_Fi(1)
0.0 107.0
1.0 113.0
4.5 110.0
10.5 117.0
12.5 109.0
24.0 105.0

INTERVALS
5
1.0
4.5
10.5
12.5
24.0

PIECEWISE-CONSTANT
E101.Fi(1)
0.50
0.28571
0.175
0.15833
0.20

PIECEWISE-CONSTANT
E101.F_NaOH(1)
0.50
0.28571
0.175
0.15833
0.20

MEASURE
E101.L(2)
0.0 138.83
0.55 145.12
2.17 154.34
3.57 158.47
6.57 165.43

MEASURE
E101.PO4_Fi(2)
0.0 594.52
0.55 530.16
2.17 631.29
3.57 554.68
6.57 643.55

MEASURE
E101.Mg_Fi(2)
0.0 165.0
0.55 156.0
2.17 155.0
3.57 138.0
6.57 150.0

INTERVALS
4
0.55
2.17
3.57
6.57

PIECEWISE-CONSTANT
E101.Fi(2)
0.69
0.64
0.63
0.67

PIECEWISE-CONSTANT
E101.F_NaOH(2)
0.69
0.64
0.63
0.67

MEASURE
E101.L(3)
0.0 133.25
0.75 148.39
2.0 173.59
3.4 184.36
7.5 192.4

MEASURE
E101.PO4_Fi(3)
0.0 594.52
0.75 585.32
2.0 499.52
3.4 478.06
7.5 487.26

MEASURE
E101.Mg_Fi(3)
0.0 147.0
0.75 146.0
2.0 128.0
3.4 138.0
7.5 124.0

INTERVALS
4
0.75
2.0
3.4
7.5

PIECEWISE-CONSTANT
E101.Fi(3)
1.0
0.9
0.714285714
1.0

E101.F_NaOH(3)

1.0
0.9
0.714285714
1.0

APPENDIX C

C.1 Coding of Parameter Estimation Modeling in gPROMS (Est.type 2 and Est.type 5)

```
#  ************************************************************************
#     PARAMETER ESTIMATION MODEL (CONSIDER THE EFFECT OF SEED SIZE)
#
#  MODEL LINK: struvite_Modelling>Est_bd_Eff_Size>EST_BD_EFF_SIZE
#           >LC_SIZE_1, LC_SIZE_2, LC_SIZE_3
#  ************************************************************************
```

PARAMETER

```
   K_w              AS REAL                    # Solubility Product of water
   A                AS REAL                    # DeBye-Huckel Constant
   Z_2              AS REAL                    # Valency of Mg
   Z_1              AS REAL                    # Valency of NH4
   Z_3              AS REAL                    # Valency of PO4
   MW_Mg            AS REAL                    # Molecular Weight of Mg (g)
   MW_NH4           AS REAL                    # Molecular Weight of NH4 (g)
   MW_PO4           AS REAL                    # Molecular Weight of PO4 (g)
   Density          AS REAL                    # Density of struvite in g/cm3 (Kg/L)
   MW_MAP           AS REAL                    # Molecular weight of struvite (g)
   pi               AS REAL                    # A constant : unitless
   NoComp           AS INTEGER                 # Number of conducted experiments

   pH               AS ARRAY(NoComp) OF REAL   # Experimental pH value
   C_NaOH           AS ARRAY(NoComp) OF REAL   # Molar concentration of NaOH feed
   pH_Fi            AS ARRAY(NoComp) OF REAL   # pH value of the inlet solution
   V0               AS ARRAY(NoComp) OF REAL   # Initial volume of solution in the reactor (L)
```

VARIABLE

C_T_PO4	AS ARRAY(NoComp) OF NoType	# Total Input Concentration of PO4(M)
C_T_Mg	AS ARRAY(NoComp) OF NoType	# Total Input Concentration of Mg(M)
C_T_NH4	AS ARRAY(NoComp) OF NoType	# Total Input concentration of NH4(M)
Mg_Fi	AS ARRAY(NoComp) OF NoType	# Concentration of Mg in mg/l
PO4_Fi	AS ARRAY(NoComp) OF NoType	# Concentration of PO4 in mg/l
NH4_Fi	AS ARRAY(NoComp) OF NoType	# Concentration of NH4 in mg/l
K_so	AS NoType	# Solubility product of struvite
L	AS ARRAY(NoComp) OF NoType	# Size of struvite crystal (microns)
H3PO4	AS ARRAY(NoComp) OF NoType	# Activity concentration of H3PO4 (molar)
H2PO4	AS ARRAY(NoComp) OF NoType	# Activity concentration of H2PO4 ion (molar)
HPO4	AS ARRAY(NoComp) OF NoType	# Activity concentration of HPO4 ion (molar)
PO4_i	AS ARRAY(NoComp) OF NoType	# Activity concentration of PO4 ion (molar)
Mg_i	AS ARRAY(NoComp) OF NoType	# Activity concentration of Mg ion (molar)
MgOH	AS ARRAY(NoComp) OF NoType	# Activity concentration of MgOH ion (molar)
NH3	AS ARRAY(NoComp) OF NoType	# Activity concentration of NH3 ion (molar)
NH4_i	AS ARRAY(NoComp) OF NoType	# Activity concentration of NH4 ion (molar)
MgPO4	AS ARRAY(NoComp) OF NoType	# Activity Concentration of MgPO4 ion (molar)
MgHPO4	AS ARRAY(NoComp) OF NoType	# Activity Concentration of MgHPO4 (molar)
MgH2PO4	AS ARRAY(NoComp) OF NoType	# Activity Concentration of MgPO4 ion (molar)
CMg_i	AS ARRAY(NoComp) OF NoType	# Ionic concentration of Mg ion (molar)
CPO4_i	AS ARRAY(NoComp) OF NoType	# Ionic concentration of PO4 ion (molar)
CNH4_i	AS ARRAY(NoComp) OF NoType	# Ionic concentration of NH4 ion (molar)
CH2PO4	AS ARRAY(NoComp) OF NoType	# Ionic concentration of H2PO4 ion (molar)
CHPO4	AS ARRAY(NoComp) OF NoType	# Ionic concentration of HPO4 ion (molar)
CMgOH	AS ARRAY(NoComp) OF NoType	# Ionic concentration of MgOH ion (molar)

```
CH3PO4          AS ARRAY(NoComp) OF NoType      # Ionic concentration of H3PO4 (molar)
CNH3            AS ARRAY(NoComp) OF NoType      # Ionic Concentration of NH3 (molar)
CMgPO4          AS ARRAY(NoComp) OF NoType      # Ionic Concentration of MgPO4 ion (molar)
CMgHPO4         AS ARRAY(NoComp) OF NoType      # Ionic Concentration of MgPO4 ion (molar)
CMgH2PO4        AS ARRAY(NoComp) OF NoType      # Ionic Concentration of MgPO4 ion (molar)

alpha_Mg        AS ARRAY(NoComp) OF NoType      # Ionization Fraction of Mg
alpha_PO4       AS ARRAY(NoComp) OF NoType      # Ionization frationof PO4
alpha_NH4       AS ARRAY(NoComp) OF NoType      # Ionization frationof NH4

I               AS ARRAY(NoComp) OF NoType      # Ionic strength (mol/L)

Gamma_1         AS ARRAY(NoComp) OF NoType      # Activity coefficient of 1 charge ion
Gamma_2         AS ARRAY(NoComp) OF NoType      # Activity coefficient of 2 charge ion
Gamma_3         AS ARRAY(NoComp) OF NoType      # Activity coefficient of 3 charge ion
Gamma_0         AS ARRAY(NoComp) OF NoType      # Activity coefficient of 0 charge ion

H               AS ARRAY(NoComp) OF NoType      # Concentration of H ion
OH              AS ARRAY(NoComp) OF NoType      # Concentration of OH ion

NH4_Feed        AS ARRAY(NoComp) OF NoType      # Input concentration of NH4 feed (mg/l)
PO4_Feed        AS ARRAY(NoComp) OF NoType      # Input concentration of PO4 feed (mg/l)
Mg_Feed         AS ARRAY(NoComp) OF NoType      # Input concentration of Mg feed (mg/l)

V               AS ARRAY(NoComp) OF NoType      # Constant operative volume of reactor(Liter)
N_MAP           AS ARRAY(NoComp) OF NoType      # Number of struvite seeds
M_MAP           AS ARRAY(NoComp) OF NoType      # Mass of struvite into the reactor (g)
F_NaOH          AS ARRAY(NoComp) OF NoType      # Feed flowrate of NaOH in l/h

NH4             AS ARRAY(NoComp) OF NoType      # Mass of ammonium into the reactor (mg)
PO4             AS ARRAY(NoComp) OF NoType      # Mass of phosphate into the reactor (mg)
Mg              AS ARRAY(NoComp) OF NoType      # Mass of magnesium into the reactor (mg)
```

```
P_cs        AS ARRAY(NoComp) OF NoType    # Condition solubility product of struvite
P_so        AS ARRAY(NoComp) OF NoType    # Concentration product of struvite
S           AS ARRAY(NoComp) OF NoType    # Supersaturation of solution (Saturation Index)
SSR         AS ARRAY(NoComp) OF NoType    # Supersaturation Ratio of solution

Fi          AS ARRAY(NoComp) OF NoType    # Feed flowrate of solution (l/h)
H_Fi        AS ARRAY(NoComp) OF NoType    # H+ concentration of inlet solution (molar)
OH_Fi       AS ARRAY(NoComp) OF NoType    # OH+ concentration of inlet solution (molar)

Lchange     AS ARRAY(NoComp) OF NoType    # Change of mean particle size (microns)
L0          AS ARRAY(NoComp) OF NoType    # Initial mean particles size as seeds (microns)
M_MAP_0     AS ARRAY(NoComp) OF NoType    # Initial mass of struvite (Kg)
Mchange     AS ARRAY(NoComp) OF NoType    # Change of mean struvite mass (g)

K_kin       AS NoType_2                   # Growth rate constant (microns/h)
n           AS NoType_1                   # Order of the growth rate equation
n1          AS Consiseed                  # Order of the growth due to crystal size
```

EQUATION

```
Mg_Fi = C_T_Mg*MW_Mg*1000;
NH4_Fi = C_T_NH4*MW_NH4*1000;
PO4_Fi = C_T_PO4*MW_PO4*1000;

MgOH = 10^2.56 *Mg_i*OH ;
NH4_i = 10^9.252 *H*NH3 ;
HPO4 = 10^12.35 *H*PO4_i ;
H2PO4 = 10^7.20 *H*HPO4 ;
H3PO4 = 10^2.15 *H*H2PO4 ;
MgPO4 = 10^(4.8)*Mg_i*PO4_i;
MgHPO4 = 10^(2.91)*Mg_i*HPO4 ;
```

```
MgH2PO4 = 10^(0.45)*Mg_i*H2PO4;

K_so = 10^(-13.26);

CMg_i = Mg_i/Gamma_2;
CPO4_i = PO4_i/Gamma_3;
CNH4_i = NH4_i/Gamma_1;
CH3PO4 = H3PO4/Gamma_0;
CH2PO4 = H2PO4/Gamma_1;
CHPO4 = HPO4/Gamma_2;
CMgOH = MgOH/Gamma_1;
CNH3 = NH3/Gamma_0;
CMgPO4 = MgPO4/Gamma_1;
CMgHPO4 = MgHPO4/Gamma_0;
CMgH2PO4 = MgH2PO4/Gamma_1;

C_T_PO4 = CH3PO4 + CH2PO4 + CHPO4 + CPO4_i + CMgPO4 + CMgHPO4 + CMgH2PO4 ;
C_T_Mg = CMg_i + CMgOH + CMgPO4 + CMgHPO4 + CMgH2PO4;
C_T_NH4 = CNH3 + CNH4_i ;

H = 10^(-pH) ;
OH = K_w/H ;

alpha_Mg = CMg_i/C_T_Mg ;
alpha_PO4 = CPO4_i/C_T_PO4 ;
alpha_NH4 = CNH4_i/C_T_NH4 ;

I = 0.5*(C_T_Mg*Z_2*Z_2 +  C_T_NH4*Z_2*Z_2 + C_T_PO4*Z_3*Z_3);

Gamma_2= 10^(-(A*Z_2^2) * ((I^0.5/(1 + I^0.5))-0.3*I)) ;
Gamma_3=  10^(-(A*Z_3^2) * ((I^0.5/(1 + I^0.5))-0.3*I)) ;
Gamma_1= 10^(-(A*Z_1^2) * ((I^0.5/(1 + I^0.5))-0.3*I)) ;
```

```
Gamma_0 = 10^(-0.1*I);


 # Conditional solubility product (Pcs) and Concentration product (Pso)
 P_so = C_T_mg*C_T_NH4*C_T_PO4 ;
 P_cs = K_so/(alpha_Mg*Gamma_2*alpha_NH4*Gamma_1*alpha_PO4*Gamma_3);

 # Supersaturation of solution
  SSR = (P_so/P_cs)^0.33333 ;                          # Supersaturation ratio
  S = LOG10(P_so) - LOG10(P_cs);                       # Supersaturation Index

 # Growth rate of crystals (microns/h)
   $L = K_kin *((SSR-1)^n)*(L^n1);                     # Based on Oversaturation (Oversaturation=SSR-1)
  # $L = K_kin *(S^n) *(L^n1);                         # Based on Saturation Index

 # Volume of solution in the reactor
    $V = Fi + F_NaOH ;

 # Ammonium mass balance in milligrams
    $NH4 = Fi*NH4_Feed - ($M_MAP*1000/MW_MAP)*MW_NH4 ;

 # Ammonia mass balance in milligrams
    $Mg = Fi*Mg_Feed - ($M_MAP*1000/MW_MAP)*MW_Mg ;

# Phosphate mass balance in milligrams
    $PO4 = Fi*PO4_Feed - ($M_MAP*1000/MW_MAP)*MW_PO4 ;
                        # Unit conversion:  1kg =1e6 mg

 # Transformation of total mass to concentrations (ppm)
    PO4_Fi = PO4/V;
    Mg_Fi = Mg/V;
    NH4_Fi = NH4/V;
```

```
    # struvite mass balance in grams
      $M_MAP = (10^(-12))*N_MAP*0.5*pi*Density*(L^2)*($L);


    # Determination of Number of struvite Crystals
       M_MAP_0 = (10^(-12)) *N_MAP*(pi/6)*Density *(L0^3);

    # Thermodynamic relation of H+ and OH- ions
       H_Fi = 10^(-pH_Fi);                                  # For feed solution
       OH_Fi = 10^(-14)/H_Fi;                               # For feed solution

    # Minimization of error of mean particle size (microns)
       Lchange = L - L0;

   # Minimization of error of mean particle size (grams)
       Mchange = M_MAP - M_MAP_0;
```

UNIT

```
  Size101 AS struvite_5_Control_PE_Eff_Size
```

SET

```
WITHIN Size101 DO
   K_w       :=10^(-14);          # Ionization Product of water
   A         := 0.5 ;             # DeBye-Huckel Constant
   Z_2       := 2.0;              # Valency of 2 chagre ions
   Z_1       := 1.0;              # Valency of 1 charge ions
   Z_3       := 3.0;              # Valency of 3 charge ions

   MW_Mg     := 24;               # Molecular weight of Mg (g)
```

```
   MW_NH4      := 18;                                  # Molecular weight of NH4 (g)
   MW_PO4      := 95;                                  # Molecular weight of PO4 (g)

   Density     := 1.72;                                # unit: Kg/L (g/cm3)
   pi          := 3.1416;                              # unitless
   MW_MAP      := 245.10;                              # Gram molecular weight of struvite-hexahydrate

   V0          := [16, 16.5, 16.8];                    # Unit: Liter
   C_NaOH      := [0.0045*18, 0.0060*18, 0.0055*18];   # Unit: molar
   pH_Fi       := [5.8, 5.75, 5.6];                    # Feed solution pH
   NoComp      := 3;                                   # Number of experiments
   pH          := [7.35, 7.22, 7.51];                  # Controlled pH of the reactive solution
END
```

ASSIGN

```
WITHIN Size101 DO
    NH4_Feed   := [0.0045*10*18000, 0.0060*10*18000, 0.0055*10*18000];   # unit: mg/l
    PO4_feed   := [0.0045*10*95000, 0.0060*10*95000, 0.0055*10*95000];   # unit: mg/l
    Mg_Feed    := [0.0045*10*24000, 0.0060*10*24000, 0.0055*10*24000];   # unit: mg/l

    L0         :=  [140.06, 138.83, 133.25];                             # unit: micrometer

    Fi(1)      := 0.5;                          # unit: l/h
    Fi(2)      :=0.690909091;                   # unit: l/h
    Fi(3)      := 1;                            # unit: l/h

    F_NaOH(1)  := 0.5;                          # unit: l/h
    F_NaOH(2)  :=0.690909091;                   # unit: l/h
    F_NaOH(3)  := 1;                            # unit: l/h

    K_kin      := 25;                           # unit: microns/h
```

```
    n         :=1.5;                          # unitless
    n1        := 0.01;

    M_MAP_0   := [30, 30, 30];                # unit: grams
END
```

INITIAL

```
WITHIN Size101 DO
      NH4_Fi(1)   = 92.32;              # unit: mg
      NH4_Fi(2)   = 112.64;             # unit: mg
      NH4_Fi(3)   = 112.64;             # unit: mg

      PO4_Fi(1)   = 487.25;             # unit: mg
      PO4_Fi(2)   = 594.52;             # unit: mg
      PO4_Fi(3)   = 594.52;             # unit: mg

      Mg_Fi(1)    = 108;                # unit: mg
      Mg_Fi(2)    = 165;                # unit: mg
      Mg_Fi(3)    = 147;                # unit: mg

      V         = V0;                   # unit: Liter
      Lchange   = 0;                    # unit: microns
      Mchange   = 0;                    # unit: microns
END
```

SOLUTIONPARAMETERS

```
   gExcelOutput := "struvite_PE_size"
```

SCHEDULE
CONTINUE for 30

ESTIMATE
Size101.K_kin
25 20 80

ESTIMATE
Size101.n
1.5 0.75 2

ESTIMATE
Size101.n1
1E-1 1E-2 2

MEASURE
Size101.L(1)
HETEROSCEDASTIC PREDICTED_VALUES (1 : 0.5 : 20; 0.5: 0.1: 1)

MEASURE
Size101.PO4_Fi(1)
HETEROSCEDASTIC PREDICTED_VALUES (1 : 1E-20 : 20; 0.5: 0.1: 1)

MEASURE
Size101.Mg_Fi(1)
HETEROSCEDASTIC PREDICTED_VALUES (1 : 0.5 : 20; 0.5: 0.1: 1)

MEASURE
Size101.L(2)
HETEROSCEDASTIC PREDICTED_VALUES (1 : 0.5 : 10; 0.5: 0.1: 1)
MEASURE
Size101.PO4_Fi(2)
HETEROSCEDASTIC PREDICTED_VALUES (1 : 0.5 : 20; 0.5: 0.1: 1)
MEASURE
Size101.Mg_Fi(2)
HETEROSCEDASTIC PREDICTED_VALUES (1 : 0.5 : 20; 0.5: 0.1: 1)

MEASURE
Size101.L(3)
HETEROSCEDASTIC PREDICTED_VALUES (1 : 0.5 : 20; 0.5: 0.1: 1)
MEASURE
Size101.PO4_Fi(3)
HETEROSCEDASTIC PREDICTED_VALUES (1 : 0.5 : 20; 0.5: 0.1: 1)
MEASURE
Size101.Mg_Fi(3)
HETEROSCEDASTIC PREDICTED_VALUES (1 : 0.5 : 20; 0.5: 0.1: 1)

RUNS
LC_SIZE_1
LC_SIZE_2
LC_SIZE_3

MEASURE
Size101.L(1)
0.0 140.06
1.0 148.54

4.5 157.41
10.5 162.02
12.5 164.22
24.0 170.9

MEASURE
Size101.PO4_Fi(1)
0.0 487.25
1.0 453.54
4.5 462.74
10.5 524.03
12.5 508.71
24.0 487.25

MEASURE
Size101.Mg_Fi(1)
0.0 107.0
1.0 113.0
4.5 110.0
10.5 117.0
12.5 109.0
24.0 105.0

INTERVALS
5
1.0
4.5
10.5
12.5
24.0

PIECEWISE-CONSTANT
Size101.Fi(1)
0.50
0.28571
0.175
0.15833
0.20

PIECEWISE-CONSTANT
Size101.F_NaOH(1)
0.50
0.28571
0.175
0.15833
0.20

MEASURE
Size101.L(2)
0.0 138.83
0.55 145.12
2.17 154.34
3.57 158.47
6.57 165.43

MEASURE
Size101.PO4_Fi(2)
0.0 594.52
0.55 530.16
2.17 631.29
3.57 554.68
6.57 643.55

MEASURE
Size101.Mg_Fi(2)
0.0 165.0
0.55 156.0
2.17 155.0
3.57 138.0
6.57 150.0

INTERVALS
4
0.55
2.17
3.57
6.57

PIECEWISE-CONSTANT
Size101.Fi(2)
0.69
0.64
0.63
0.67

PIECEWISE-CONSTANT
Size101.F_NaOH(2)
0.69
0.64
0.63
0.67

MEASURE
Size101.L(3)
0.0 133.25
0.75 148.39
2.0 173.59
3.4 184.36
7.5 192.4

MEASURE
Size101.PO4_Fi(3)
0.0 594.52
0.75 585.32
2.0 499.52
3.4 478.06
7.5 487.26

MEASURE
Size101.Mg_Fi(3)
0.0 147.0
0.75 146.0
2.0 128.0
3.4 138.0
7.5 124.0

INTERVALS
4
0.75
2.0
3.4
7.5

PIECEWISE-CONSTANT
Size101.Fi(3)
1.0
0.9
0.714285714
1.0

PIECEWISE-CONSTANT
Size101.F_NaOH(3)
1.0
0.9
0.714285714
1.0

APPENDIX D

D.1 Coding of Parameter Estimation Modeling in gPROMS (Est.type 3 and Est.type 6)

```
#  ************************************************************************
#  THIS PROGRAM IS DEVELOPED TO IDENTIFY THE STRUVITE GROWTH KINETICS
#  CONSIDERING THE FLEXIBLE SEED SIZE TO AVOID THE EFFECT OF EXPERIMENTAL
#  SETUP ON SEED SIZE
#
#  MODEL LINK: struvite_Modelling>struvite_6_Control_PE_Lchange>Est_bd_Lchange
#          >EST_BD_LCHANGE>LC_LCHANGE_1,LCHANGE_2,LCHANGE_3
#  ************************************************************************
```

PARAMETER

```
  K_w           AS REAL          # Solubility Product of water
  A             AS REAL          # DeBye-Huckel Constant
  Z_2           AS REAL          # Valency of Mg
  Z_1           AS REAL          # Valency of NH4
  Z_3           AS REAL          # Valency of PO4
  MW_Mg         AS REAL          # Molecular Weight of Mg (g)
  MW_NH4        AS REAL          # Molecular Weight of NH4 (g)
  MW_PO4        AS REAL          # Molecular Weight of PO4 (g)
  Density       AS REAL          # Density of struvite in g/cm3 (Kg/L)
  MW_MAP        AS REAL          # Molecular weight of struvite (g)
  pi            AS REAL          # A constant : unitless
  NoComp        AS INTEGER       # Number of conducted experiments

  pH      AS ARRAY(NoComp) OF REAL      # Experimental pH value
  C_NaOH  AS ARRAY(NoComp) OF REAL      # Molar concentration of NaOH feed
```

```
  pH_Fi       AS ARRAY(NoComp) OF REAL        # pH value of the inlet solution
  V0          AS ARRAY(NoComp) OF REAL        # Initial volume of solution in the reactor (L)


VARIABLE
  C_T_PO4   AS ARRAY(NoComp) OF NoType  # Total Input Concentration of PO4(M)
  C_T_Mg    AS ARRAY(NoComp) OF NoType  # Total Input Concentration of Mg(M)
  C_T_NH4   AS ARRAY(NoComp) OF NoType  # Total Input concentration of NH4(M)

  Mg_Fi     AS ARRAY(NoComp) OF NoType  # Concentration of Mg in mg/l
  PO4_Fi    AS ARRAY(NoComp) OF NoType  # Concentration of PO4 in mg/l
  NH4_Fi    AS ARRAY(NoComp) OF NoType  # Concentration of NH4 in mg/l

  K_so      AS NoType                   # Solubility product of struvite
  L         AS ARRAY(NoComp) OF NoType  # Size of struvite crystal (microns)

  H3PO4     AS ARRAY(NoComp) OF NoType  # Activity concentration of H3PO4 (molar)
  H2PO4     AS ARRAY(NoComp) OF NoType  # Activity concentration of H2PO4 ion (molar)
  HPO4      AS ARRAY(NoComp) OF NoType  # Activity concentration of HPO4 ion (molar)
  PO4_i     AS ARRAY(NoComp) OF NoType  # Activity concentration of PO4 ion (molar)
  Mg_i      AS ARRAY(NoComp) OF NoType  # Activity concentration of Mg ion (molar)
  MgOH      AS ARRAY(NoComp) OF NoType  # Activity concentration of MgOH ion (molar)
  NH3       AS ARRAY(NoComp) OF NoType  # Activity concentration of NH3 ion (molar)
  NH4_i     AS ARRAY(NoComp) OF NoType  # Activity concentration of NH4 ion (molar)
  MgPO4     AS ARRAY(NoComp) OF NoType  # Activity Concentration of MgPO4 ion (molar)
  MgHPO4    AS ARRAY(NoComp) OF NoType  # Activity Concentration of MgHPO4 (molar)
  MgH2PO4   AS ARRAY(NoComp) OF NoType  # Activity Concentration of MgPO4 ion (molar)

  CMg_i       AS ARRAY(NoComp) OF NoType  # Ionic concentration of Mg ion (molar)
  CPO4_i      AS ARRAY(NoComp) OF NoType  # Ionic concentration of PO4 ion (molar)
  CNH4_i      AS ARRAY(NoComp) OF NoType  # Ionic concentration of NH4 ion (molar)
  CH2PO4      AS ARRAY(NoComp) OF NoType  # Ionic concentration of H2PO4 ion (molar)
```

```
CHPO4       AS ARRAY(NoComp) OF NoType  # Ionic concentration of HPO4 ion (molar)
CMgOH       AS ARRAY(NoComp) OF NoType  # Ionic concentration of MgOH ion (molar)
CH3PO4      AS ARRAY(NoComp) OF NoType  # Ionic concentration of H3PO4 (molar)
CNH3        AS ARRAY(NoComp) OF NoType  # Ionic Concentration of NH3 (molar)
CMgPO4      AS ARRAY(NoComp) OF NoType  # Ionic Concentration of MgPO4 ion (molar)
CMgHPO4     AS ARRAY(NoComp) OF NoType  # Ionic Concentration of MgPO4 ion (molar)
CMgH2PO4    AS ARRAY(NoComp) OF NoType  # Ionic Concentration of MgPO4 ion (molar)

alpha_Mg    AS ARRAY(NoComp) OF NoType  # Ionization Fraction of Mg
alpha_PO4   AS ARRAY(NoComp) OF NoType  # Ionization fration of PO4
alpha_NH4   AS ARRAY(NoComp) OF NoType  # Ionization fration of NH4

I           AS ARRAY(NoComp) OF NoType  # Ionic strength (mol/L)

Gamma_1     AS ARRAY(NoComp) OF NoType  # Activity coefficient of 1 charge ion
Gamma_2     AS ARRAY(NoComp) OF NoType  # Activity coefficient of 2 charge ion
Gamma_3     AS ARRAY(NoComp) OF NoType  # Activity coefficient of 3 charge ion
Gamma_0     AS ARRAY(NoComp) OF NoType  # Activity coefficient of 0 charge ion

H           AS ARRAY(NoComp) OF NoType  # Concentration of H ion
OH          AS ARRAY(NoComp) OF NoType  # Concentration of OH ion

NH4_Feed    AS ARRAY(NoComp) OF NoType  # Input concentration of NH4 feed (mg/l)
PO4_Feed    AS ARRAY(NoComp) OF NoType  # Input concentration of PO4 feed (mg/l)
Mg_Feed     AS ARRAY(NoComp) OF NoType  # Input concentration of Mg feed (mg/l)

V           AS ARRAY(NoComp) OF NoType  # Constant operative volume of reactor(Liter)
N_MAP       AS ARRAY(NoComp) OF NoType  # Number of struvite seeds
M_MAP       AS ARRAY(NoComp) OF NoType  # Mass of struvite into the reactor (g)
F_NaOH      AS ARRAY(NoComp) OF NoType  # Feed flowrate of NaOH in l/h

NH4         AS ARRAY(NoComp) OF NoType  # Mass of ammonium into the reactor (mg)
```

```
PO4             AS ARRAY(NoComp) OF NoType   # Mass of phosphate into the reactor (mg)
Mg              AS ARRAY(NoComp) OF NoType   # Mass of magnesium into the reactor (mg)

P_cs            AS ARRAY(NoComp) OF NoType   # Condition solubility product of struvite
P_so            AS ARRAY(NoComp) OF NoType   # Concentration product of struvite
S               AS ARRAY(NoComp) OF NoType   # Supersaturation of solution (Saturation Index)
SSR             AS ARRAY(NoComp) OF NoType   # Supersaturation Ratio of solution

Fi              AS ARRAY(NoComp) OF NoType   # Feed flowrate of solution (l/h)
H_Fi            AS ARRAY(NoComp) OF NoType   # H+ concentration of inlet solution (molar)
OH_Fi           AS ARRAY(NoComp) OF NoType   # OH+ concentration of inlet solution (molar)

Lchange         AS ARRAY(NoComp) OF NoType   # Change of mean particle size (microns)

L0              AS NoType   # Initial mean particles size as seeds (microns)

M_MAP_0         AS ARRAY(NoComp) OF NoType   # Initial mass of struvite (Kg)
Mchange         AS ARRAY(NoComp) OF NoType   # Change of mean struvite mass (g)

K_kin           AS NoType_2                   # Growth rate constant (microns/h)
n               AS NoType_1                  # Order of the growth rate equation
```

EQUATION

```
Mg_Fi = C_T_Mg*MW_Mg*1000;
NH4_Fi = C_T_NH4*MW_NH4*1000;
PO4_Fi = C_T_PO4*MW_PO4*1000;

MgOH = 10^2.56 *Mg_i*OH ;
NH4_i = 10^9.252 *H*NH3 ;
HPO4 = 10^12.35 *H*PO4_i ;
H2PO4 = 10^7.20 *H*HPO4 ;
```

```
H3PO4 = 10^2.15 *H*H2PO4 ;
MgPO4 = 10^(4.8)*Mg_i*PO4_i;
MgHPO4 = 10^(2.91)*Mg_i*HPO4 ;
MgH2PO4 = 10^(0.45)*Mg_i*H2PO4;

K_so = 10^(-13.26);

CMg_i = Mg_i/Gamma_2;
CPO4_i = PO4_i/Gamma_3;
CNH4_i = NH4_i/Gamma_1;
CH3PO4 = H3PO4/Gamma_0;
CH2PO4 = H2PO4/Gamma_1;
CHPO4 = HPO4/Gamma_2;
CMgOH = MgOH/Gamma_1;
CNH3 = NH3/Gamma_0;
CMgPO4 = MgPO4/Gamma_1;
CMgHPO4 = MgHPO4/Gamma_0;
CMgH2PO4 = MgH2PO4/Gamma_1;

C_T_PO4 = CH3PO4 + CH2PO4 + CHPO4 + CPO4_i + CMgPO4 + CMgHPO4 + CMgH2PO4 ;
C_T_Mg = CMg_i + CMgOH + CMgPO4 + CMgHPO4 + CMgH2PO4;
C_T_NH4 = CNH3 + CNH4_i ;

H = 10^(-pH) ;
OH = K_w/H ;

alpha_Mg = CMg_i/C_T_Mg ;
alpha_PO4 = CPO4_i/C_T_PO4 ;
alpha_NH4 = CNH4_i/C_T_NH4 ;

I = 0.5*(C_T_Mg*Z_2*Z_2 +  C_T_NH4*Z_2*Z_2 + C_T_PO4*Z_3*Z_3);
```

```
Gamma_2= 10^(-(A*Z_2^2) * ((I^0.5/(1 + I^0.5))-0.3*I)) ;
Gamma_3=  10^(-(A*Z_3^2) * ((I^0.5/(1 + I^0.5))-0.3*I)) ;
Gamma_1= 10^(-(A*Z_1^2) * ((I^0.5/(1 + I^0.5))-0.3*I)) ;
Gamma_0 = 10^(-0.1*I);


 # Conditional solubility product (Pcs) and Concentration product (Pso)
 P_so = C_T_mg*C_T_NH4*C_T_PO4 ;
 P_cs = K_so/(alpha_Mg*Gamma_2*alpha_NH4*Gamma_1*alpha_PO4*Gamma_3);

 # Supersaturation of solution
  SSR = (P_so/P_cs)^0.33333 ;                                  # Supersaturation ratio
  S = LOG10(P_so) - LOG10(P_cs);                               # Supersaturation Index

 # Growth rate of crystals (microns/h)
   $L = K_kin *((SSR-1)^n);                                    # Based on Oversaturation (Oversaturation=SSR-1)
 #  $L = K_kin *(S^n);                                         # Based on Saturation Index

 # Volume of solution in the reactor
    $V = Fi + F_NaOH ;

 # Ammonium mass balance in milligrams
    $NH4 = Fi*NH4_Feed - ($M_MAP*1000/MW_MAP)*MW_NH4 ;

 # Ammonia mass balance in milligrams
    $Mg = Fi*Mg_Feed - ($M_MAP*1000/MW_MAP)*MW_Mg ;

# Phosphate mass balance in milligrams
    $PO4 = Fi*PO4_Feed - ($M_MAP*1000/MW_MAP)*MW_PO4 ;
                        # Unit conversion:  1kg =1e6 mg

 # Transformation of total mass to concentrations (ppm)
```

```
    PO4_Fi = PO4/V;
    Mg_Fi = Mg/V;
    NH4_Fi = NH4/V;

  # struvite mass balance in grams
    $M_MAP = (10^(-12))*N_MAP*0.5*pi*Density*(L^2)*($L);


  # Determination of Number of struvite Crystals
     M_MAP_0 = (10^(-12)) *N_MAP*(pi/6)*Density *(L0^3);

  # Thermodynamic relation of H+ and OH- ions
     H_Fi = 10^(-pH_Fi);                                    # For feed solution
     OH_Fi = 10^(-14)/H_Fi;                                 # For feed solution

  # Minimization of error of mean particle size (microns)
     Lchange = L - L0;

 # Minimization of error of mean particle size (grams)
     Mchange = M_MAP - M_MAP_0;


UNIT
  Lchange101 AS struvite_6_Control_PE_Lchange

SET
WITHIN Lchange101 DO
   K_w       :=10^(-14);                                  # Ionization Product of water
   A         := 0.5 ;                                     # DeBye-Huckel Constant
   Z_2       := 2.0;                                      # Valency of 2 chagre ions
   Z_1       := 1.0;                                      # Valency of 1 charge ions
   Z_3       := 3.0;                                      # Valency of 3 charge ions
```

```
   MW_Mg       := 24;                                  # Molecular weight of Mg (g)
   MW_NH4      := 18;                                  # Molecular weight of NH4 (g)
   MW_PO4      := 95;                                  # Molecular weight of PO4 (g)

   Density     := 1.72;                                # unit: Kg/L (g/cm3)
   pi          := 3.1416;                              # unitless
   MW_MAP      := 245.10;                              # Gram molecular weight of struvite-hexahydrate

   V0          := [16, 16.5, 16.8];                    # Unit: Liter
   C_NaOH      := [0.0045*18, 0.0060*18, 0.0055*18];   # Unit: molar
   pH_Fi       := [5.8, 5.75, 5.6];                    # Feed solution pH
   NoComp      := 3;                                   # Number of experiments
   pH          := [7.35, 7.22, 7.51];                  # Controlled pH of the reactive solution
END
```

ASSIGN

```
   WITHIN Lchange101 DO
    NH4_Feed   := [0.0045*10*18000, 0.0060*10*18000, 0.0055*10*18000];   # unit: mg/l
    PO4_feed   := [0.0045*10*95000, 0.0060*10*95000, 0.0055*10*95000];   # unit: mg/l
    Mg_Feed    := [0.0045*10*24000, 0.0060*10*24000, 0.0055*10*24000];   # unit: mg/l

    L0         :=  140.0;                  # unit: micrometer

    Fi(1)      := 0.5;                     # unit: l/h
    Fi(2)      :=0.690909091;              # unit: l/h
    Fi(3)      := 1;                       # unit: l/h

    F_NaOH(1)  := 0.5;                     # unit: l/h
    F_NaOH(2)  :=0.690909091;              # unit: l/h
    F_NaOH(3)  := 1;                       # unit: l/h
```

```
    K_kin      := 25;                    # unit: microns/h
    n          :=1.5;                    # unitless

    M_MAP_0    := [30, 30, 30];          # unit: grams
END


INITIAL
   WITHIN Lchange101 DO
      NH4_Fi(1)   = 92.32;              # unit: mg
      NH4_Fi(2)   = 112.64;             # unit: mg
      NH4_Fi(3)   = 112.64;             # unit: mg

      PO4_Fi(1)   = 487.25;             # unit: mg
      PO4_Fi(2)   = 594.52;             # unit: mg
      PO4_Fi(3)   = 594.52;             # unit: mg

      Mg_Fi(1)    = 108;                # unit: mg
      Mg_Fi(2)    = 165;                # unit: mg
      Mg_Fi(3)    = 147;                # unit: mg

      V          = V0;                  # unit: Liter
      Lchange    = 0;                   # unit: microns
      Mchange    = 0;                   # unit: microns
END


SOLUTIONPARAMETERS
   gExcelOutput := "struvite_PE_Lchange"
```

SCHEDULE
CONTINUE for 30

ESTIMATE
Lchange101.K_kin
25 20 80

ESTIMATE
Lchange101.n
1.5 0.75 2

ESTIMATE
Lchange101.L0
140 100 200

{ESTIMATE
Lchange101.L0(2)
133 100 200

ESTIMATE
Lchange101.L0(3)
138 100 200}

MEASURE
Lchange101.L(1)
HETEROSCEDASTIC PREDICTED_VALUES (1 : 0.5 : 20; 0.5: 0.1: 1)

MEASURE
Lchange101.PO4_Fi(1)

HETEROSCEDASTIC PREDICTED_VALUES (1 : 1E-20 : 20; 0.5: 0.1: 1)

MEASURE
Lchange101.Mg_Fi(1)
HETEROSCEDASTIC PREDICTED_VALUES (1 : 0.5 : 20; 0.5: 0.1: 1)

MEASURE
Lchange101.L(2)
HETEROSCEDASTIC PREDICTED_VALUES (1 : 0.5 : 10; 0.5: 0.1: 1)
MEASURE
Lchange101.PO4_Fi(2)
HETEROSCEDASTIC PREDICTED_VALUES (1 : 0.5 : 20; 0.5: 0.1: 1)
MEASURE
Lchange101.Mg_Fi(2)
HETEROSCEDASTIC PREDICTED_VALUES (1 : 0.5 : 20; 0.5: 0.1: 1)

MEASURE
Lchange101.L(3)
HETEROSCEDASTIC PREDICTED_VALUES (1 : 0.5 : 20; 0.5: 0.1: 1)
MEASURE
Lchange101.PO4_Fi(3)
HETEROSCEDASTIC PREDICTED_VALUES (1 : 0.5 : 20; 0.5: 0.1: 1)
MEASURE
Lchange101.Mg_Fi(3)
HETEROSCEDASTIC PREDICTED_VALUES (1 : 0.5 : 20; 0.5: 0.1: 1)

RUNS
LC_LCHANGE_1
LC_LCHANGE_2

LC_LCHANGE_3

MEASURE
Lchange101.L(1)
0.0 140.06
1.0 148.54
4.5 157.41
10.5 162.02
12.5 164.22
24.0 170.9

MEASURE
Lchange101.PO4_Fi(1)
0.0 487.25
1.0 453.54
4.5 462.74
10.5 524.03
12.5 508.71
24.0 487.25

MEASURE
Lchange101.Mg_Fi(1)
0.0 107.0
1.0 113.0
4.5 110.0
10.5 117.0
12.5 109.0
24.0 105.0

INTERVALS
5

1.0
4.5
10.5
12.5
24.0

PIECEWISE-CONSTANT
Lchange101.Fi(1)
0.50
0.28571
0.175
0.15833
0.20

PIECEWISE-CONSTANT
Lchange101.F_NaOH(1)
0.50
0.28571
0.175
0.15833
0.20

MEASURE
Lchange101.L(2)
0.0 138.83
0.55 145.12
2.17 154.34
3.57 158.47
6.57 165.43

MEASURE
Lchange101.PO4_Fi(2)
0.0 594.52
0.55 530.16
2.17 631.29
3.57 554.68
6.57 643.55

MEASURE
Lchange101.Mg_Fi(2)
0.0 165.0
0.55 156.0
2.17 155.0
3.57 138.0
6.57 150.0

INTERVALS
4
0.55
2.17
3.57
6.57

PIECEWISE-CONSTANT
Lchange101.Fi(2)
0.69
0.64
0.63
0.67

PIECEWISE-CONSTANT
Lchange101.F_NaOH(2)

0.69
0.64
0.63
0.67

MEASURE
Lchange101.L(3)
0.0 133.25
0.75 148.39
2.0 173.59
3.4 184.36
7.5 192.4

MEASURE
Lchange101.PO4_Fi(3)
0.0 594.52
0.75 585.32
2.0 499.52
3.4 478.06
7.5 487.26

MEASURE
Lchange101.Mg_Fi(3)
0.0 147.0
0.75 146.0
2.0 128.0
3.4 138.0
7.5 124.0

INTERVALS
4

0.75
2.0
3.4
7.5

PIECEWISE-CONSTANT
Lchange101.Fi(3)
1.0
0.9
0.714285714
1.0

PIECEWISE-CONSTANT
Lchange101.F_NaOH(3)
1.0
0.9
0.714285714
1.0

APPENDIX E

E.1 gPROMS Coding for Thermodynamic Modeling

```
#  ************************************************************************
#                THERMODYNAMIC MODEL
#  THIS PROGRAM IS DEVELOPED TO STUDY SOLUTION SPECIATION OF SOLUTION RELATING
#  TO STRUVITE THERMODYNAMICS AND RELEVANT SUPERSATURATION.
#  SOLUTION CONTRATION: CABARLAH PARK PRIMARY POND DATA
#
#  MODEL LINK: struvite_Modelling>struvite_1_Thermodynamic>struvite_thermodynamic
#  ************************************************************************

PARAMETER
   NoComp          AS INTEGER # Number of variable pH
   pH              AS ARRAY(NoComp) OF REAL   # pH value of the solution
   K_w             AS REAL                    # Ionization Product of water
   A               AS REAL                    # DeBye-Huckel Constant
   Z_1             AS REAL                    # Valency of Mg ion
   Z_2             AS REAL                    # Valency of NH4 ion
   Z_3             AS REAL                    # Valency of PO4 ion

   MW_Mg           AS REAL                    # Molecular Weight of Mg (g)
   MW_NH4          AS REAL                    # Molecular Weight of NH4 (g)
   MW_PO4          AS REAL                    # Molecular Weight of PO4 (g)


VARIABLE
   PO4_Fi          AS NoType                  # Total Input Concentration of PO4 (ppm)
```

```
Mg_Fi           AS NoType                       # Total Input Concentration of Mg (ppm)
NH4_Fi          AS NoType                       # Total Input concentration of NH4 (ppm)

C_T_PO4         AS NoType                       # Total Input molar Concentration of PO4
C_T_Mg          AS NoType                       # Total Input molar Concentration of Mg
C_T_NH4         AS NoType                       # Total Input molar concentration of NH4

H3PO4           AS ARRAY(NoComp) OF NoType  # Activity concentration of aq H3PO4 (molar)
H2PO4           AS ARRAY(NoComp) OF NoType  # Activity concentration of H2PO4 ion (molar)
HPO4            AS ARRAY(NoComp) OF NoType  # Activity concentration of HPO4 ion (molar)
PO4_i           AS ARRAY(NoComp) OF NoType  # Activity concentration of PO4 ion (molar)

Mg_i            AS ARRAY(NoComp) OF NoType  # Activity concentration of Mg ion (molar)
MgOH            AS ARRAY(NoComp) OF NoType  # Activity concentration of MgOH ion (molar)

NH3             AS ARRAY(NoComp) OF NoType  # Activity concentration of NH3 ion (molar)
NH4_i           AS ARRAY(NoComp) OF NoType  # Activity concentration of NH4 ion (molar)

MgPO4           AS ARRAY(NoComp) OF NoType  # Activity Concentration of MgPO4 ion
MgHPO4          AS ARRAY(NoComp) OF NoType  # Activity Concentration of MgPO4 ion
MgH2PO4         AS ARRAY(NoComp) OF NoType  # Activity Concentration of MgPO4 ion

alpha_Mg        AS ARRAY(NoComp) OF NoType  # Ionization Fraction of Mg (unitless)
alpha_PO4       AS ARRAY(NoComp) OF NoType  # Ionization fration of PO4 (unitless)
alpha_NH4       AS ARRAY(NoComp) OF NoType  # Ionization fration of NH4 (unitless)

I               AS NoType           # Ionic strength (mol/L)

Gamma_1         AS NoType           # Activity coefficient of 1 charge ion
Gamma_2         AS NoType           # Activity coefficient of 2 charge ion
Gamma_3         AS NoType           # Activity coefficient of 3 charge ion
Gamma_0         AS NoType           # Activity coefficient of 0 charge ion
```

```
H               AS ARRAY(NoComp) OF NoType   # Molar concentration (ionic) of H ion
OH              AS ARRAY(NoComp) OF NoType   # Molar concentration (ionic) of OH ion

K_so            AS NoType                    # Solubility product of struvite
P_cs            AS ARRAY(NoComp) OF NoType   # Condition solubility product of struvite
P_so            AS ARRAY(NoComp) OF NoType   # Concentration Product of struvite

Sup             AS ARRAY(NoComp) OF NoType   # Saturation Index
S               AS ARRAY(NoComp) OF NoType   # Critical Supersaturation

CMg_i           AS ARRAY(NoComp) OF NoType   # Ionic Concentration of Free Magnesium ion
CPO4_i          AS ARRAY(NoComp) OF NoType   # Ionic Concentration of free phosphate ion
CNH4_i          AS ARRAY(NoComp) OF NoType   # Ionic Concentration of free ammonium ion
CH2PO4          AS ARRAY(NoComp) OF NoType   # Ionic Concentration of H2PO4 ion
CHPO4           AS ARRAY(NoComp) OF NoType   # Ionic Concentration of HPO4 ion
CMgOH           AS ARRAY(NoComp) OF NoType   # Ionic Concentration of MgOH ion
CH3PO4          AS ARRAY(NoComp) OF NoType   # Ionic Concentration of H3PO4
CNH3            AS ARRAY(NoComp) OF NoType   # Ionic Concentration of NH3
CMgPO4          AS ARRAY(NoComp) OF NoType   # Ionic Concentration of MgPO4 ion
CMgHPO4         AS ARRAY(NoComp) OF NoType   # Ionic Concentration of MgPO4 ion
CMgH2PO4        AS ARRAY(NoComp) OF NoType   # Ionic Concentration of MgPO4 ion
```

EQUATION

```
Mg_Fi = C_T_Mg*MW_Mg*1000;
NH4_Fi = C_T_NH4*MW_NH4*1000;
PO4_Fi = C_T_PO4*MW_PO4*1000;

MgOH = 10^2.56 *Mg_i*OH ;
NH4_i = 10^9.252 *H*NH3 ;
HPO4 = 10^12.35 *H*PO4_i ;
```

```
H2PO4 = 10^7.20 *H*HPO4 ;
H3PO4 = 10^2.15 *H*H2PO4 ;
MgPO4 = 10^(4.8)*Mg_i*PO4_i;
MgHPO4 = 10^(2.91)*Mg_i*HPO4 ;
MgH2PO4 = 10^(0.45)*Mg_i*H2PO4;

K_so = 10^(-13.26);

CMg_i = Mg_i/Gamma_2;
CPO4_i = PO4_i/Gamma_3;
CNH4_i = NH4_i/Gamma_1;
CH3PO4 = H3PO4/Gamma_0;
CH2PO4 = H2PO4/Gamma_1;
CHPO4 = HPO4/Gamma_2;
CMgOH = MgOH/Gamma_1;

CNH3 = NH3/Gamma_0;

CMgPO4 = MgPO4/Gamma_1;
CMgHPO4 = MgHPO4/Gamma_0;
CMgH2PO4 = MgH2PO4/Gamma_1;

C_T_PO4 = CH3PO4 + CH2PO4 + CHPO4 + CPO4_i + CMgPO4 + CMgHPO4 + CMgH2PO4 ;
C_T_Mg = CMg_i + CMgOH + CMgPO4 + CMgHPO4 + CMgH2PO4;
C_T_NH4 = CNH3 + CNH4_i ;

H = 10^(-pH) ;
OH = K_w/H ;

alpha_Mg = CMg_i/C_T_Mg ;
alpha_PO4 = CPO4_i/C_T_PO4 ;
alpha_NH4 = CNH4_i/C_T_NH4 ;
```

```
   I = 0.5*(C_T_Mg*Z_2^2 + C_T_PO4*Z_3^2 + C_T_NH4*Z_1^2) ;

{
  -LOG10(Gamma_2)= (A*Z_2^2) * ((I^0.5/(1 + I^0.5))-0.3*I) ;
   -LOG10(Gamma_3)=  (A*Z_3^2) * ((I^0.5/(1 + I^0.5))-0.3*I) ;
   -LOG10(Gamma_1)= (A*Z_1^2) * ((I^0.5/(1 + I^0.5))-0.3*I) ;
   -LOG10(Gamma_0) = 0.1*I;
}

   Gamma_2= 10^(-(A*Z_2^2) * ((I^0.5/(1 + I^0.5))-0.3*I)) ;
   Gamma_3=  10^(-(A*Z_3^2) * ((I^0.5/(1 + I^0.5))-0.3*I)) ;
   Gamma_1= 10^(-(A*Z_1^2) * ((I^0.5/(1 + I^0.5))-0.3*I)) ;
   Gamma_0 = 10^(-0.1*I);

  P_cs = K_so/(alpha_Mg*Gamma_2*alpha_NH4*Gamma_1*alpha_PO4*Gamma_3);
  P_so = C_T_mg * C_T_NH4 * C_T_PO4 ;
  Sup = LOG10(P_so) - LOG10(P_cs);
  S = (P_so/P_cs)^0.333;


UNIT
  Thermo101 AS struvite_1_Thermodynamic


SET
WITHIN Thermo101 DO
   K_w :=10^(-14);            # Ionization Product of water
   A   := 0.5 ;               # DeBye-Huckel Constant
   Z_2 := 2.0;                # Valency of Mg
   Z_1 := 1.0;                # Valency of NH4
   Z_3 := 3.0;                # Valency of PO4
```

```
   MW_Mg := 24;              # Molecular weight of Mg (g)
   MW_NH4 := 18;             # Molecular weight of NH4 (g)
   MW_PO4 := 95;             # Molecular weight of PO4 (g)

   NoComp := 19;             # Number of pH value
   pH := [5,5.5, 6, 6.5, 7, 7.5, 8, 8.5, 9, 9.5, 10, 10.5, 11, 11.5, 12, 12.5, 13, 13.5, 14];
                             # pH value of the solution
END


ASSIGN
   WITHIN Thermo101 DO
      NH4_Fi          := 199.7;      # unit: mg/l
      PO4_Fi          := 34.1;       # unit: mg/l
      Mg_Fi           := 26;         # unit: mg/l
END


SOLUTIONPARAMETERS
  gExcelOutput := "Thesis_Therodynamics"
```

APPENDIX F

F.1 Modeling of PHREEQC for Design the Feed Mixing

```
SOLUTION 1
    temp      25
    pH        5.38
    pe        4
    redox     pe
    units     mol/l
    density   1
    Mg        0.07
    N(-3)     0.07
    P         0.07
    -water    1 # kg

SOLUTION 2
    temp      25
    pH        5.38
    pe        4
    redox     pe
    units     mol/l
    density   1
    Mg        0.06
    N(-3)     0.06
    P         0.06
    -water    1 # kg

SOLUTION 3
    temp      25
    pH        5.38
    pe        4
    redox     pe
    units     mol/l
    density   1
    Mg        0.05
    N(-3)     0.05
    P         0.05
    -water    1 # kg

SOLUTION 4
    temp      25
    pH        5.38
    pe        4
    redox     pe
    units     mol/l
    density   1
    Mg        0.04
    N(-3)     0.04
    P         0.04
    -water    1 # kg

SOLUTION 5
    temp      25
    pH        5.38
    pe        4
```

```
    redox     pe
    units     mol/l
    density   1
    Mg        0.03
    N(-3)     0.03
    P         0.03
    -water    1 # kg

SOLUTION 6
    temp      25
    pH        5.38
    pe        4
    redox     pe
    units     mol/l
    density   1
    Mg        0.02
    N(-3)     0.02
    P         0.02
    -water    1 # kg

SOLUTION 7
    temp      25
    pH        5.38
    pe        4
    redox     pe
    units     mol/l
    density   1
    Mg        0.01
    N(-3)     0.01
    P         0.01
    -water    1 # kg
END

SOLUTION_SPREAD
    -units    mol/l
    Mg          Cl          Na       Water         pH
Mol/l  Mol/l       Mol/l
  0.01        0.01        0.02           1       10.0
  0.01        0.01        0.02           1       10.5
  0.01        0.01        0.02           1       11.0
  0.01        0.01        0.02           1       11.5
  0.01        0.01        0.02           1       12.0
  0.01        0.01        0.02           1       12.5
  0.01        0.01        0.02           1       13.0
  0.01        0.01        0.02           1       13.5
  0.01        0.01        0.02           1       14.0

SOLUTION_SPREAD
    -units    mol/l
    Mg          Cl          Na       Water         pH
Mol/l  Mol/l       Mol/l
  0.02        0.02        0.04           1       10.0
  0.02        0.02        0.04           1       10.5
  0.02        0.02        0.04           1       11.0
  0.02        0.02        0.04           1       11.5
  0.02        0.02        0.04           1       12.0
  0.02        0.02        0.04           1       12.5
  0.02        0.02        0.04           1       13.0
  0.02        0.02        0.04           1       13.5
  0.02        0.02        0.04           1       14.0
```

```
SOLUTION_SPREAD
    -units    mol/l
    Mg          Cl          Na       Water         pH
Mol/l  Mol/l       Mol/l
  0.03        0.03        0.06           1       10.0
  0.03        0.03        0.06           1       10.5
  0.03        0.03        0.06           1       11.0
  0.03        0.03        0.06           1       11.5
  0.03        0.03        0.06           1       12.0
  0.03        0.03        0.06           1       12.5
  0.03        0.03        0.06           1       13.0
  0.03        0.03        0.06           1       13.5
  0.03        0.03        0.06           1       14.0

SOLUTION_SPREAD
    -units    mol/l
    Mg          Cl          Na       Water         pH
Mol/l  Mol/l       Mol/l
  0.04        0.04        0.08           1       10.0
  0.04        0.04        0.08           1       10.5
  0.04        0.04        0.08           1       11.0
  0.04        0.04        0.08           1       11.5
  0.04        0.04        0.08           1       12.0
  0.04        0.04        0.08           1       12.5
  0.04        0.04        0.08           1       13.0
  0.04        0.04        0.08           1       13.5
  0.04        0.04        0.08           1       14.0

SOLUTION_SPREAD
    -units    mol/l
    Mg          Cl          Na       Water         pH
Mol/l  Mol/l       Mol/l
  0.05        0.05        0.10           1       10.0
  0.05        0.05        0.10           1       10.5
  0.05        0.05        0.10           1       11.0
  0.05        0.05        0.10           1       11.5
  0.05        0.05        0.10           1       12.0
  0.05        0.05        0.10           1       12.5
  0.05        0.05        0.10           1       13.0
  0.05        0.05        0.10           1       13.5
  0.05        0.05        0.10           1       14.0

SOLUTION_SPREAD
    -units    mol/l
    Mg          Cl          Na       Water         pH
Mol/l  Mol/l       Mol/l
  0.06        0.06        0.12           1       10.0
  0.06        0.06        0.12           1       10.5
  0.06        0.06        0.12           1       11.0
  0.06        0.06        0.12           1       11.5
  0.06        0.06        0.12           1       12.0
  0.06        0.06        0.12           1       12.5
  0.06        0.06        0.12           1       13.0
  0.06        0.06        0.12           1       13.5
  0.06        0.06        0.12           1       14.0
SOLUTION_SPREAD
    -units    mol/l
    Mg          Cl          Na       Water         pH
Mol/l  Mol/l       Mol/l
  0.07        0.07        0.07           1       10.0
  0.07        0.07        0.07           1       10.5
```

```
  0.07        0.07        0.07           1       11.0
  0.07        0.07        0.07           1       11.5
  0.07        0.07        0.07           1       12.0
  0.07        0.07        0.07           1       12.5
  0.07        0.07        0.07           1       13.0
  0.07        0.07        0.07           1       13.5
  0.07        0.07        0.07           1       14.0
END

SOLUTION_SPREAD
    -units    mol/l
 N(-3)           P          Na       Water         pH
Mol/l  Mol/l       Mol/l
  0.01        0.01        0.02           1        8.0
  0.01        0.01        0.02           1        9.0
  0.01        0.01        0.02           1       10.0
  0.01        0.01        0.02           1       11.0
  0.01        0.01        0.02           1       12.0
  0.01        0.01        0.02           1       13.0
  0.01        0.01        0.02           1       14.0

SOLUTION_SPREAD
    -units    mol/l
 N(-3)           P          Na       Water         pH
Mol/l  Mol/l       Mol/l
  0.02        0.02        0.04           1        8.0
  0.02        0.02        0.04           1        9.0
  0.02        0.02        0.04           1       10.0
  0.02        0.02        0.04           1       11.0
  0.02        0.02        0.04           1       12.0
  0.02        0.02        0.04           1       13.0
  0.02        0.02        0.04           1       14.0

SOLUTION_SPREAD
    -units    mol/l
 N(-3)           P          Na       Water         pH
Mol/l  Mol/l       Mol/l
  0.03        0.03        0.06           1        8.0
  0.03        0.03        0.06           1        9.0
  0.03        0.03        0.06           1       10.0
  0.03        0.03        0.06           1       11.0
  0.03        0.03        0.06           1       12.0
  0.03        0.03        0.06           1       13.0
  0.03        0.03        0.06           1       14.0

SOLUTION_SPREAD
    -units    mol/l
 N(-3)           P          Na       Water         pH
Mol/l  Mol/l       Mol/l
  0.04        0.04        0.08           1        8.0
  0.04        0.04        0.08           1        9.0
  0.04        0.04        0.08           1       10.0
  0.04        0.04        0.08           1       11.0
  0.04        0.04        0.08           1       12.0
  0.04        0.04        0.08           1       13.0
  0.04        0.04        0.08           1       14.0

SOLUTION_SPREAD
    -units    mol/l
 N(-3)           P          Na       Water         pH
Mol/l  Mol/l       Mol/l
```

```
  0.05        0.05        0.10           1        8.0
  0.05        0.05        0.10           1        9.0
  0.05        0.05        0.10           1       10.0
  0.05        0.05        0.10           1       11.0
  0.05        0.05        0.10           1       12.0
  0.05        0.05        0.10           1       13.0
  0.05        0.05        0.10           1       14.0

SOLUTION_SPREAD
    -units    mol/l
 N(-3)           P          Na       Water         pH
Mol/l  Mol/l       Mol/l
  0.06        0.06        0.12           1        8.0
  0.06        0.06        0.12           1        9.0
  0.06        0.06        0.12           1       10.0
  0.06        0.06        0.12           1       11.0
  0.06        0.06        0.12           1       12.0
  0.06        0.06        0.12           1       13.0
  0.06        0.06        0.12           1       14.0

SOLUTION_SPREAD
    -units    mol/l
 N(-3)           P          Na       Water         pH
Mol/l  Mol/l       Mol/l
  0.07        0.07        0.14           1        8.0
  0.07        0.07        0.14           1        9.0
  0.07        0.07        0.14           1       10.0
  0.07        0.07        0.14           1       11.0
  0.07        0.07        0.14           1       12.0
  0.07        0.07        0.14           1       13.0
  0.07        0.07        0.14           1       14.0
END
```

APPENDIX G

G.1 PHREEQC Thermodynamic Modeling to Design the Minimum Operating Supersaturation

```
SOLUTION_SPREAD
    -units    mg/l
      Mg        N(-3)            P       pH   Water
  Mol/l         Mol/l        Mol/l
 0.00428     0.00579     0.00429     7.5        1
 0.00428     0.00579     0.00429       8        1
 0.00428     0.00579     0.00429     8.5        1

PHASES
STRUVITE
    MgNH4PO4:6H2O = 6H2O + Mg+2 + NH4+ + PO4-3
    log_k     -13.27
```

APPENDIX H

H.1 CSD Data for Particles for the Observation of Particles Breakage

Material: Quartz sand
Apparatus: Malvern particle-sizer
Analyzing Technique: Analysis with 300 mm lens- range 0.5 to 600 μm of particle size

Table H. 1 Mean particle size of quartz sand during experiment

Sampling Interval (hrs)	Mean particle size (μm)
0	344.02
3.5	341.96
10	337.84
28	338.29

APPENDIX I

I.1 Experimental Data for Fed-batch Experiment

Table I. 1 Observations of the mean particle size of developing struvite for experimen-1

Operating Volume (V)	Mean Particle Size (μm)
15.00	133.25
16.00	140.60
17.00	148.54
19.00	157.41
21.10	162.02
23.00	164.22
26.00	170.90
28.00	163.16
31.00	162.16

Table I. 2 Observations of the mean particle size of developing struvite for experiment-2

Operating Volume (L)	Mean Particle Size (μm)
15.00	127.77
16.50	138.83
17.15	145.12
19.25	154.34
21.00	158.47
25.00	165.43
29.00	156.39
33.00	149.50

Table I. 3 Observations of the mean particle size of developing struvite for experimen-3

Operating Volume (L)	Mean Particle Size (μm)
15	133.25
16.8	148.39
20	173.59
22.25	184.36
24.75	192.40
29.00	184.36

Table I. 4 Constituents concentration of experiment-1

Time internal	Mg (mg/l)	P (mg/l)	PO_4 (mg/l)	Mg Conc. (M)	PO_4 Conc. (M)	Volume of reactive solution (L)
0	123	166	1017.42	0.00513	0.00535	15
0.25	124	154	943.87	0.00517	0.00497	15
0.5	114	167	1023.55	0.00475	0.00539	15
0.75	113	159	974.52	0.00471	0.00513	15
1	137	195	1195.16	0.00571	0.00629	15
1.25	140	168	1029.68	0.00583	0.00542	15
1.5	142	193	1182.90	0.00592	0.00623	15
1.75	137	177	1084.84	0.00571	0.00571	15
2.25	147	194	1189.03	0.00613	0.00626	16.8
3	146	191	1170.65	0.00608	0.00616	20
4.25	128	163	999.03	0.00533	0.00526	22.25
5.65	138	156	956.13	0.00575	0.00503	24.75
9.25	125	156	956.13	0.00521	0.00503	28
9.75	124	159	974.52	0.00517	0.00513	29
	131.2857143	171.28571	1049.82	**0.00547**	**0.00553**	

Table I. 5 Constituents concentration of experiment-2

Time internal	Mg (mg/l)	P (mg/l)	PO_4 (mg/l)	Mg Conc. (M)	PO_4 Conc. (M)	Volume of reactive solution (L)
0	164	198	1213.55	0.00683	0.00639	15
0.25	155	188	1152.26	0.00646	0.00606	15
0.5	156	186	1140.00	0.00650	0.00600	15
0.75	153	191	1170.65	0.00638	0.00616	15
1	154	186	1140.00	0.00642	0.00600	15
1.25	167	189	1158.39	0.00696	0.00610	15
2	165	194	1189.03	0.00688	0.00626	16.5
2.55	156	173	1060.32	0.00650	0.00558	17.15
4.17	155	206	1262.58	0.00646	0.00665	19.25
5.57	138	181	1109.35	0.00575	0.00584	21
8.57	150	210	1287.10	0.00625	0.00677	25
	155.7272727	191.09091				

Table I. 6 Constituents concentration of experiment-3

Time interval (h)	Mg (mg/l)	P (mg/l)	PO_4 (mg/l)	Mg Conc. (M)	PO_4 Conc. (M)	Volume of reactive solution (L)
0	113	148	907.10	0.00471	0.00477	15
0.25	104	141	864.19	0.00433	0.00455	15
0.5	106	141	864.19	0.00442	0.00455	15
0.75	106	152	931.61	0.00442	0.00490	15
2.25	107	159	974.52	0.00446	0.00513	16
3.25	113	148	907.10	0.00471	0.00477	17
6.75	110	151	925.48	0.00458	0.00487	19
12.75	117	171	1048.06	0.00488	0.00552	21.1
18.75	109	166	1017.42	0.00454	0.00535	23
26.25	105	159	974.52	0.00438	0.00513	26
31.25	108	136	833.55	0.00450	0.00439	28
38.25	105	156	956.13	0.00438	0.00503	31
	108.5833333	152.3333333				

Table I. 7 Consistency of plastic coating to prevent the dissolution of copper into solution due to corrosion of copper coil (Fed-batch experiment)

Observation Time (hrs)	Concentration of **Mg** (mg/l)	Concentration of **P** (mg/l)	Concentration of **Cu** (mg/l)
1	55.00	65.1	<=0.1
3	49.90	59.00	<=0.1
5	44.20	54.30	<=0.1
7	36.50	43.60	<=0.1
9	25.80	19.60	<=0.1
11	118.00	70.10	<=0.1
15	112	41.50	<=0.1

APPENDIX J

J.1 Description of gPROMS Functions

This research incorporates gPROMS for simulation of the mathematical model described in Chapter 3. It is worthwhile pointing out that gPROMS is a process simulation software and equation solver, which can perform statistical calculations using it's built in functions. The first step of modeling a new process is to create a new gPROMS project, which normally consists of the following project entities.

- VARIABLE TYPES
- MODEL
- PROCESSES

VARIABLE TYPES defines the numerical range of variables along with their default units.

MODEL entity: In gPROMS, the declaration of primitive process models is done via MODELs. A gPROMS project should contain at least one Model. A Model contains a mathematical description of the physical behavior of a given system. It comprises the following sections, containing a different type of information regarding the system being controlled.

> ***PARAMETER:*** A set of parameters that characterize the system. These correspond to quantities that will never be calculated by any simulation or other type of calculation making use of this model. Their values must always be specified before the simulation begins and remain unchanged thereafter. Parameters can be defined as *REAL* or *INTEGER* type.

VARIABLES: This section defines the time-dependent behavior of the system. These values may be specified in later section of the gPROMS project or left to be calculated by the simulation.

EQUATION: A set of equations involving the declared variables and parameters are coded in this section. These equations include algebraic, differential and differential-algebraic equations. The multi-component parameters/variables/equations may be defined by ARRAY functions.

PROCESSES entity: The simulation activity to study the behavior of the system under different circumstances is defined in this project entity. A process is partitioned into the following sections, containing information required to define the corresponding simulation activity.

UNIT: This section declares the process equipment (process identity number).

SET: This section set the fixed values of all the defined Parameters.

ASSIGN: The specification of input variables is provided in this section to maintain the zero degrees of freedom in the simulation for successful model execution.

INITIAL: This section declares the initial-condition (at time zero) of variables pertaining to the simulation activity.

SCHEDULE: The external manipulation, such as deliberate control action, and/or disturbances, is provided in this section. Scheduling can be constructed Conventional Scheduling (specified time range condition) and Dynamic Scheduling (dynamic variable condition). A detailed description can be obtained in gPROMS User Guide (gPROMS 2002). The simulation result of Conventional Scheduling is previously demonstrated previously (Ali *et al.*

2005a). The simulation result of Dynamic Scheduling is also shown previously by (Ali *et al*. 2004).

For parameter estimation, the following project entities are also included in gPROMS coding along with the abovementioned project entities.

PARAMETER ESTIMATION: The complete specification of parameter estimation problem requires some additional information, which includes the unknown parameters to be estimated, the number of experiments performed and the statistical variance model to be used. Detailed descriptions are available in gPROMS Advanced User Guide (gPROMS 2002a).

EXPERIMENT: The project entity specifies the condition of experiment, which includes the initial condition of experiments, time varying control variables, and time invariant control variables.

J.2 Exporting the Output to Microsoft Excel

When a simulation of a process is conducted, the results are exported to gRMS (output storage file in gPROMS). gRMS has limited capabilities of plotting graphs (gPROMS 2002a). gExcelOutput can be switched on in the *SOLUTION PARAMETER* section of the Process entity, and the calculated variables in the simulation is exported to Excel. Exporting output of the simulation is useful for producing higher quality graphs.

Table J. 1 Summary of the model response for Mg^{2+}, NH_4^+ and PO_4^3 (concentrations are in molar)

Solution pH	6	7	8	9	10	11	12	13
Mg^{2+}	0.001072	0.001029	0.000994	0.000984	0.000943	0.000701	0.000229	3.41E-05
Total Mg	0.001083	0.001083	0.001083	0.001083	0.001083	0.001083	0.001083	0.001083
NH_4^+	0.011065	0.011014	0.010525	0.007265	0.001743	0.000202	2.12E-05	2.44E-06
Total NH_4	0.011094	0.011094	0.011094	0.011094	0.011094	0.011094	0.011094	0.011094
PO_4^{3-}	1.98E-11	1.02E-09	1.76E-08	1.89E-07	1.77E-06	1.13E-05	5.2E-05	0.000204
Total PO_4	0.000359	0.000359	0.000359	0.000359	0.000359	0.000359	0.000359	0.000359

APPENDIX K

K 1. Fischer Information Matrices

Table K. 1 Fischer information matrix and computed F-value for Est.type 1

Parameter	Optimal Value	Parameter Number	1	2	3	4	5	6	7	8	9	10	11	12	13	14	15	16	17	18	19
E101.K_KIN	46.64	**1.00**	0.21	-10.29	0.06	-0.06	-0.48	0.18	-0.53	0.20	0.49	-0.22	-1.93	-0.25	-1.56	-0.14	-0.46	1.80	0.46	0.39	2.54
E101.N	1.48	**2.00**	-10.29	542.58	-13.70	2.80	22.59	-9.34	40.50	-12.43	-28.96	12.23	106.10	13.56	85.80	4.99	17.77	-79.27	-37.72	-21.64	-132.36
LC1 E101.L(1).Gamma	0.56	**3.00**	0.06	-13.70	180.98	-0.03	-0.33	-1.92	-2.62	-0.10	0.08	-0.11	-0.03	-0.17	-0.96	0.21	0.34	-6.38	1.33	0.09	0.48
LC1 E101.PO4_FI(1).Omega	1.16	**4.00**	-0.06	2.80	-0.03	8.03	61.58	0.07	0.13	0.02	0.00	0.01	0.02	0.02	0.13	0.01	0.01	-0.08	-0.06	0.02	-0.03
LC1 E101.PO4_FI(1).Gamma	0.59	**5.00**	-0.48	22.59	-0.33	61.58	475.13	0.65	1.14	0.13	0.00	0.11	0.14	0.17	0.99	0.09	0.08	-0.05	-0.55	0.14	-0.28
LC1 E101.MG_FI(1).Omega	1.65	**6.00**	0.18	-9.34	-1.92	0.07	0.65	13.64	25.22	0.21	-0.13	0.21	0.10	0.33	1.91	-0.33	-0.53	10.53	-2.38	-0.10	-0.89
LC1 E101.MG_FI(1).Gamma	0.25	**7.00**	-0.53	40.50	-2.62	0.13	1.14	25.22	146.31	0.40	-0.15	0.37	0.29	0.59	3.41	-0.27	-0.51	12.07	-3.43	0.05	-1.36
LC2 E101.L(2).Omega	0.53	**8.00**	0.20	-12.43	-0.10	0.02	0.13	0.21	0.40	121.88	191.41	0.04	0.06	0.07	0.41	0.05	0.05	-0.32	-0.19	0.07	-0.10
LC2 E101.L(2).Gamma	0.60	**9.00**	0.49	-28.96	0.08	0.00	0.00	-0.13	-0.15	191.41	335.79	0.00	0.02	0.00	0.02	0.04	0.05	-0.73	0.08	0.03	0.02
LC2 E101.PO4_FI(2).Omega	1.21	**10.00**	-0.22	12.23	-0.11	0.01	0.11	0.21	0.37	0.04	0.00	5.56	50.27	0.06	0.33	0.03	0.03	-0.04	-0.18	0.05	-0.09
LC2 E101.PO4_FI(2).Gamma	0.63	**11.00**	-1.93	106.10	-0.03	0.02	0.14	0.10	0.29	0.06	0.02	50.27	564.87	0.08	0.45	0.09	0.10	-1.01	-0.13	0.10	-0.09
LC2 E101.MG_FI(2).Omega	1.16	**12.00**	-0.25	13.56	-0.17	0.02	0.17	0.33	0.59	0.07	0.00	0.06	0.08	5.61	35.37	0.05	0.05	-0.07	-0.29	0.07	-0.15
LC2 E101.MG_FI(2).Gamma	0.60	**13.00**	-1.56	85.80	-0.96	0.13	0.99	1.91	3.41	0.41	0.02	0.33	0.45	35.37	231.98	0.30	0.30	-0.78	-1.65	0.45	-0.85
LC3 E101.L(3).Omega	0.68	**14.00**	-0.14	4.99	0.21	0.01	0.09	-0.33	-0.27	0.05	0.04	0.03	0.09	0.05	0.30	14.74	27.92	-2.61	0.15	0.13	0.00
LC3 E101.L(3).Gamma	0.49	**15.00**	-0.46	17.77	0.34	0.01	0.08	-0.53	-0.51	0.05	0.05	0.03	0.10	0.05	0.30	27.92	132.53	-3.61	0.28	0.17	0.04
LC3 E101.PO4_FI(3).Omega	0.94	**16.00**	1.80	-79.27	-6.38	-0.08	-0.05	10.53	12.07	-0.32	-0.73	-0.04	-1.01	-0.07	-0.78	-2.61	-3.61	153.37	37.75	-2.01	-1.60
LC3 E101.PO4_FI(3).Gamma	0.43	**17.00**	0.46	-37.72	1.33	-0.06	-0.55	-2.38	-3.43	-0.19	0.08	-0.18	-0.13	-0.29	-1.65	0.15	0.28	37.75	218.90	-0.01	0.68
LC3 E101.MG_FI(3).Omega	1.57	**18.00**	0.39	-21.64	0.09	0.02	0.14	-0.10	0.05	0.07	0.03	0.05	0.10	0.07	0.45	0.13	0.17	-2.01	-0.01	16.18	64.95
LC3 E101.MG_FI(3).Gamma	0.37	**19.00**	2.54	-132.3	0.48	-0.03	-0.28	-0.89	-1.36	-0.10	0.02	-0.09	-0.09	-0.15	-0.85	0.00	0.04	-1.60	0.68	64.95	289.02

F values for this matrix:	**90%**	**95%**	**99%**
	1.684906185	1.958145797	2.598744258

Table K. 2 Fischer information matrix and computed F-value for Est.type 2

Parameter		Optimal Value	Parameter Number	1	2	3	4	5	6	7	8	9	10	11	12	13	14	15	16	17	18	19	20	21
	SIZE101.K_KIN	27.83	**1.00**	1.00	-0.59	-1.00	-0.01	0.01	-0.03	0.06	-0.05	0.06	0.00	0.02	-0.01	0.04	0.01	0.02	-0.06	0.07	0.33	-0.09	0.17	-0.15
	SIZE101.N	1.52	**2.00**	-0.59	1.00	0.63	0.05	-0.02	0.00	-0.02	0.27	-0.28	-0.02	0.01	0.04	-0.07	0.01	-0.07	0.01	0.00	-0.25	0.17	-0.09	0.09
	SIZE101.N1	0.11	**3.00**	-1.00	0.63	1.00	0.01	-0.01	0.03	-0.06	0.07	-0.07	0.00	-0.02	0.01	-0.04	-0.01	-0.02	0.06	-0.07	-0.34	0.10	-0.17	0.15
LC_SIZE_1	SIZE101.L(1).Omega	0.72	**4.00**	-0.01	0.05	0.01	1.00	-0.97	-0.01	0.01	-0.06	0.06	0.00	0.00	0.00	0.00	0.00	0.00	0.00	0.00	0.01	-0.01	0.00	0.00
LC_SIZE_1	SIZE101.L(1).Gamma	0.48	**5.00**	0.01	-0.02	-0.01	-0.97	1.00	0.01	-0.01	0.07	-0.07	0.00	0.00	0.00	0.00	0.00	0.00	0.00	0.00	-0.01	0.00	0.00	0.00
LC_SIZE_1	SIZE101.PO4_FI(1).Omega	1.14	**6.00**	-0.03	0.00	0.03	-0.01	0.01	1.00	-0.99	-0.08	0.08	0.00	0.00	-0.01	0.01	0.00	0.00	0.00	0.00	-0.04	0.03	0.00	0.00
LC_SIZE_1	SIZE101.PO4_FI(1).Gamma	0.60	**7.00**	0.06	-0.02	-0.06	0.01	-0.01	-0.99	1.00	0.08	-0.08	0.00	0.00	0.00	0.00	0.00	0.00	0.00	0.00	0.05	-0.04	0.00	0.00
LC_SIZE_1	SIZE101.MG_FI(1).Omega	0.90	**8.00**	-0.05	0.27	0.07	-0.06	0.07	-0.08	0.08	1.00	-1.00	0.02	-0.01	-0.05	0.05	-0.01	0.01	0.00	0.01	-0.02	0.04	0.02	-0.02
LC_SIZE_1	SIZE101.MG_FI(1).Gamma	0.38	**9.00**	0.06	-0.28	-0.07	0.06	-0.07	0.08	-0.08	-1.00	1.00	-0.02	0.01	0.05	-0.05	0.01	-0.01	0.00	-0.01	0.02	-0.05	-0.02	0.02
LC_SIZE_2	SIZE101.L(2).Omega	0.72	**10.00**	0.00	-0.02	0.00	0.00	0.00	0.00	0.00	0.02	-0.02	1.00	-0.99	0.00	0.00	0.00	0.00	0.00	0.00	-0.01	0.01	0.00	0.00
LC_SIZE_2	SIZE101.L(2).Gamma	0.54	**11.00**	0.02	0.01	-0.02	0.00	0.00	0.00	0.00	-0.01	0.01	-0.99	1.00	0.00	0.00	0.00	-0.01	0.00	0.00	0.03	-0.02	0.01	0.00
LC_SIZE_2	SIZE101.PO4_FI(2).Omega	1.21	**12.00**	-0.01	0.04	0.01	0.00	0.00	-0.01	0.00	-0.05	0.05	0.00	0.00	1.00	-0.99	0.00	-0.01	-0.01	0.00	0.01	0.00	0.00	0.00
LC_SIZE_2	SIZE101.PO4_FI(2).Gamma	0.64	**13.00**	0.04	-0.07	-0.04	0.00	0.00	0.01	0.00	0.05	-0.05	0.00	0.00	-0.99	1.00	0.00	0.01	0.01	0.00	0.00	0.00	0.00	0.00
LC_SIZE_2	SIZE101.MG_FI(2).Omega	1.16	**14.00**	0.01	0.01	-0.01	0.00	0.00	0.00	0.00	-0.01	0.01	0.00	0.00	0.00	0.00	1.00	-0.91	0.00	0.00	0.01	-0.01	0.00	0.00
LC_SIZE_2	SIZE101.MG_FI(2).Gamma	0.61	**15.00**	0.02	-0.07	-0.02	0.00	0.00	0.00	0.00	0.01	-0.01	0.00	-0.01	-0.01	0.01	-0.91	1.00	0.01	0.00	-0.02	0.02	-0.02	0.02
LC_SIZE_3	SIZE101.L(3).Omega	0.81	**16.00**	-0.06	0.01	0.06	0.00	0.00	0.00	0.00	0.00	0.00	0.00	0.00	-0.01	0.01	0.00	0.01	1.00	-0.87	-0.08	0.07	-0.02	0.02
LC_SIZE_3	SIZE101.L(3).Gamma	0.45	**17.00**	0.07	0.00	-0.07	0.00	0.00	0.00	0.00	0.01	-0.01	0.00	0.00	0.00	0.00	0.00	0.00	-0.87	1.00	0.08	-0.07	0.01	-0.01
LC_SIZE_3	SIZE101.PO4_FI(3).Omega	1.06	**18.00**	0.33	-0.25	-0.34	0.01	-0.01	-0.04	0.05	-0.02	0.02	-0.01	0.03	0.01	0.00	0.01	-0.02	-0.08	0.08	1.00	-0.86	0.26	-0.24
LC_SIZE_3	SIZE101.PO4_FI(3).Gamma	0.42	**19.00**	-0.09	0.17	0.10	-0.01	0.00	0.03	-0.04	0.04	-0.05	0.01	-0.02	0.00	0.00	-0.01	0.02	0.07	-0.07	-0.86	1.00	-0.22	0.21
LC_SIZE_3	SIZE101.MG_FI(3).Omega	1.27	**20.00**	0.17	-0.09	-0.17	0.00	0.00	0.00	0.00	0.02	-0.02	0.00	0.01	0.00	0.00	0.00	-0.02	-0.02	0.01	0.26	-0.22	1.00	-1.00
LC_SIZE_3	SIZE101.MG_FI(3).Gamma	0.42	**21.00**	-0.15	0.09	0.15	0.00	0.00	0.00	0.00	-0.02	0.02	0.00	0.00	0.00	0.00	0.00	0.02	0.02	-0.01	-0.24	0.21	-1.00	1.00

F values for this matrix:

90%	95%	99%
1.687010825	1.9613114	2.609

Table K. 3 Fischer information matrix and computed F value for Est.type 3

Parameter	Optimal Value	Parameter Number	1	2	3	4	5	6	7	8	9	10	11	12	13	14	15	16	17	18	19	20	21
LCHANGE101.K_KIN	45.21	**1.00**	0.22	-10.20	-0.05	-0.01	-0.11	-0.05	-0.40	-0.20	-0.18	0.06	0.36	-0.16	-1.31	-0.27	-1.43	-0.19	-0.35	0.57	-2.29	0.39	2.31
LCHANGE101.N	1.45	**2.00**	-10.20	516.31	1.97	-1.57	4.14	1.69	16.30	11.07	10.31	-5.68	-28.00	8.48	70.26	14.47	77.35	-1.09	8.63	-25.60	69.89	-19.74	-117.13
LCHANGE101.L0	134.96	**3.00**	-0.05	1.97	0.36	-0.59	-0.91	0.02	0.14	0.06	0.08	0.08	1.06	0.05	0.44	0.09	0.48	-1.44	-0.76	-0.18	0.73	-0.13	-0.78
LC_LCHANGE_1LCHANGE101.L(1).Omega	1.15	**4.00**	-0.01	-1.57	-0.59	40.08	33.31	-0.01	-0.08	0.07	-0.52	20.09	70.46	0.02	-0.09	-0.04	-0.24	77.20	26.57	-0.23	0.55	0.02	0.11
LC_LCHANGE_1LCHANGE101.L(1).Gamma	0.37	**5.00**	-0.11	4.14	-0.91	33.31	145.15	0.00	-0.01	0.09	-0.44	6.14	21.54	0.01	0.00	0.00	-0.03	23.75	8.25	-0.46	1.21	0.01	0.09
LC_LCHANGE_1LCHANGE101.PO4_FI(1).Omega	1.11	**6.00**	-0.05	1.69	0.02	-0.01	0.00	6.45	48.72	0.00	0.11	0.00	-0.01	-0.01	0.05	0.02	0.12	0.01	0.02	-0.05	0.16	-0.01	-0.03
LC_LCHANGE_1LCHANGE101.PO4_FI(1).Gamma	0.60	**7.00**	-0.40	16.30	0.14	-0.08	-0.01	48.72	383.89	-0.09	1.23	-0.05	-0.23	-0.08	0.38	0.16	0.95	-0.22	-0.03	-0.06	0.42	-0.07	-0.27
LC_LCHANGE_1LCHANGE101.MG_FI(1).Omega	0.96	**8.00**	-0.20	11.07	0.06	0.07	0.09	0.00	-0.09	9.66	15.41	0.13	0.48	0.04	-0.07	-0.04	-0.24	0.96	0.55	-1.15	2.98	0.04	0.27
LC_LCHANGE_1LCHANGE101.MG_FI(1).Gamma	0.36	**9.00**	-0.18	10.31	0.08	-0.52	-0.44	0.11	1.23	15.41	175.74	-0.70	-2.71	-0.38	1.26	0.57	3.49	-4.77	-2.46	4.89	-11.97	-0.35	-1.87
LC_LCHANGE_2LCHANGE101.L(2).Omega	1.11	**10.00**	0.06	-5.68	0.08	20.09	6.14	0.00	-0.05	0.13	-0.70	31.77	127.32	0.02	-0.04	-0.02	-0.15	55.90	19.32	-0.58	1.49	0.02	0.14
LC_LCHANGE_2LCHANGE101.L(2).Gamma	0.42	**11.00**	0.36	-28.00	1.06	70.46	21.54	-0.01	-0.23	0.48	-2.71	127.32	527.01	0.09	-0.21	-0.10	-0.65	196.09	67.80	-2.11	5.41	0.09	0.56
LC_LCHANGE_2LCHANGE101.PO4_FI(2).Omega	1.17	**12.00**	-0.16	8.48	0.05	0.02	0.01	-0.01	-0.08	0.04	-0.38	0.02	0.09	15.39	61.29	-0.04	-0.24	0.12	0.04	-0.07	0.11	0.02	0.08
LC_LCHANGE_2LCHANGE101.PO4_FI(2).Gamma	0.65	**13.00**	-1.31	70.26	0.44	-0.09	0.00	0.05	0.38	-0.07	1.26	-0.04	-0.21	61.29	320.49	0.19	1.10	-0.12	0.05	-0.23	0.94	-0.07	-0.28
LC_LCHANGE_2LCHANGE101.MG_FI(2).Omega	1.10	**14.00**	-0.27	14.47	0.09	-0.04	0.00	0.02	0.16	-0.04	0.57	-0.02	-0.10	-0.04	0.19	8.15	36.82	-0.08	0.01	-0.07	0.32	-0.03	-0.13
LC_LCHANGE_2LCHANGE101.MG_FI(2).Gamma	0.61	**15.00**	-1.43	77.35	0.48	-0.24	-0.03	0.12	0.95	-0.24	3.49	-0.15	-0.65	-0.24	1.10	36.82	186.61	-0.60	-0.05	-0.22	1.38	-0.19	-0.77
LC_LCHANGE_3LCHANGE101.L(3).Omega	0.76	**16.00**	-0.19	-1.09	-1.44	77.20	23.75	0.01	-0.22	0.96	-4.77	55.90	196.09	0.12	-0.12	-0.08	-0.60	325.25	138.55	-4.56	11.93	0.14	0.97
LC_LCHANGE_3LCHANGE101.L(3).Gamma	0.46	**17.00**	-0.35	8.63	-0.76	26.57	8.25	0.02	-0.03	0.55	-2.46	19.32	67.80	0.04	0.05	0.01	-0.05	138.55	160.12	-2.75	7.27	0.06	0.49
LC_LCHANGE_3LCHANGE101.PO4_FI(3).Omega	0.93	**18.00**	0.57	-25.60	-0.18	-0.23	-0.46	-0.05	-0.06	-1.15	4.89	-0.58	-2.11	-0.07	-0.23	-0.07	-0.22	-4.56	-2.75	32.23	-0.69	-0.11	-0.97
LC_LCHANGE_3LCHANGE101.PO4_FI(3).Gamma	0.44	**19.00**	-2.29	69.89	0.73	0.55	1.21	0.16	0.42	2.98	-11.97	1.49	5.41	0.11	0.94	0.32	1.38	11.93	7.27	-0.69	272.29	0.23	2.35
LC_LCHANGE_3LCHANGE101.MG_FI(3).Omega	1.22	**20.00**	0.39	-19.74	-0.13	0.02	0.01	-0.01	-0.07	0.04	-0.35	0.02	0.09	0.02	-0.07	-0.03	-0.19	0.14	0.06	-0.11	0.23	6.47	40.05
LC_LCHANGE_3LCHANGE101.MG_FI(3).Gamma	0.42	**21.00**	2.31	-117.13	-0.78	0.11	0.09	-0.03	-0.27	0.27	-1.87	0.14	0.56	0.08	-0.28	-0.13	-0.77	0.97	0.49	-0.97	2.35	40.05	248.78

F values for this matrix:	**90%**	**95%**	**99%**
	1.687010825	1.9613114	2.609

Table K. 4 Fischer information matrix and computed F value for Est.type 4

Parameter	Optimal Value	Parameter Number	1	2	3	4	5	6	7	8	9	10	11	12	13	14	15	16	17	18	19
E101.K_KIN	47.06	**1.00**	0.18	-7.82	0.04	0.11	-0.07	-0.45	-0.27	-0.53	0.42	-0.18	-1.39	-0.25	-1.43	-0.09	-0.42	-0.11	0.97	0.44	2.63
E101.N	1.64	**2.00**	-7.82	377.99	-4.81	-14.72	2.82	18.96	16.13	35.42	-21.89	8.94	69.72	12.64	72.05	2.56	14.62	1.51	-61.42	-22.31	-125.61
LC1E101.L(1).Omega	0.65	**3.00**	0.04	-4.81	95.22	163.70	0.01	0.18	-0.54	1.62	-0.28	-0.04	0.21	0.12	0.73	-0.04	-0.09	-0.95	-0.73	0.03	-0.35
LC1E101.L(1).Gamma	0.51	**4.00**	0.11	-14.72	163.70	331.16	0.01	0.12	-0.18	0.66	-0.15	-0.02	0.14	0.07	0.44	0.04	0.02	-0.27	-0.38	0.07	-0.15
LC1E101.PO4_FI(1).Omega	1.13	**5.00**	-0.07	2.82	0.01	0.01	10.43	68.07	-0.01	0.09	-0.03	0.00	0.04	0.02	0.10	0.02	0.02	0.01	-0.08	0.03	-0.02
LC1E101.PO4_FI(1).Gamma	0.60	**6.00**	-0.45	18.96	0.18	0.12	68.07	447.37	-0.21	1.02	-0.29	-0.03	0.29	0.15	0.89	0.14	0.13	-0.21	-0.71	0.21	-0.24
LC1E101.MG_FI(1).Omega	1.16	**7.00**	-0.27	16.13	-0.54	-0.18	-0.01	-0.21	20.11	9.01	0.43	0.06	-0.26	-0.16	-1.01	0.22	0.35	2.20	1.17	0.11	0.67
LC1E101.MG_FI(1).Gamma	0.32	**8.00**	-0.53	35.42	1.62	0.66	0.09	1.02	9.01	147.94	-1.61	-0.22	1.23	0.70	4.25	-0.21	-0.53	-5.54	-4.24	0.19	-2.05
LC2E101.L(2).Gamma	0.61	**9.00**	0.42	-21.89	-0.28	-0.15	-0.03	-0.29	0.43	-1.61	156.58	0.05	-0.34	-0.18	-1.08	-0.10	-0.06	0.62	0.93	-0.19	0.36
LC2E101.PO4_FI(2).Omega	1.20	**10.00**	-0.18	8.94	-0.04	-0.02	0.00	-0.03	0.06	-0.22	0.05	11.24	61.61	-0.02	-0.13	-0.01	0.00	0.10	0.12	-0.02	0.05
LC2E101.PO4_FI(2).Gamma	0.64	**11.00**	-1.39	69.72	0.21	0.14	0.04	0.29	-0.26	1.23	-0.34	61.61	375.79	0.17	1.04	0.16	0.14	-0.28	-0.84	0.24	-0.28
LC2E101.MG_FI(2).Omega	1.14	**12.00**	-0.25	12.64	0.12	0.07	0.02	0.15	-0.16	0.70	-0.18	-0.02	0.17	6.69	36.41	0.07	0.06	-0.21	-0.45	0.11	-0.16
LC2E101.MG_FI(2).Gamma	0.60	**13.00**	-1.43	72.05	0.73	0.44	0.10	0.89	-1.01	4.25	-1.08	-0.13	1.04	36.41	202.52	0.41	0.33	-1.31	-2.68	0.66	-0.97
LC3E101.L(3).Omega	0.87	**14.00**	-0.09	2.56	-0.04	0.04	0.02	0.14	0.22	-0.21	-0.10	-0.01	0.16	0.07	0.41	22.49	16.92	0.57	-0.20	0.21	0.03
LC3E101.L(3).Gamma	0.44	**15.00**	-0.42	14.62	-0.09	0.02	0.02	0.13	0.35	-0.53	-0.06	0.00	0.14	0.06	0.33	16.92	124.33	0.81	-0.09	0.23	0.09
LC3E101.PO4_FI(3).Omega	0.97	**16.00**	-0.11	1.51	-0.95	-0.27	0.01	-0.21	2.20	-5.54	0.62	0.10	-0.28	-0.21	-1.31	0.57	0.81	19.61	25.32	0.40	1.16
LC3E101.PO4_FI(3).Gamma	0.44	**17.00**	0.97	-61.42	-0.73	-0.38	-0.08	-0.71	1.17	-4.24	0.93	0.12	-0.84	-0.45	-2.68	-0.20	-0.09	25.32	190.68	-0.42	0.95
LC3E101.MG_FI(3).Omega	1.64	**18.00**	0.44	-22.31	0.03	0.07	0.03	0.21	0.11	0.19	-0.19	-0.02	0.24	0.11	0.66	0.21	0.23	0.40	-0.42	22.16	77.05
LC3E101.MG_FI(3).Gamma	0.36	**19.00**	2.63	-125.61	-0.35	-0.15	-0.02	-0.24	0.67	-2.05	0.36	0.05	-0.28	-0.16	-0.97	0.03	0.09	1.16	0.95	77.05	307.25

F values for this matrix:	**90%**	**95%**	**99%**
	1.68491	1.9581458	2.5987

Table K. 5 Fischer information matrix and computed F value for Est.type 5

Parameter	Optimal Value	Parameter Number	1	2	3	4	5	6	7	8	9	10	11	12	13	14	15	16	17	18	19	20	21
SIZE101.K_KIN	28.24	**1.00**	0.52	-13.72	74.13	0.01	0.07	-0.17	-1.06	-0.68	-1.54	0.17	0.72	-0.26	-2.28	-0.39	-2.32	-0.20	-0.88	0.80	1.51	0.38	3.90
SIZE101.N	1.67	**2.00**	-13.72	396.94	-1975.38	-2.54	-12.05	4.10	27.00	24.07	57.85	-5.57	-24.39	7.66	68.21	11.61	69.85	4.28	19.21	-25.42	-60.60	-11.76	-112.87
SIZE101.N1	0.11	**3.00**	74.13	-1975.38	10639.73	1.72	11.37	-22.71	-146.87	-96.29	-217.11	24.65	107.38	-36.70	-324.37	-55.51	-332.66	-27.71	-124.00	119.46	233.11	56.23	568.11
LC_SIZE_1SIZE101.L(1).Omega	0.88	**4.00**	0.01	-2.54	1.72	22.83	91.82	0.06	0.58	0.22	1.16	0.09	0.44	0.06	0.57	0.05	0.33	0.04	0.17	-0.38	0.74	-0.04	-0.03
LC_SIZE_1SIZE101.L(1).Gamma	0.45	**5.00**	0.07	-12.05	11.37	91.82	373.51	0.26	2.22	0.91	3.80	0.35	1.66	0.25	2.04	0.17	1.02	0.17	0.67	-1.61	3.00	-0.15	-0.04
LC_SIZE_1SIZE101.PO4_FI(1).Omega	1.28	**6.00**	-0.17	4.10	-22.71	0.06	0.26	16.57	82.17	0.38	0.53	0.11	0.51	0.11	0.52	0.01	0.03	0.07	0.27	-0.69	1.21	-0.05	0.10
LC_SIZE_1SIZE101.PO4_FI(1).Gamma	0.58	**7.00**	-1.06	27.00	-146.87	0.58	2.22	82.17	455.65	2.56	6.34	0.85	3.93	0.72	4.38	0.22	1.26	0.46	1.84	-4.59	8.23	-0.37	0.37
LC_SIZE_1SIZE101.MG_FI(1).Omega	0.87	**8.00**	-0.68	24.07	-96.29	0.22	0.91	0.38	2.56	23.64	28.88	0.38	1.75	0.35	1.85	0.06	0.30	0.23	0.92	-2.32	3.91	-0.16	0.27
LC_SIZE_1SIZE101.MG_FI(1).Gamma	0.39	**9.00**	-1.54	57.85	-217.11	1.16	3.80	0.53	6.34	28.88	149.40	1.06	5.14	0.56	7.07	0.80	5.16	0.40	1.63	-3.56	7.28	-0.44	-0.92
LC_SIZE_2SIZE101.L(2).Omega	0.83	**10.00**	0.17	-5.57	24.65	0.09	0.35	0.11	0.85	0.38	1.06	20.98	97.06	0.11	0.68	0.03	0.18	0.06	0.26	-0.67	1.31	-0.06	0.06
LC_SIZE_2SIZE101.L(2).Gamma	0.51	**11.00**	0.72	-24.39	107.38	0.44	1.66	0.51	3.93	1.75	5.14	97.06	450.53	0.51	3.23	0.18	1.01	0.30	1.23	-3.11	5.92	-0.29	0.23
LC_SIZE_2SIZE101.PO4_FI(2).Omega	1.34	**12.00**	-0.26	7.66	-36.70	0.06	0.25	0.11	0.72	0.35	0.56	0.11	0.51	12.90	53.38	-0.01	-0.11	0.05	0.21	-0.60	1.40	-0.07	0.16
LC_SIZE_2SIZE101.PO4_FI(2).Gamma	0.63	**13.00**	-2.28	68.21	-324.37	0.57	2.04	0.52	4.38	1.85	7.07	0.68	3.23	53.38	308.75	0.35	2.15	0.37	1.44	-3.34	5.55	-0.25	-0.14
LC_SIZE_2SIZE101.MG_FI(2).Omega	1.24	**14.00**	-0.39	11.61	-55.51	0.05	0.17	0.01	0.22	0.06	0.80	0.03	0.18	-0.01	0.35	6.32	33.11	0.03	0.11	-0.14	-0.14	0.02	-0.16
LC_SIZE_2SIZE101.MG_FI(2).Gamma	0.59	**15.00**	-2.32	69.85	-332.66	0.33	1.02	0.03	1.26	0.30	5.16	0.18	1.01	-0.11	2.15	33.11	190.17	0.19	0.64	-0.73	-1.25	0.13	-1.06
LC_SIZE_3SIZE101.L(3).Omega	0.88	**16.00**	-0.20	4.28	-27.71	0.04	0.17	0.07	0.46	0.23	0.40	0.06	0.30	0.05	0.37	0.03	0.19	6.19	28.44	-0.44	0.50	-0.01	-0.01
LC_SIZE_3SIZE101.L(3).Gamma	0.43	**17.00**	-0.88	19.21	-124.00	0.17	0.67	0.27	1.84	0.92	1.63	0.26	1.23	0.21	1.44	0.11	0.64	28.44	135.46	-1.73	2.20	-0.06	0.02
LC_SIZE_3SIZE101.PO4_FI(3).Omega	1.47	**18.00**	0.80	-25.42	119.46	-0.38	-1.61	-0.69	-4.59	-2.32	-3.56	-0.67	-3.11	-0.60	-3.34	-0.14	-0.73	-0.44	-1.73	11.61	21.78	0.25	-0.40
LC_SIZE_3SIZE101.PO4_FI(3).Gamma	0.37	**19.00**	1.51	-60.60	233.11	0.74	3.00	1.21	8.23	3.91	7.28	1.31	5.92	1.40	5.55	-0.14	-1.25	0.50	2.20	21.78	221.89	-0.90	1.80
LC_SIZE_3SIZE101.MG_FI(3).Omega	2.74	**20.00**	0.38	-11.76	56.23	-0.04	-0.15	-0.05	-0.37	-0.16	-0.44	-0.06	-0.29	-0.07	-0.25	0.02	0.13	-0.01	-0.06	0.25	-0.90	5.30	35.94
LC_SIZE_3SIZE101.MG_FI(3).Gamma	0.26	**21.00**	3.90	-112.87	568.11	-0.03	-0.04	0.10	0.37	0.27	-0.92	0.06	0.23	0.16	-0.14	-0.16	-1.06	-0.01	0.02	-0.40	1.80	35.94	276.10

F values for this matrix:	**90%**	**95%**	**99%**
	1.687010825	1.9613114	2.609

Table K. 6 Fischer information matrix and computed F value for Est.type 6

Parameter	Optimal Value	Parameter Number	1	2	3	4	5	6	7	8	9	10	11	12	13	14	15	16	17	18	19
LCHANGE101.K_KIN	49.16	**1.00**	0.19	-8.81	-0.05	0.02	-0.09	-0.08	-0.36	-0.15	-0.29	0.23	-0.12	-1.06	-0.25	-1.35	-0.27	2.14	1.10	0.21	2.03
LCHANGE101.N	1.68	**2.00**	-8.81	433.11	2.00	-0.36	4.02	2.93	13.31	9.50	24.20	-13.41	6.02	55.84	13.06	71.67	8.82	-93.83	-66.52	-10.01	-100.35
LCHANGE101.L0	135.02	**3.00**	-0.05	2.00	0.34	-0.29	-0.82	0.03	0.13	0.05	0.10	1.59	0.04	0.38	0.09	0.49	-0.16	-0.80	-0.40	-0.07	-0.74
LC_LCHANGE_1LCHANGE101.L(1).Omega	1.35	**4.00**	0.02	-0.36	-0.29	23.43	23.75	-0.06	-0.16	-0.06	0.76	-5.71	-0.01	-0.03	-0.01	-0.05	-0.20	2.94	0.10	0.01	-0.02
LC_LCHANGE_1LCHANGE101.L(1).Gamma	0.34	**5.00**	-0.09	4.02	-0.82	23.75	140.28	0.01	0.02	0.01	-0.12	-1.68	0.00	0.00	0.00	0.00	0.02	-0.40	0.00	0.00	0.01
LC_LCHANGE_1LCHANGE101.PO4_FI(1).Omega	1.08	**6.00**	-0.08	2.93	0.03	-0.06	0.01	25.10	89.81	0.04	-0.73	0.05	0.03	-0.06	-0.03	-0.17	0.09	-1.70	0.13	0.01	0.09
LC_LCHANGE_1LCHANGE101.PO4_FI(1).Gamma	0.61	**7.00**	-0.36	13.31	0.13	-0.16	0.02	89.81	388.09	0.08	-0.85	0.05	0.00	0.08	0.03	0.16	0.23	-3.87	-0.22	-0.02	-0.01
LC_LCHANGE_1LCHANGE101.MG_FI(1).Omega	1.34	**8.00**	-0.15	9.50	0.05	-0.06	0.01	0.04	0.08	4.34	16.15	0.03	0.01	-0.01	-0.01	-0.06	0.09	-1.61	0.02	0.00	0.04
LC_LCHANGE_1LCHANGE101.MG_FI(1).Gamma	0.29	**9.00**	-0.29	24.20	0.10	0.76	-0.12	-0.73	-0.85	16.15	162.39	-0.95	-0.73	1.70	0.81	4.78	-1.08	22.11	-4.06	-0.27	-2.09
LC_LCHANGE_2LCHANGE101.L(2).Gamma	0.59	**10.00**	0.23	-13.41	1.59	-5.71	-1.68	0.05	0.05	0.03	-0.95	130.77	0.06	-0.14	-0.06	-0.38	0.08	-1.36	0.33	0.02	0.16
LC_LCHANGE_2LCHANGE101.PO4_FI(2).Omega	1.19	**11.00**	-0.12	6.02	0.04	-0.01	0.00	0.03	0.00	0.01	-0.73	0.06	18.98	59.45	-0.07	-0.39	0.01	-0.47	0.36	0.03	0.15
LC_LCHANGE_2LCHANGE101.PO4_FI(2).Gamma	0.65	**12.00**	-1.06	55.84	0.38	-0.03	0.00	-0.06	0.08	-0.01	1.70	-0.14	59.45	287.15	0.20	1.13	0.05	-0.04	-1.05	-0.08	-0.42
LC_LCHANGE_2LCHANGE101.MG_FI(2).Omega	1.10	**13.00**	-0.25	13.06	0.09	-0.01	0.00	-0.03	0.03	-0.01	0.81	-0.06	-0.07	0.20	7.24	37.27	0.02	0.10	-0.48	-0.03	-0.19
LC_LCHANGE_2LCHANGE101.MG_FI(2).Gamma	0.60	**14.00**	-1.35	71.67	0.49	-0.05	0.00	-0.17	0.16	-0.06	4.78	-0.38	-0.39	1.13	37.27	198.42	0.08	0.89	-2.77	-0.20	-1.13
LC_LCHANGE_3LCHANGE101.L(3).Gamma	0.54	**15.00**	-0.27	8.82	-0.16	-0.20	0.02	0.09	0.23	0.09	-1.08	0.08	0.01	0.05	0.02	0.08	117.72	-4.26	-0.15	-0.02	0.03
LC_LCHANGE_3LCHANGE101.PO4_FI(3).Omega	0.95	**16.00**	2.14	-93.83	-0.80	2.94	-0.40	-1.70	-3.87	-1.61	22.11	-1.36	-0.47	-0.04	0.10	0.89	-4.26	219.22	61.52	0.14	-1.32
LC_LCHANGE_3LCHANGE101.PO4_FI(3).Gamma	0.43	**17.00**	1.10	-66.52	-0.40	0.10	0.00	0.13	-0.22	0.02	-4.06	0.33	0.36	-1.05	-0.48	-2.77	-0.15	61.52	225.57	0.19	1.03
LC_LCHANGE_3LCHANGE101.MG_FI(3).Omega	2.01	**18.00**	0.21	-10.01	-0.07	0.01	0.00	0.01	-0.02	0.00	-0.27	0.02	0.03	-0.08	-0.03	-0.20	-0.02	0.14	0.19	1.85	20.64
LC_LCHANGE_3LCHANGE101.MG_FI(3).Gamma	0.33	**19.00**	2.03	-100.35	-0.74	-0.02	0.01	0.09	-0.01	0.04	-2.09	0.16	0.15	-0.42	-0.19	-1.13	0.03	-1.32	1.03	20.64	236.80

F values for this matrix:	**90%**	**95%**	**99%**
	1.684906185	1.9581458	2.5987

APPENDIX L

L.1 Model Response in terms of Saturation Index (Est.type 4)

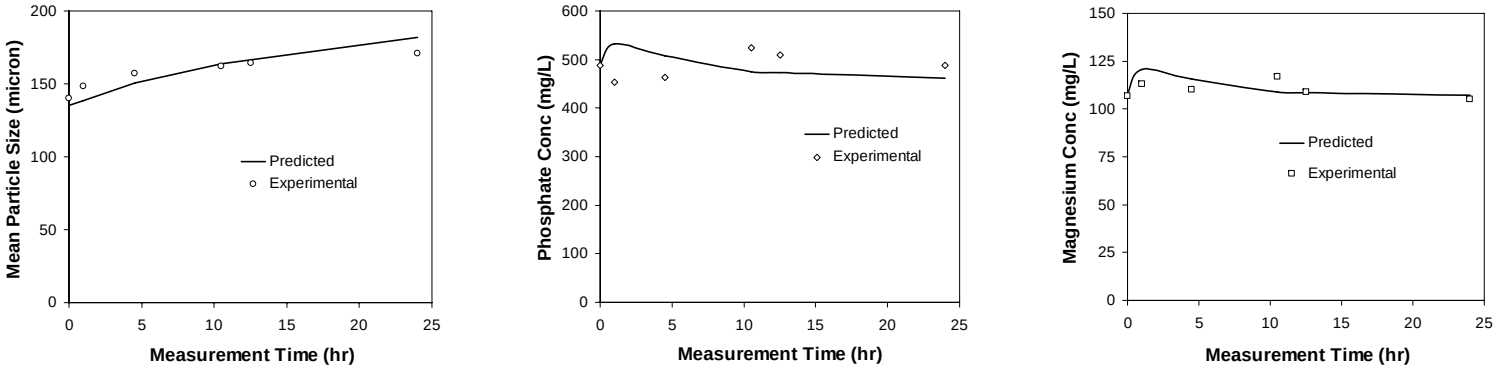

Figure L. 1 Overlay charts of experiment 1 (Est.type 4)

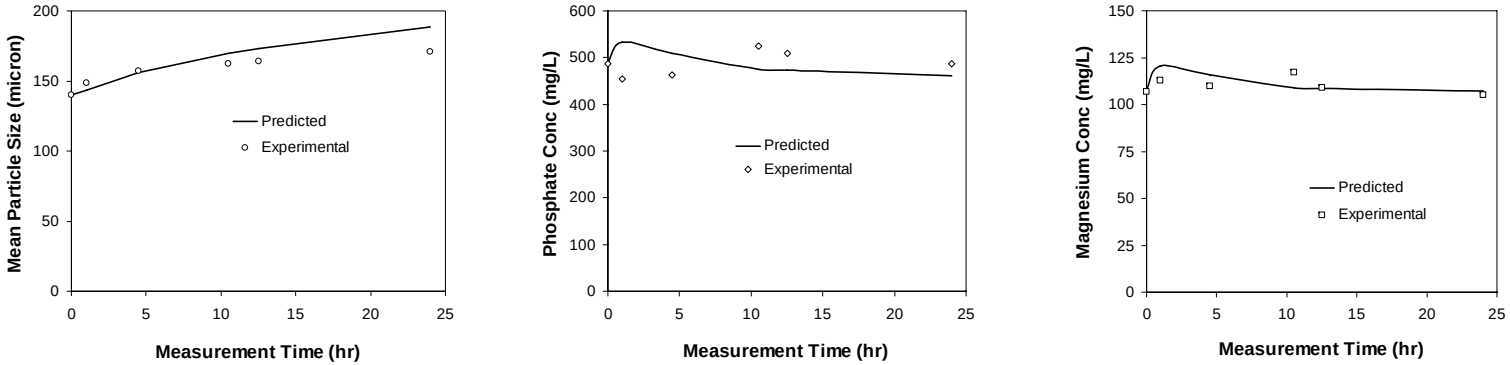

Figure L. 2 Overlay charts of experiment 2 (Est.type 4)

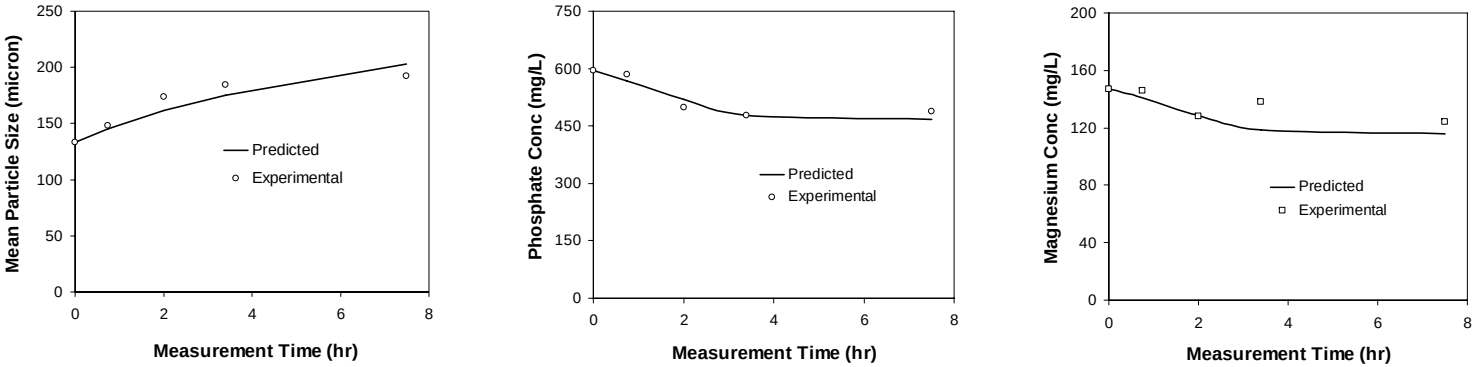

Figure L. 3 Overlay charts of experiment 3 (Est.type 4)

APPENDIX M

M1. Model Response in terms of Saturation Index (Est.type 5)

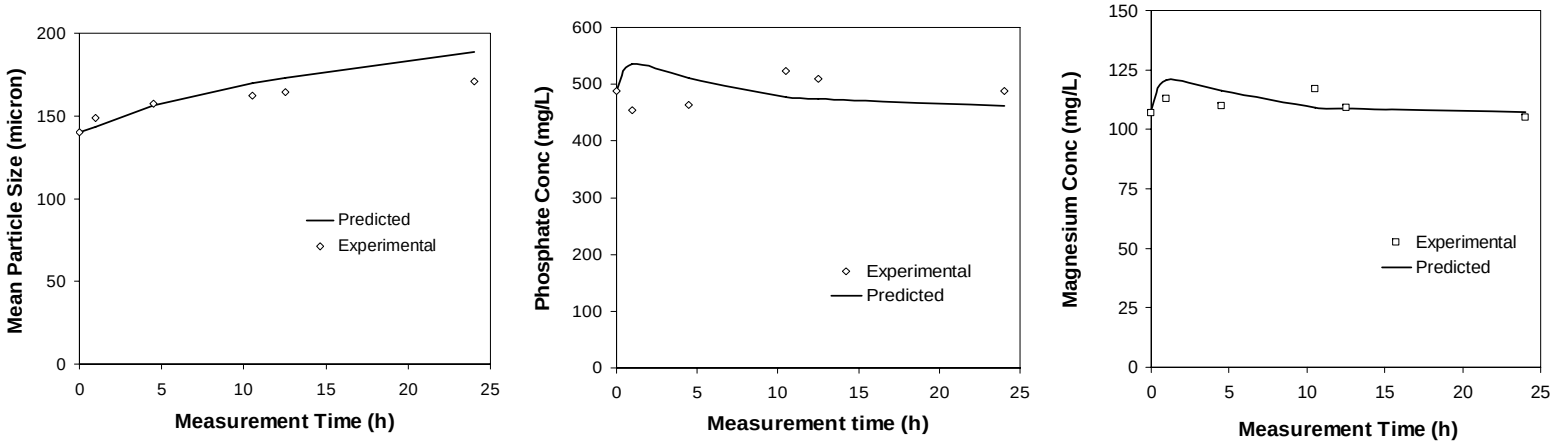

Figure M. 1 Overlay charts of experiment 1 (Est.type 5)

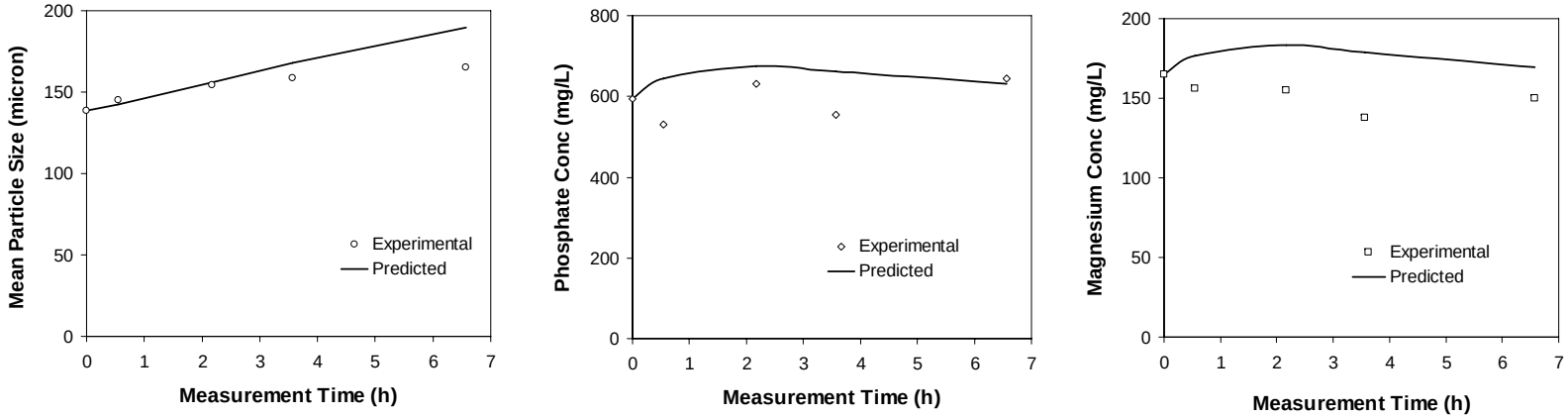

Figure M. 2 Overlay charts of experiment 2 (Est.type 5)

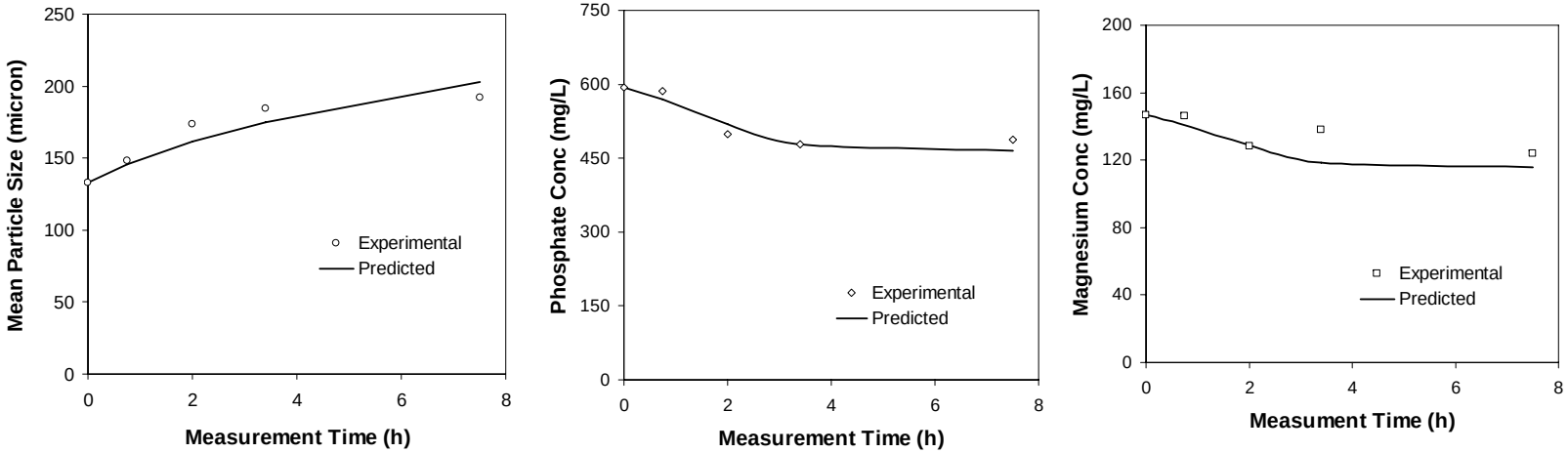

Figure M. 3 Overlay charts of experiment 3 (Est.type 5)

APPENDIX N

N.1 Model Response in terms of Saturation Index (Est.type 6)

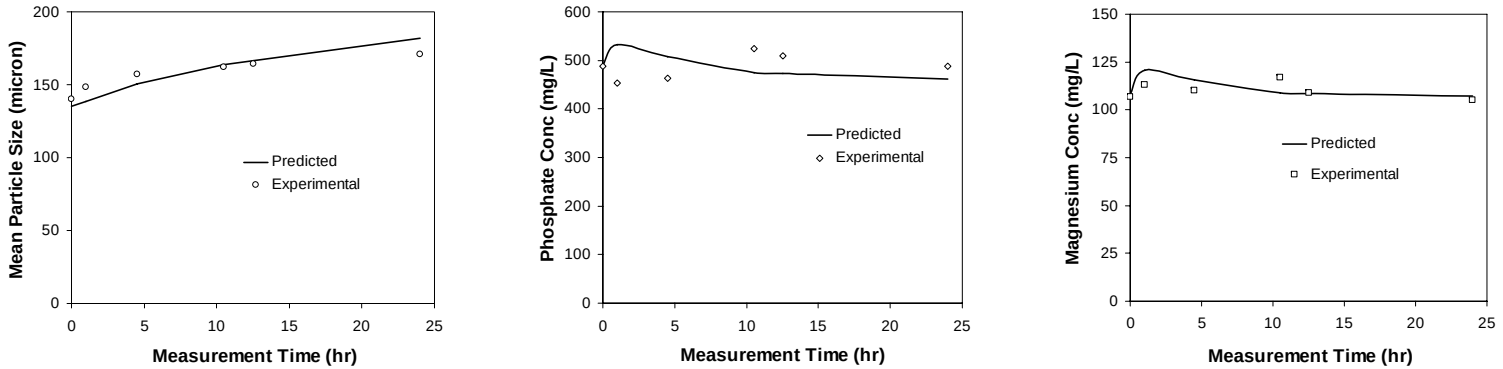

Figure N. 1 Overlay charts of experiment 1 (Est.type 6)

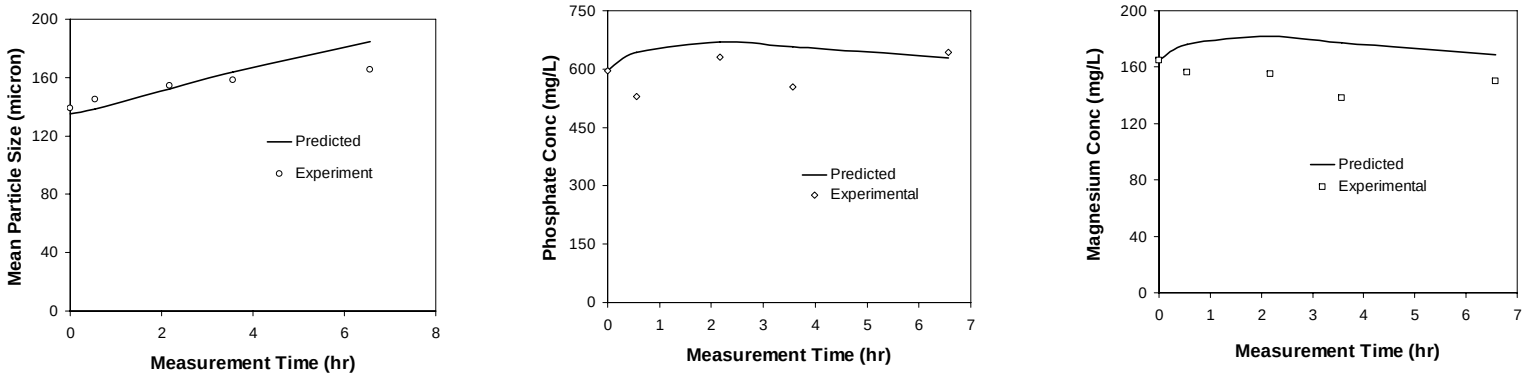

Figure N. 2 Overlay charts of experiment 2 (Est.type 6)

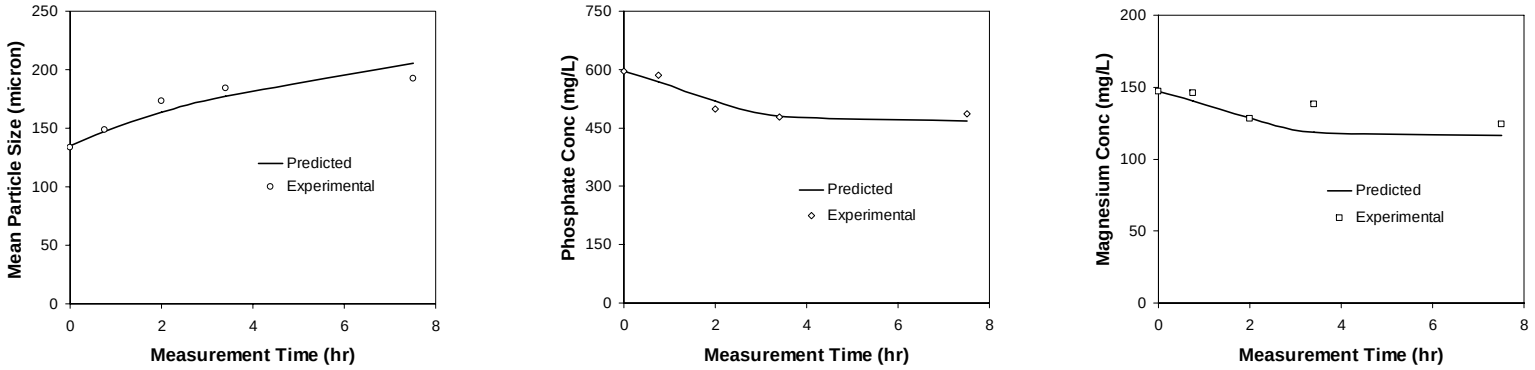

Figure N. 3 Overlay charts of experiment 3 (Est.type 6)

Table N. 1 Objective Function Contributions when supersaturation is expressed in terms of Saturation Index (SI)

Experiment	Variables	Objective Function Contribution (Est.type 4))	Objective Function Contribution (Est.type 5)	Objective Function Contribution (Est.type 6)
1	L	15.78	15.808	14.77
	Total PO_4^{3-}	25.89	25.981	25.85
	Total Mg^{2+}	12.95	13.023	12.86
2	L	14.39	14.415	13.48
	Total PO_4^{3-}	23.84	23.907	23.76
	Total Mg^{2+}	18.62	18.637	18.47
3	L	12.89	12.895	12.56
	Total PO_4^{3-}	16.04	16.111	15.95
	Total Mg^{2+}	14.01	14.015	13.92
Total Objective Functions		198.431	198.863	195.706